HIGH GRADE METAMORPHIC AND STRUCTURAL RELATIONSHIPS NEAR AMATA, MUSGRAVE RANGES, CENTRAL AUSTRALIA

Volume 2

by

Kenneth David Collerson, B.Sc.(Hons) (New England)

Department of Geology and Mineralogy
University of Adelaide

August, 1972

CONTENTS

VOLUME 2

TEXT FIGURES

FIGURE A.1.1

Map showing stations and specimen locations referred to in the text.
(Located in pocket at back of Volume 2)

FIGURE 1.1

Location map of the Musgrave Block showing regional geological and geographical features.
(Located in pocket at back of Volume 2)

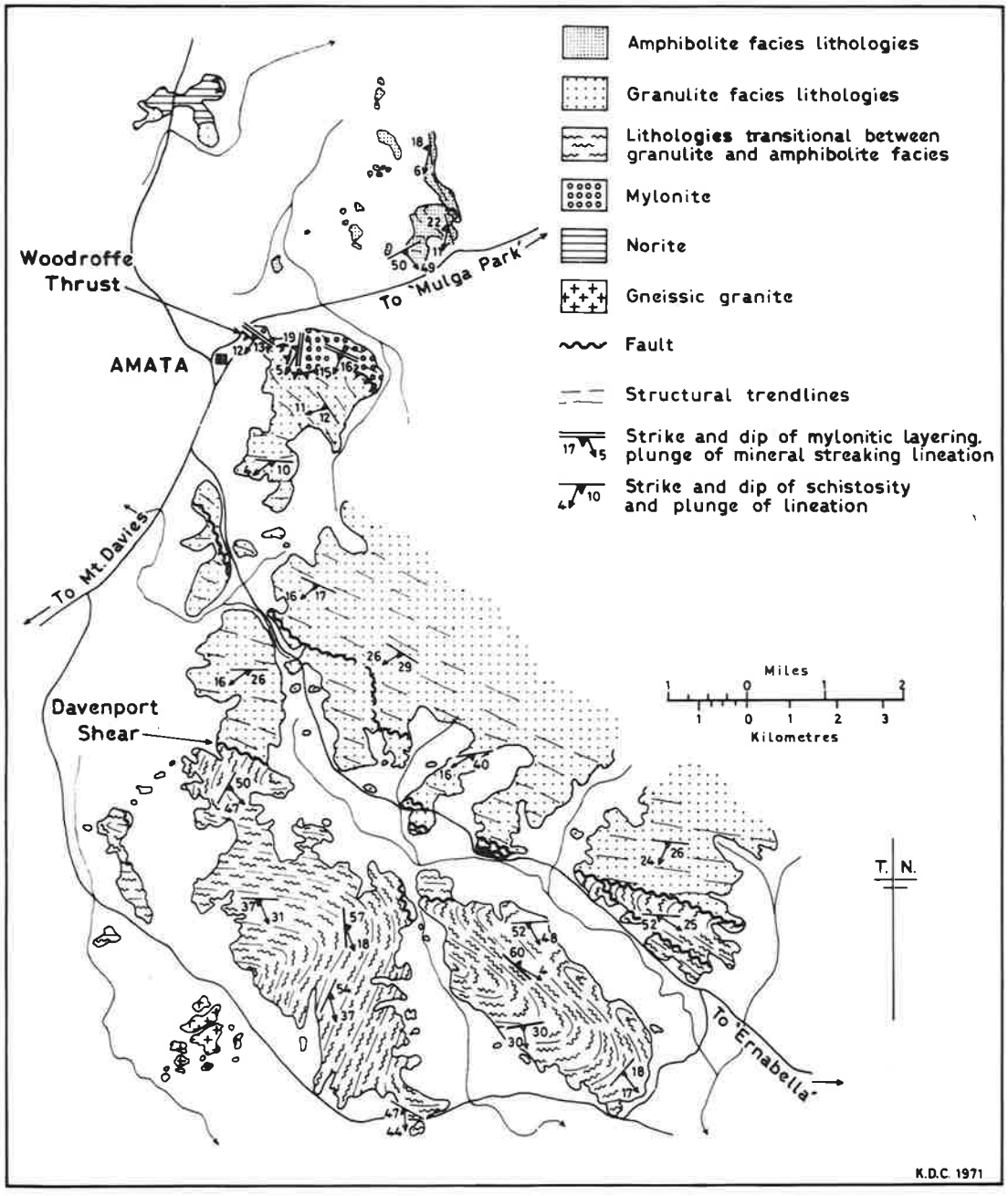

Figure 1.2 Simplified geological map of the Amata area showing structural trend lines and the distribution of metamorphic facies.

FIGURE 1.3

Geological map of the Amata area, Musgrave Ranges.
(Located in the back pocket of Volume 2)

FIGURE 2.1

Map of the Amata area showing the strike and dip of planar structural elements.
(Located in the back pocket of Volume 2)

FIGURE 2.2

Map of the Amata area showing the trend and plunge of linear structural elements.
(Located in the back pocket of Volume 2)

FIGURE 2.3

Stereograms of mesoscopic structural elements, Amata region, central Musgrave Ranges.
(Located in the back pocket of Volume 2)

FIGURE 2.4

(a) Compositional layering in interbanded mafic and quartzo-feldspathic granulites.

(b) Hinge region of a rootless gF_1 intra-folial fold in banded mafic granulite. Note the strongly developed gS_1 schistosity in the surrounding quartzo-feldspathic granulite and the granoblastic microstructure in the mafic unit.

A325-579
Width of field: 6 cm.
Crossed polars.

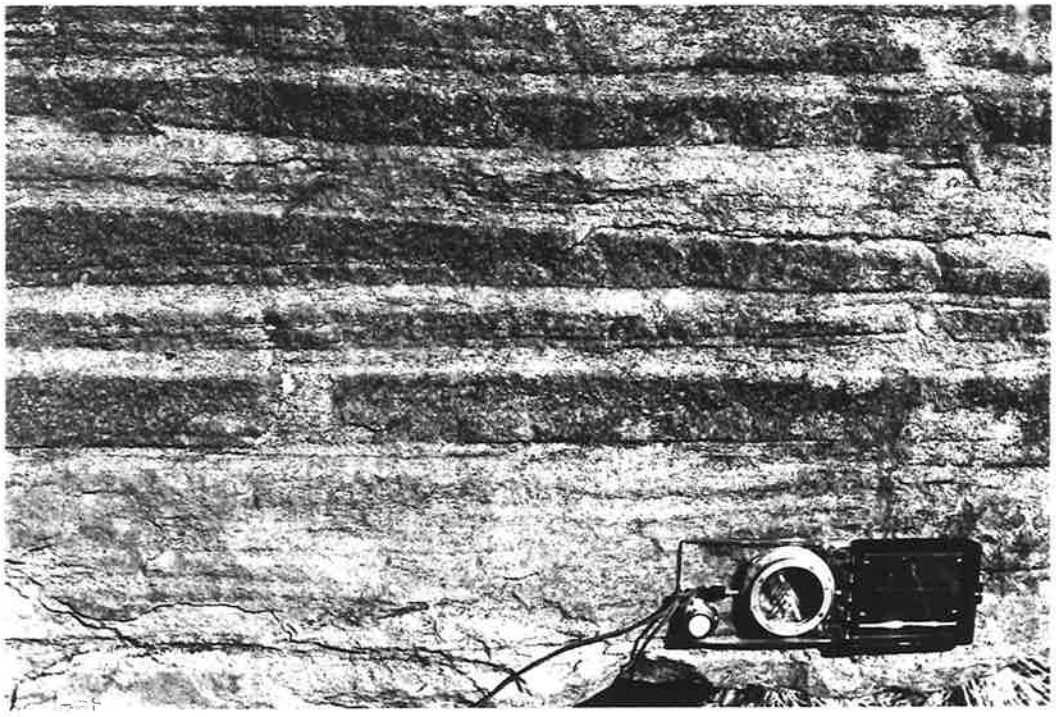

a

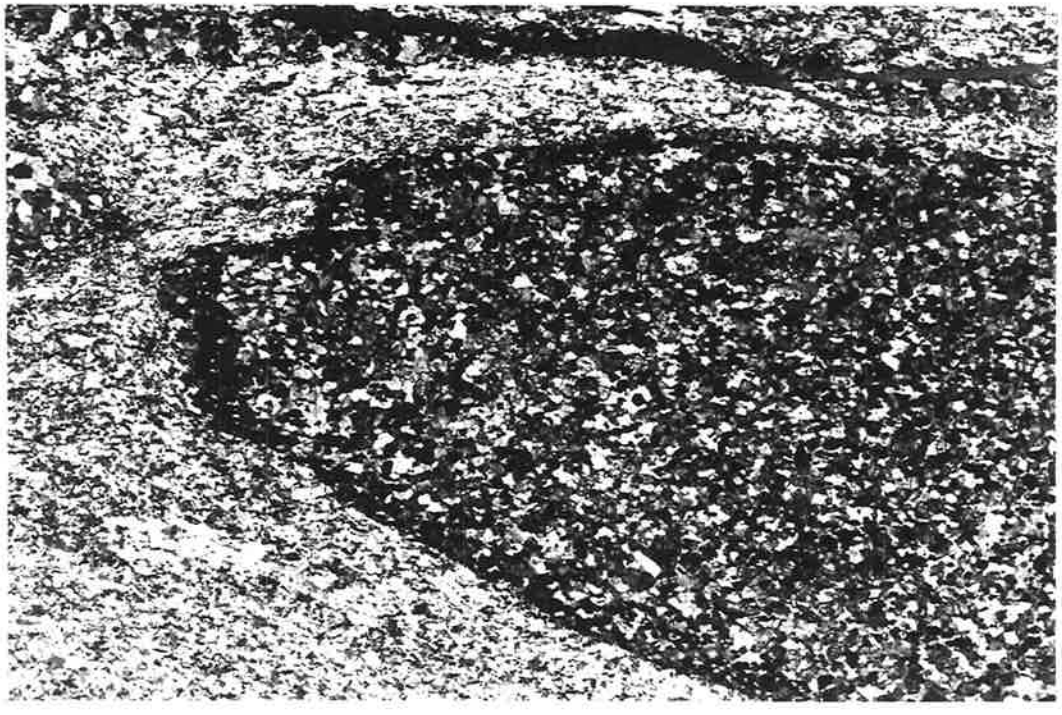

b

FIGURE 2.5

Sketches of typical mesoscopic folds from the granulite facies terrain.

A - pre gF_1 fold refolded by gF_1 fold
B,C,D,E,F - gF_1 folds
G,H,I - gF_2 folds

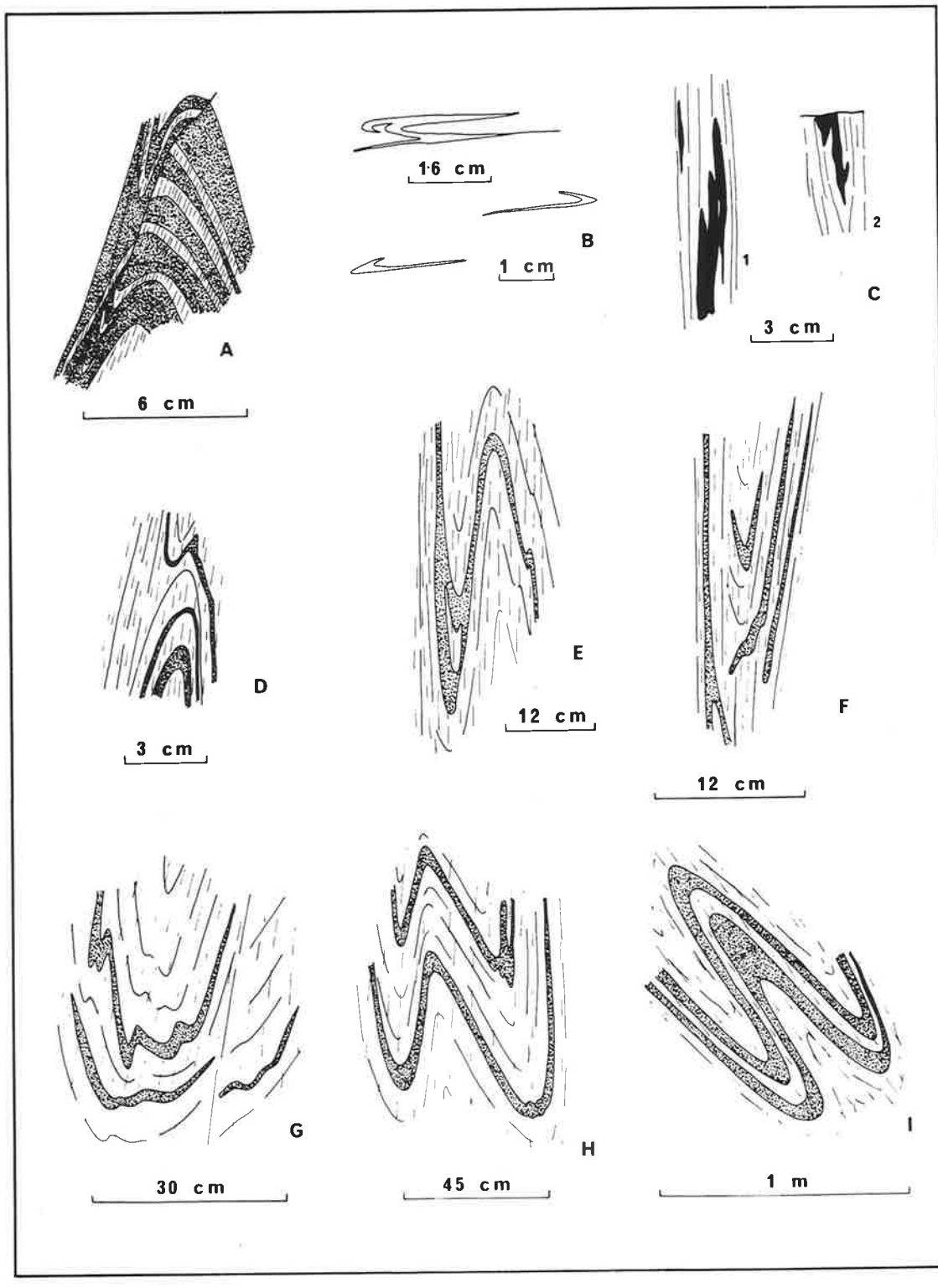
A
6 cm
1·6 cm
B
1 cm
1
2
C
3 cm
D
3 cm
E
12 cm
F
12 cm
G
30 cm
H
45 cm
I
1 m

FIGURE 2.6

(a) Rootless non-profile gF_1 folds in a garnetiferous quartzo-feldspathic granulite.

(b) Mesoscopic isoclinal gF_2(?) intrafolial fold in garnetiferous quartzo-feldspathic granulite folded by an open gF_3 fold. Axial plane schistosity gS_3 is weakly developed.

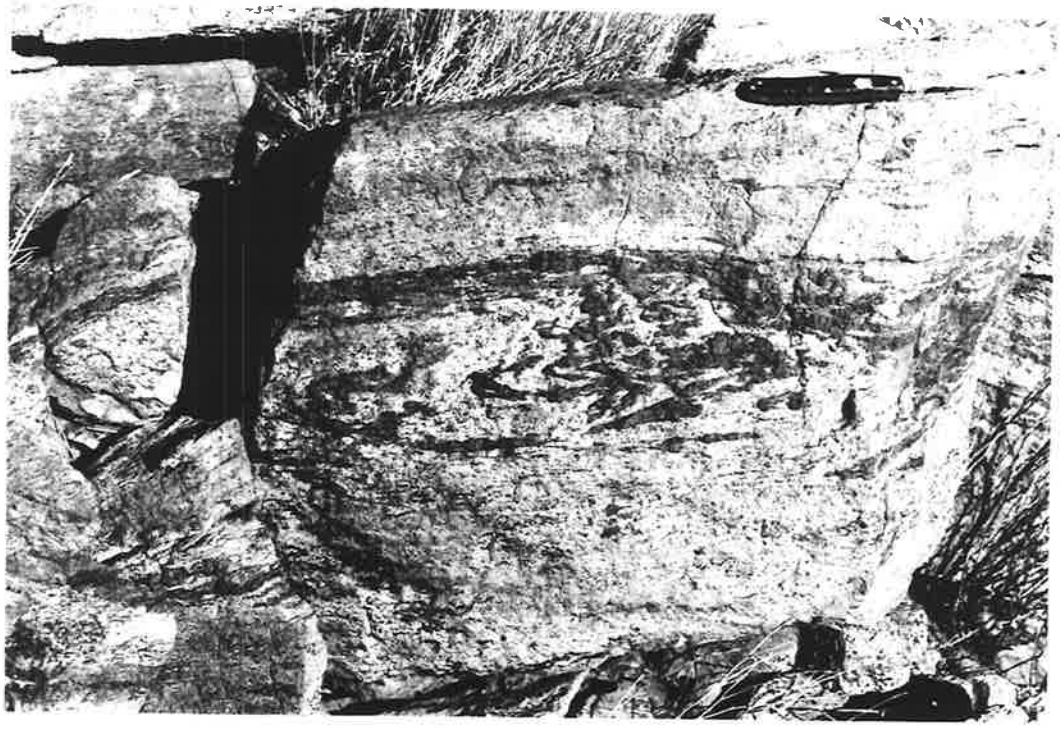

a

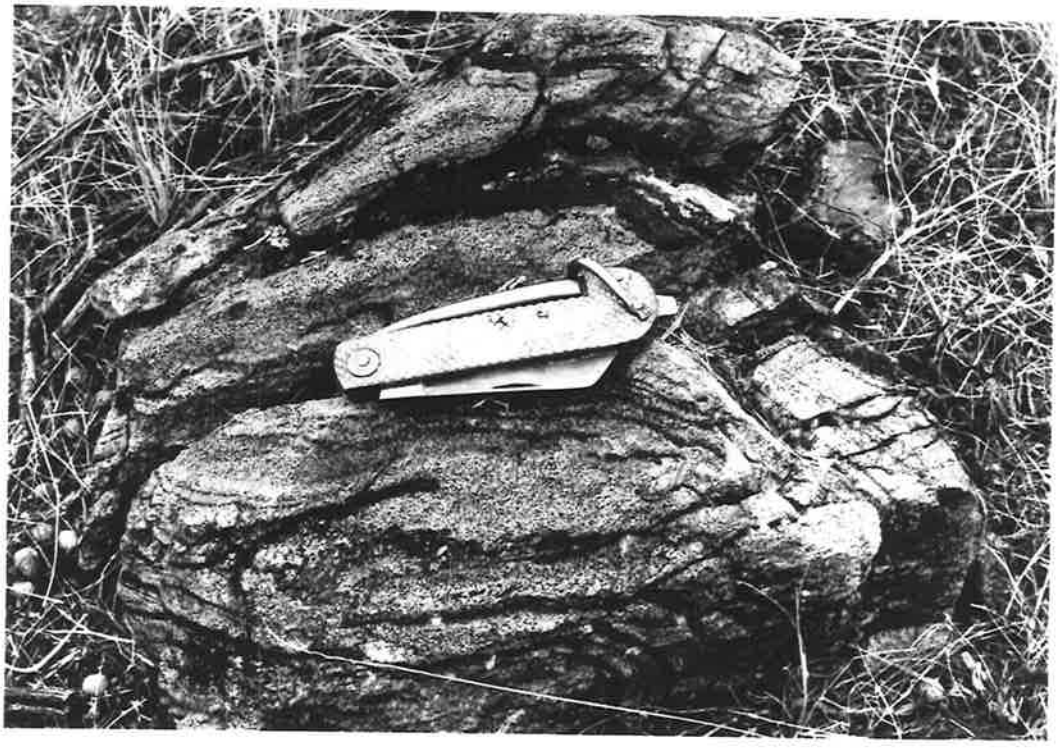

b

FIGURE 2.7

Lower hemisphere Schmidt net projections showing:

(a) Fold plunges and poles to axial planes in the granulite facies terrain.

Ornamentation:
- solid triangles - gF_1 fold axes
- open triangles - poles to gF_1 axial planes
- solid circles - gF_2 fold axes
- open circles - poles to gF_2 axial planes
- solid squares - gF_5 fold axes

(b) and (c) Fold plunges and poles to axial planes in the transitional terrain.

Ornamentation:
- solid triangles - tF_1 fold axes
- open triangles - poles to tF_1 axial planes
- solid circles - tF_2 fold axes
- open circles - poles to tF_2 axial planes
- open squares - tF_3 fold axes

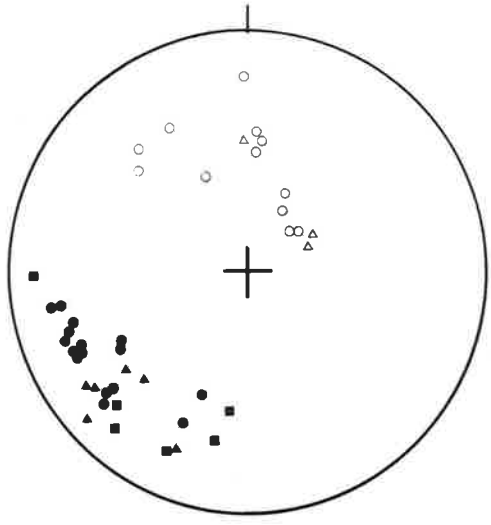

a

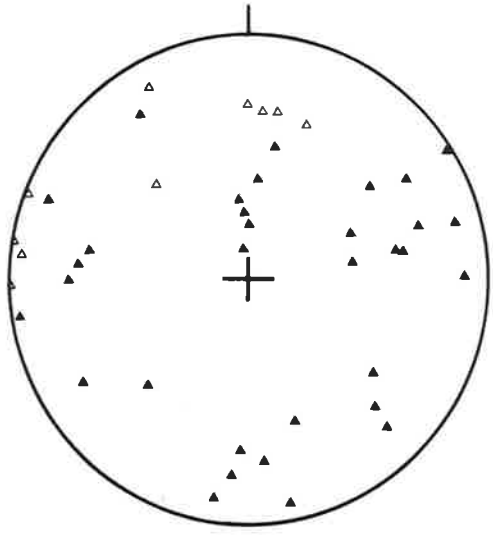

b

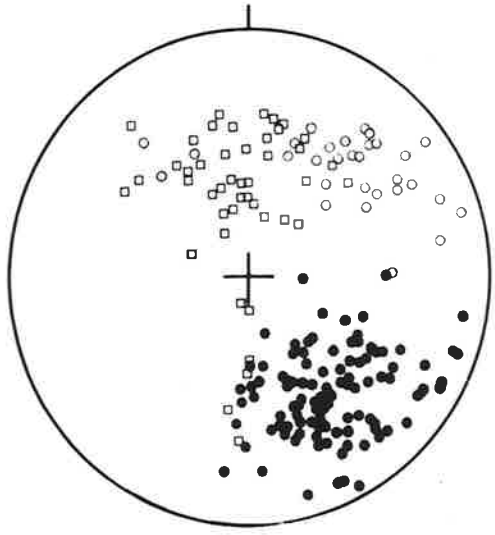

c

FIGURE 2.8

(a) Strongly developed gL_1 lineation in mafic granulite produced by the alignment of elongate xenoblastic grains of pyroxene and feldspar. The schistosity and layering are parallel to the photographed surface.

(b) Strongly developed gL_1 lineation in garnetiferous quartzo-feldspathic granulite. The schistosity and layering are parallel to the photographed surface.

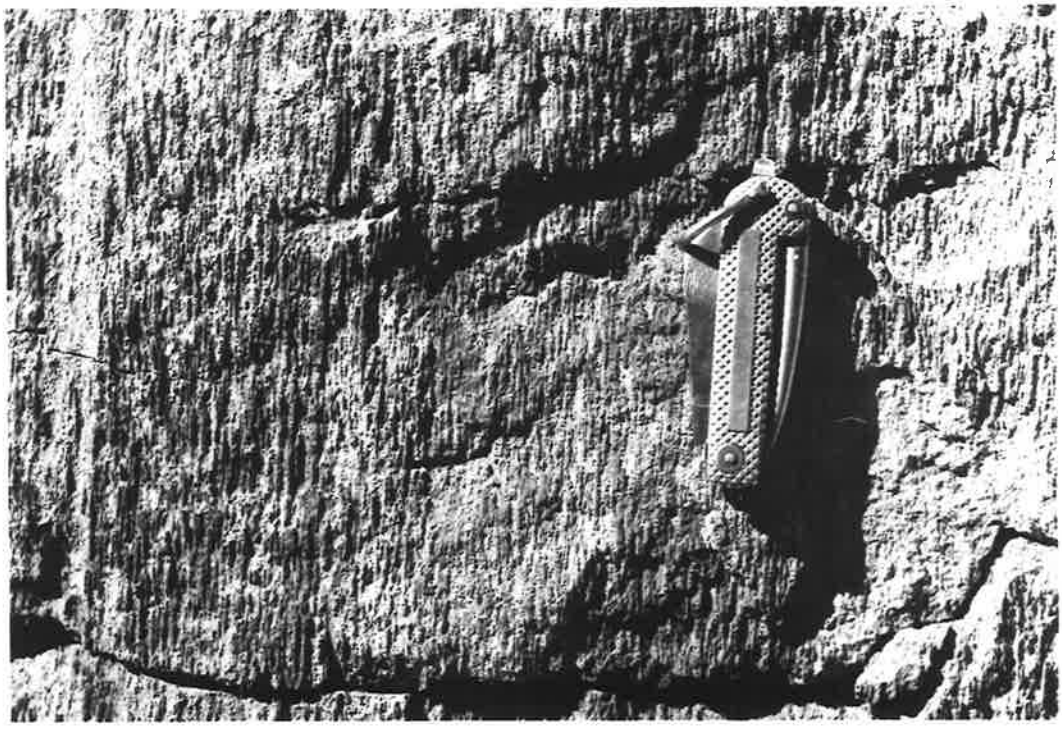

a

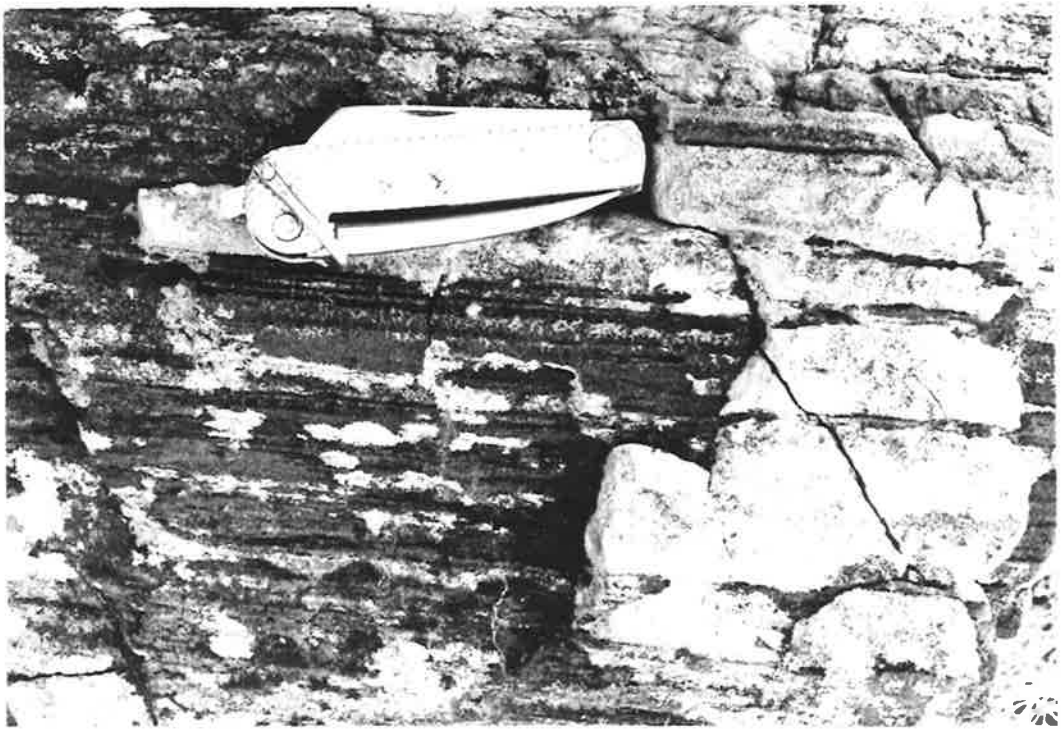

b

FIGURE 2.9

(a) Transposed gF_3 fold hinge zone. Note the steeply dipping layering on the right of the photograph. The layering in the foreground is dipping away from the viewer.

(b) Schmidt net lower hemisphere projection giving the orientation of gS_1 and gL_1 in the gF_3 fold shown in Figure 2.9a. Note the plunge of β towards the north-east.

Ornamentation:
- small solid circles - poles to gS_1 in hinge
- large solid circles - poles to gS_1 in the transposed limb
- small open circle - plunges to gL_1 lineations in the hinge
- large open circle - plunges of gL_1 lineation in the transposed limb.

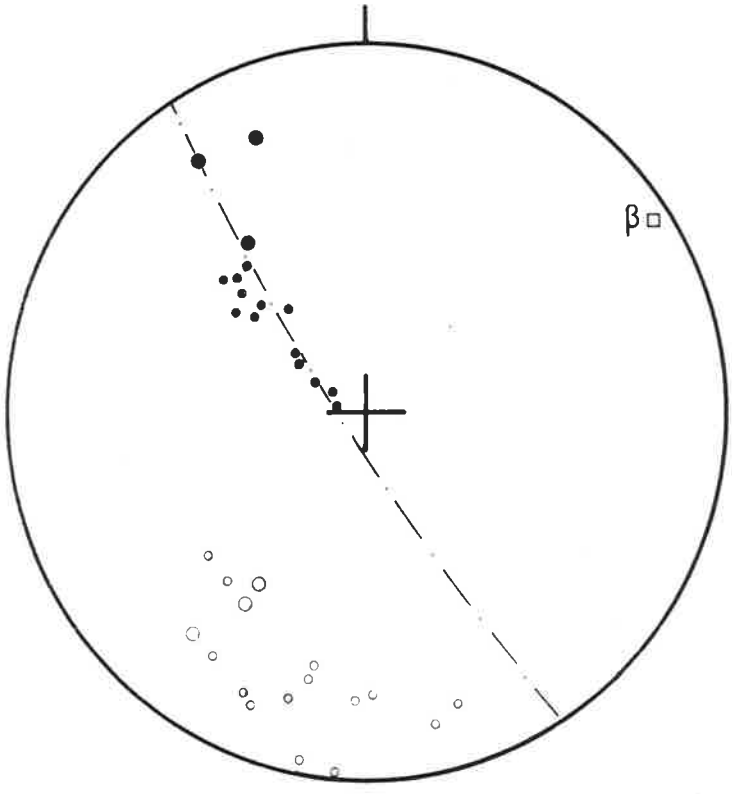

b

FIGURE 2.10

Schmidt net lower hemisphere projections showing the similarity in orientation of poles to schistosity and plunges of lineations in the dolerite dykes and fault zones.

(a) granulite facies terrain

(b) transitional terrain

(c) amphibolite facies terrain

Ornamentation:
- large closed circles - poles to schistosity in dykes (S_4)
- small closed circles - poles to mylonitic layering
- small open circles - plunges of mineral streaking lineation in fault zones (L_4)
- large open circles - plunges of mineral lineation in dykes (L_4)

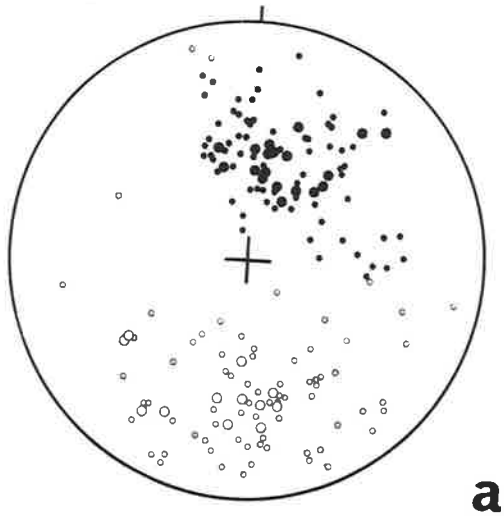

a

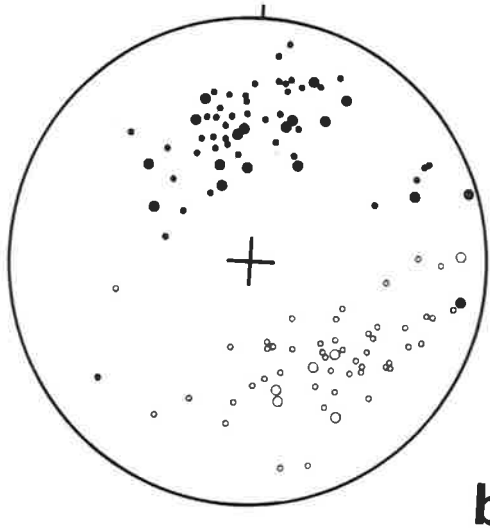

b

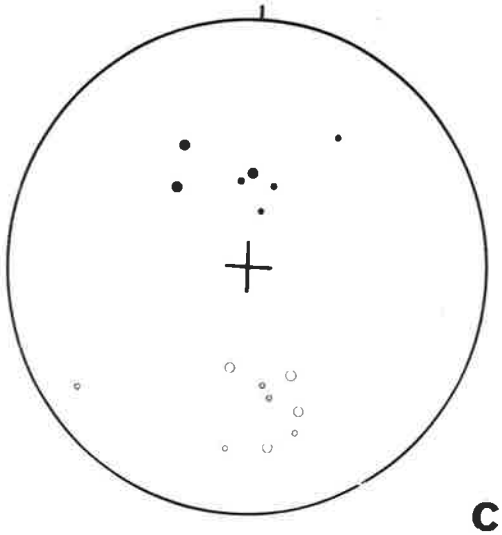

c

FIGURE 2.11

(a) Compositional layering and aS_1 schistosity in banded quartzo-feldspathic gneiss from the amphibolite facies terrain.

(b) Steeply dipping mafic interlayers in banded quartzo-feldspathic gneiss from the transitional terrain.

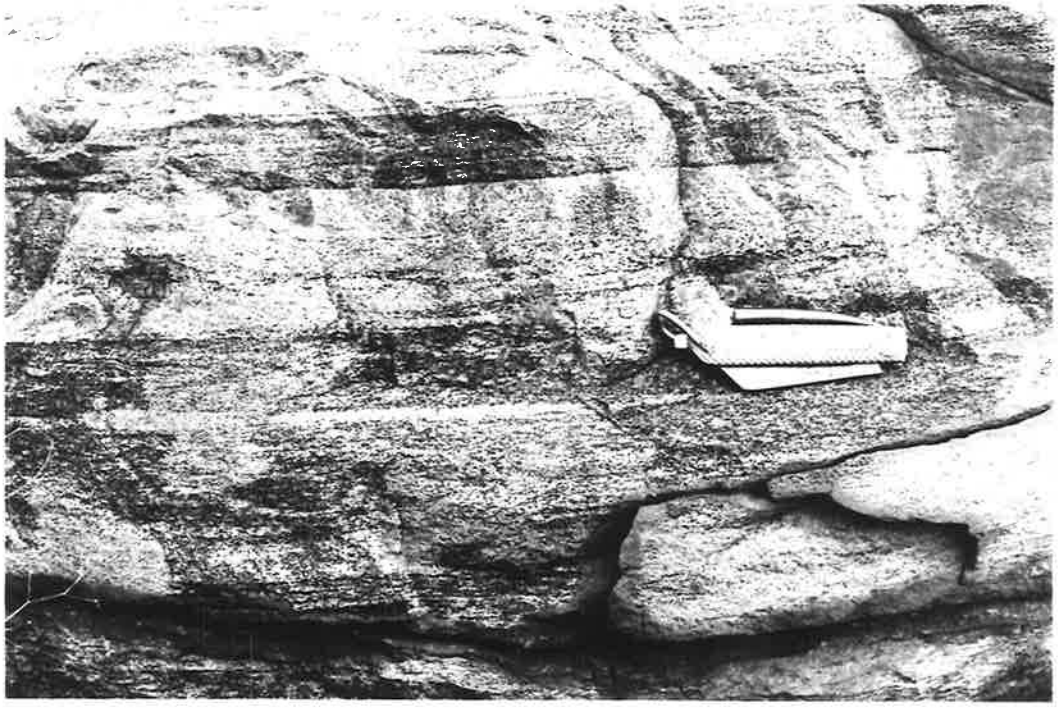

a

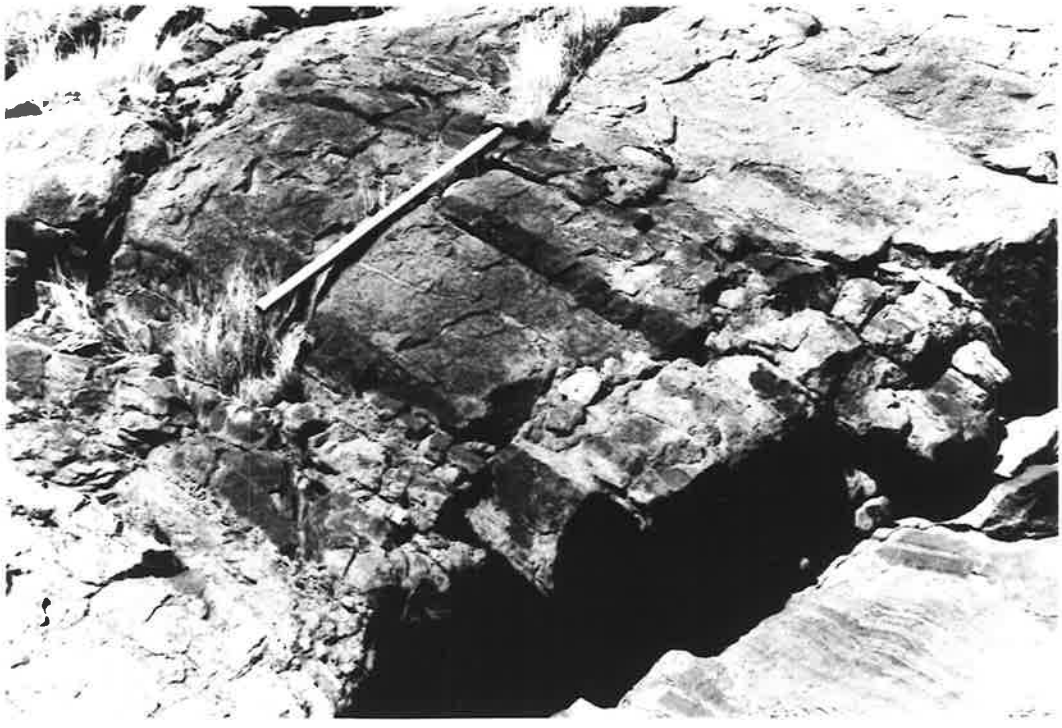

b

FIGURE 2.12

(a) Mesoscopic tF_1 intrafolial fold in garnet-bearing quartzo-feldspathic gneiss.

(b) Banded quartzo-feldspathic gneiss showing the nose of a mesoscopic tF_2 fold with refracted axial plane schistosity tS_2 (parallel to the white ink line) in layers of differing anisotropy.

a

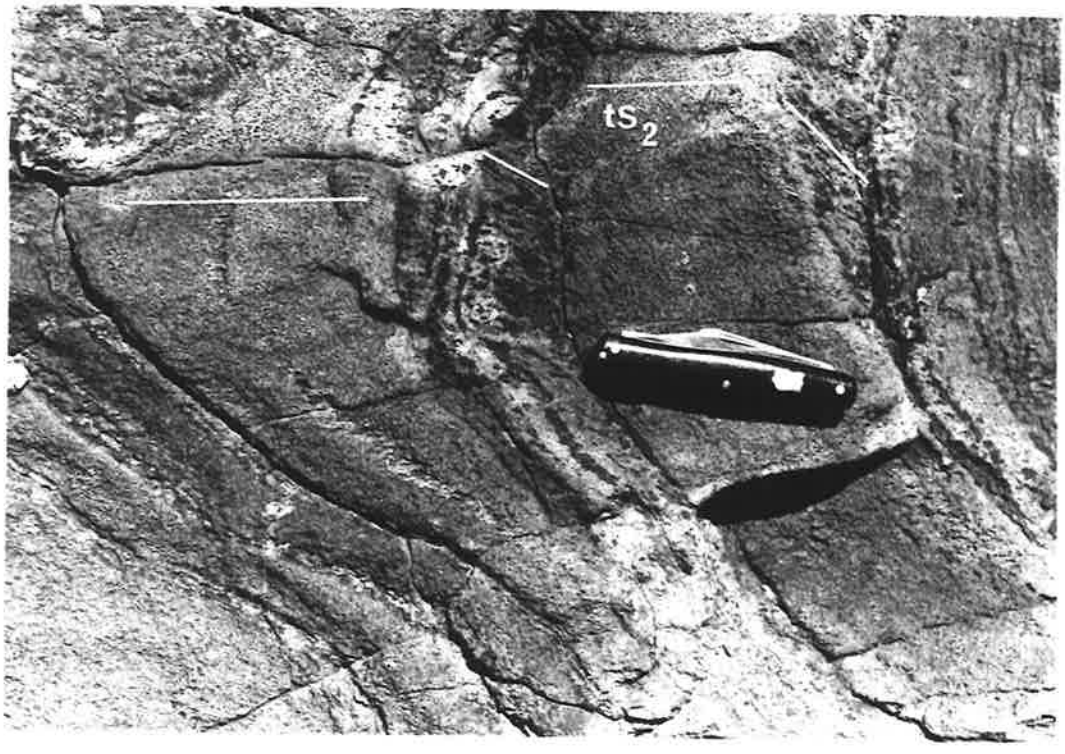

b

FIGURE 2.13

Sketches of typical mesoscopic folds from the transitional terrain.

A,B,C - tF_1 intrafolial folds
D,E,F,G,H - profiles of tF_2 folds
I,J,K,L - tF_3 folds

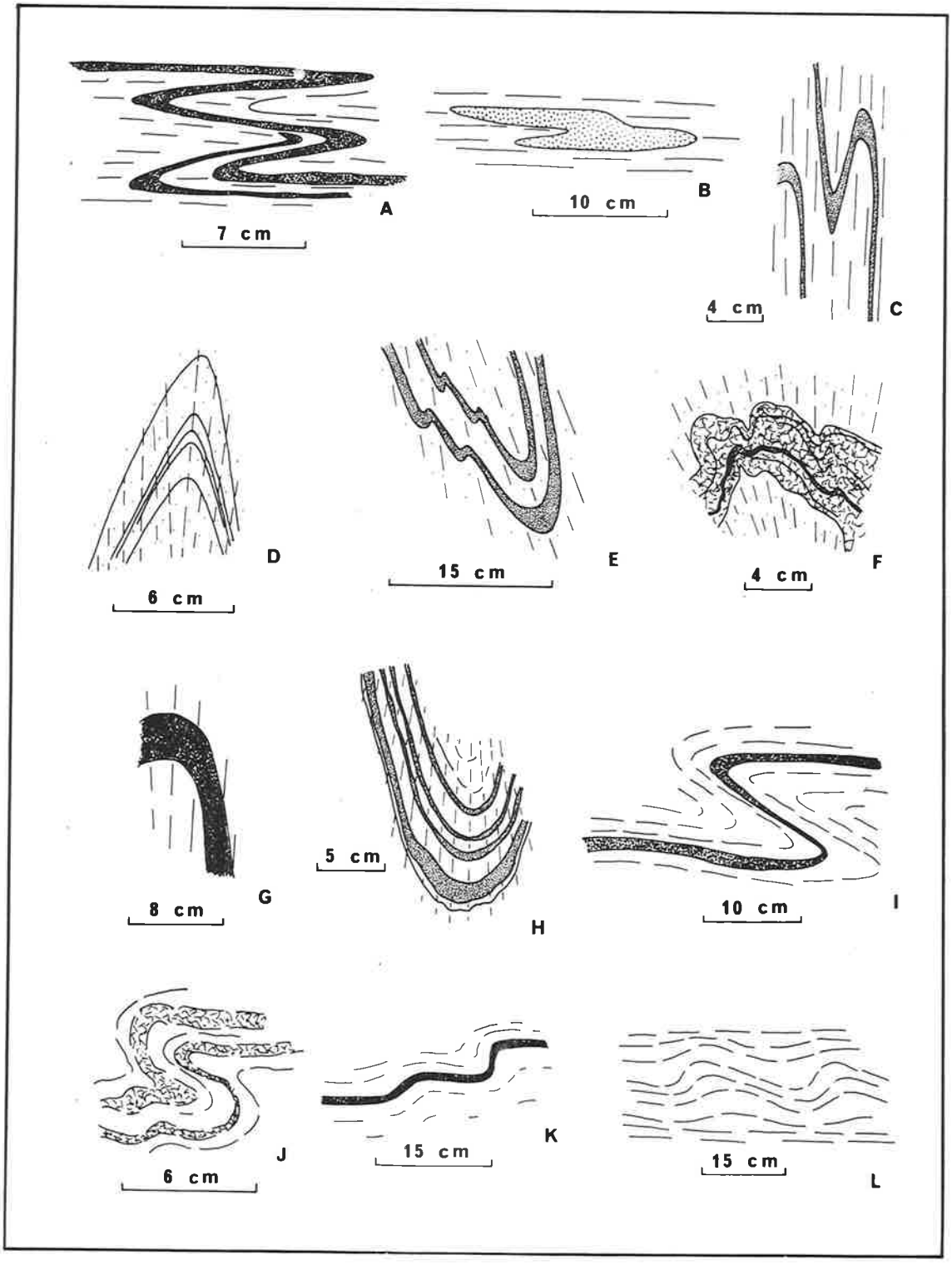
A
7 cm
B
10 cm
C
4 cm
D
6 cm
E
15 cm
F
4 cm
G
8 cm
H
5 cm
I
10 cm
J
6 cm
K
15 cm
L
15 cm

FIGURE 2.14

(a) Lower hemisphere Schmidt net projections showing poles to aF_2 (open circles) and aF_3 (open squares with dot) axial planes, aF_2 (solid circles) and aF_3 (open squares) fold axes, and the β orientation of a macroscopic aF_5 fold axis (solid square).

(b) Lower hemisphere Schmidt net projections showing the orientation of pre-tL_2 lineations.

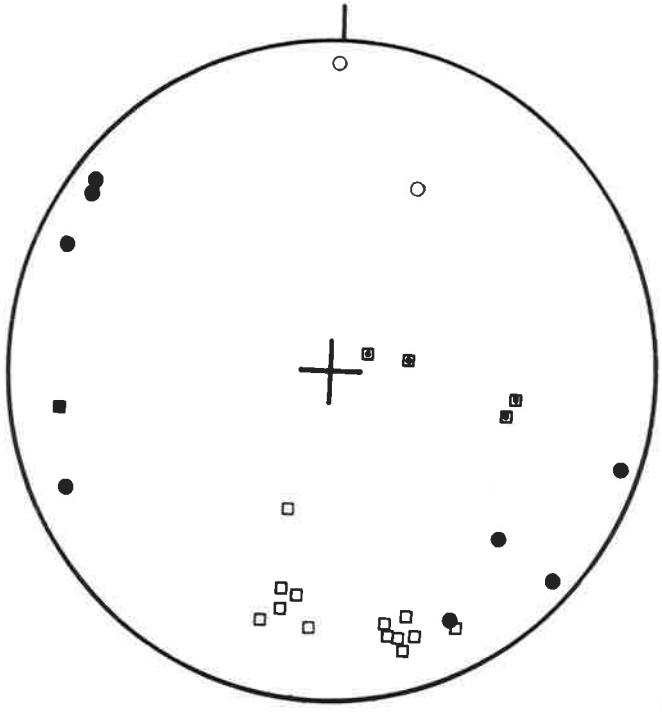

a

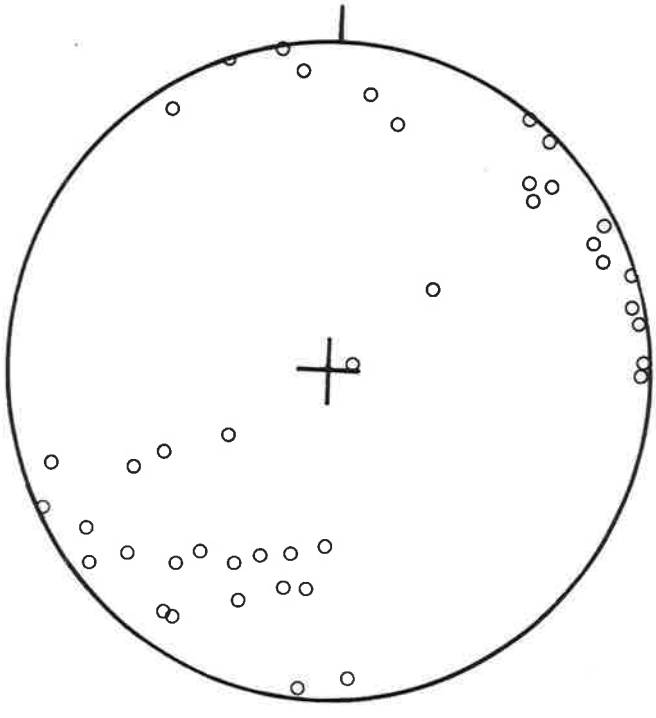

b

FIGURE 2.15

(a) Mesoscopic tF_2 fold in mafic and quartzo-feldspathic lithologies. Note the thickening of the nose and the inclined axial plane.

(b) Non-profile view of mesoscopic aF_2 fold in banded quartzo-feldspathic gneiss.

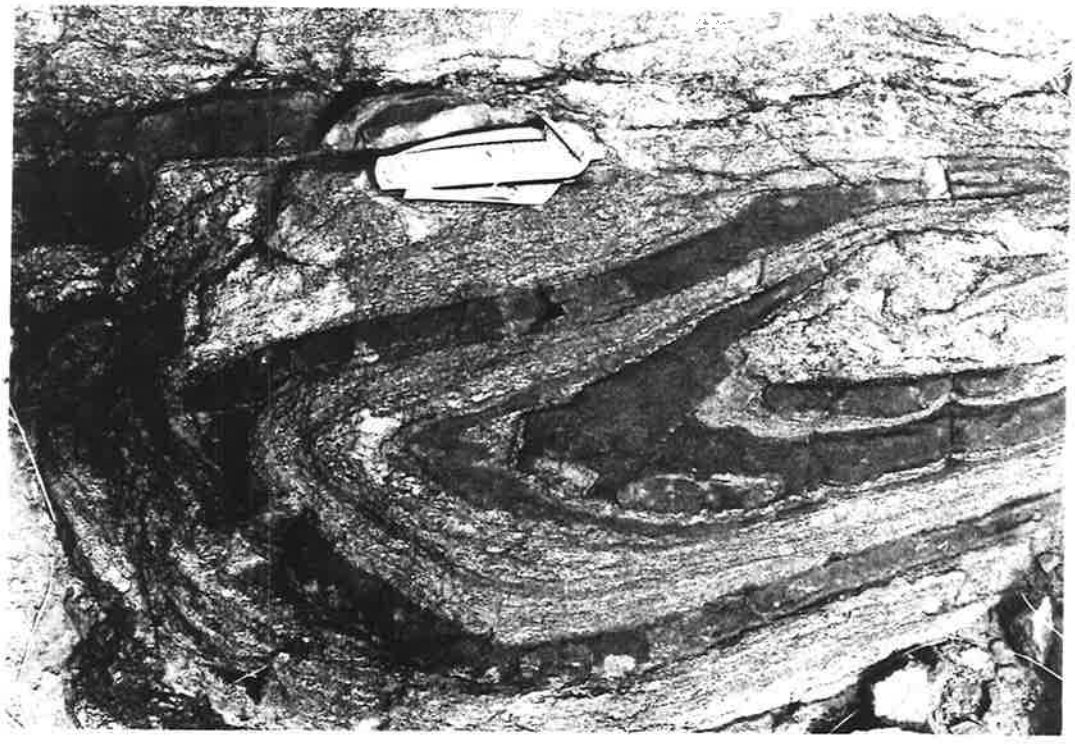

a

b

FIGURE 2.16

(a) Hinge region of a small mesoscopic tF_2 fold in mafic and quartzo-feldspathic lithologies showing the strongly developed tS_2 axial plane schistosity in the quartzo-feldspathic gneiss and the more isotropic nature of the mafic unit.

A325-669
Width of field: 4 cm.
Crossed polars.

(b) Mesoscopic tF_2 fold in quartzo-feldspathic vein through mafic lithology. Note the strongly developed tS_2 axial plane schistosity in the quartzo-feldspathic vein.

A325-850
Width of field: 7 cm.
Crossed polars.

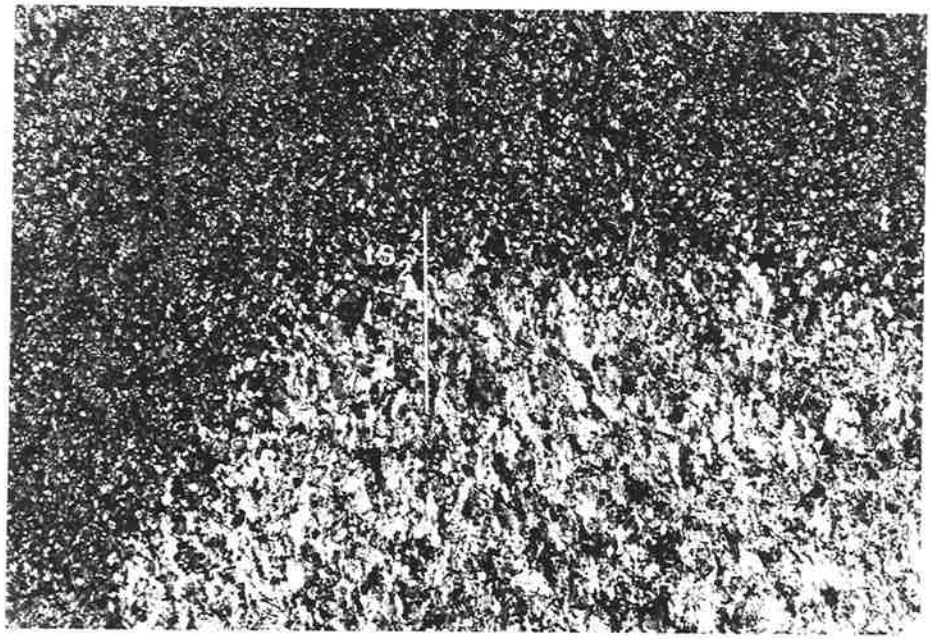

a

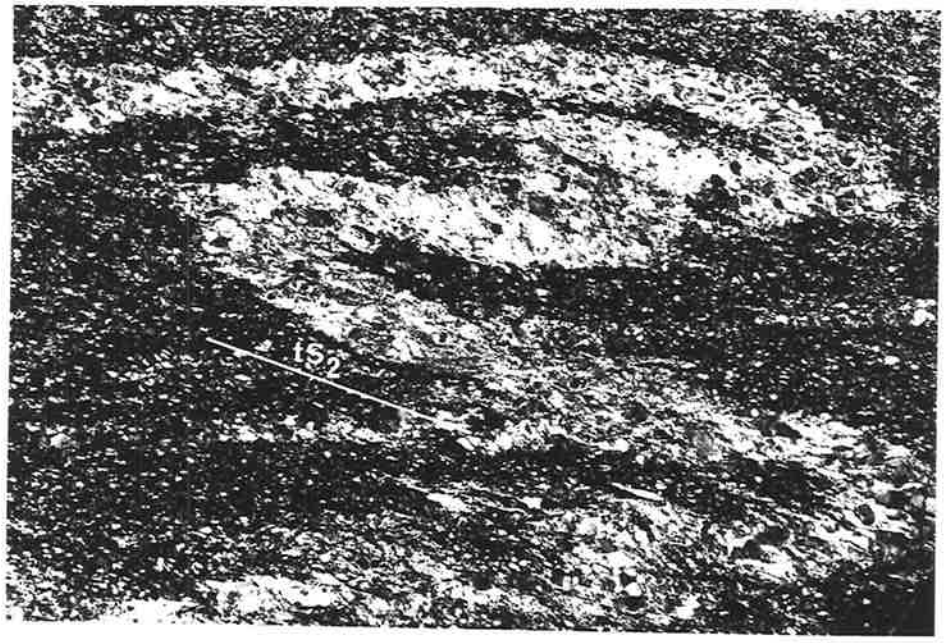

b

FIGURE 2.17

(a) Quartzo-feldspathic gneiss with well developed tL_2 lineation defined by the alignment of prismatic clusters of quartz and feldspar. The schistosity and layering are parallel to the photographed surface.

(b) Schistosity surface showing refolding of the tL_2 lineation by tF_3 corrugations.

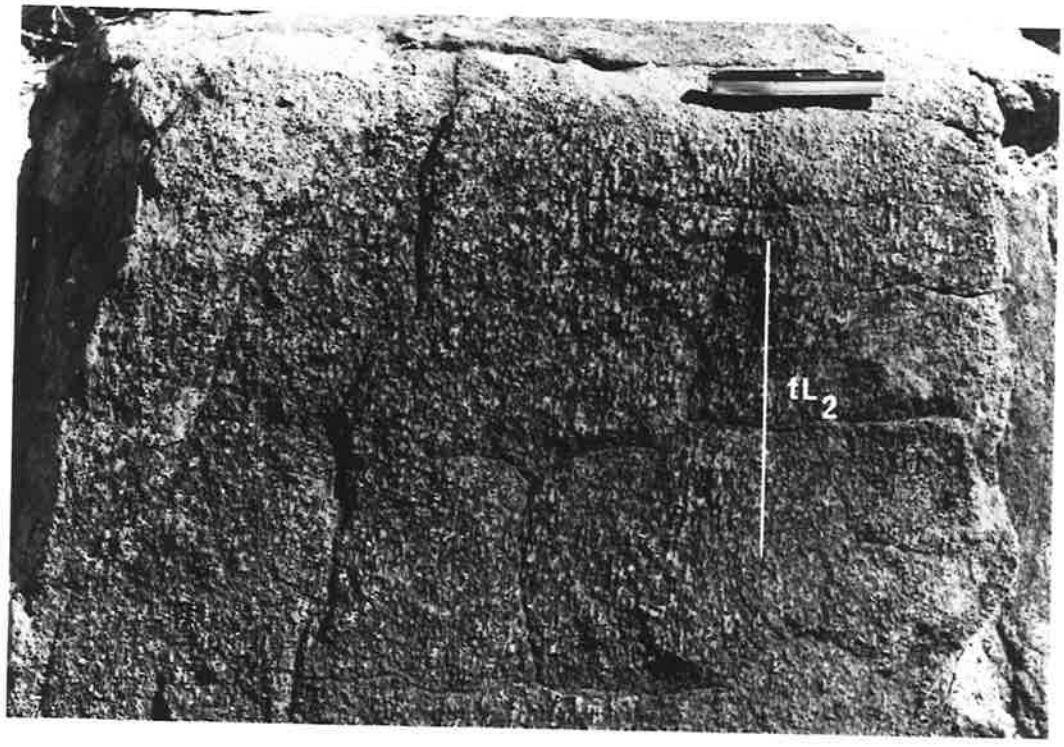

a

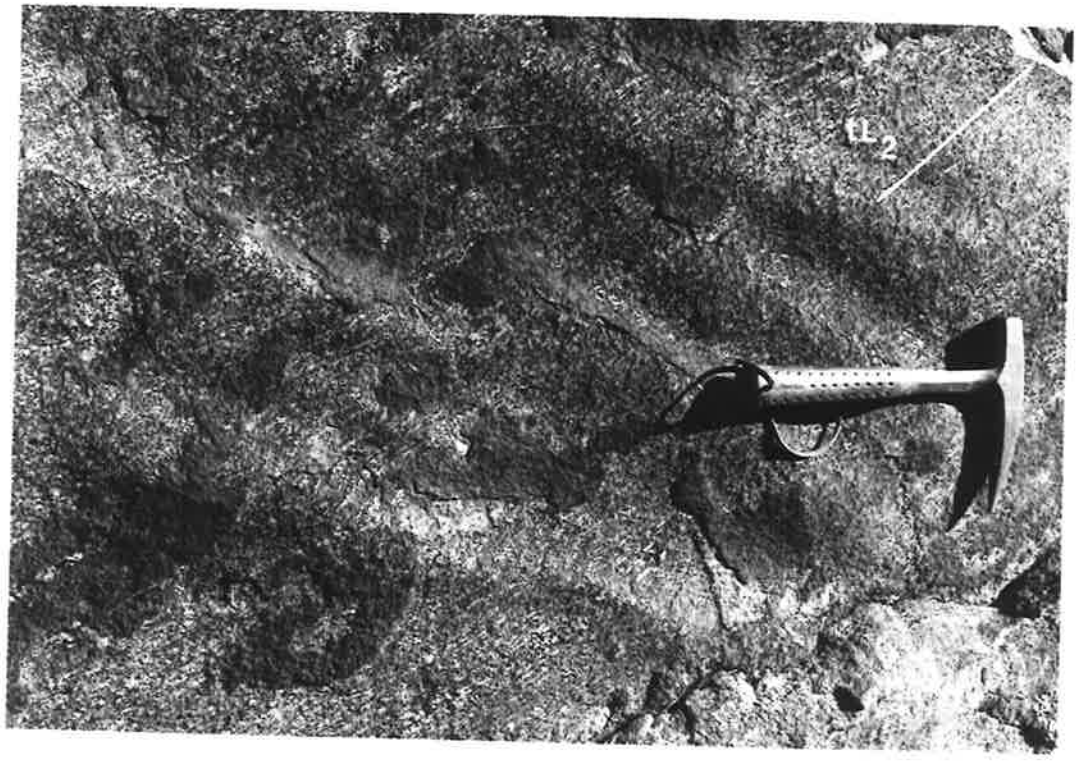

b

FIGURE 2.18

Schmidt net lower hemisphere projections showing:

(a) the orientation of the layering/schistosity (solid circles), the streaking lineation (open circles) and the plunges of mesoscopic fold axes (solid squares) in the Davenport Shear zone.

(b) the effect of the Davenport shear on the orientation of gS_1 and gL_1 near station 2053.

(1) 30 metres from shear;
(2) 1.2 metres from shear;
(3) 1 metre from shear;
(4) 90 centimetres from shear;
(5) 30 centimetres from shear.

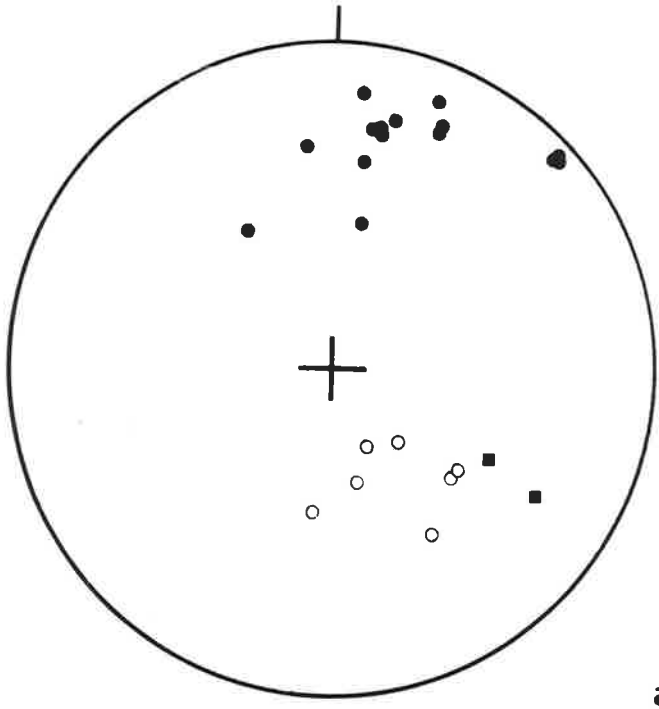

a

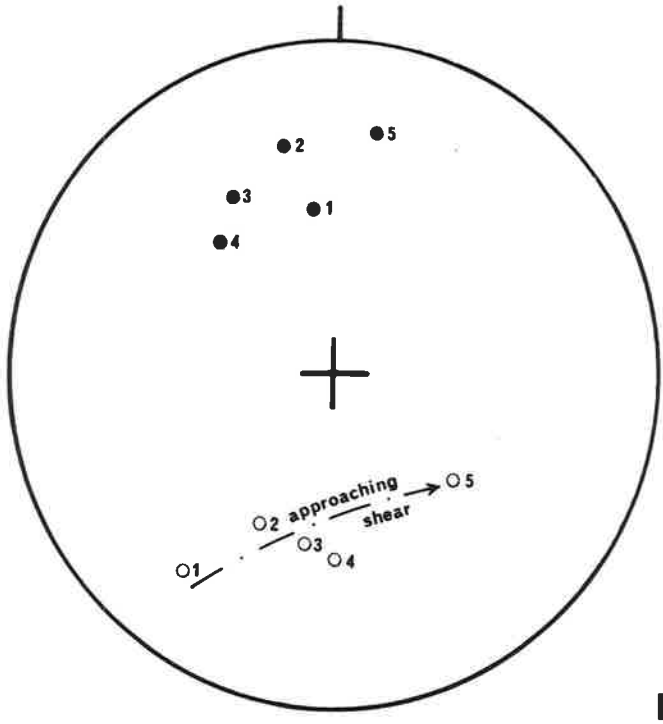

b

FIGURE 2.19

(a) View towards the east south east from north of Amata, showing the abrupt escarpment of the Woodroffe Thrust and the gently dipping layered granulites above the thrust.

(b) Typical outcrop pattern of the massive quartzo-feldspathic gneisses in the transitional terrain south of Amata.

a

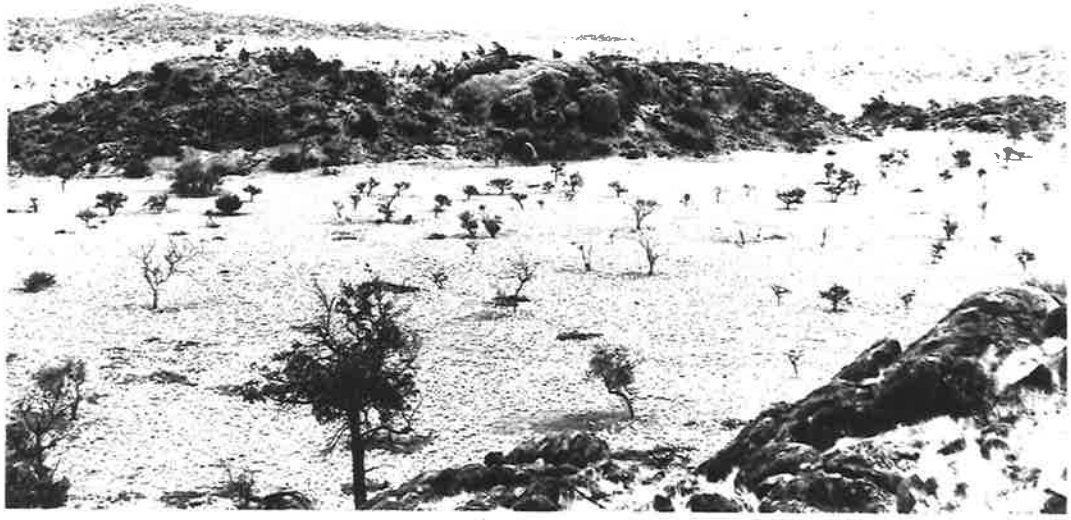

b

FIGURE 3.1

Diagram showing the orientation of thin sections with respect to the main linear feature in the rocks.

FIGURE 3.2

Classification of grain boundary shapes, taken from Spry (1969)
Figure 1

a straight
b curved
c embayed
d scalloped, cuspate
e sutured: (1) lobate
(2) serrated
f rational unilateral
g rational bilateral

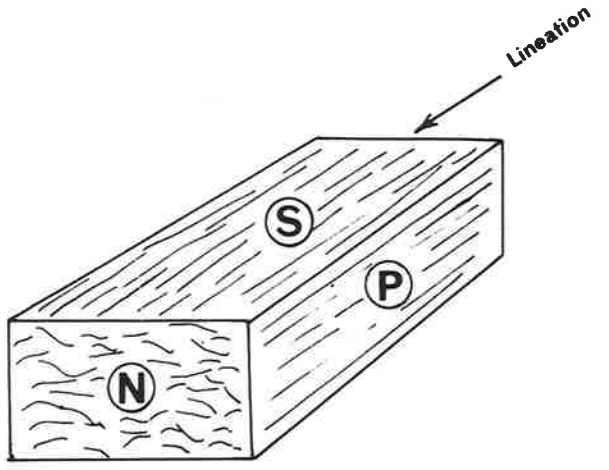
Lineation
S
P
N

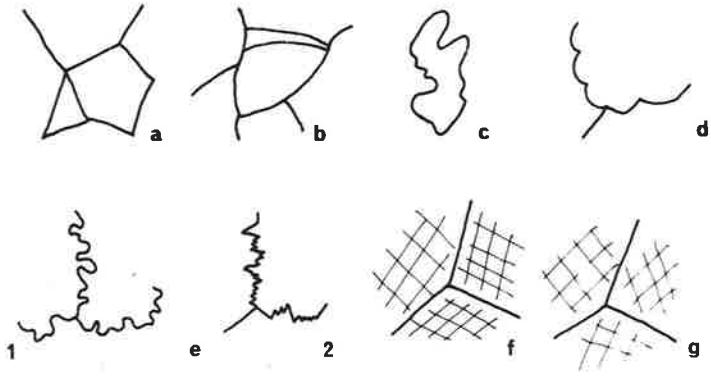
a
b
c
d
1
e
2
f
g

FIGURE 3.3

(a) Mafic granulite with xenoblastic inequigranular to equigranular microstructure defined by grains with straight or gently curved boundaries.
A325-1117aN
Plane polarized light
Width of field: 6 mm.

(b) Intercalated compositional bands of elongate xenoblastic ferromagnesian and felsic grains in mafic granulite.
A325-2000P
Plane polarized light
Width of field: 6 mm.

(c) Mafic granulite composed of straight sided or gently curved grains defining an equigranular granoblastic microstructure. Note the coronas around the orthopyroxene grain.
A325-949bN
Plane polarized light.
Width of field: 2 mm.

(d) Garnetiferous quartzo-feldspathic granulite with platy aggregates of margarite pseudomorphing basal sections of sillimanite.
A325-927
Plane polarized light
Width of field: 0.6 mm.

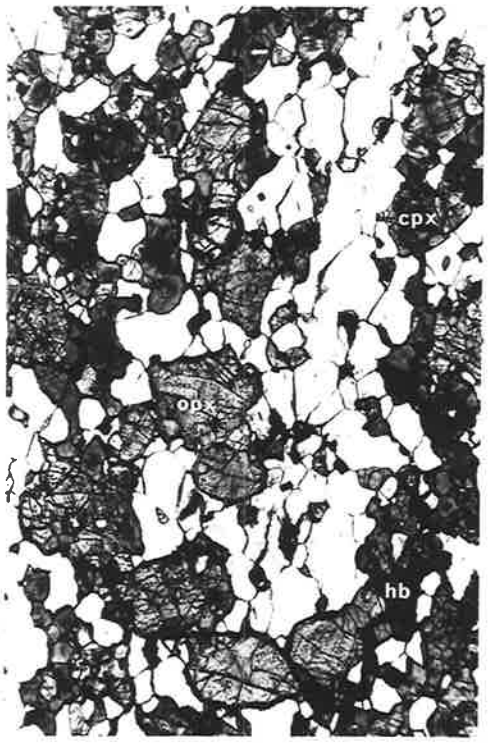

a

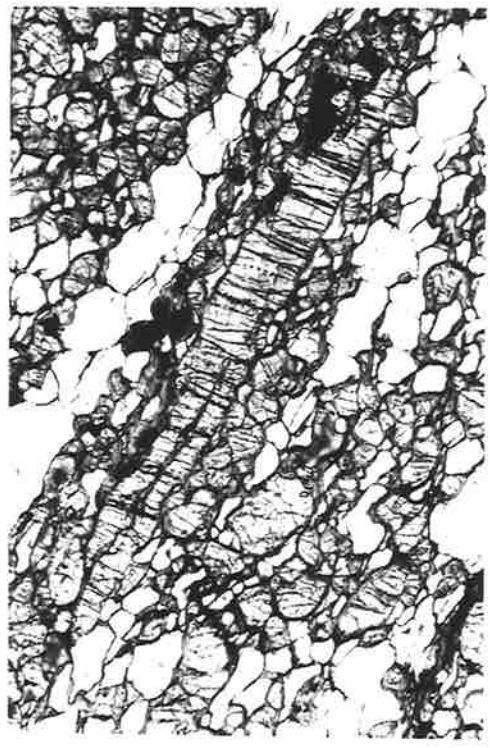

b

c

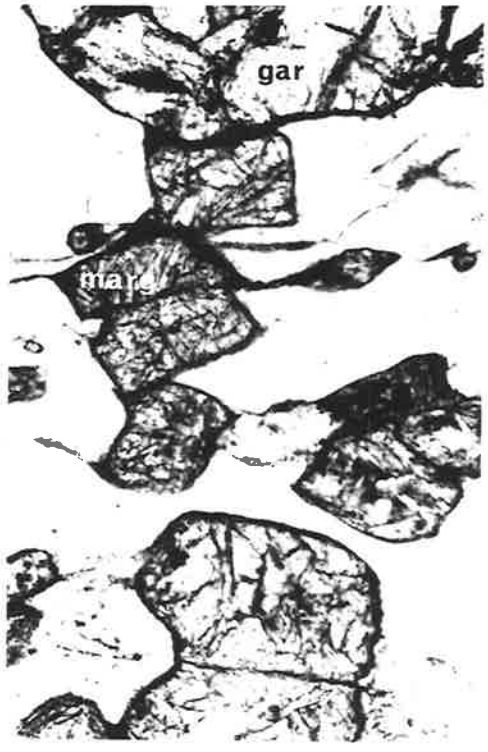

d

FIGURE 3.4

(a) Garnetiferous mafic granulite with inequigranular granoblastic microstructure. Fine stipple, clinopyroxene; heavy stipple, garnet; moderate stipple, orthopyroxene.
A325-1115aN
Length of bar: 1 mm.

(b) Xenoblastic grains of ferromagnesian and felsic phases showing straight or gently rounded interfaces with adjacent grains.
Dense stipple, hornblende.
A325-1117aN
Lenght of bar: 1 mm.

(c) Mafic granulite with inequigranular granoblastic microstructure. Note the development of coronas around orthopyroxene.
A325-953bN
Length of bar: 1 mm.

a

b

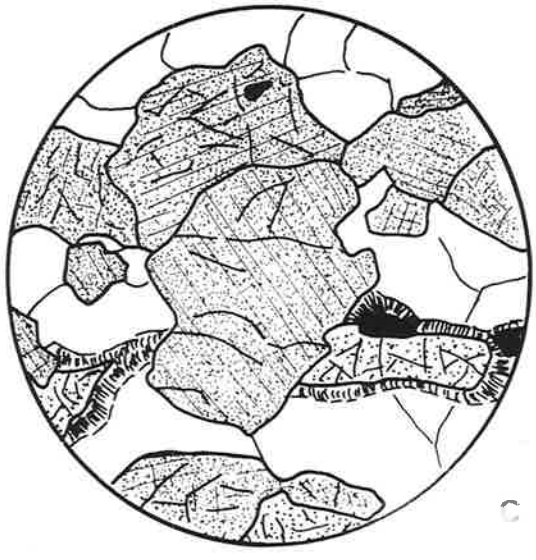

FIGURE 3.5

(a) Ribbon-type exsolution in mesoperthite from quartzo-feldspathic granulite.
A325-138P
Crossed polars
Width of field: 0.6 mm.

(b) Kink bands in plagioclase from mafic granulite developed normal to glide lamellae. Note the gentle bending of some of the lamellae.
A325-1207P
Crossed polars
Width of field: 0.6 mm.

(c) Mechanical twinning on both albite and pericline laws in a plagioclase grain.
A325-2074
Crossed polars
Width of field: 0.6 mm.

(d) Mechanical twinning in plagioclase from mafic transitional terrain lithology. Note the wedging of the twin lamellae.
A325-1353
Crossed polars
Width of field: 0.6 mm.

a

b

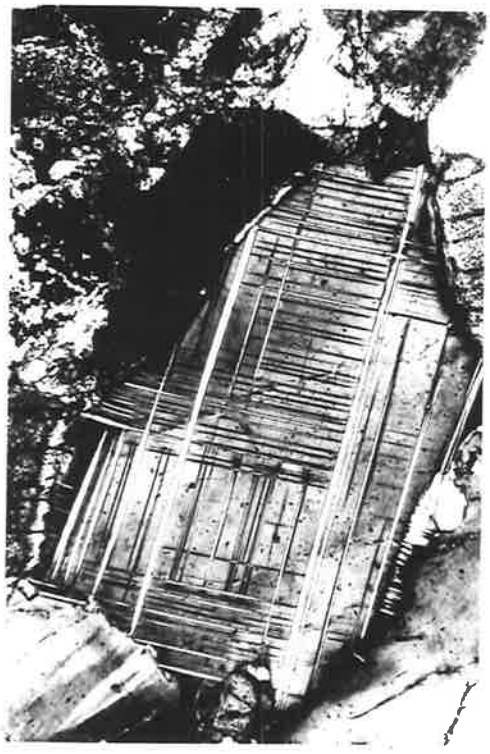

c

d

FIGURE 3.6

(a) Typical microstructural appearance of deformed quartzite from granulite terrain. Note the highly strained wavey lenticles of quartz and fine grained marginal recrystallization zones.
A325-140
Crossed polars
Width of field: 2.0 mm.

(b) Quartzo-feldspathic granulite with elongate tabular lenticles of quartz wrapping around garnet porphyroblast.
A325-1175P
Crossed polars
Width of field: 3.8 cm.

(c) Well developed exsolution lamellae of orthopyroxene in host grain of clinopyroxene.
A325-1761P
Crossed polars
Width of field: 0.6 mm.

(d) Ascicular needles of rutile in orthopyroxene from ultramafic granulite.
A325-2050c
Plane polarized light
Width of field: 0.25 mm.

a

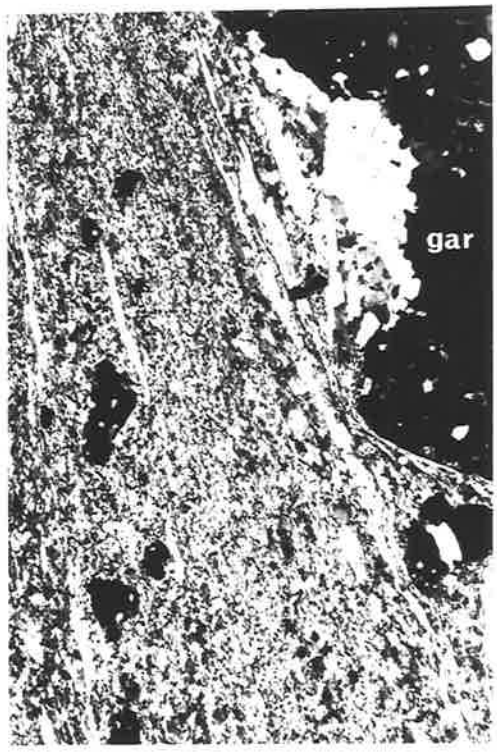

b

c

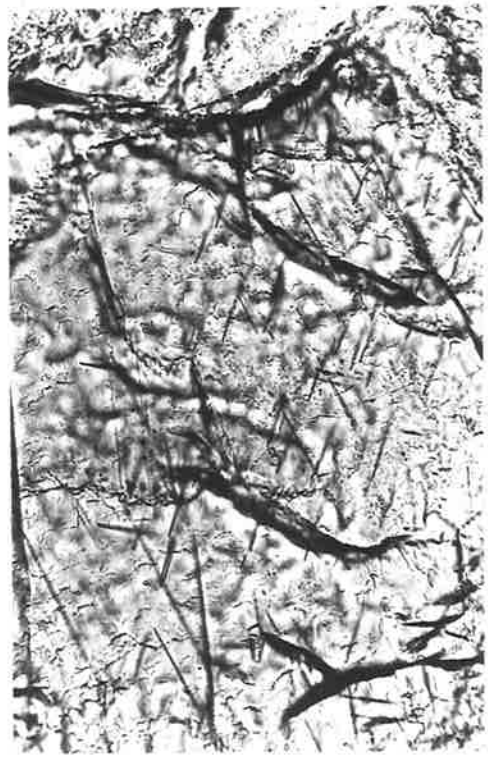

d

FIGURE 3.7

(a) Coronas of clinopyroxene and secondary amphibole around orthopyroxene.
A325-949bN
Plane polarized light
Width of field: 0.6 mm.

(b) Corona of garnet and clinopyroxene around orthopyroxene, and garnet around opaque oxides. Note the needle-like inclusions in the plagioclase.
A325-953bN
Plane polarized light
Width of field: 1.4 mm.

(c) Corona of garnet around orthopyroxene. Note the absence of coronal development around clinopyroxene and the turbid nature of the clinopyroxene due to the presence of opaque inclusions.
A325-953bN
Plane polarized light
Width of field: 1.4 mm.

(d) Fine lamellar twinning and kink bands in orthopyroxene.
A325-952N
Crossed polars
Width of field: 0.6 mm.

a

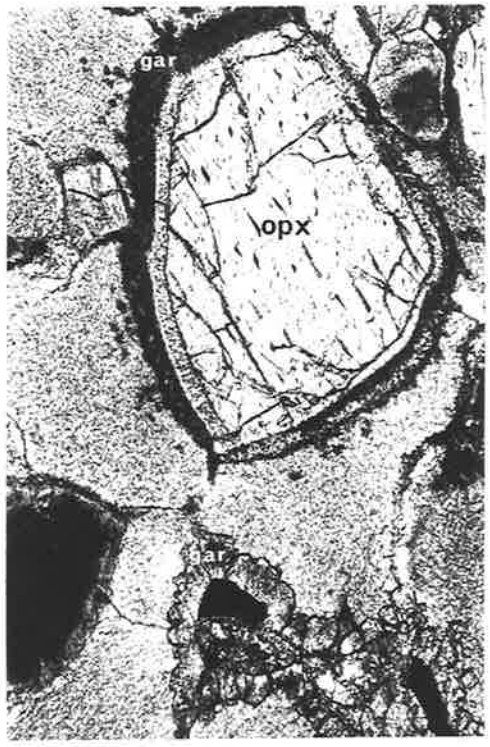

b

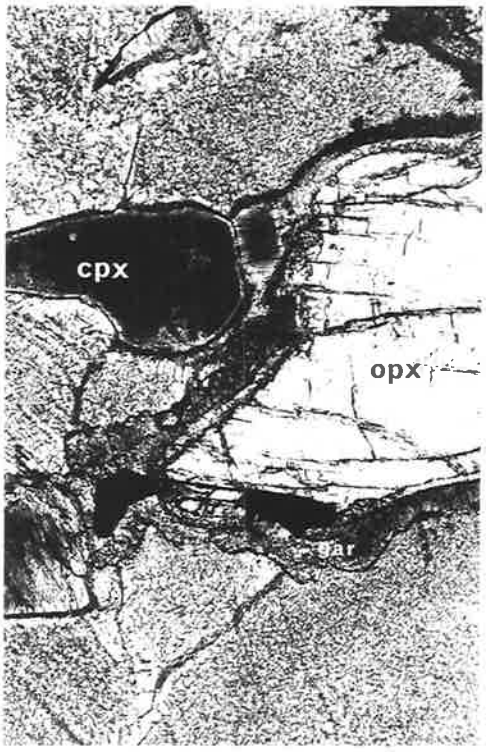

c

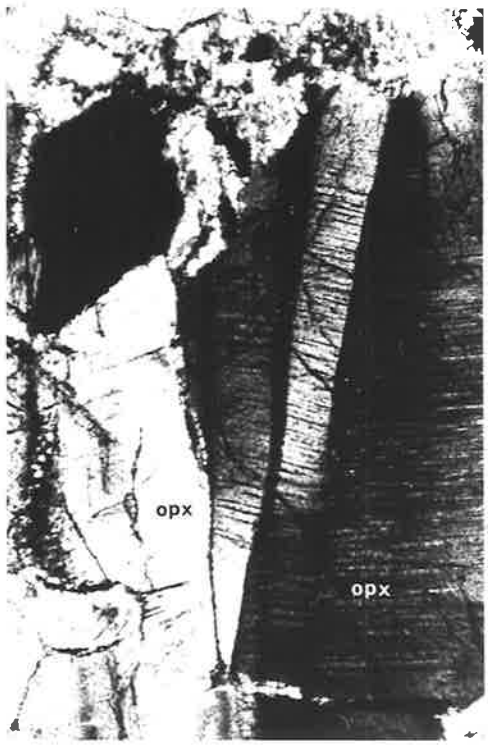

d

FIGURE 3.8

(a) Ultramafic granulite with straight or gently curved grain boundaries. Irregular xenoblastic intergrowths of clinopyroxene are present in the orthopyroxene.
A325-2050c
Length of bar: 1 mm.

(b) Mafic granulite with xenoblastic inequigranular microstructure. Some of the orthopyroxene boundaries are embayed.
A325-1152P
Length of bar: 1 mm.

(c) Ultramafic granulite with microstructure dominated by the presence of xenoblastic pyroxene grains (with gently curved boundaries) which form inequigranular or equigranular aggregates.
A325-952N
Length of bar: 1 mm.

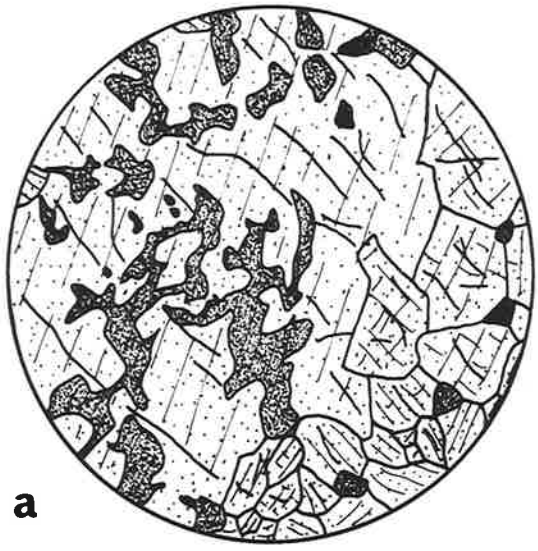

a

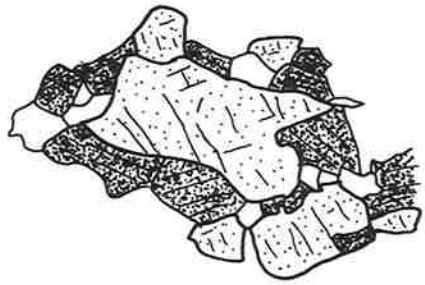

b

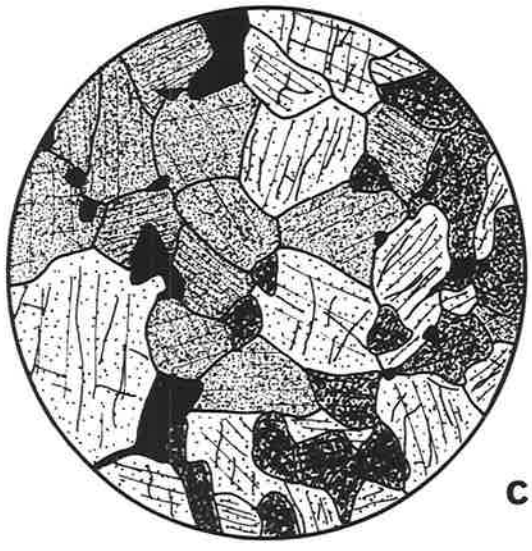

c

FIGURE 3.9

(a) Quartzo-feldspathic granulite with equigranular to platey inequigranular granoblastic microstructure.
A325-126bP
Crossed polars
Width of field: 3.8 cm.

(b) Quartzo-feldspathic granulite with equigranular to slightly inequigranular granoblastic microstructure.
A325-126bN
Crossed polars
Width of field: 3.8 cm.

(c) Quartzo-feldspathic granulite with variable microstructure, interbanded platey inequigranular and equigranular granoblastic.
A325-1110bP
Crossed polars
Width of field: 3.8 cm.

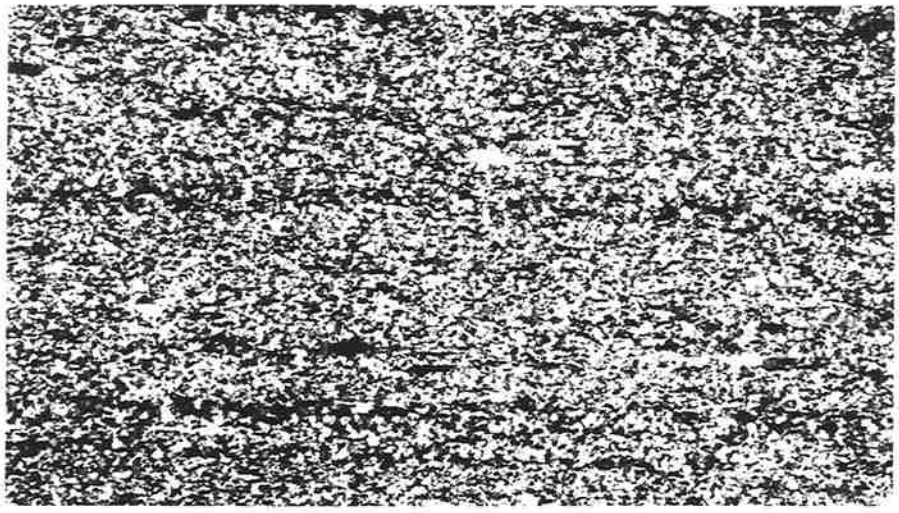

a

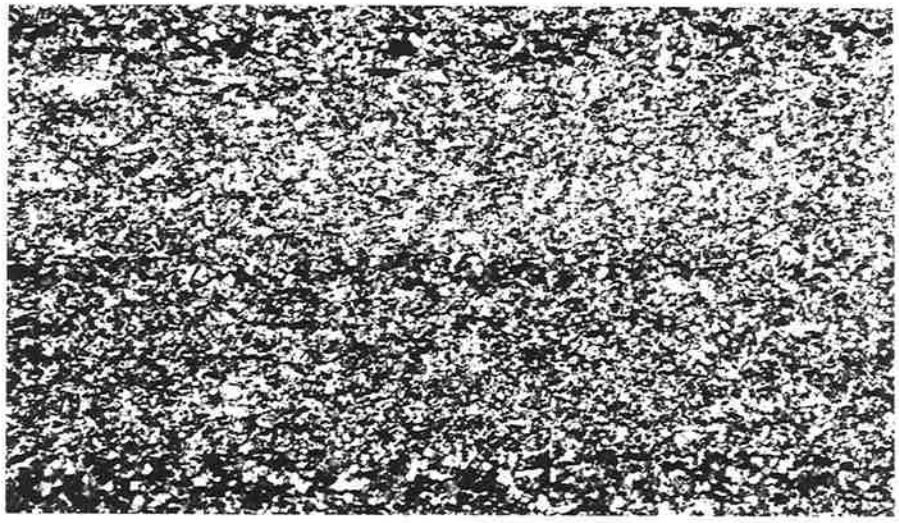

b

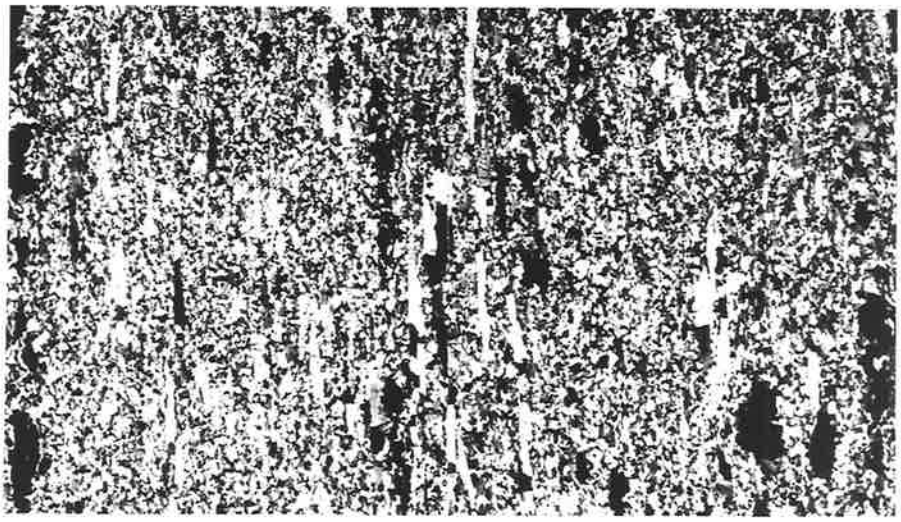

c

FIGURE 3.10

(a) Garnetiferous quartzo-feldspathic granulite with elongate tabular aggregates of quartz and feldspar, and xenoblastic porphyroblasts.
A325-1144P
Crossed polars
Width of field: 3.8 cm.

(b) Quartzo-feldspathic granulite with well developed platey granoblastic microstructure.
A325-928gP
Crossed polars
Width of field: 3.8 cm.

(c) Quartzo-feldspathic granulite with lozenge shaped granoblastic aggregate of feldspar in a platey granoblastic to granoblastic groundmass. Note the slightly anastomosing nature of the groundmass.
A325-928jP
Crossed polars
Width of field: 3.8 cm.

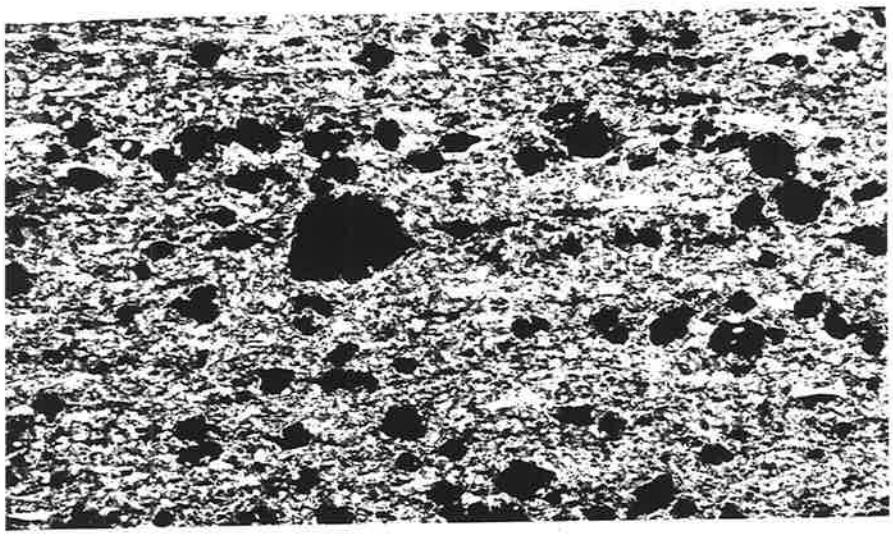

a

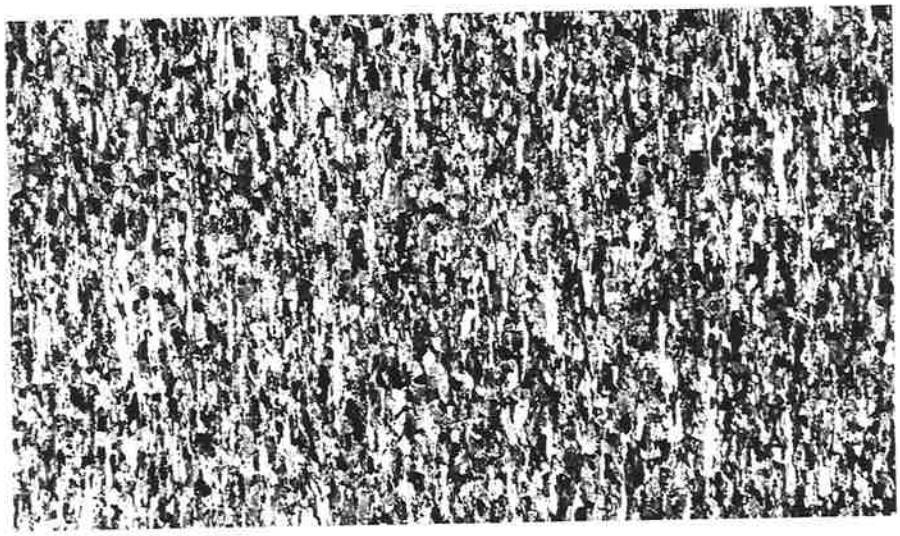

b

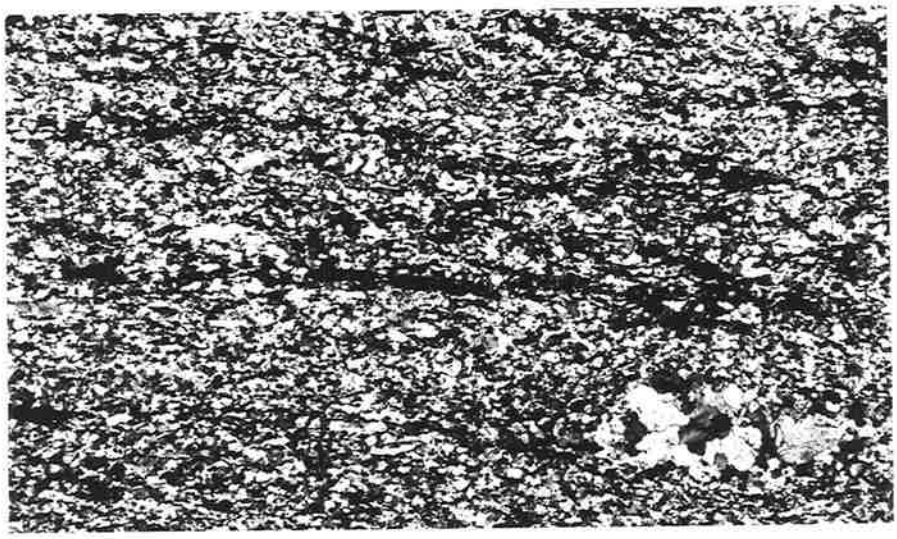

c

FIGURE 3.11

(a) Xenolith of coarse grained gneiss enclosed in granite gneiss from the amphibolite facies terrain north of Amata.

(b) Quartz microcline pegmatite segregation vein through lineated quartzo-feldspathic granulite.

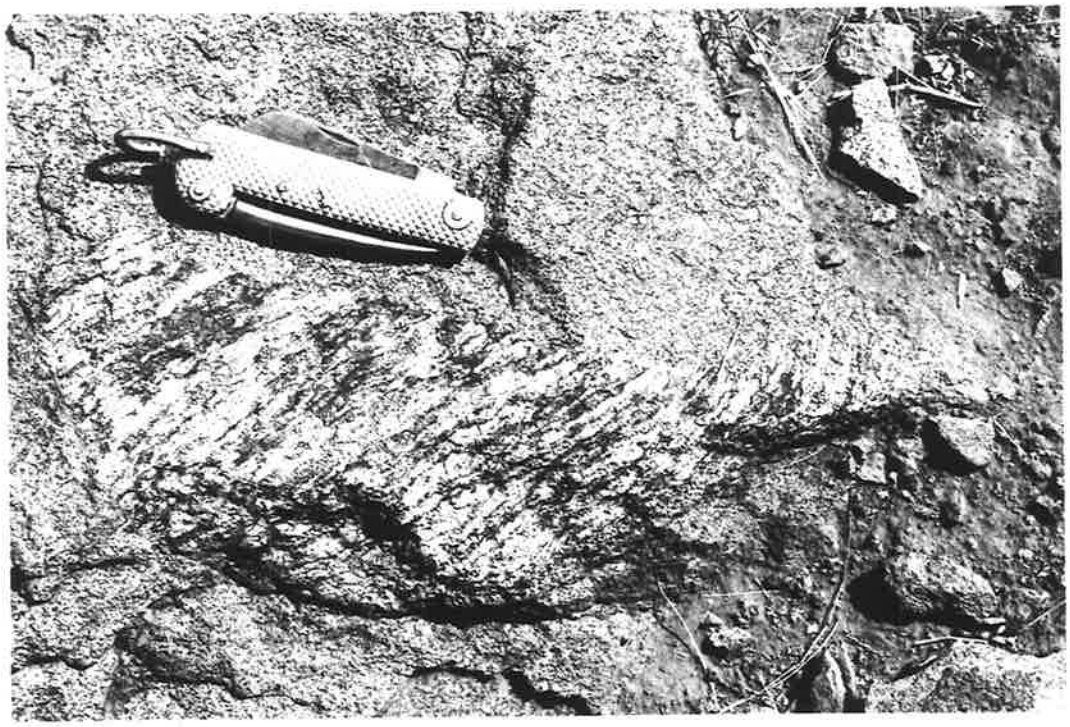

a

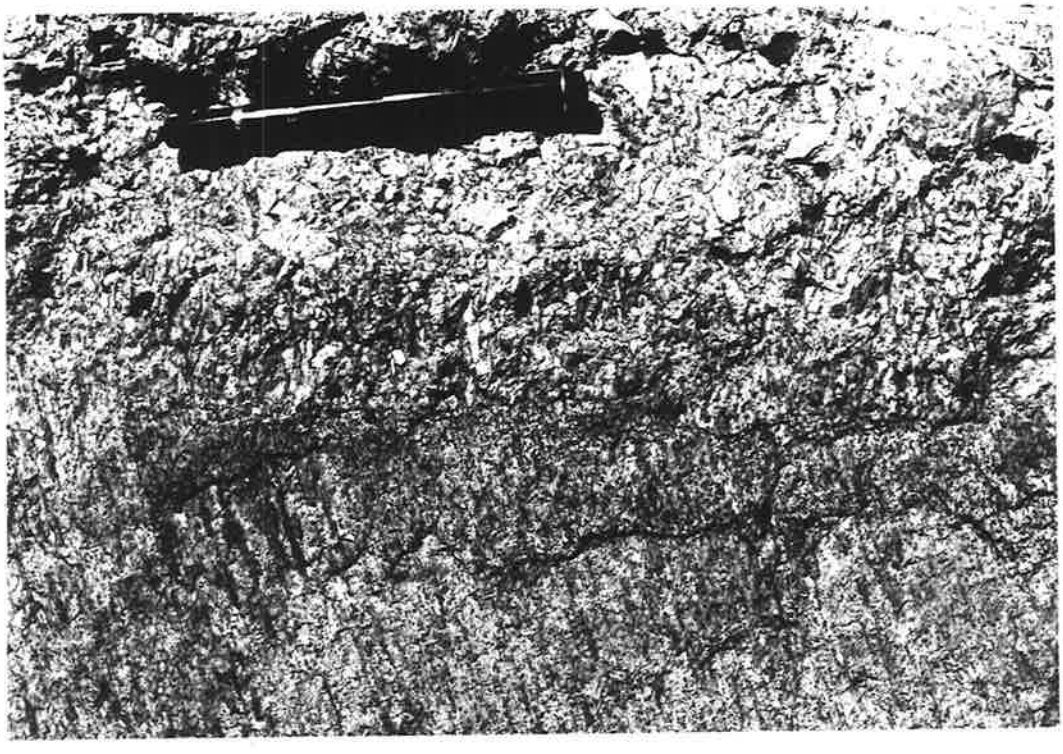

b

FIGURE 3.12

(a) Quartzo-feldspathic gneiss from the amphibolite facies terrain showing characteristic anastomosing microstructure.
A325-1640N
Crossed polars
Width of field: 4 cm.

(b) Gross microstructural relationships in tourmaline bearing pegmatite from the granulite facies terrain.
A325-953
Crossed polars
Width of field: 4 cm.

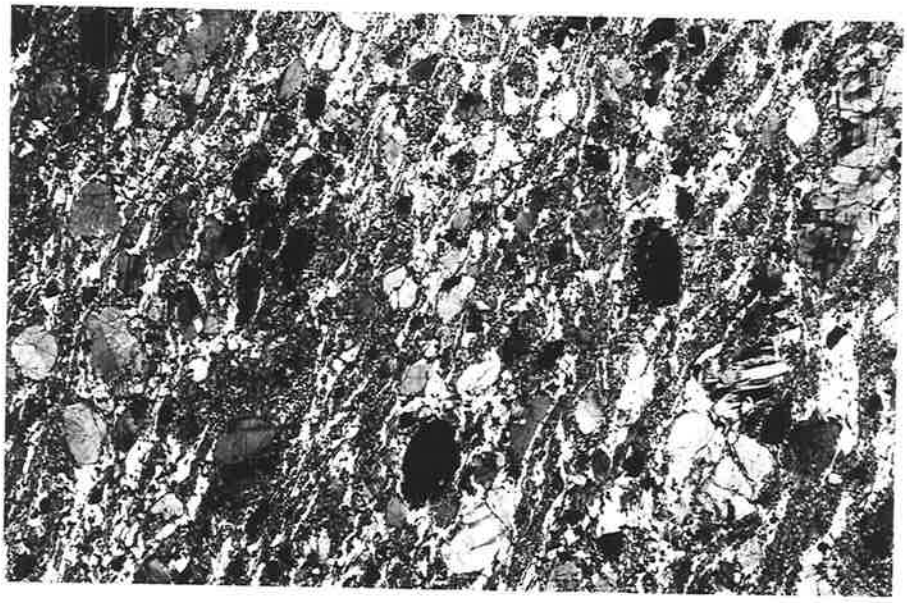

a

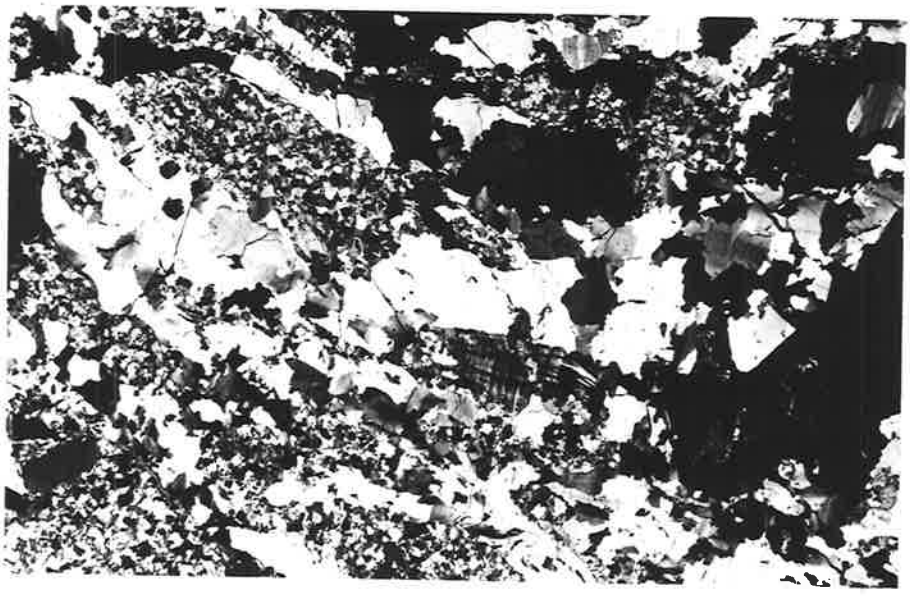

b

FIGURE 3.13

(a) Typical microstructure of calc silicate rock from the transitional terrain. Note the narrow radiating coronas of clinozoisite and zoisite around the clinopyroxene grains.
A325-425
Plane polarized light
Width of field: 2 mm.

(b) Complexly kinked biotite with serrated kink planes showing the development of recrystallized grains.
A325-682N
Plane polarized light
Width of field: 0.6 mm.

(c) Amphibolite with inequigranular granoblastic microstructure.
A325-1684N
Plane polarized light
Width of field: 6 mm.

(d) Amphibolite with inequigranular granoblastic microstructure.
A325-1748
Plane polarized light
Width of field: 6 mm.

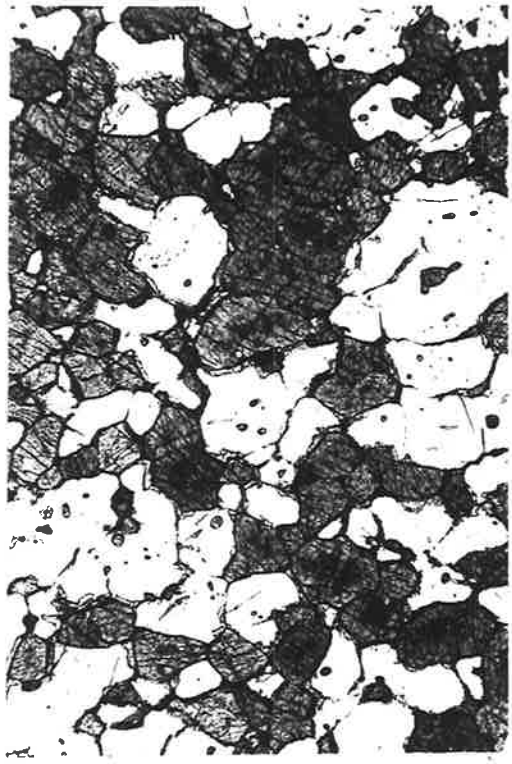

a

b

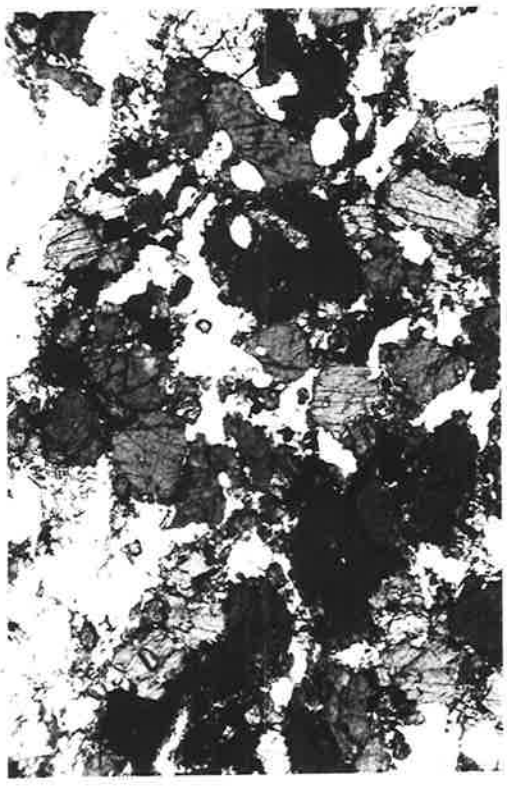

c

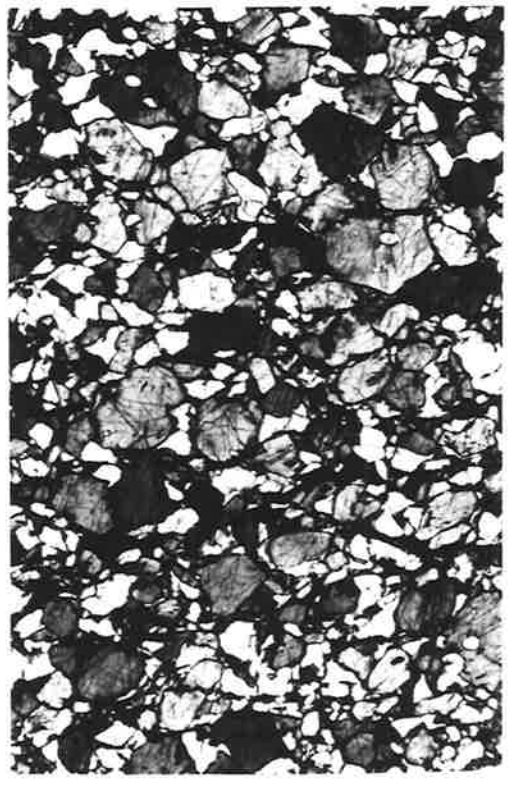

d

FIGURE 3.14

(a) Mafic rock from the transitional terrain composed predominantly of hornblende (dense stipple) together with clinopyroxene (light stipple) orthopyroxene (moderate stipple) and plagioclase with inequigranular granoblastic microstructure. Note the development of coronas.
A325-896N
Length of bar: 1 mm.

(b) Inequigranular to equigranular granoblastic microstructure in plagioclase, clinopyroxene, hornblende rock from the transitional terrain.
A325-630a
Length of bar: 1 mm.

(c) Inequigranular granoblastic microstructure exhibited by amphibolite from the transitional terrain.
A325-936g
Length of bar: 1 mm.

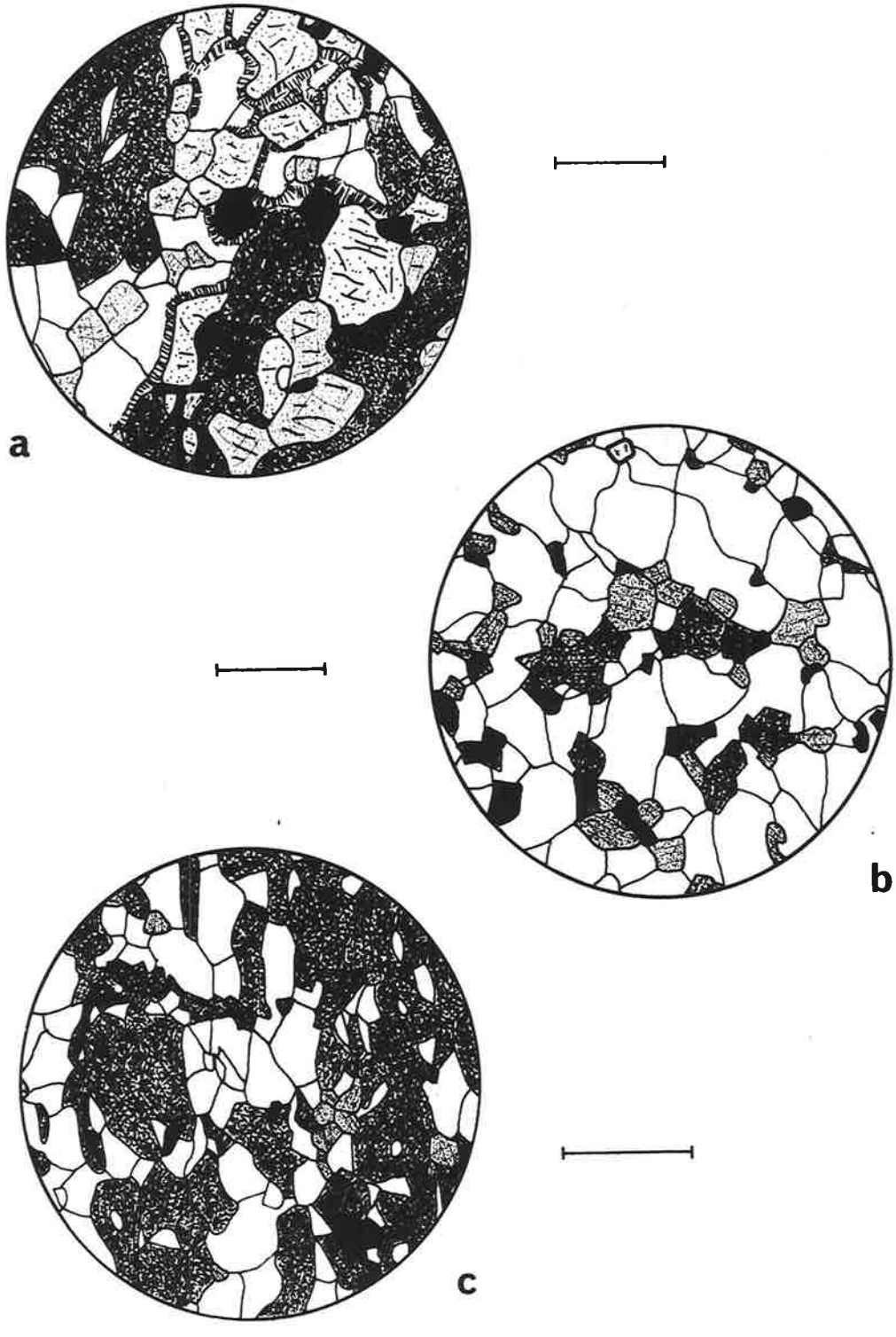
a
b
c

FIGURE 3.15

(a) Poikiloblastic porphyroblast of orthopyroxene in mafic rock from the transitional terrain. Note the rounded shapes of the inclusions.
A325-664N
Length of bar: 1 mm.

(b) Embayed xenoblast of orthopyroxene in micaceous mafic rock from the transitional terrain with slight development of sieve structure. Inclusions include phlogopite and apatite. Note the rational boundary of biotite against the orthopyroxene.
A325-990N
Length of bar: 1 mm.

(c) Hornblende, orthopyroxene, clinopyroxene, plagioclase bearing mafic rock from the transitional terrain. Note the rational boundaries displayed by the large hornblende porphyroblast.
A325-523
Length of bar: 1 mm.

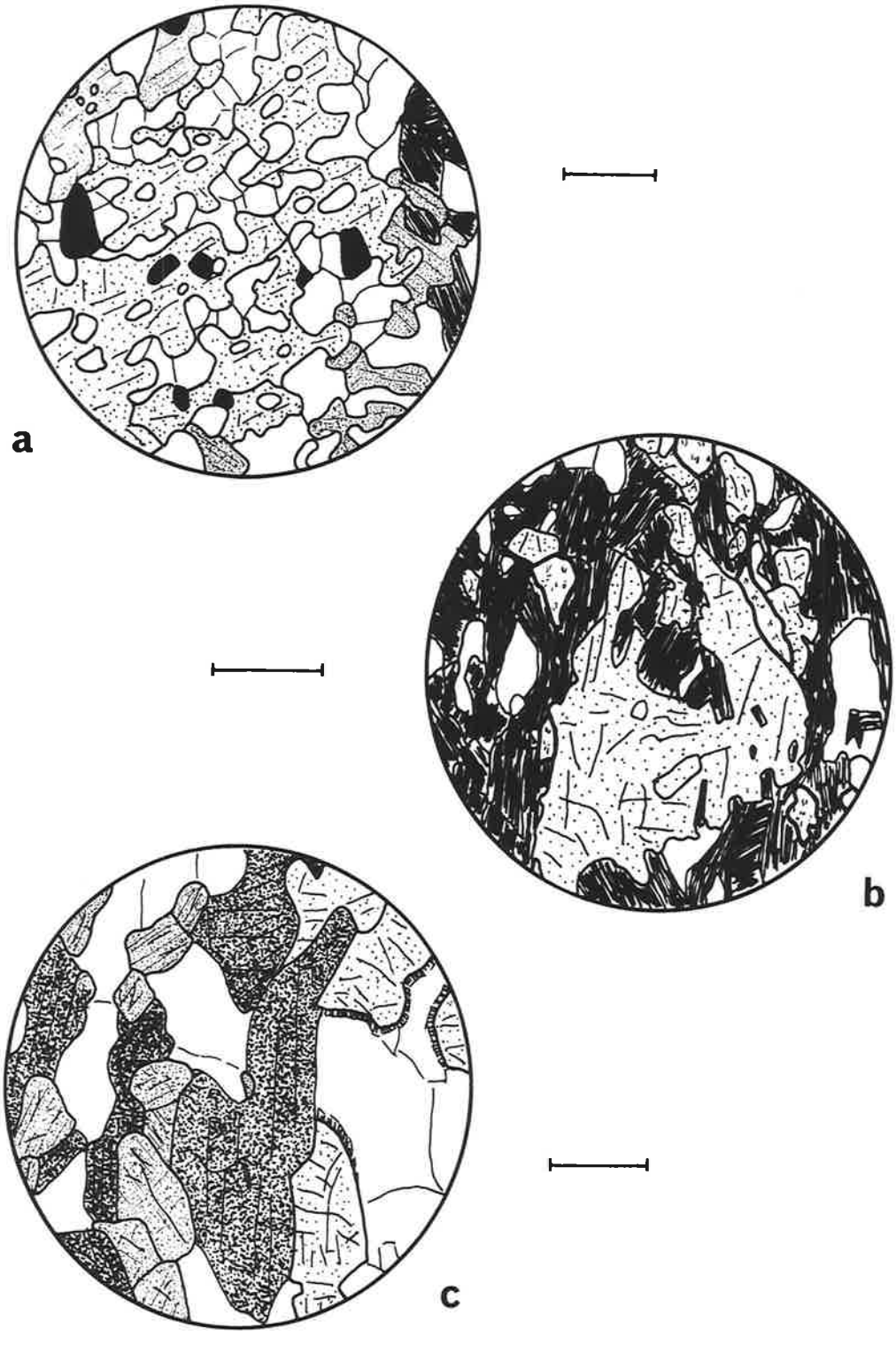
a
b
c

FIGURE 3.16

(a) Mafic rock from the transitional terrain with well developed tS_1 layering and tS_2 schistosity.
A325-846N
Plane polarized light
Width of field: 3.8 cm.

(b) Porphyroblastic or glomeroporphyroblastic mafic rock from the transitional terrain. Note the anastomosing layering engulfing small diamond shaped grains.
A325-874N
Plane polarized light
Width of field: 2 mm.

(c) Rounded grains of garnet associated with xenoblastic grains of bead perthite.
A325-345P
Plane polarized light
Width of field: 1.4 mm.

(d) Rounded inclusions of quartz and feldspar in poikiloblastic xenoblastic porphyroblast of garnet.
A325-698N
Plane polarized light
Width of field: 6 mm.

a

b

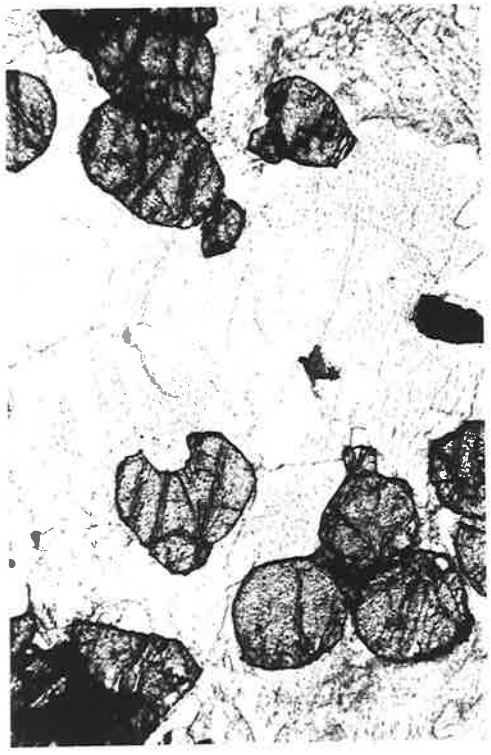

c

d

FIGURE 3.17

(a) Ramifying coronas of hornblende developed around opaque oxides and orthopyroxene in a mafic rock from the transitional terrain.
A325-1273
Plane polarized light
Width of field: 1.4 mm.

(b) Intergrowths (and coronas) of garnet with biotite in amphibolite from the transitional terrain.
A325-936e
Plane polarized light
Width of field: 2 mm.

(c) Garnet-quartz symplectites occurring as coronas around hornblende and opaque oxides.
A325-611
Plane polarized light
Width of field: 0.6 mm.

(d) Decussate aggregates of secondary hornblende occurring as coronas around opaque oxides.
A325-49
Plane polarized light
Width of field: 1.4 mm.

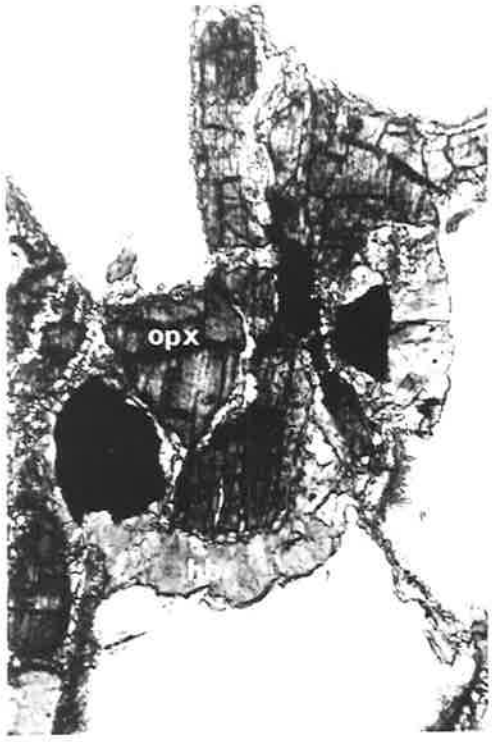

a

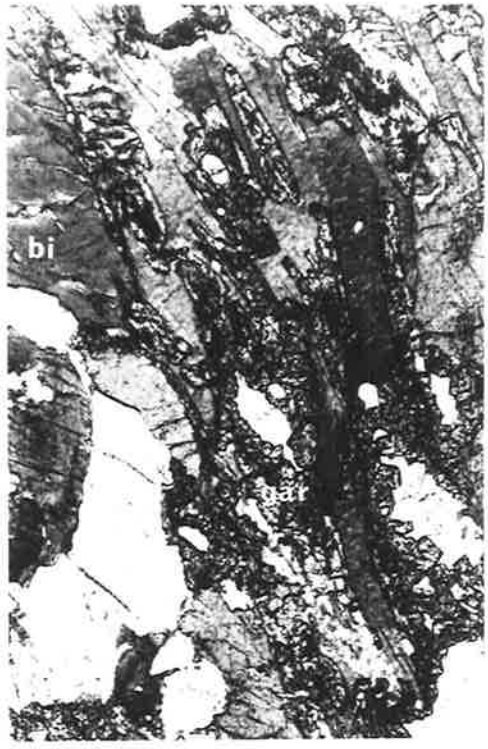

b

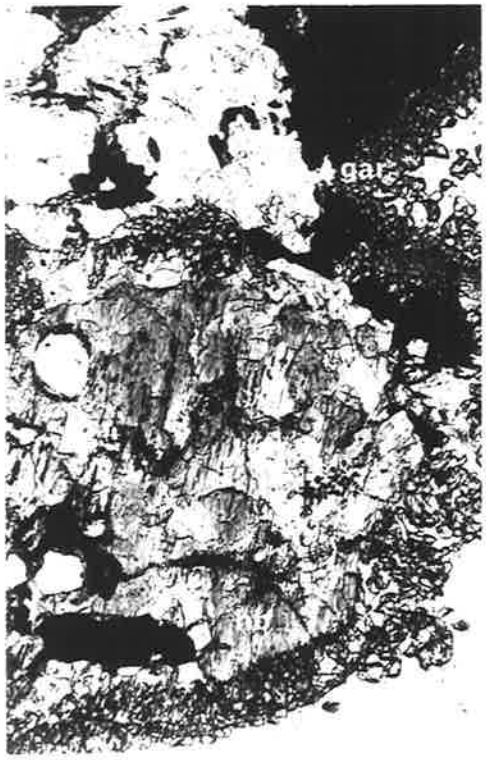

c

d

FIGURE 3.18

(a) Fine grained coronas of garnet around irregular grains of opaque oxides. Note the sillimanite inclusions in the plagioclase.
A325-705bN
Plane polarized light
Width of field: 0.6 mm.

(b) Ragged decussate aggregates, or discrete subidioblastic grains of hornblende intergrown with secondary garnet and biotite.
A325-400P
Plane polarized light
Width of field: 2 mm.

(c) Orhtopyroxene surrounded by symplectites of quartz and garnet. Coronas of garnet also surround grains of opaque oxide.
A325-705bN
Plane polarized light
Width of field: 0.6 mm.

(d) Coronas of decussate cummingtonite developed along a plagioclase interface. Note the complex deformation twinning in the plagioclase.
A325-523
Crossed polars
Width of field: 0.6 mm.

a

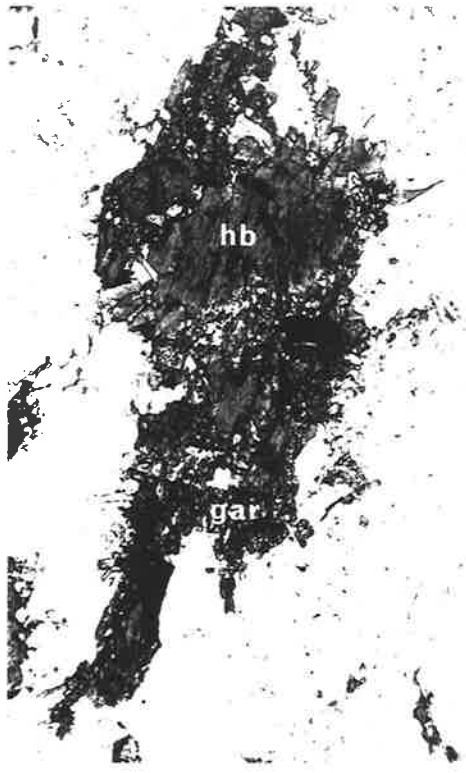

b

c

d

FIGURE 3.19

(a) Irregular grain of magnetite (light grey) and grains of ilmenite (dark grey) in amphibolite from the transitional terrain. Note the presence of spinel exsolution lamellae and martite in the magnetite.
A325-6
Plane polarized light
Width of field: 0.21 mm.

(b) Embayed, poikiloblastic grain of ilmenite with flame-like exsolution lamellae of haematite from a mafic granulite. Note the straight idioblastic interface developed between rutile and ilmenite.
A325-81
Plane polarized light
Width of field: 0.21 mm.

(c) Ilmenite (with flame-like haematite exsolution lamellae) partially surrounded by magnetite (showing abundant martite development). Haematite exsolution is absent close to the magnetite.
A325-564
Plane polarized light
Width of field: 0.21 mm.

(d) Magnetite (with martite alteration) intergrown with ilmenite showing rod-like (black) lamellae of corundum.
A325-564
Plane polarized light
Width of field: 0.21 mm.

a

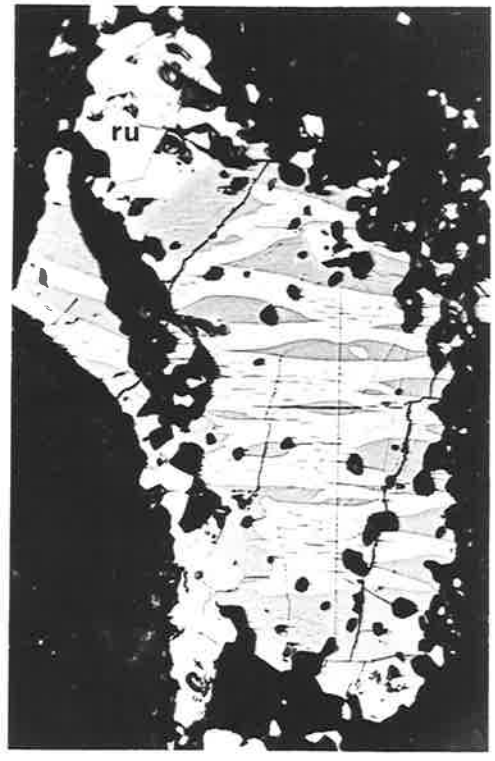

b

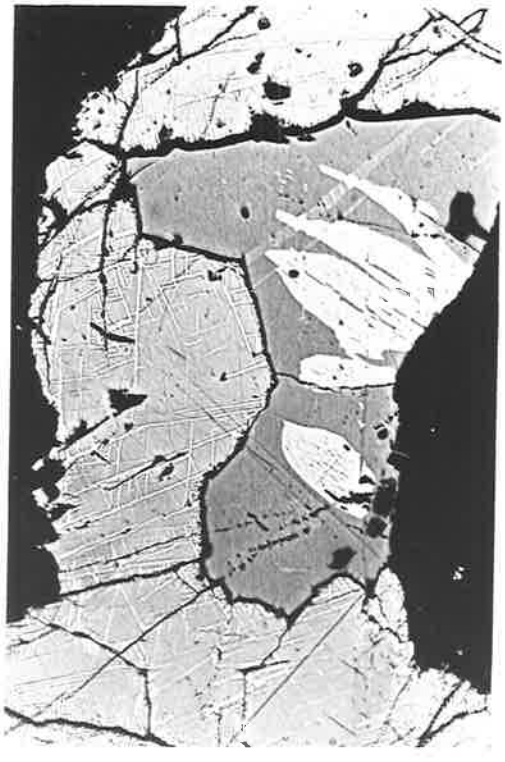

c

d

FIGURE 3.20

(a) Intermediate rock from the transitional terrain, composed of xenoblastic plagioclase (clear), quartz (very light stipple), orthopyroxene (coarse stipple), clinopyroxene (fine dense stipple) and opaque oxides (black). Note the weakly developed preferred orientation displayed by the grains.
A325-1410N
Length of bar: 1 mm.

(b) Twin-like intergrowth between clinopyroxene and orthopyroxene in ultramafic rock from the transitional terrain.
A325-776N
Length of bar: 1 mm.

(c) Complex intergrowths between hornblende (very dense stipple), clinopyroxene (fine stipple) and orthopyroxene (widely spaced stipple) in ultramafic rock from the transitional terrain.
A325-295N
Length of bar: 1 mm.

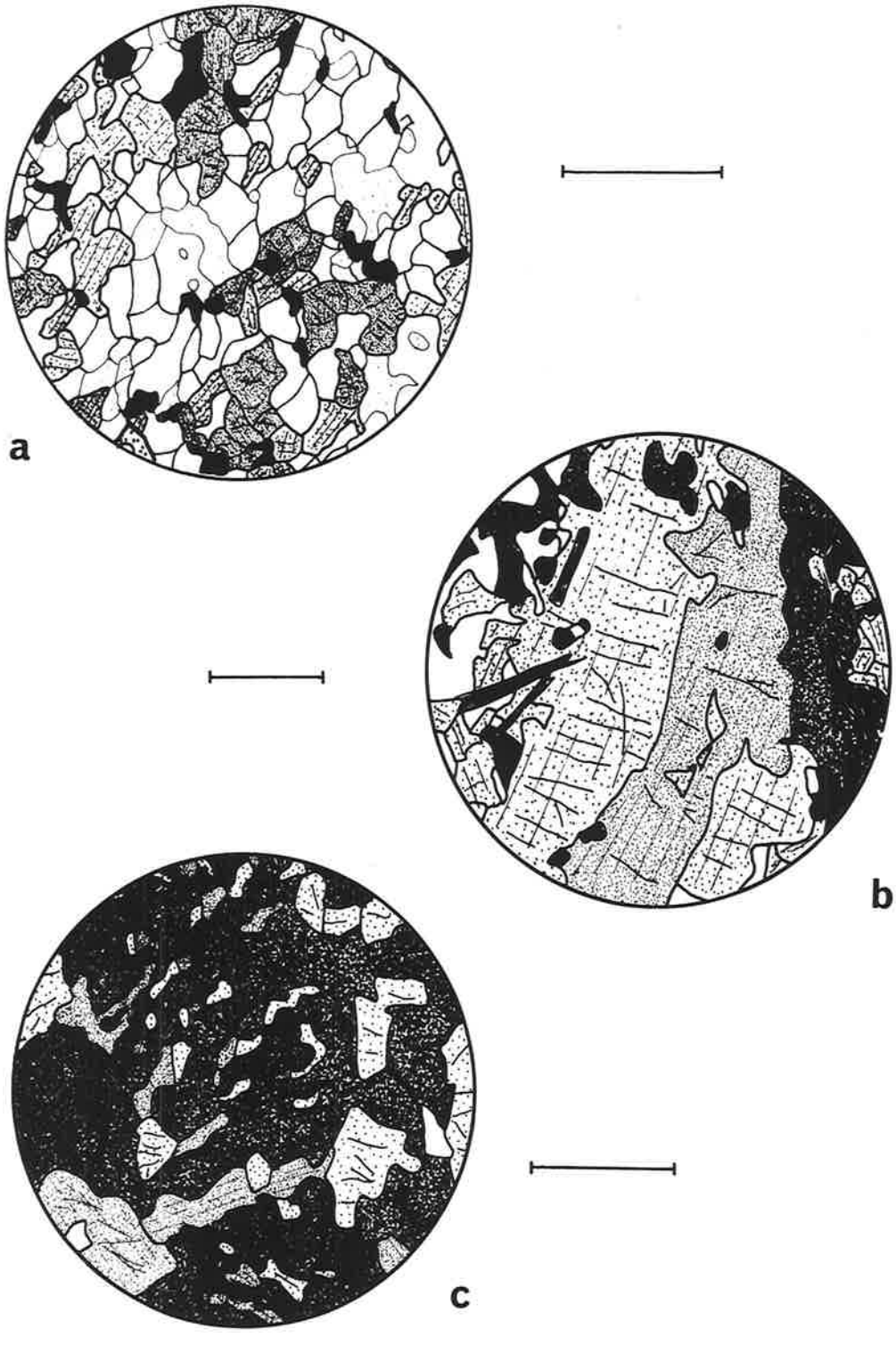
a
b
c

FIGURE 3.21

(a) Quartzo-feldspathic gneiss from the transitional terrain, consisting of xenoblastic elongate grains of quartz and microcline perthite with minor amounts of opaque oxides. Note the porphyroblastic nature of the microstructure and the dimensional preferred orientation of the phases.
A325-940
Crossed polars
Width of field: 3.8 cm.

(b) Quartz-microcline perthite-plagioclase-biotite gneiss from the transitional terrain. The microstructure is medium to coarse grained inequigranular granoblastic and a weakly defined schistosity is present.
A325-474N
Crossed polars
Width of field: 3.8 cm.

(c) Quartz-perthite-plagioclase-orthopyroxene-biotite-hornblende gneiss from the transitional terrain showing inequigranular to equigranular granoblastic microstructure defined by grains displaying curved, embayed and serrated interfaces.
A325-49N
Crossed polars
Width of field: 3.8 cm.

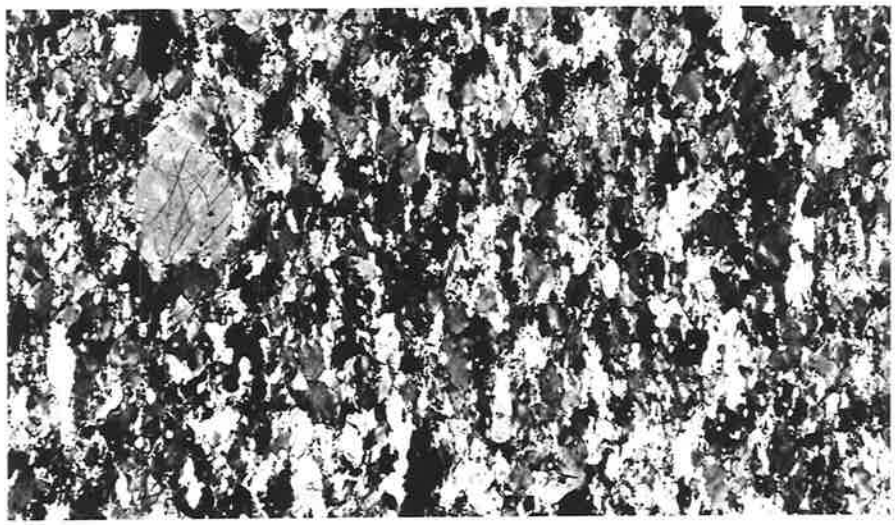

a

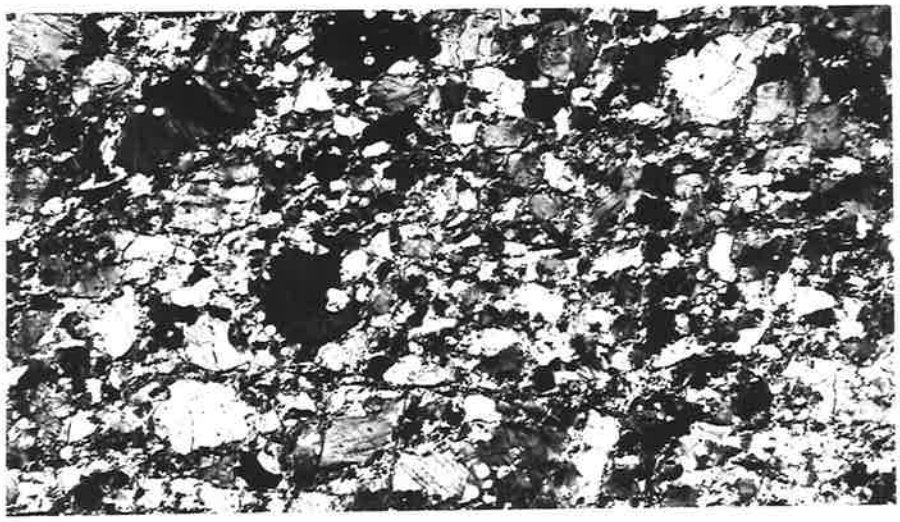

b

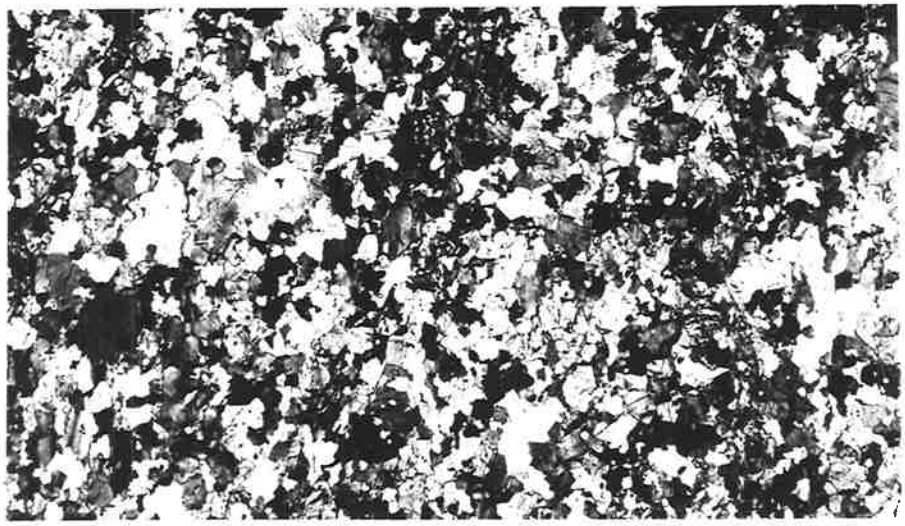

c

FIGURE 3.22

(a) Quartzo-feldspathic gneiss from the transitional terrain with a banded equigranular granoblastic microstructure. Note the compositional layering $tS_0//tS_1$ and the weakly developed tS_2 schistosity defined by wavy lenticles of quartz and feldspar, and prismatic aggregates of ferromagnesian phases.
A325-788N
Crossed polars
Width of field: 3.8 cm.

(b) Quartzo-feldspathic gneiss from the transitional terrain with an inequigranular granoblastic microstructure. The dimensional preferred orientation is dominantly the tS_2 schistosity.
A325-620cN
Crossed polars
Width of field: 3.8 cm.

(c) Garnetiferous quartzo-feldspathic gneiss with well developed anastomosing microstructure and lozenge shaped feldspar and garnet porphyroblasts (or -clasts).
A325-318bN
Crossed polars
Width of field: 3.8 cm.

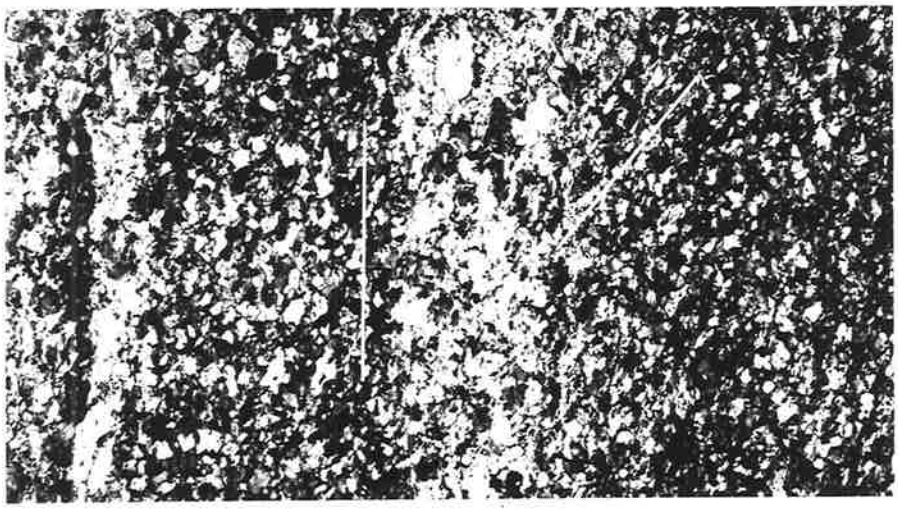

a

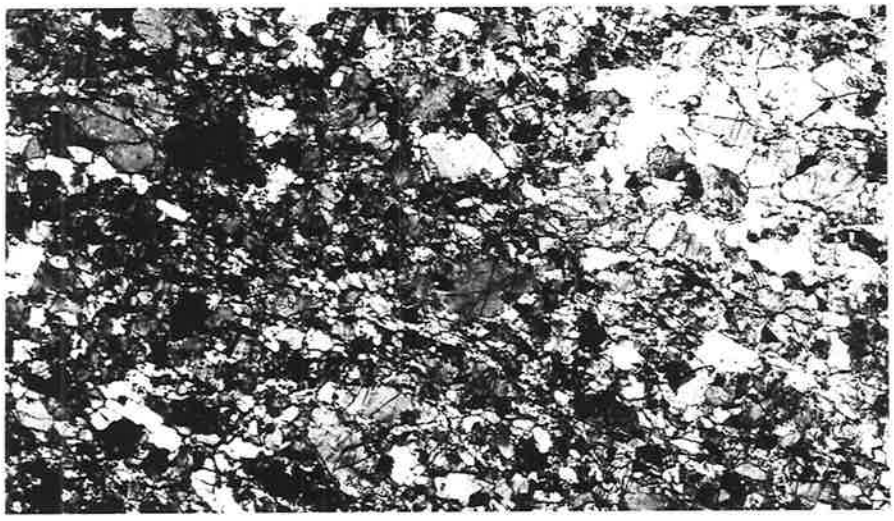

b

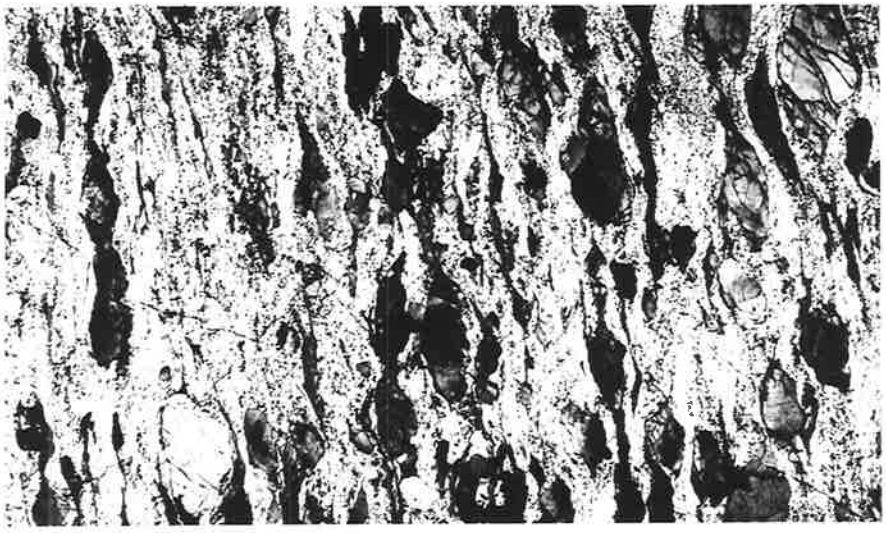

c

FIGURE 3.23

(a) Quartzo-feldspathic gneiss from the amphibolite facies terrain. The microstructure is defined by the presence of coarse grained lozenge shaped porphyroblasts of feldspar in a fine grained inequigranular granoblastic groundmass.
A325-1744N
Crossed polars
Width of field: 4.5 cm.

(b) Quartzo-feldspathic gneiss from the amphibolite facies terrain. The microstructure is inequigranular granoblastic. A weakly defined anastomosing schistosity is present.
A325-1657N
Crossed polars
Width of field: 4 cm.

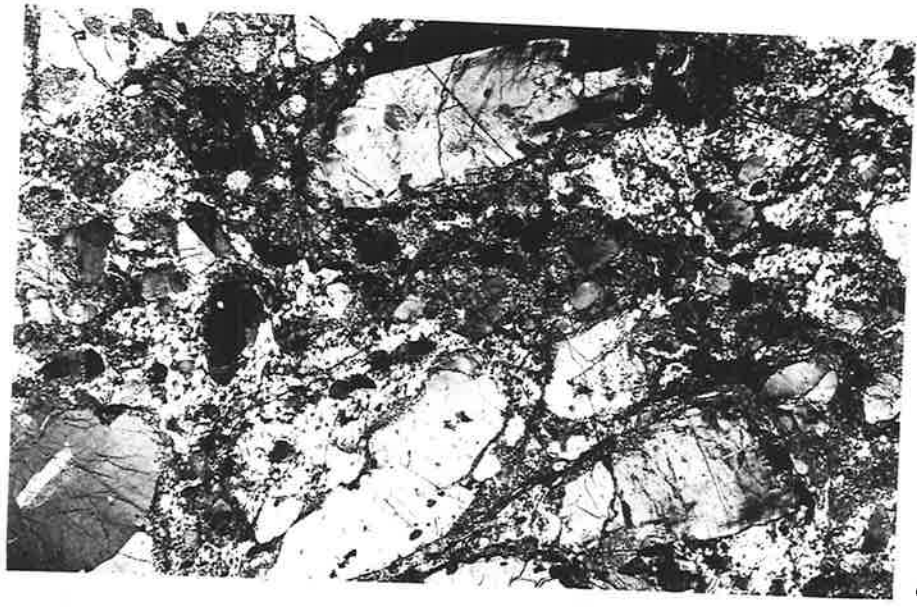

a

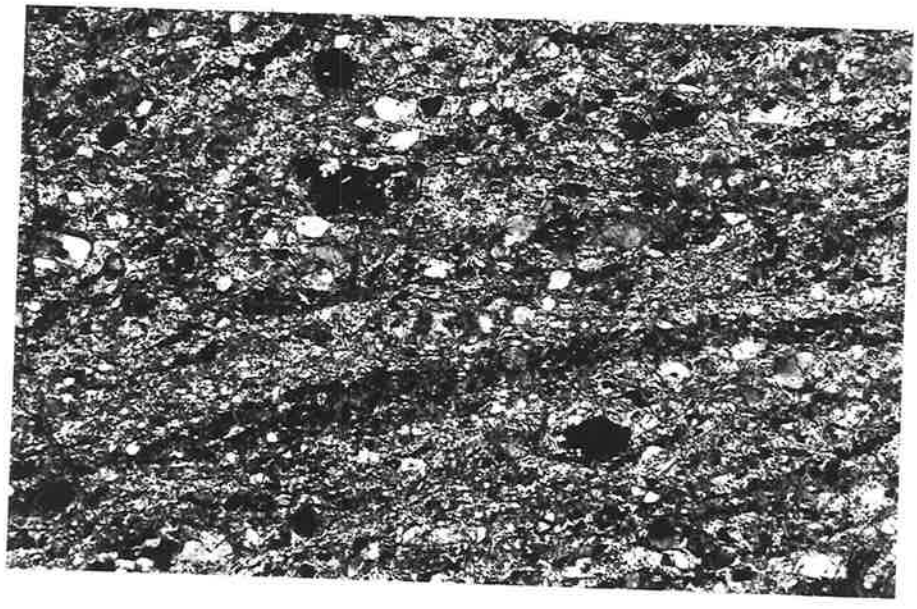

b

FIGURE 4.1

Ternary plot of quartz, feldspar and other phases.

(a) Granulite facies terrain.

Ornamentation:

small open circles - quartzo-feldspathic lithologies
small closed circles - mafic lithologies containing antiperthitic plagioclase
large closed circles - mafic lithologies containing non-antiperthitic plagioclase
closed square - ultramafic lithology
open triangle - calc silicate lithology
open square - manganiferous lithology.

(b) Transitional terrain.

Ornamentation:

small open circles - quartzo-feldspathic lithologies
small closed circles - non-micaceous mafic lithologies
large closed circles - micaceous mafic lithologies
closed square - ultramafic lithology
open triangle - calc silicate lithology.

(c) Amphibolite facies terrain.

Ornamentation:

small open circles - quartzo-feldspathic lithologies
small closed circles - mafic lithologies
half open circle - pelitic lithology.

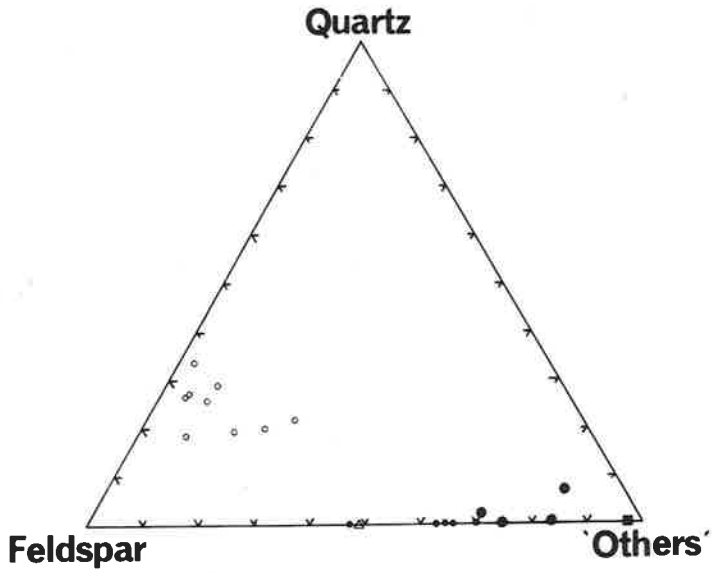
Quartz
Feldspar
`Others´

b

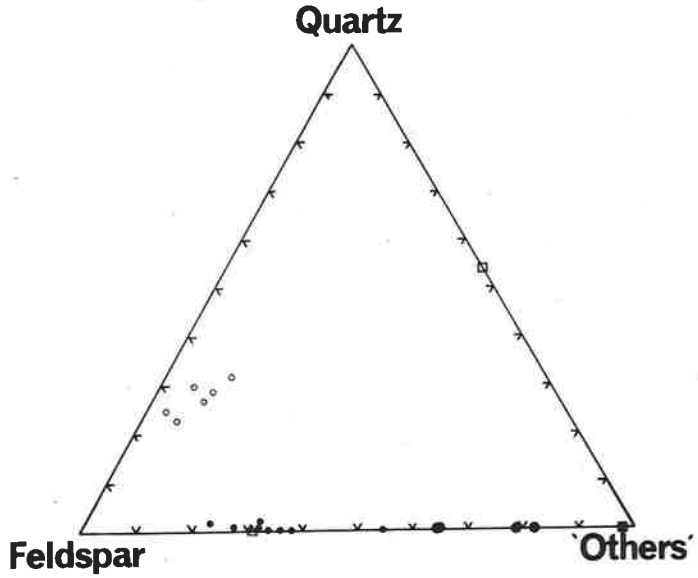
Quartz
Feldspar
`Others´

a

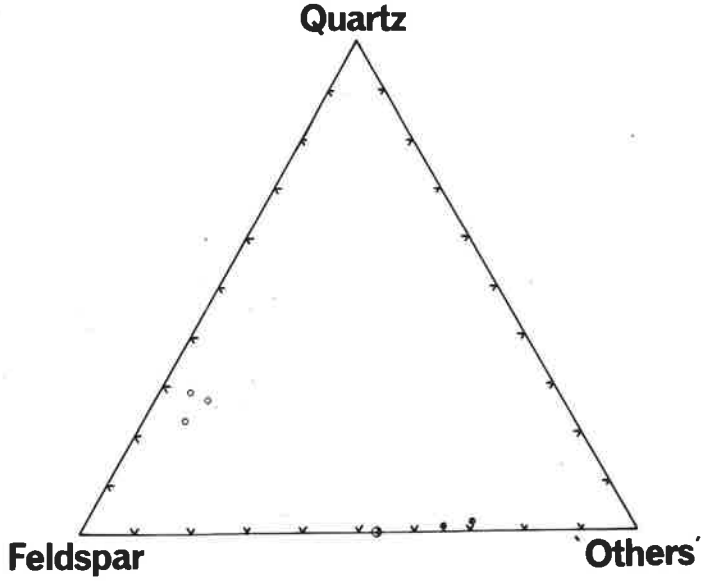
Quartz
Feldspar
`Others´

c

FIGURE 4.2

Normative Q-Or-Ab proportions (a) and Or-Ab-An proportions (b) for the quartzo-feldspathic rocks from the Amata area.

A line representing the variation in position of minimum melting in the system $NaAlSi_3O_8$ - $KAlSi_3O_8$ - SiO_2 - H_2O for variations in water pressure from 500-10,000 bars (after Tuttle and Bowen, 1958; and Luth, Jahns and Tuttle, 1964) is shown in Figure a, as are contours representing the distribution of normative Q, Or, Ab in the 571 analysed plutonic rocks from Washington's Tables (after Tuttle and Bowen, 1958).

The position of the thermal trough in the system $KAlSi_3O_8$ - $NaAlSi_3O_8$ - $CaAl_2Si_2O_8$ - SiO_2 (after Kleeman, 1965) is shown in Figure b.

FIGURE 4.2.1

Granulite facies terrain.
open circles, C.I.P.W. normative values
closed circles, catanormative values.

1. A325-205
2. A325-199
3. A325-1165a
4. A325-138
5. A325-1121
6. A325-77

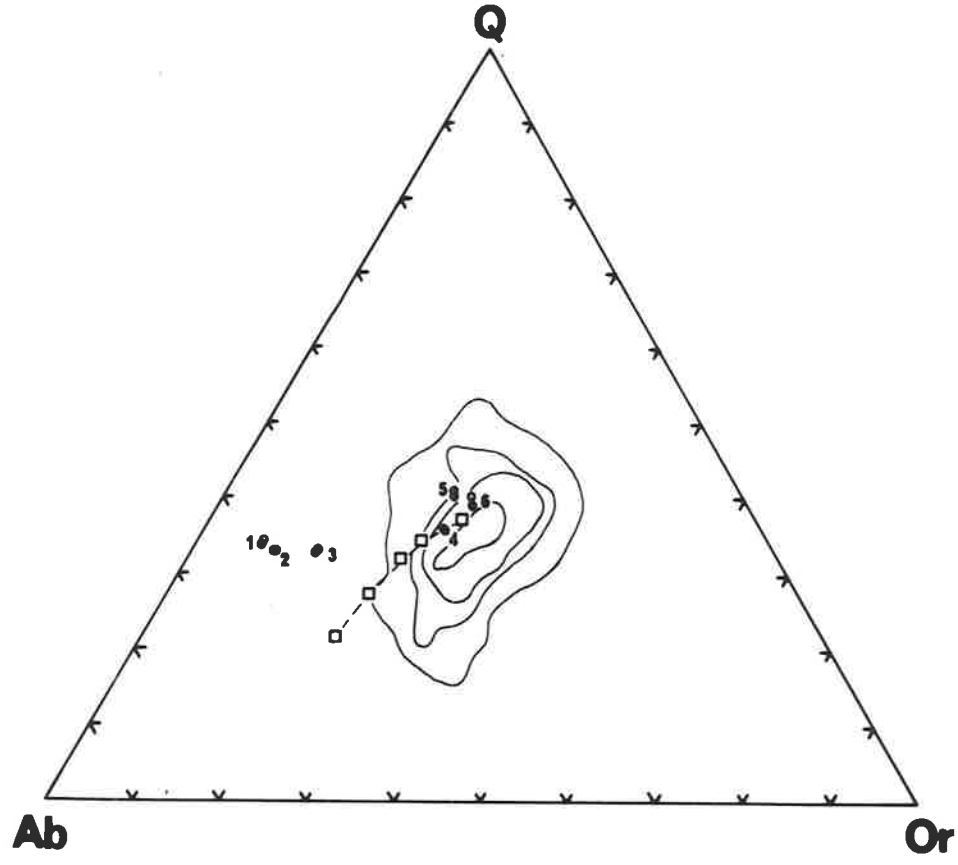

a

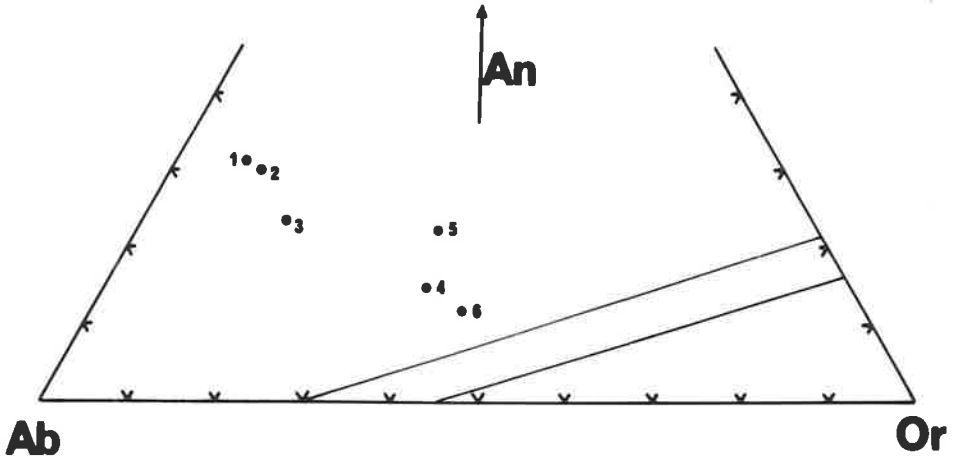

b

FIGURE 4.2.2

Transitional terrain.

open circles, C.I.P.W. normative values

closed circles, mesonormative values.

1. A325-531
2. A325-396
3. A325-400
4. A325-323
5. A325-783
6. A325-474
7. A325-18
8. A325-326
9. A325-405

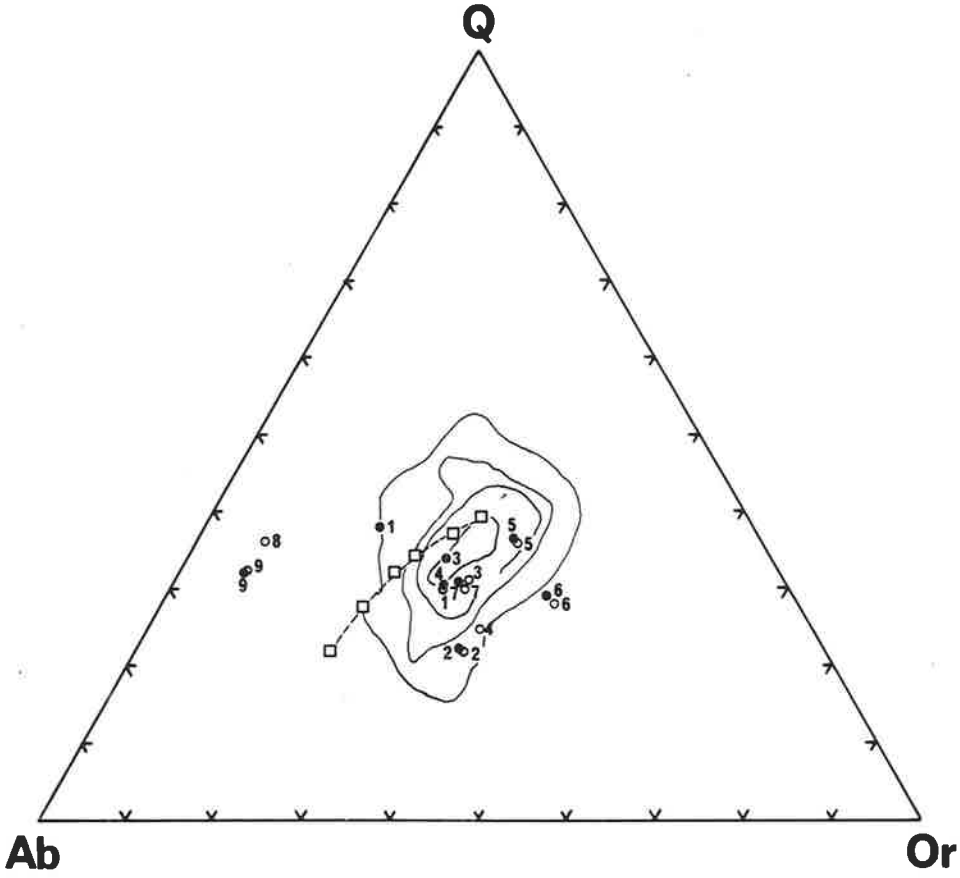

a

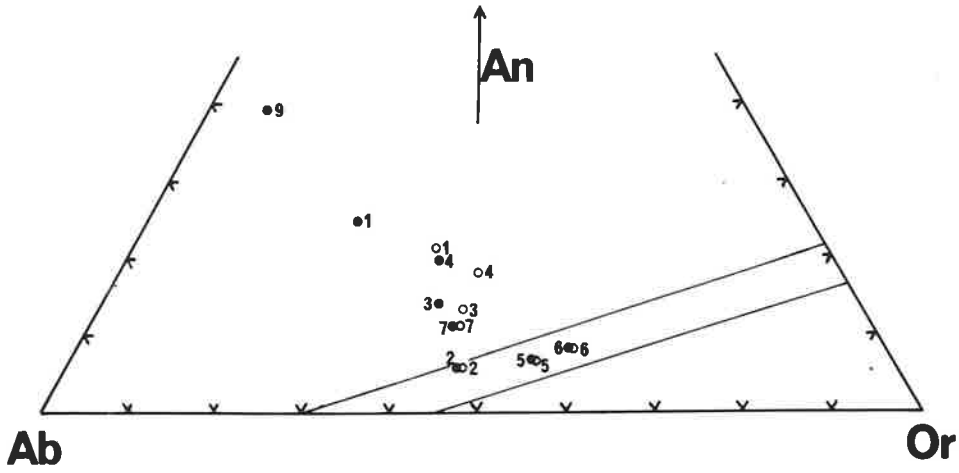

b

FIGURE 4.2.3

Amphibolite facies terrain.

open circles, C.I.P.W. normative values

closed circles, mesonormative values.

1. A325-1744
2. A325-1636a
3. A325-1659

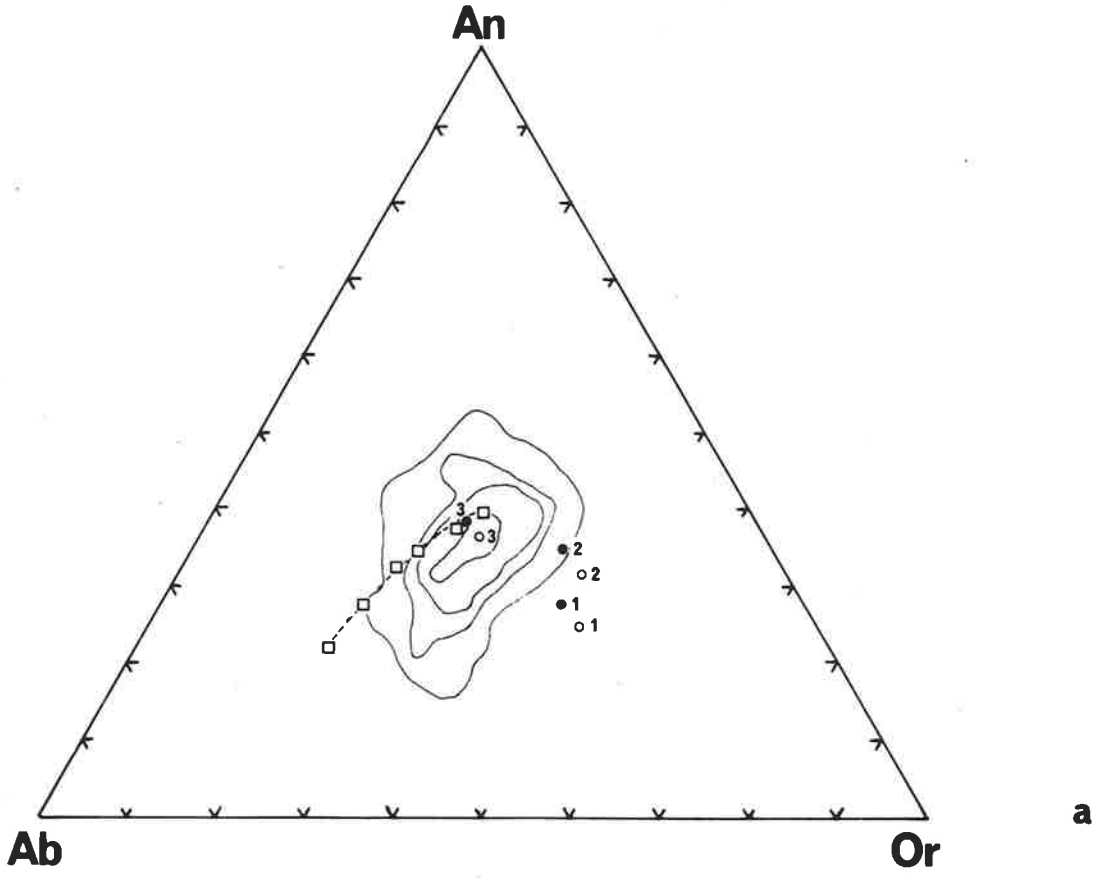

a

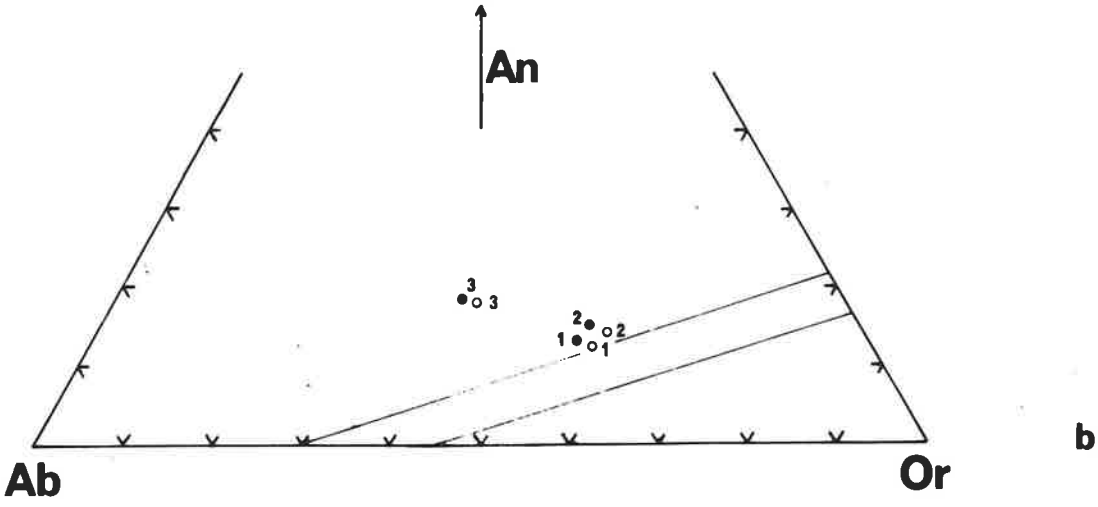

b

FIGURE 4.3

Ternary normative Or-Ab-An diagram showing compositional trend lines.

Amata Rocks - Solid lines

A-A Quartzo-feldspathic granulites with minor K feldspar

A'-A' Quartzo-feldspathic granulites with two feldspars

B-B Composite quartzo-feldspathic granulites

C-C Composite quartzo-feldspathic transitional rocks.

- Broken lines

D-D Hypersthene granulites)
D'-D' Quartz feldspar granulites) Mont Tremblant (after Katz, 1969)

E-E Charnockitic rocks, Langöy, Norway)
F-F Charnockitic rocks, Arendal, Norway) (after Barth, 1969)

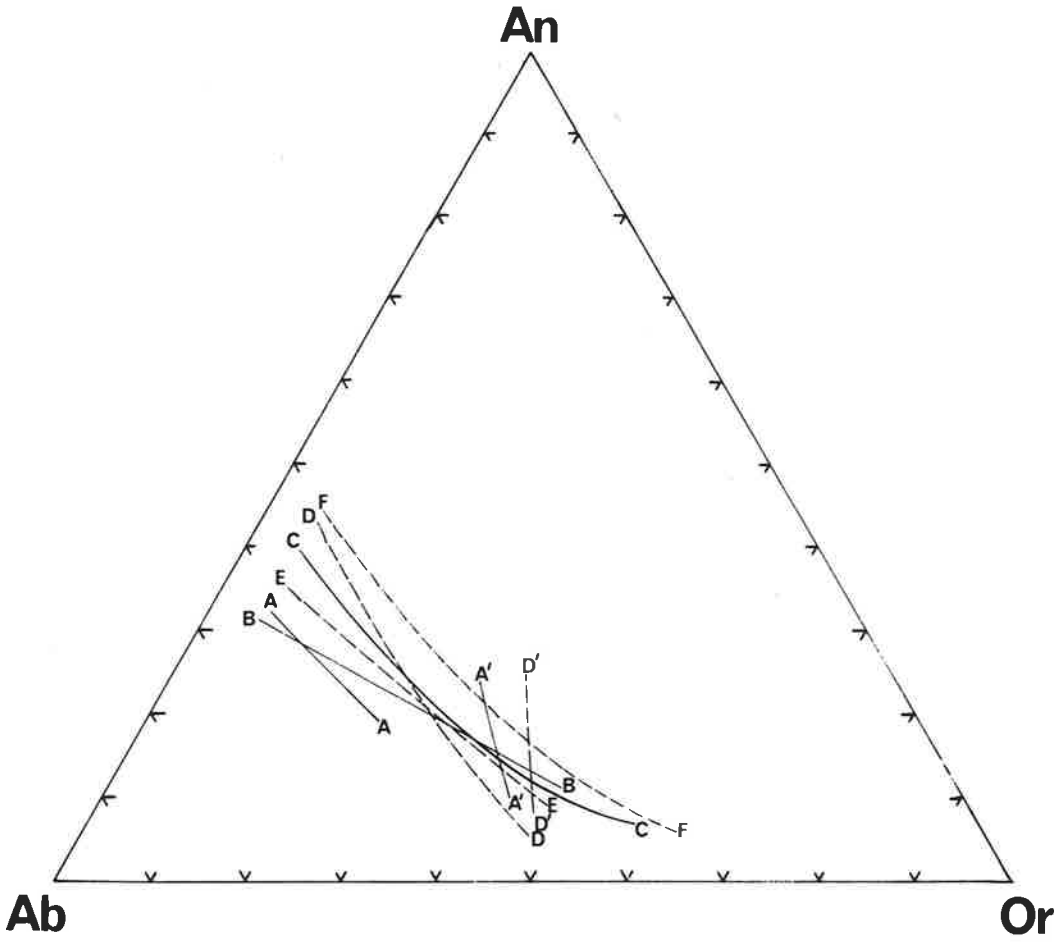
An
Ab
Or
A
B
C
D
E
F
A'
D'

FIGURE 4.4

(a) Plot of rock oxidation ratio against total iron for the granulite facies terrain.

Ornamentation:

Open circles - quartzo-feldspathic lithologies
closed circles - mafic lithologies
closed square - ultramafic lithology
triangle - calc silicate lithology
open square - manganiferous lithology

(after Chinner, 1960)

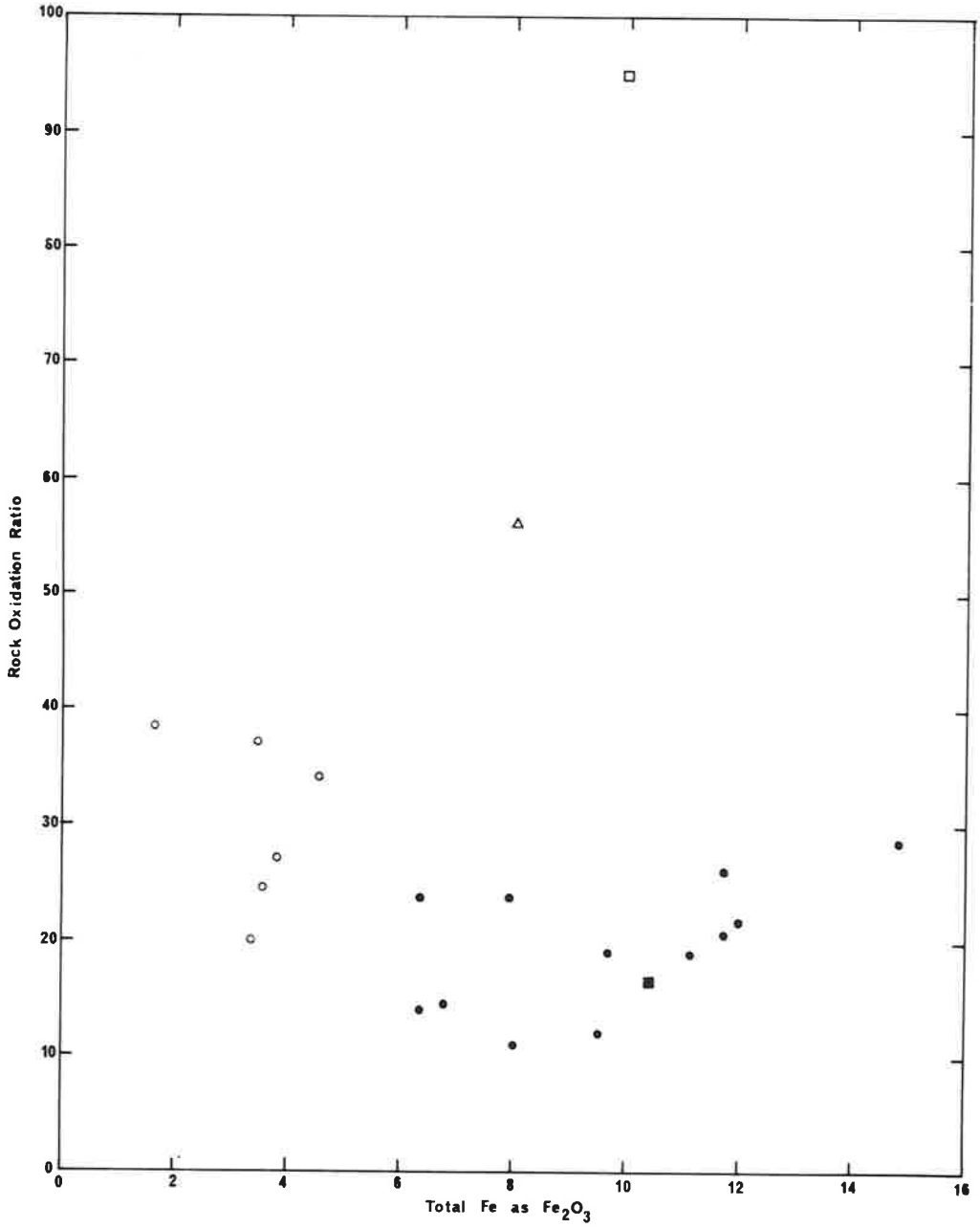
Rock Oxidation Ratio
100
90
50
70
60
50
40
30
20
10
0
0
2
4
6
8
10
12
14
16
Total Fe as Fe_2O_3

a

FIGURE 4.4

(b) Plot of rock oxidation ratio against total iron for the transitional terrain.

Ornamentation:

open circles	- quartzo-feldspathic lithologies with K_2O > Na_2O
inverted triangle	- quartzo-feldspathic lithologies with Na_2O > K_2O
small closed circles	- mica-free mafic lithologies
large closed circles	- micaceous mafic lithologies
closed square	- ultramafic lithologies
triangle	- calc silicate lithologies

(after Chinner, 1960)

(c) Plot of rock oxidation ratio against total iron for the amphibolite facies terrain.

Ornamentation:

open circles	- quartzo-feldspathic lithologies
closed circles	- mafic lithologies
half open circle	- pelitic lithology.

(after Chinner, 1960)

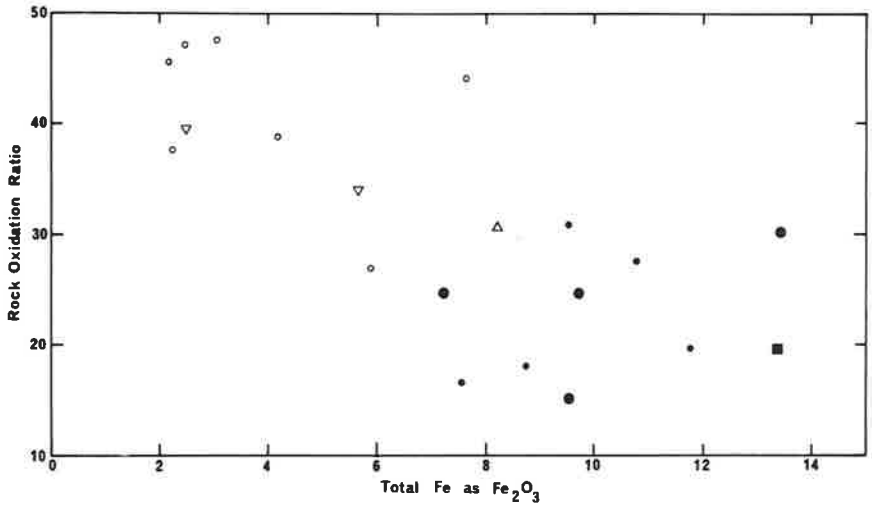
Rock Oxidation Ratio
50
40
30
20
10
0
2
4
6
8
10
12
14
Total Fe as Fe_2O_3

b

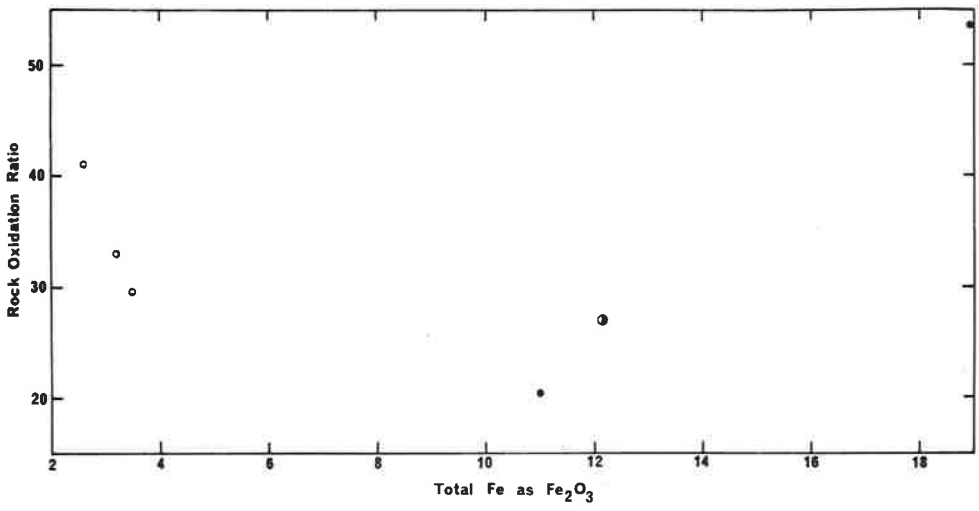
Rock Oxidation Ratio
50
40
30
20
2
4
6
8
10
12
14
16
18
Total Fe as Fe_2O_3

c

FIGURE 4.5

(a) Plot of rock oxidation ratio against manganese for the granulite facies terrain.

(after Chinner, 1960)

Ornamentation:
(same as Figure 4.4a).

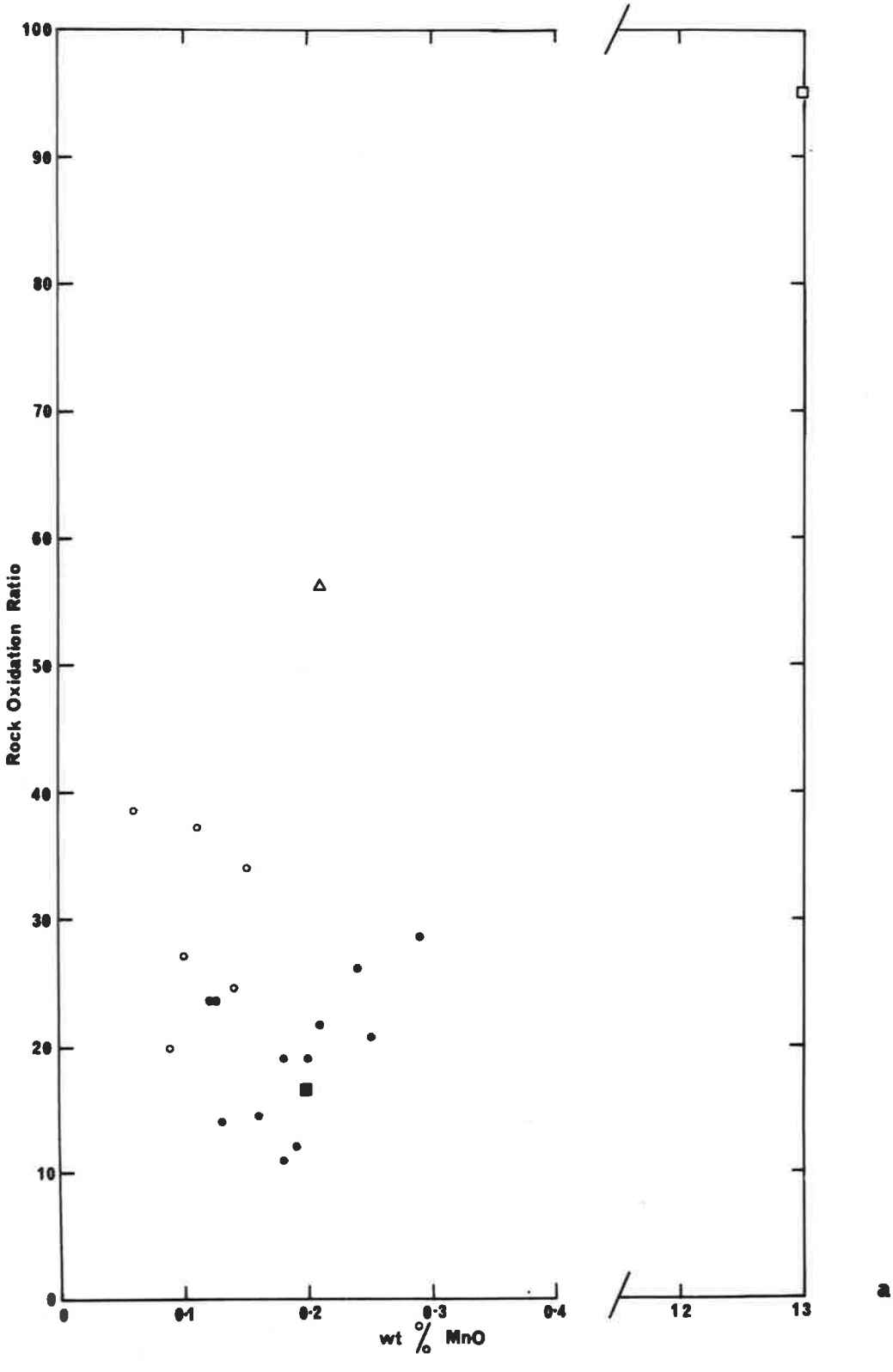
100
90
80
70
60
50
40
30
20
10
0
Rock Oxidation Ratio
0
0·1
0·2
0·3
0·4
12
13
wt % MnO

a

FIGURE 4.5

(b) Plot of rock oxidation ratio against manganese for the transitional terrain.

(after Chinner, 1960)

Ornamentation:
(same as Figure 4.4b)

(c) Plot of rock oxidation ratio against manganese for the amphibolite facies terrain.

(after Chinner, 1960)

Ornamentation:
(same as Figure 4.4c)

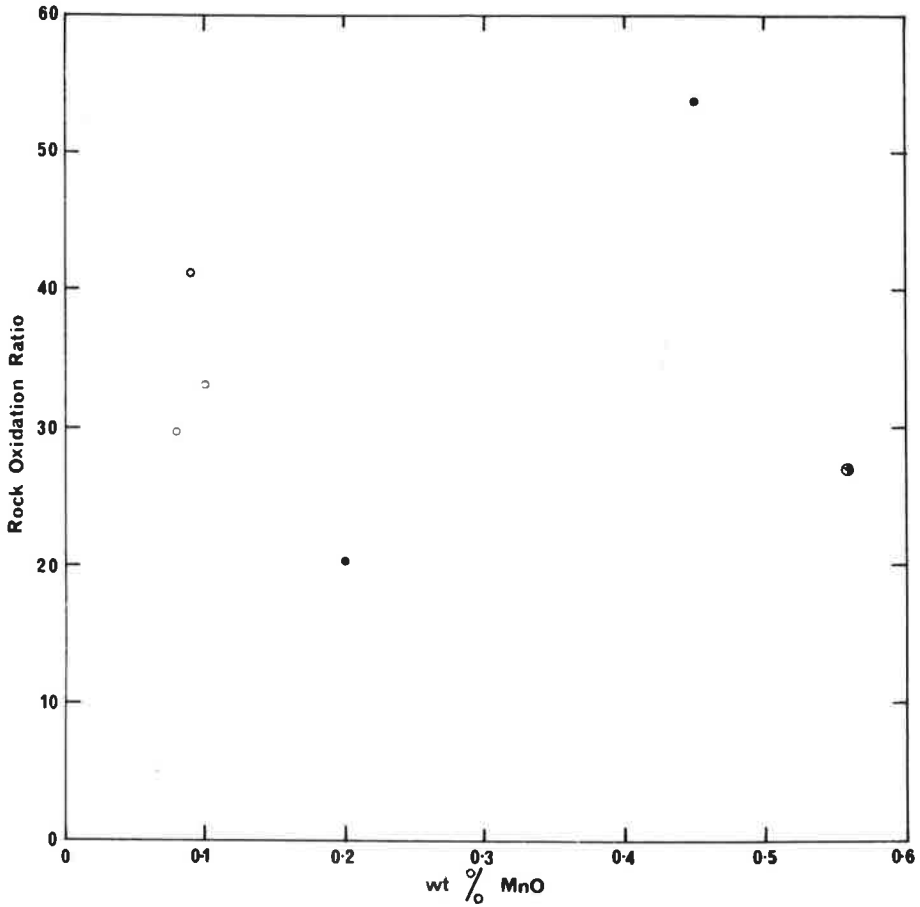
Rock Oxidation Ratio
60
50
40
30
20
10
0
0
0·1
0·2
0·3
0·4
0·5
0·6
wt % MnO

c

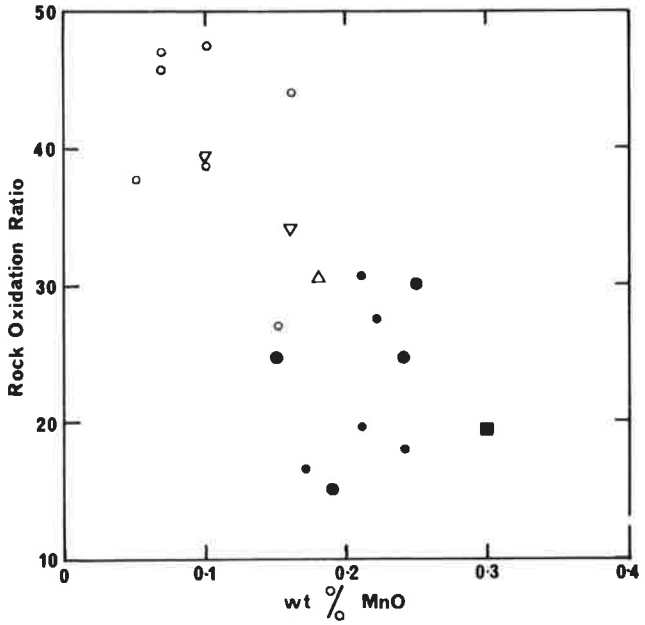
Rock Oxidation Ratio
50
40
30
20
10
0
0·1
0·2
0·3
0·4
wt % MnO

b

FIGURE 4.6

Ternary ACF plots for:

(a) the granulite facies terrain;

(b) the transitional terrain.

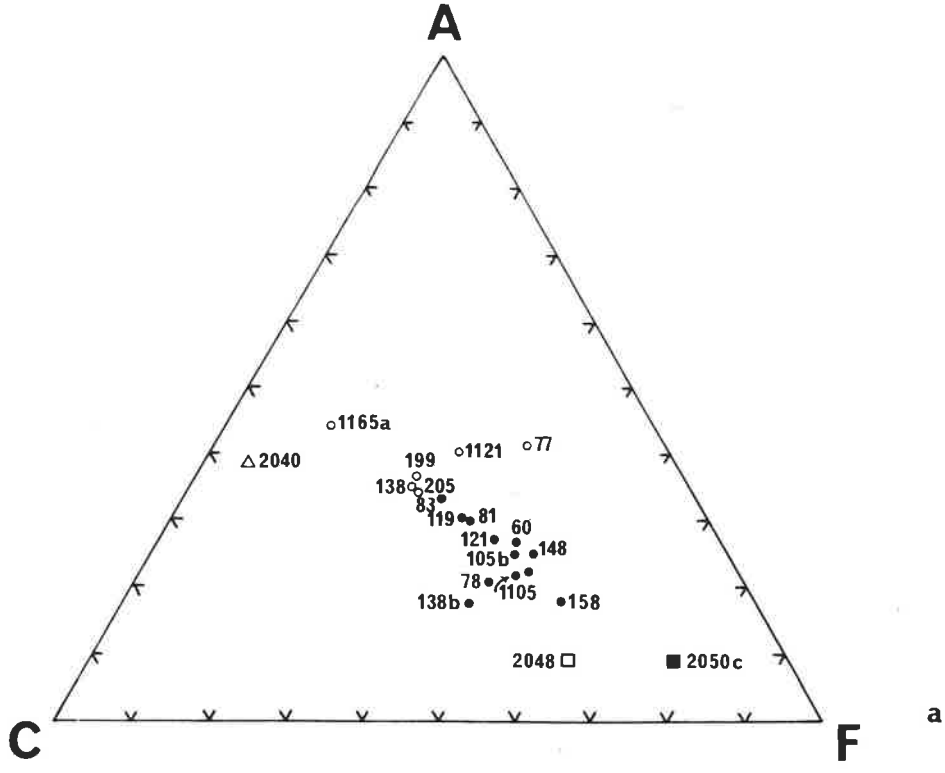
A
C
F
1165a
2040
199
1121
77
138c
205
83
119
81
60
121
148
105b
78
1105
138b
158
2048
2050c

a

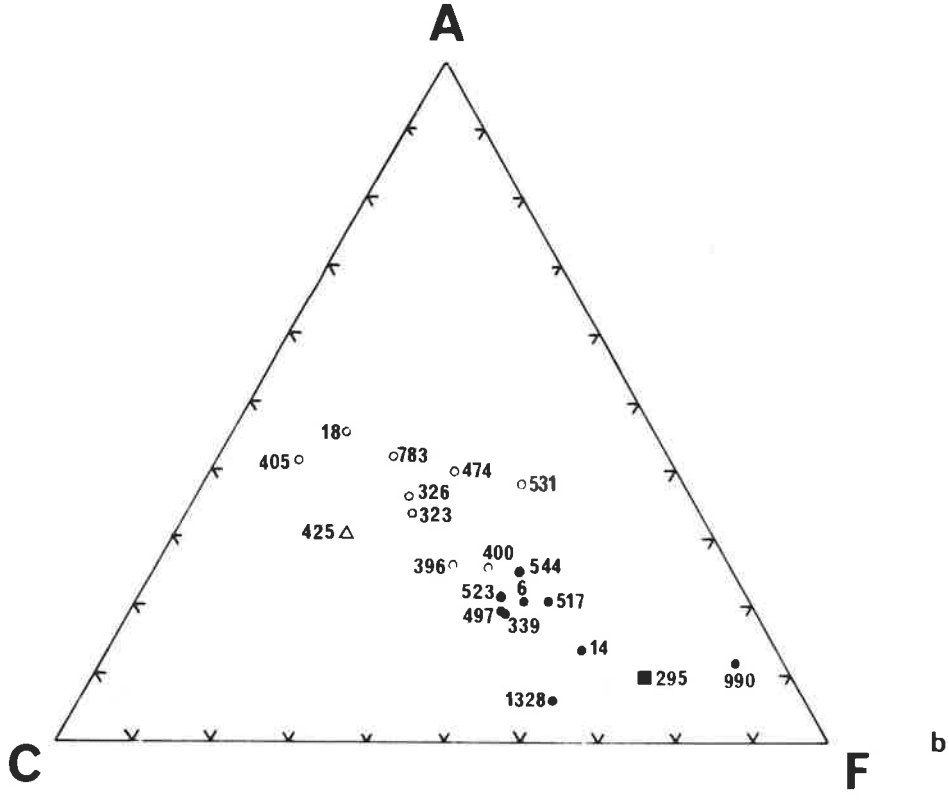
A
C
F
18
405
783
474
531
326
323
425
400
396
544
523
6
517
497
339
14
295
990
1328

b

FIGURE 4.6

Ternary ACF plots for

(c) the amphibolite facies terrain;

(d) the average rocks listed in Table 4.8.

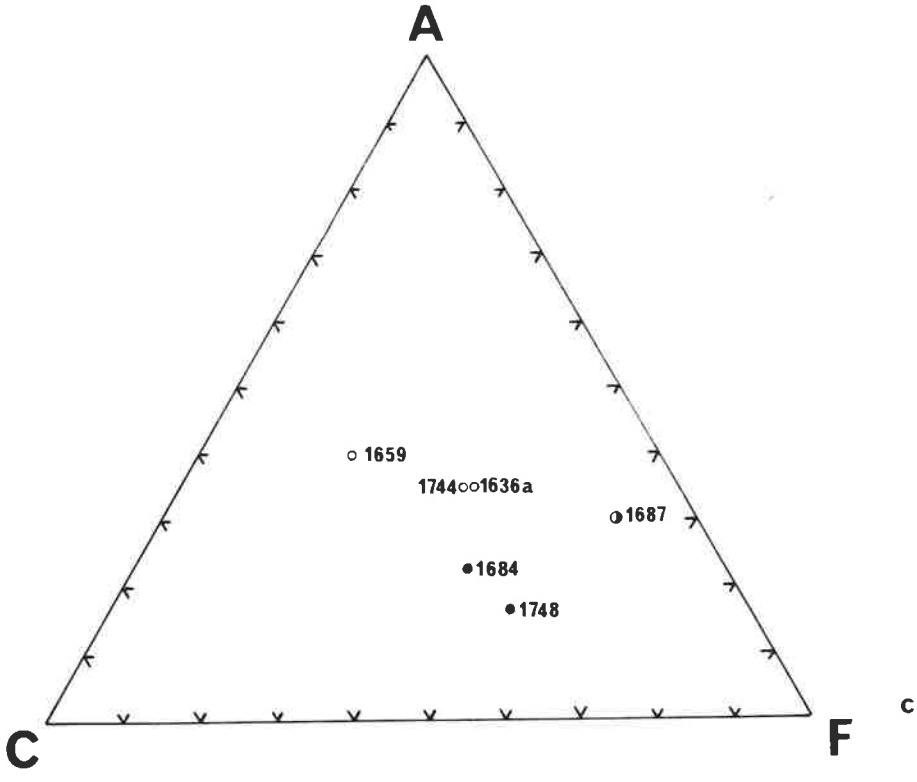

c

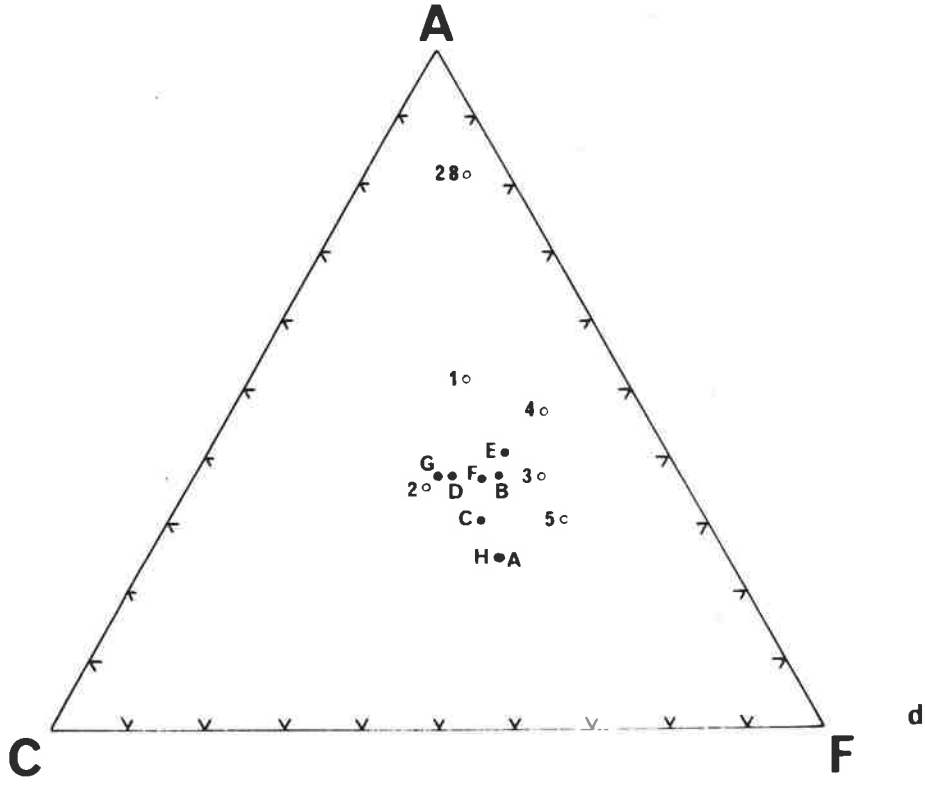

d

FIGURE 4.7

Ternary A.K.F. plots for:

(a) the granulite facies terrain;

(b) the transitional terrain.

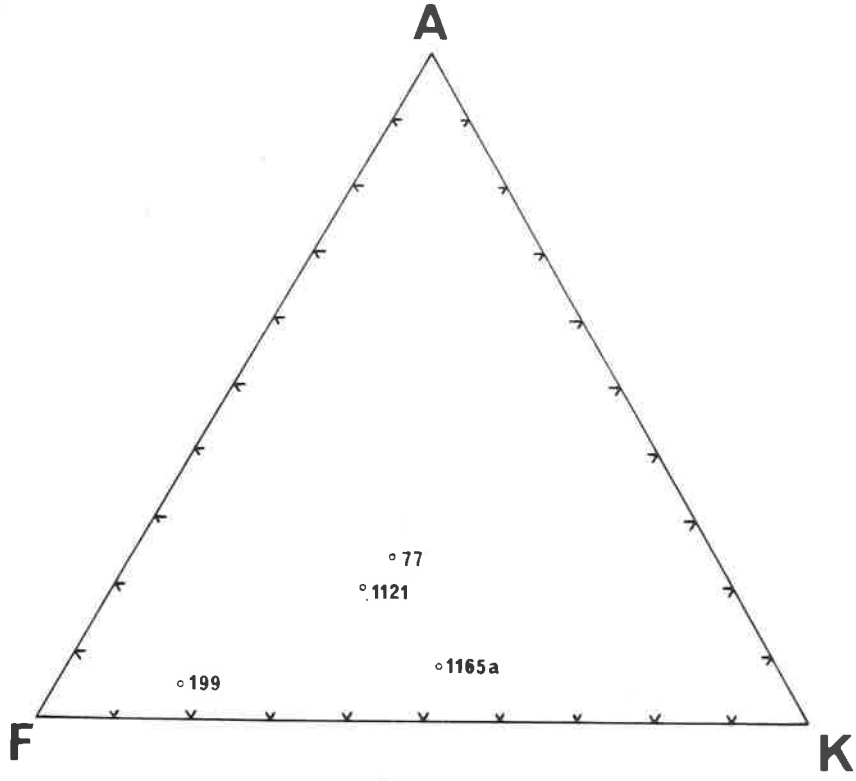

a

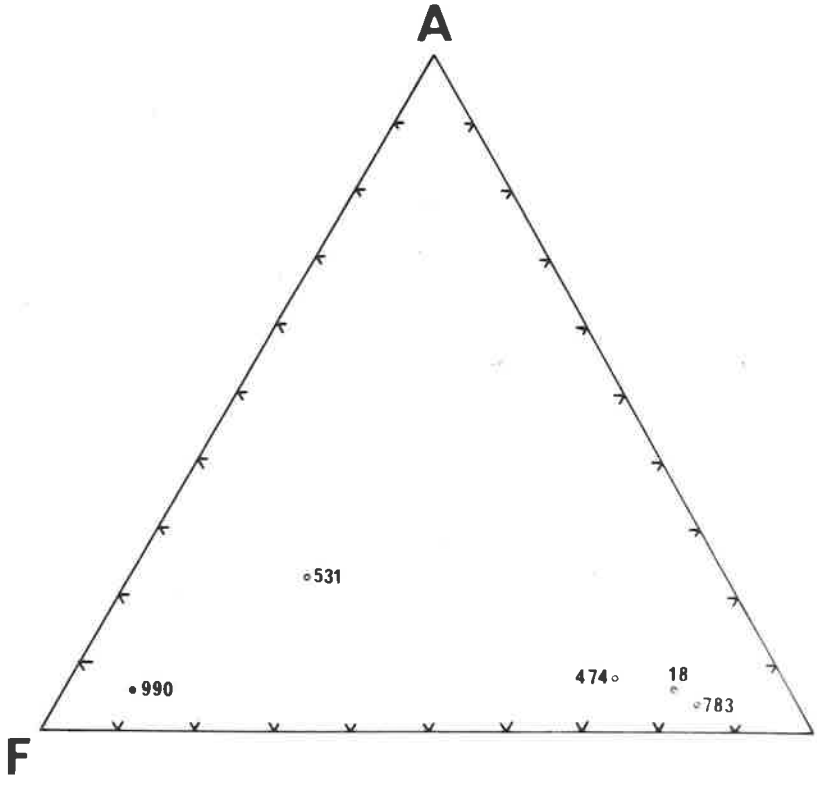

b

FIGURE 4.7

Ternary A.K.F. plots for:

(c) the amphibolite facies terrain;

(d) the average rocks listed in Table 4.8.

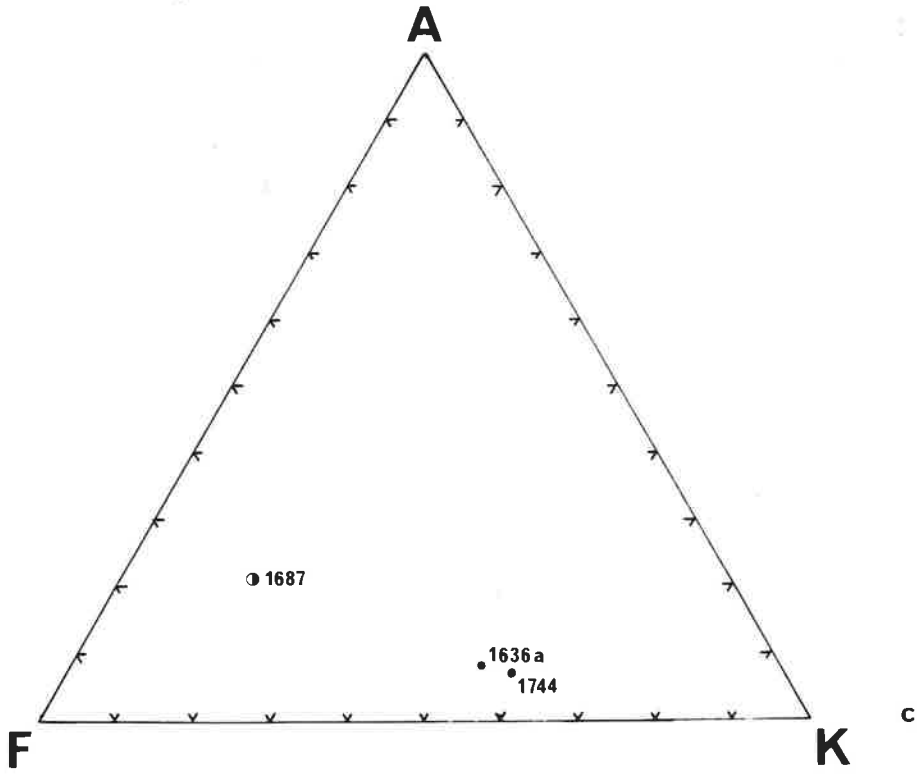

c

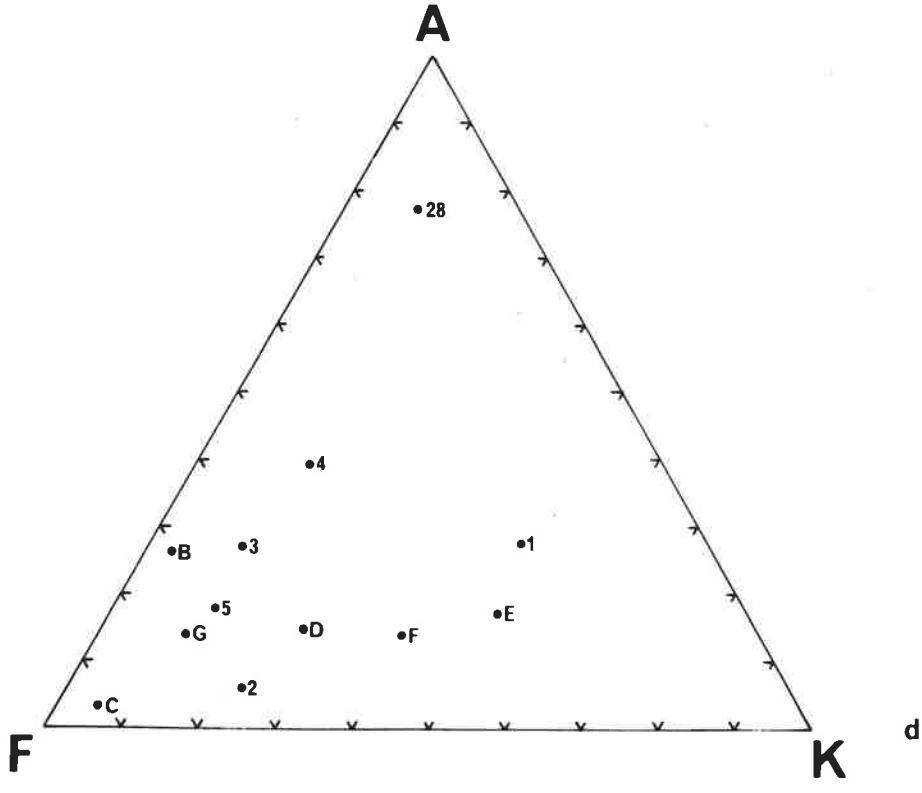

d

FIGURE 4.8

(a) Log-log plots of potassium against rubidium for the granulite facies terrain.

Ornamentation:

open circles	-	quartzo-feldspathic lithologies
closed circles	-	mafic lithologies
square	-	ultramafic lithology

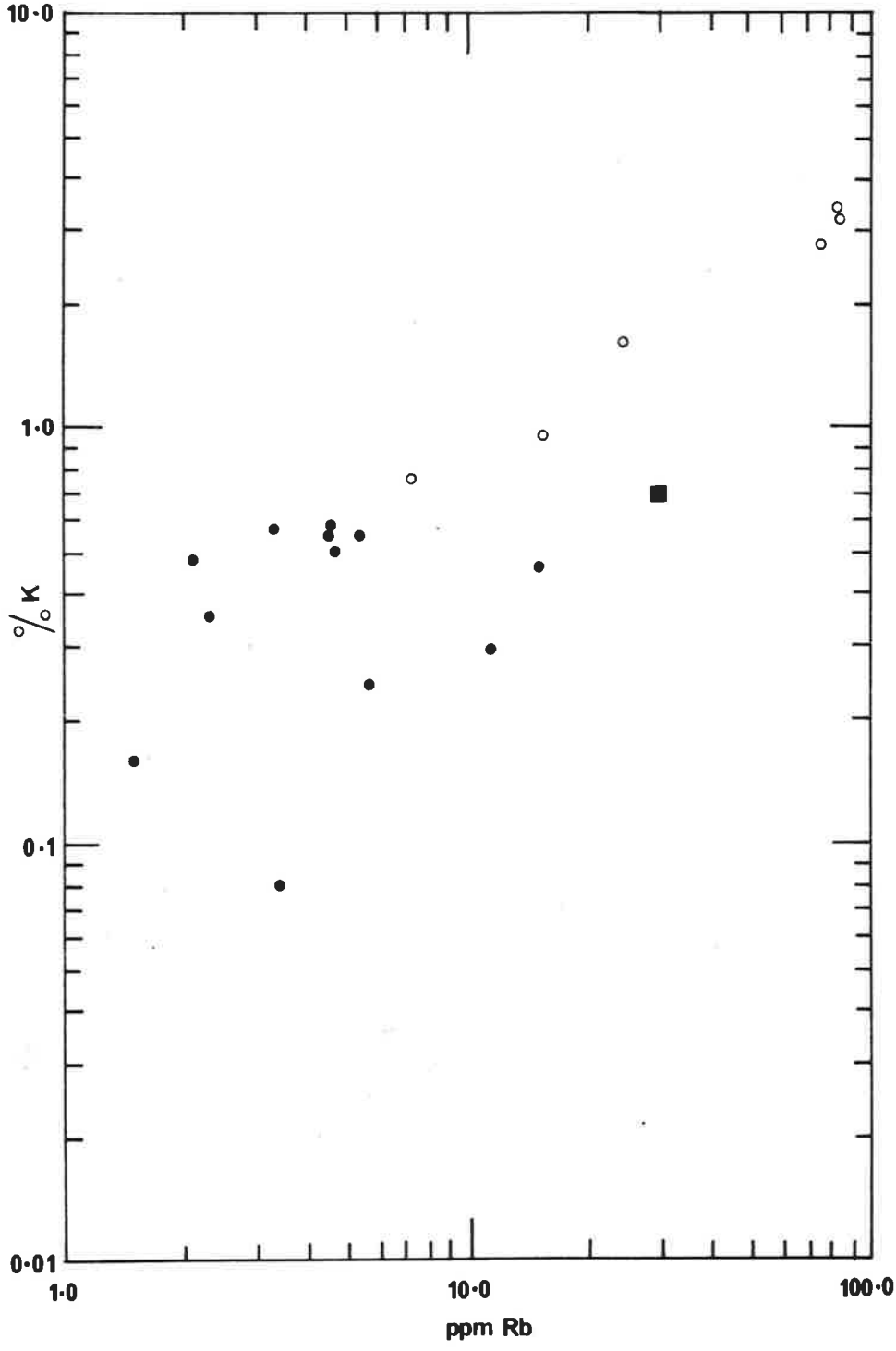

a

FIGURE 4.8

(b) Log-log plot of potassium against rubidium for the transitional terrain.

Ornamentation:

open circles	- quartzo-feldspathic lithologies with $K_2O > Na_2O$
inverted triangle	- quartzo-feldspathic lithologies with $Na_2O > K_2O$
small closed circles	- mica free mafic lithologies
large closed circles	- micaceous mafic lithologies
closed square	- ultramafic lithology.

(c) Log-log plot of potassium against rubidium for the amphibolite facies terrain.

Ornamentation:

open circles	- quartzo-feldspathic lithologies
closed circles	- mafic lithologies
half open circle	- pelitic lithology

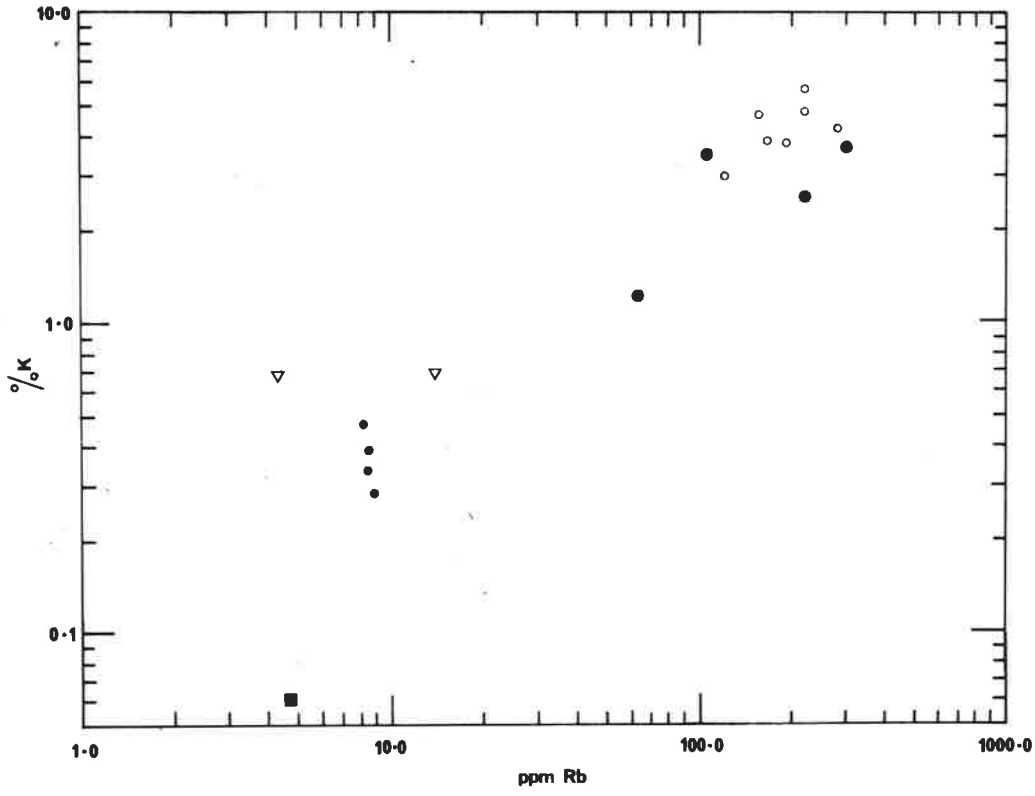
10·0
1·0
0·1
%K
1·0
10·0
100·0
1000·0
ppm Rb

b

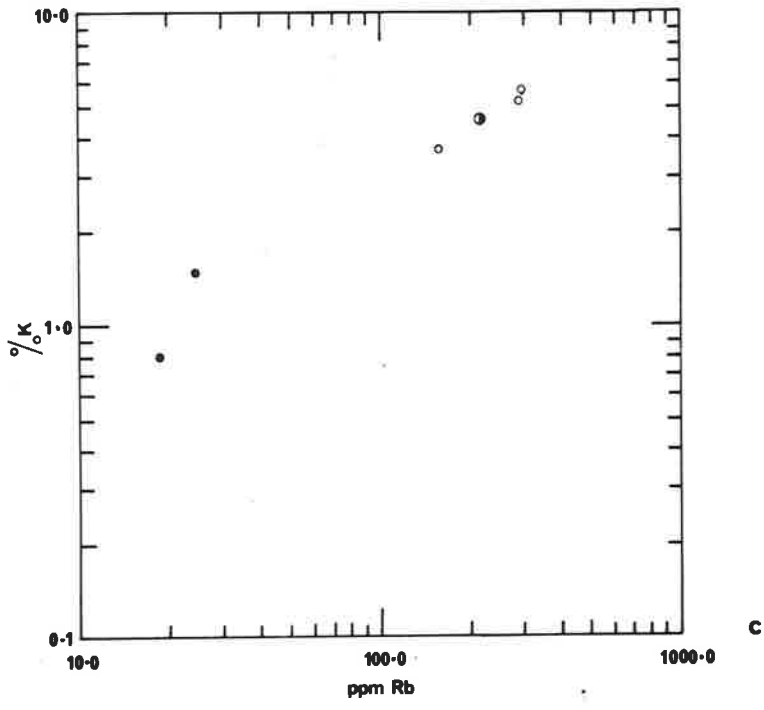
10·0
1·0
0·1
%K
10·0
100·0
1000·0
ppm Rb

c

FIGURE 4.9

(a) K-Rb regression lines for quartzo-feldspathic, mafic and quartzo-feldspathic plus mafic granulites.

(b) K-Rb reduced major axes for:

A. quartzo-feldspathic granulites

B. mafic granulites

C. quartzo-feldspathic plus mafic granulites.

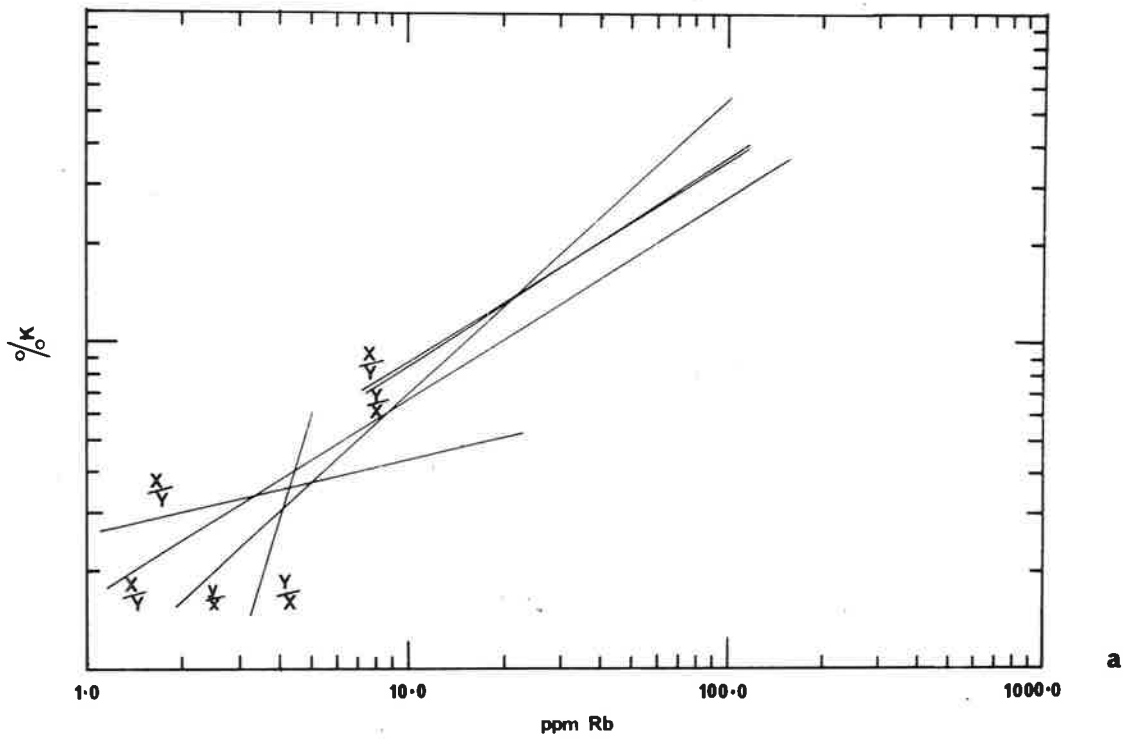
%K
X/Y
Y/X
X/Y
Y/X
X/Y
Y/X
1·0
10·0
100·0
1000·0
ppm Rb

a

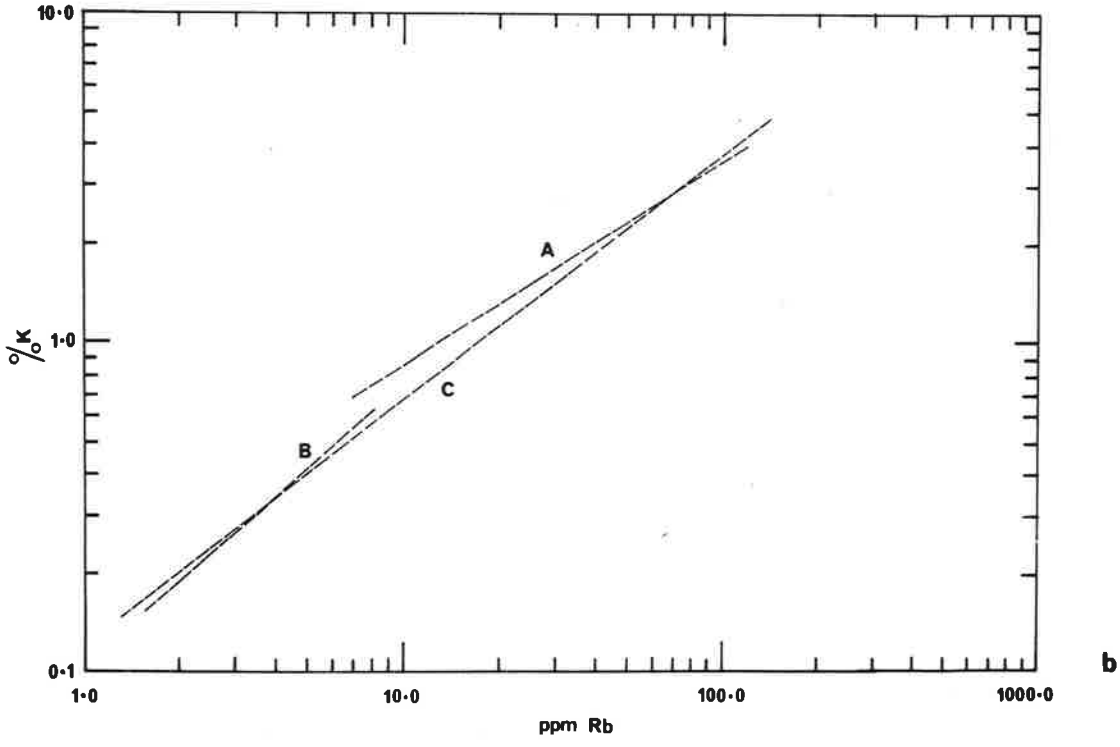
10·0
%K
1·0
0·1
A
B
C
1·0
10·0
100·0
1000·0
ppm Rb

b

FIGURE 4.9

(c) K-Rb regression lines for transitional terrain.

(d) K-Rb reduced major axes for transitional terrain.

A. quartzo-feldspathic lithologies
B. total population
C. mica free mafic lithologies
D. micaceous mafic lithologies
E. total population of mafic lithologies.

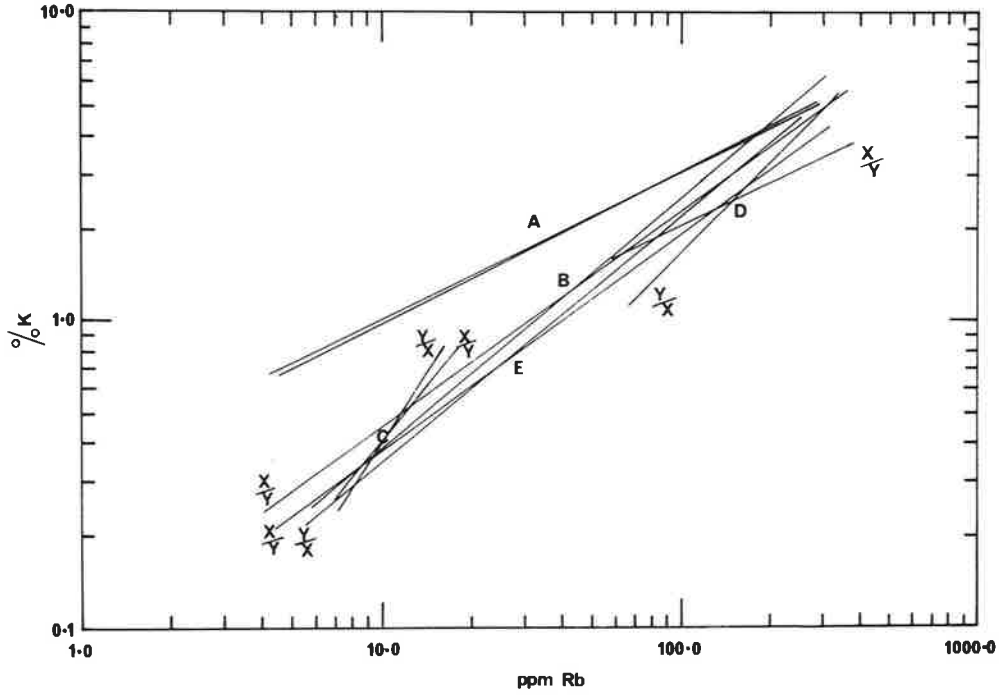
10·0
1·0
0·1
%K
1·0
10·0
100·0
1000·0
ppm Rb
A
B
C
D
E
X/Y
Y/X

c

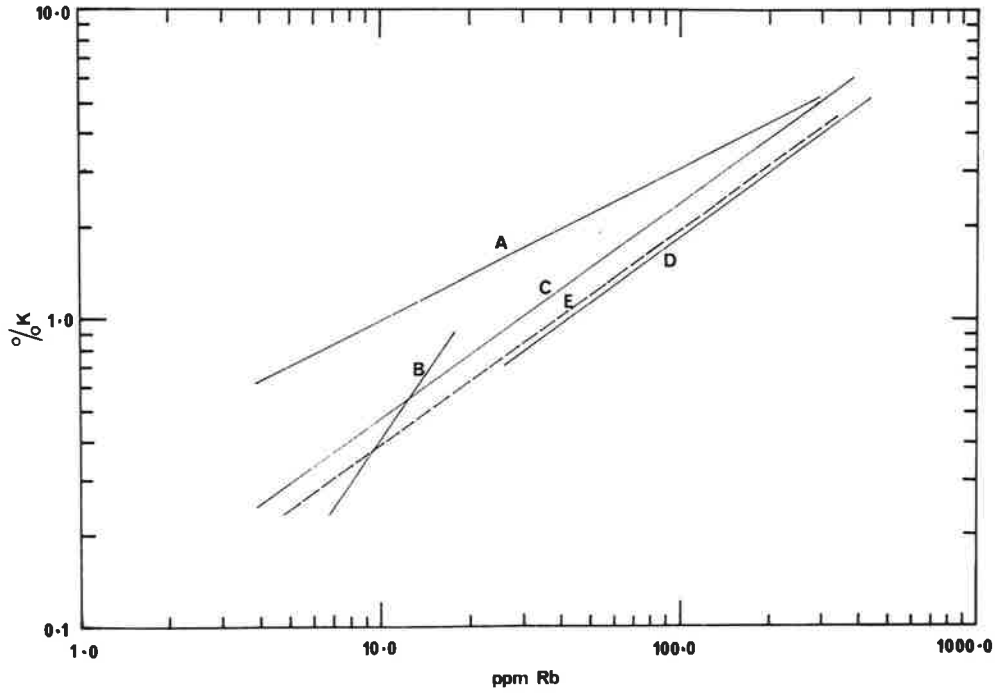
10·0
1·0
0·1
%K
1·0
10·0
100·0
1000·0
ppm Rb
A
B
C
D
E

d

FIGURE 4.10

(a) K-Rb reduced major axes for the total populations of quartzo-feldspathic and mafic lithologies from the granulite facies, transitional and amphibolite facies terrains.

(b) K-Rb reduced major axes for data from other high grade metamorphic terrains.

A. Granulite facies paragneiss
B. Amphibolite facies paragneiss
C.

} Adirondack Mountains (after Whitney, 1969)

a amphibolite facies
g granulite facies

} Valle Strona (after Sighinolfi, 1969)

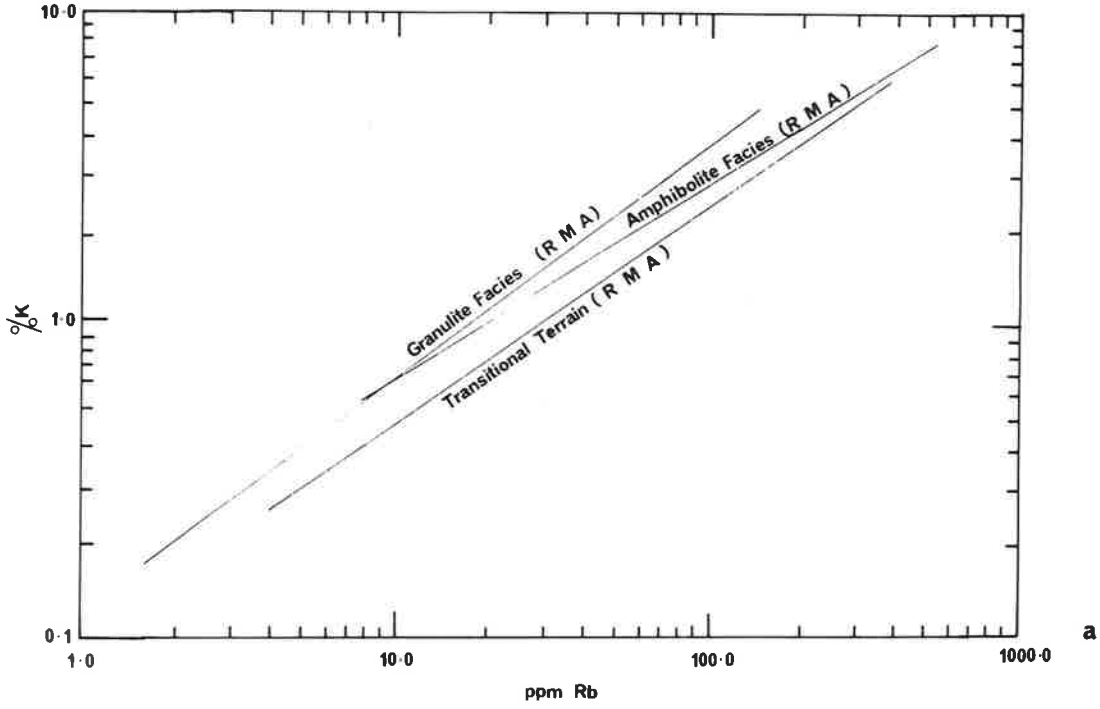
10·0
1·0
0·1
%K
1·0
10·0
100·0
1000·0
ppm Rb
Granulite Facies (R M A)
Amphibolite Facies (R M A)
Transitional Terrain (R M A)

a

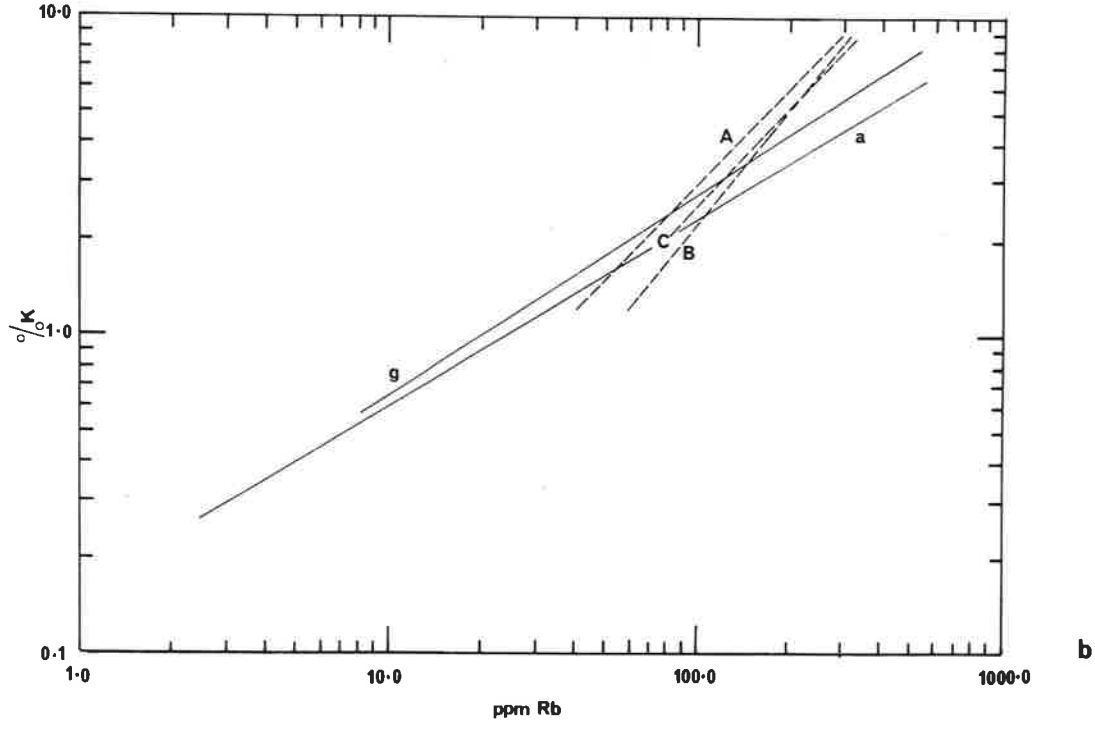
10·0
1·0
0·1
%K
1·0
10·0
100·0
1000·0
ppm Rb
A
a
C
B
g

b

FIGURE 4.11

(a) K/Rb ratio against potassium for the granulite facies terrain.

Ornamentation:

open circles	- quartzo-feldspathic granulites
closed circles	- mafic granulites
square	- ultramafic granulite.

(b) K/Rb ratio against potassium for the transitional terrain.

Ornamentation:

open circles	- quartzo-feldspathic lithologies
small closed circles	- mica free mafic lithologies
large closed circles	- micaceous mafic lithologies
square	- ultramafic lithology

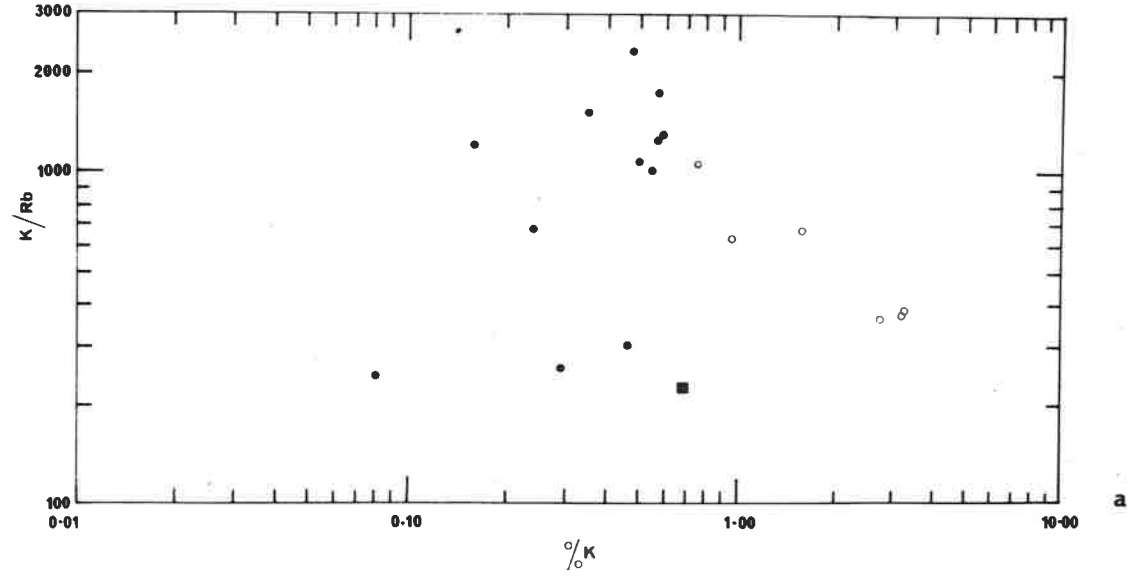
3000
2000
1000
100
K/Rb
0·01
0·10
1·00
10·00
%K

a

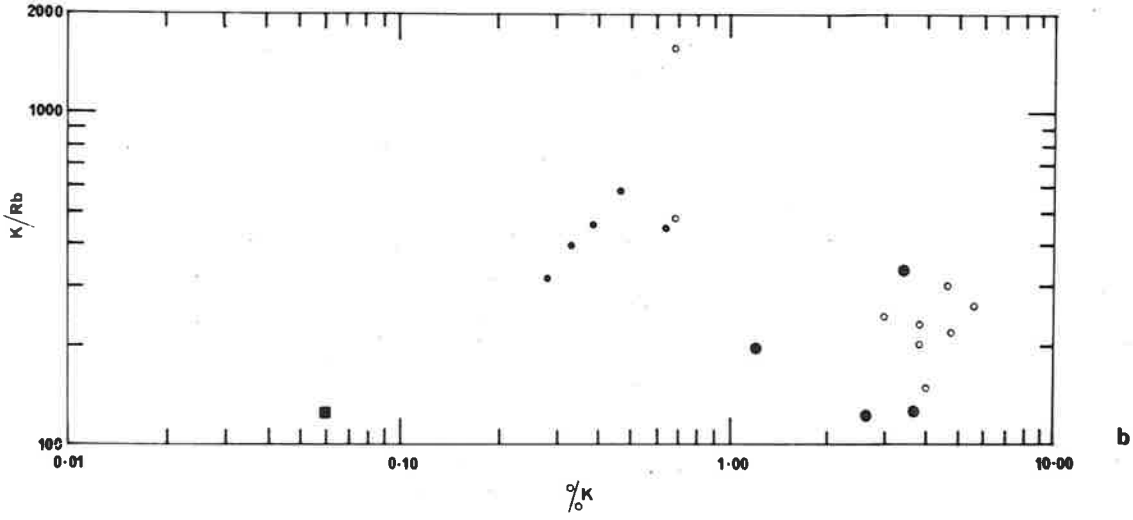
2000
1000
100
K/Rb
0·01
0·10
1·00
10·00
%K

b

FIGURE 4.11

(c) K/Rb ratio against potassium for the amphibolite facies terrain.

Ornamentation:

open circles - quartzo-feldspathic lithologies
closed circles - mafic lithologies
half open circle - pelitic lithology

(d) K/Rb ratio against potassium for selected feldspars from:

Granulite Facies

open circles - Ceylon
small closed circles - Musgrave Ranges
large closed circles - Broken Hill

Amphibolite Facies

square - Pewsey Vale)
plus sign - Springton) Mount Lofty Ranges
triangle - Palmer)

(data from Virgo, 1966)

cross - basic igneous rock
diamond - anorthosites

(data from Murthy and Griffin, 1970)

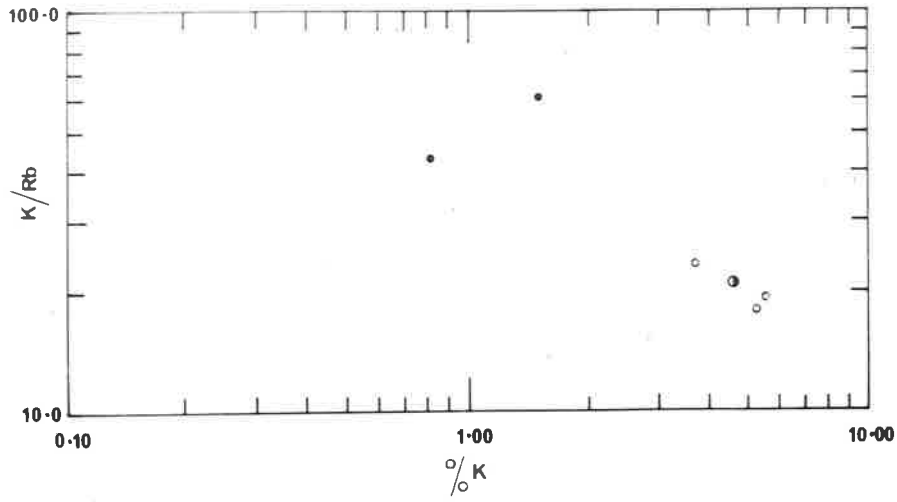
100·0
10·0
K/Rb
0·10
1·00
10·00
%K

c

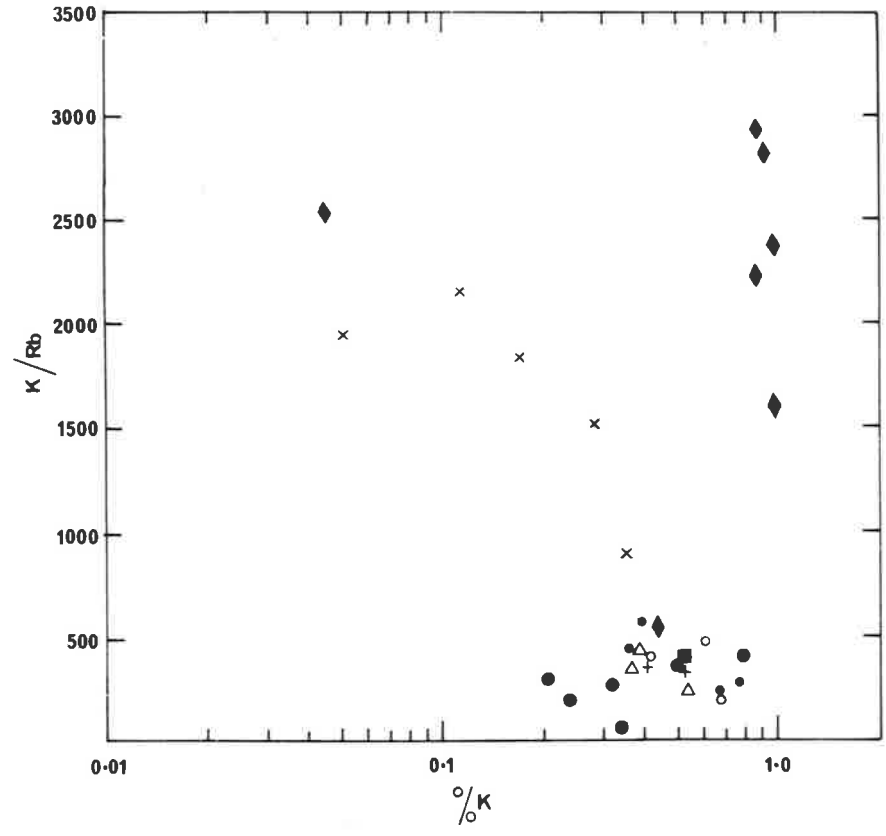
3500
3000
2500
2000
1500
1000
500
K/Rb
0·01
0·1
1·0
%K

d

FIGURE 4.12

(a) Rb-Sr relationships in the granulite facies terrain.

Ornamentation:

open circles	- quartzo-feldspathic granulites with K_2O > Na_2O
inverted triangles	- quartzo-feldspathic granulites with Na_2O > K_2O
closed circles	- mafic granulites
square	- ultramafic granulite

(b) Rb-Sr relationships in the transitional terrain.

Ornamentation:

open circles	- quartzo-feldspathic lithologies with K_2O > Na_2O
inverted triangles	- quartzo-feldspathic lithologies with Na_2O > K_2O
small closed circles	- mica free mafic lithologies
large closed circles	- micaceous mafic lithologies
square	- ultramafic lithology.

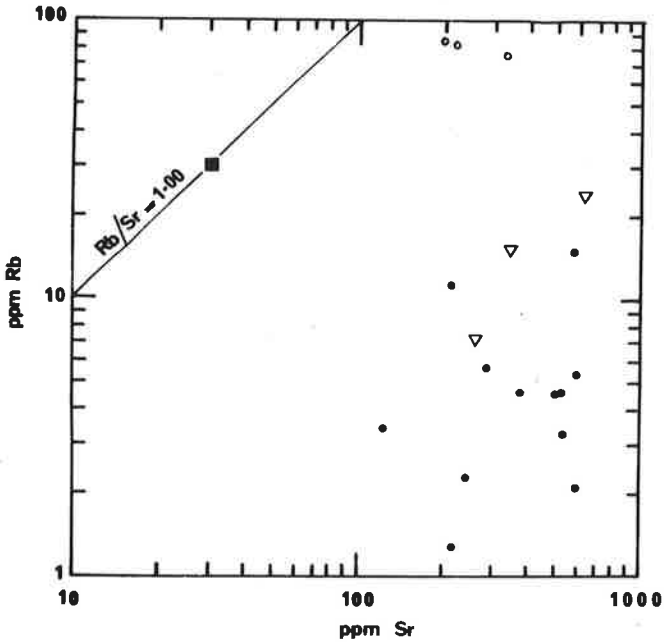
100
10
1
10
100
1000
ppm Rb
ppm Sr
Rb/Sr = 1·00

a

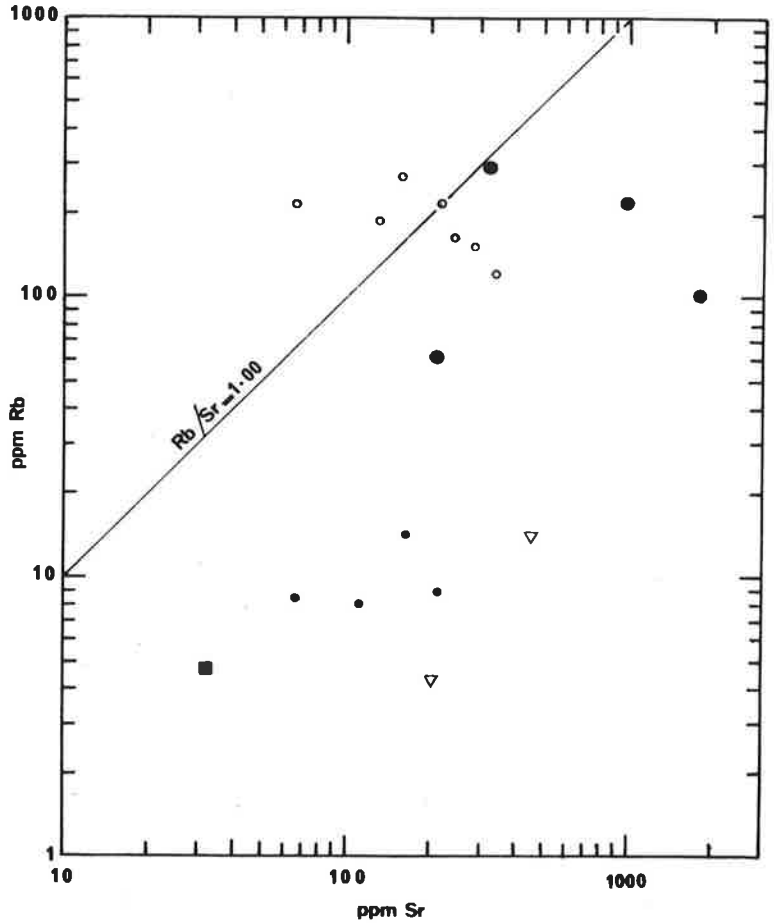
1000
100
10
1
10
100
1000
ppm Rb
ppm Sr
Rb/Sr = 1·00

b

FIGURE 4.12

(c) Rb-Sr relationships in the amphibolite facies terrain.

Ornamentation:
(same as in Figure 4.11c)

(d) Potassium against Rb/Sr ratio for the amphibolite facies terrain.

(e) Calcium against Rb/Sr ratio for the amphibolite facies terrain.

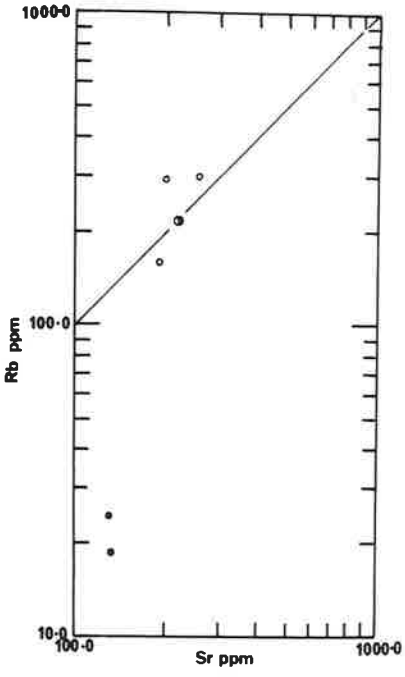
1000·0
100·0
10·0
Rb ppm
100·0
Sr ppm
1000·0

c

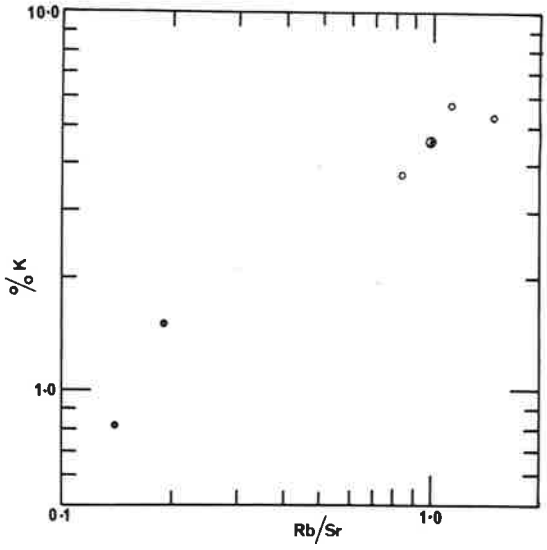
10·0
1·0
0·1
% K
Rb/Sr
1·0

d

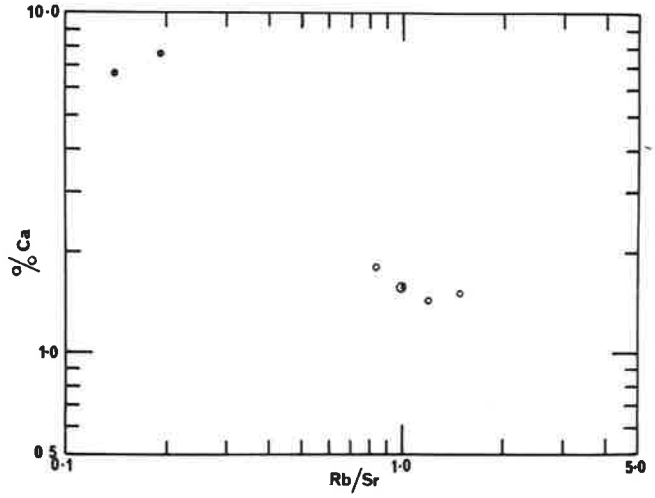
10·0
1·0
0·5
% Ca
0·1
Rb/Sr
1·0
5·0

e

FIGURE 4.12

(f) Potassium against Rb/Sr ratio for the granulite facies terrain.

Ornamentation:

open circles - quartzo-feldspathic granulites

closed circles - mafic granulites

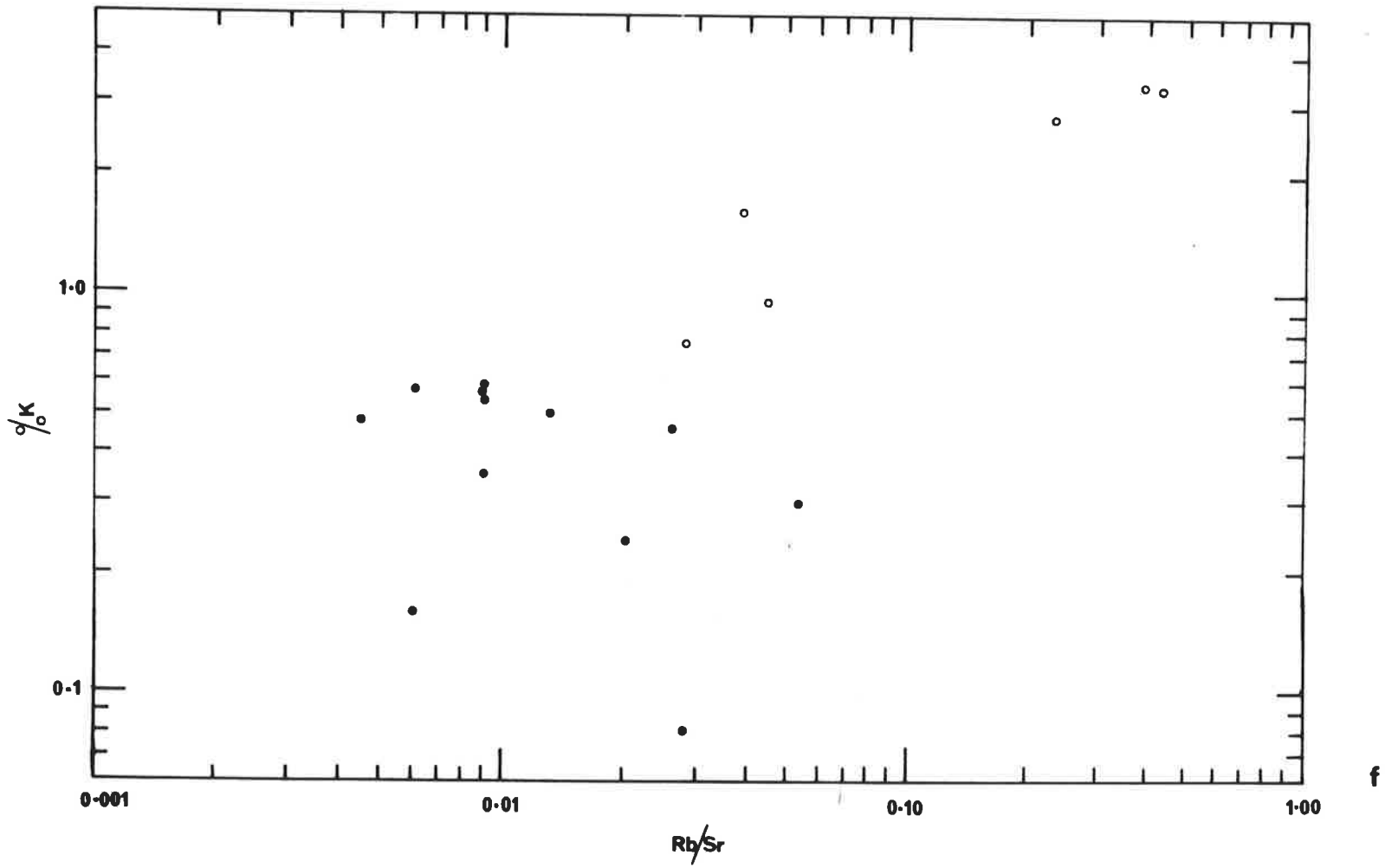

f

FIGURE 4.12

(g) Potassium against Rb/Sr ratio for the transitional terrain.

Ornamentation:

(same as in Figure 4.12b)

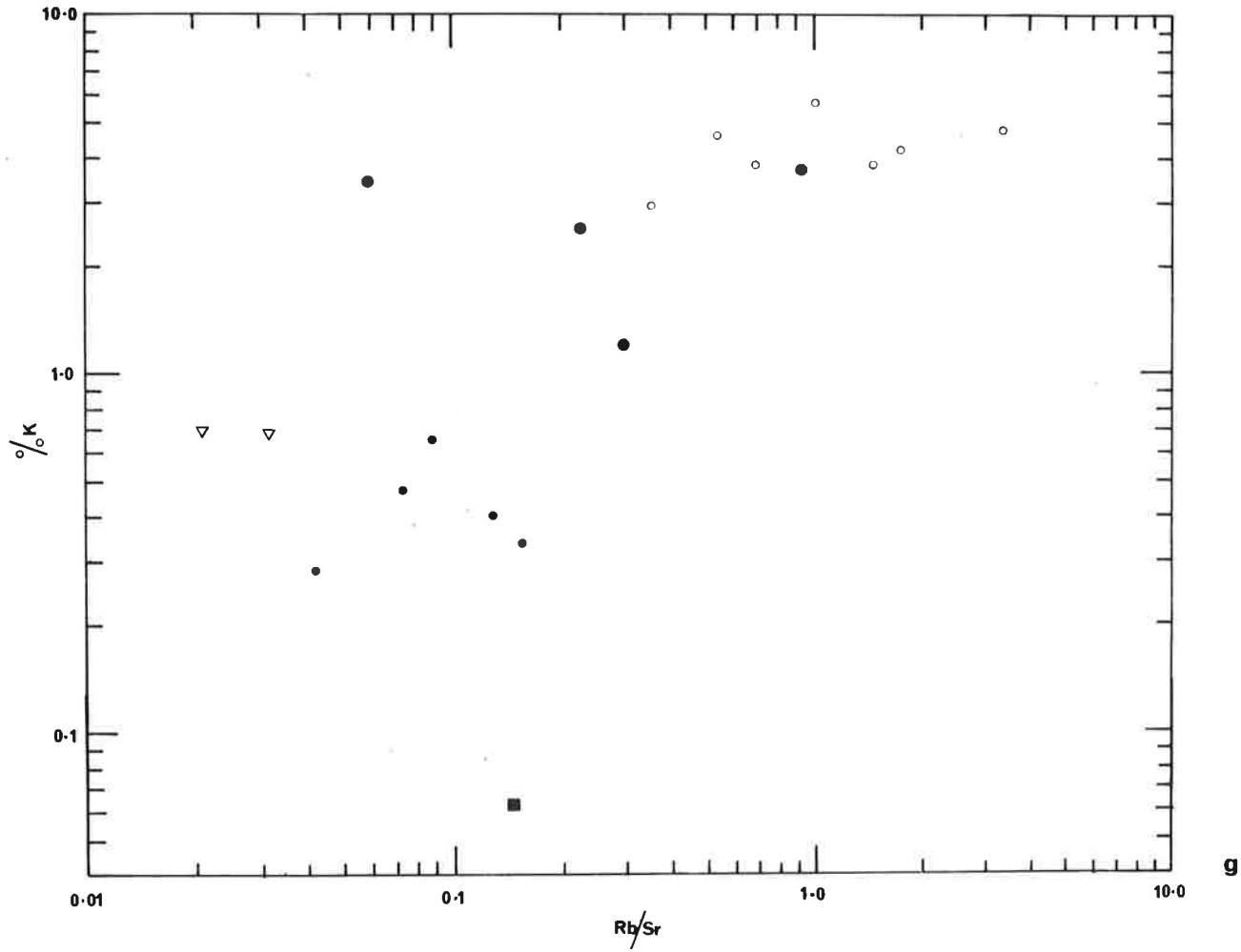

g

FIGURE 4.12

Calcium against Rb/Sr ratio for the:

(h) granulite facies terrain;

(i) transitional terrain.

Ornamentation:

Open circles - quartzo-feldspathic lithologies

Closed circles - mafic lithologies

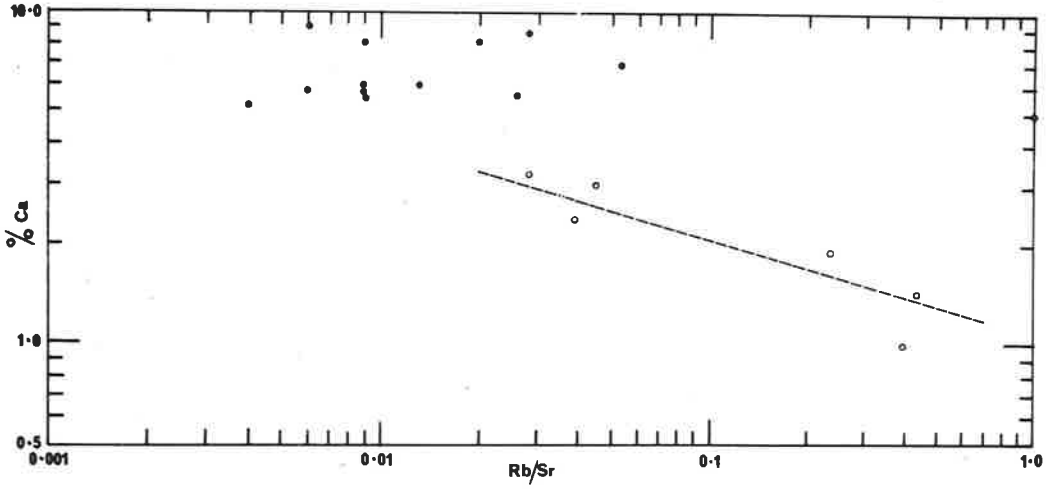

h

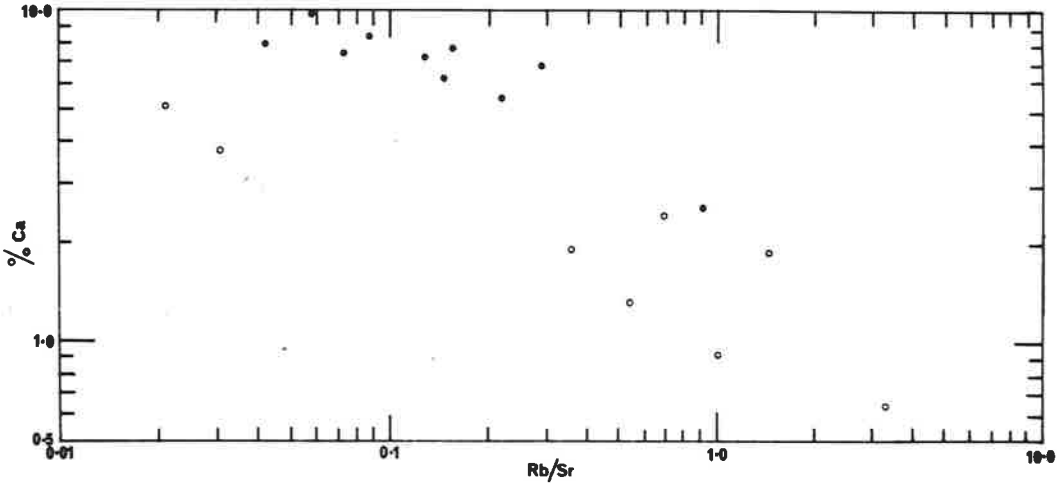

i

FIGURE 4.13

Titanium against Ti/Zr ratio for the:

(a) granulite facies terrain;

(b) transitional terrain;

(c) amphibolite facies terrain.

Ornamentation:

small open circles	- quartzo-feldspathic lithologies
small closed circles	- mica free mafic lithologies
large closed circles	- micaceous mafic lithologies
square	- ultramafic lithology
triangle	- calc silicate lithology
half open circle	- pelitic lithology

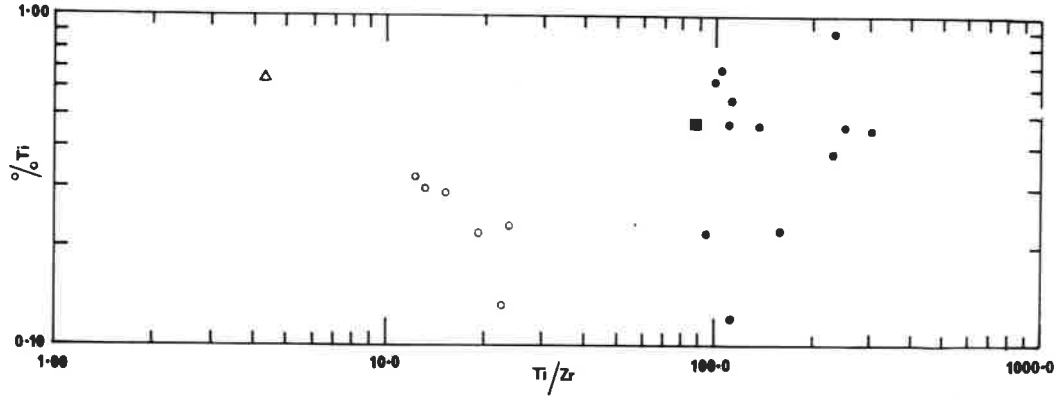
1·00
0·10
%Ti
1·00
10·0
100·0
1000·0
Ti/Zr

a

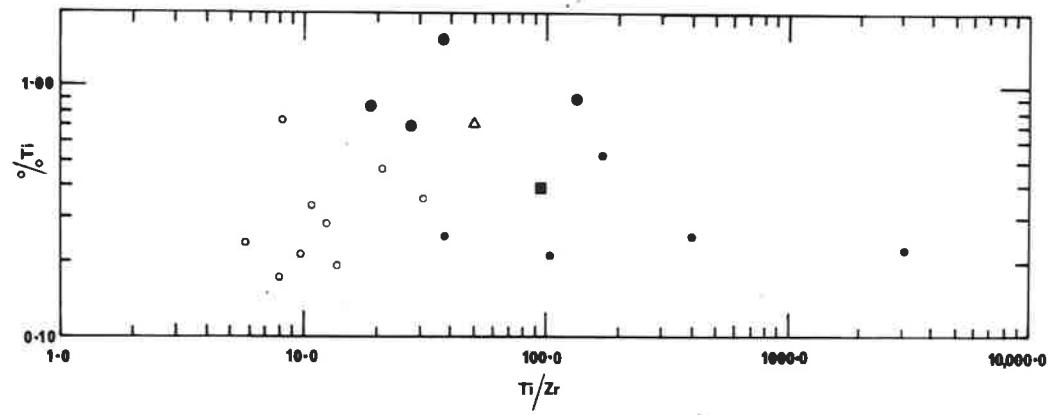
1·00
0·10
%Ti
1·0
10·0
100·0
1000·0
10,000·0
Ti/Zr

b

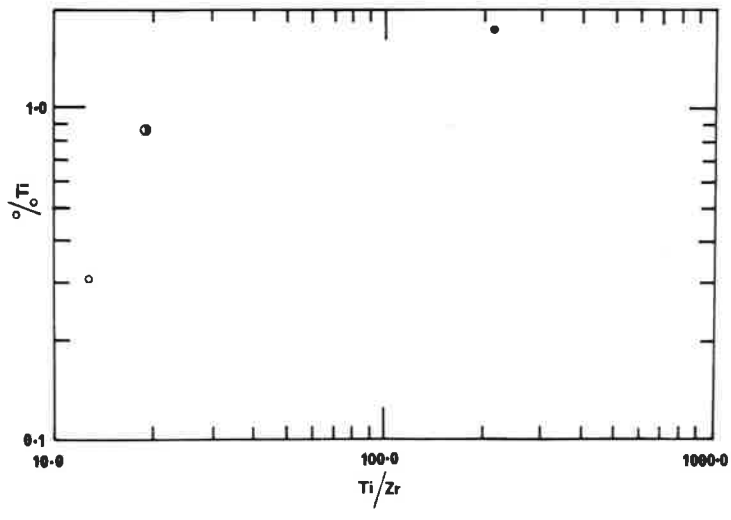
1·0
0·1
%Ti
10·0
100·0
1000·0
Ti/Zr

c

FIGURE 4.14

(a) La-Ce relationship for the Amata rocks.

(b) Zr-(La+Ce) relationship for the Amata rocks.

Ornamentation:

closed circles - granulite facies terrain
open circles - transitional terrain
squares - amphibolite facies terrain

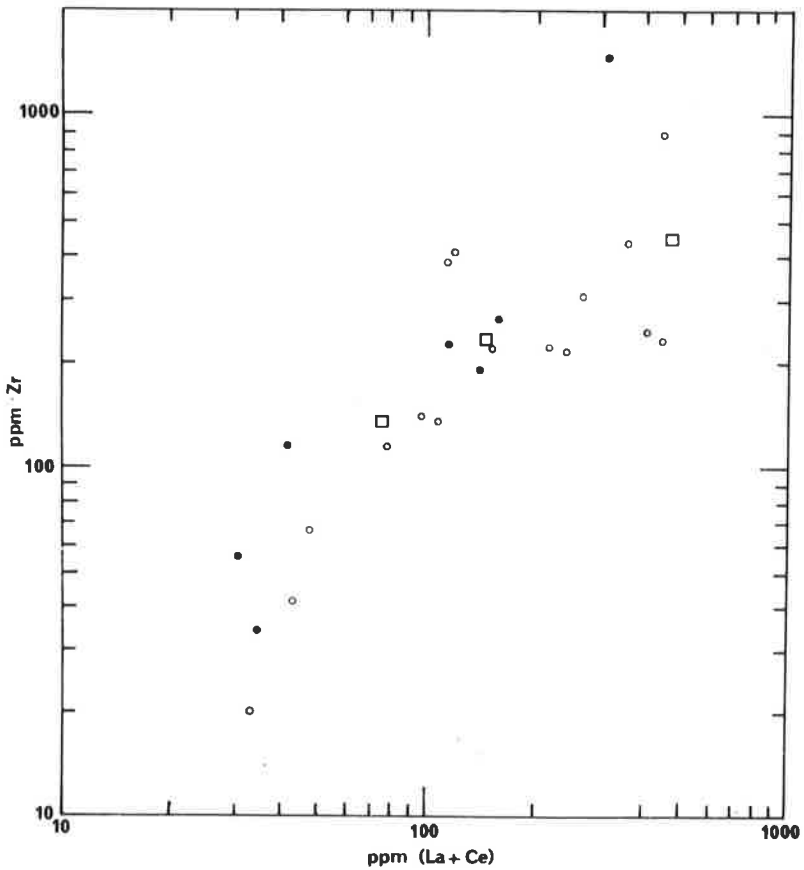
1000
100
10
10
100
1000
ppm Zr
ppm (La + Ce)

b

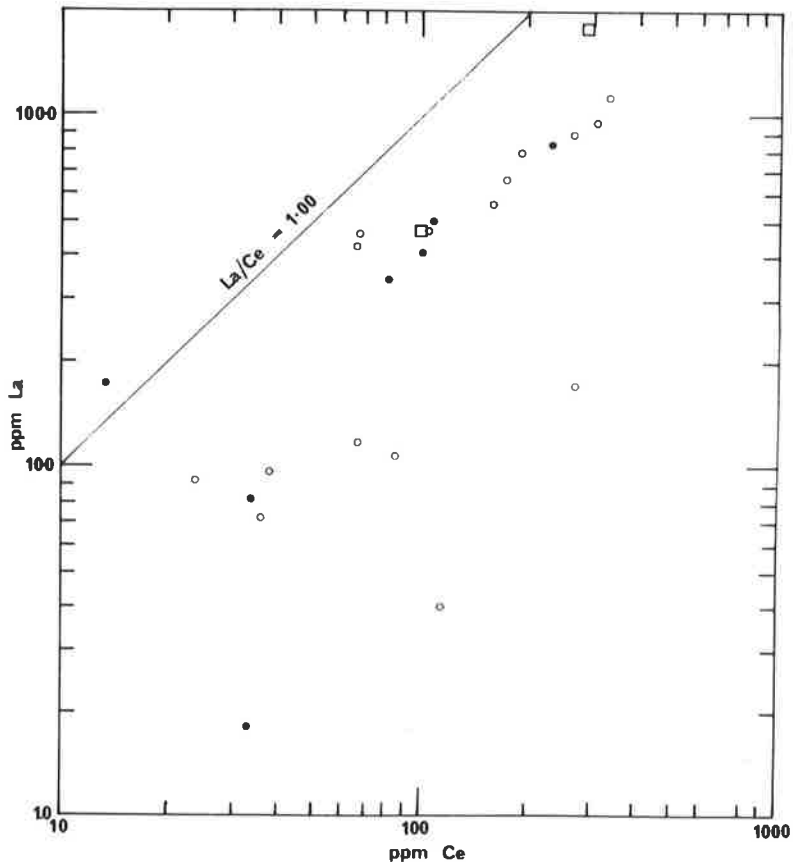
La/Ce = 1·00
1000
100
10
10
100
1000
ppm La
ppm Ce

a

FIGURE 4.15

(a) Th-K relationship for the granulite facies terrain lithologies.

Ornamentation:

small open circles - quartzo-feldspathic
small closed circles - mafic
triangle - calc silicate

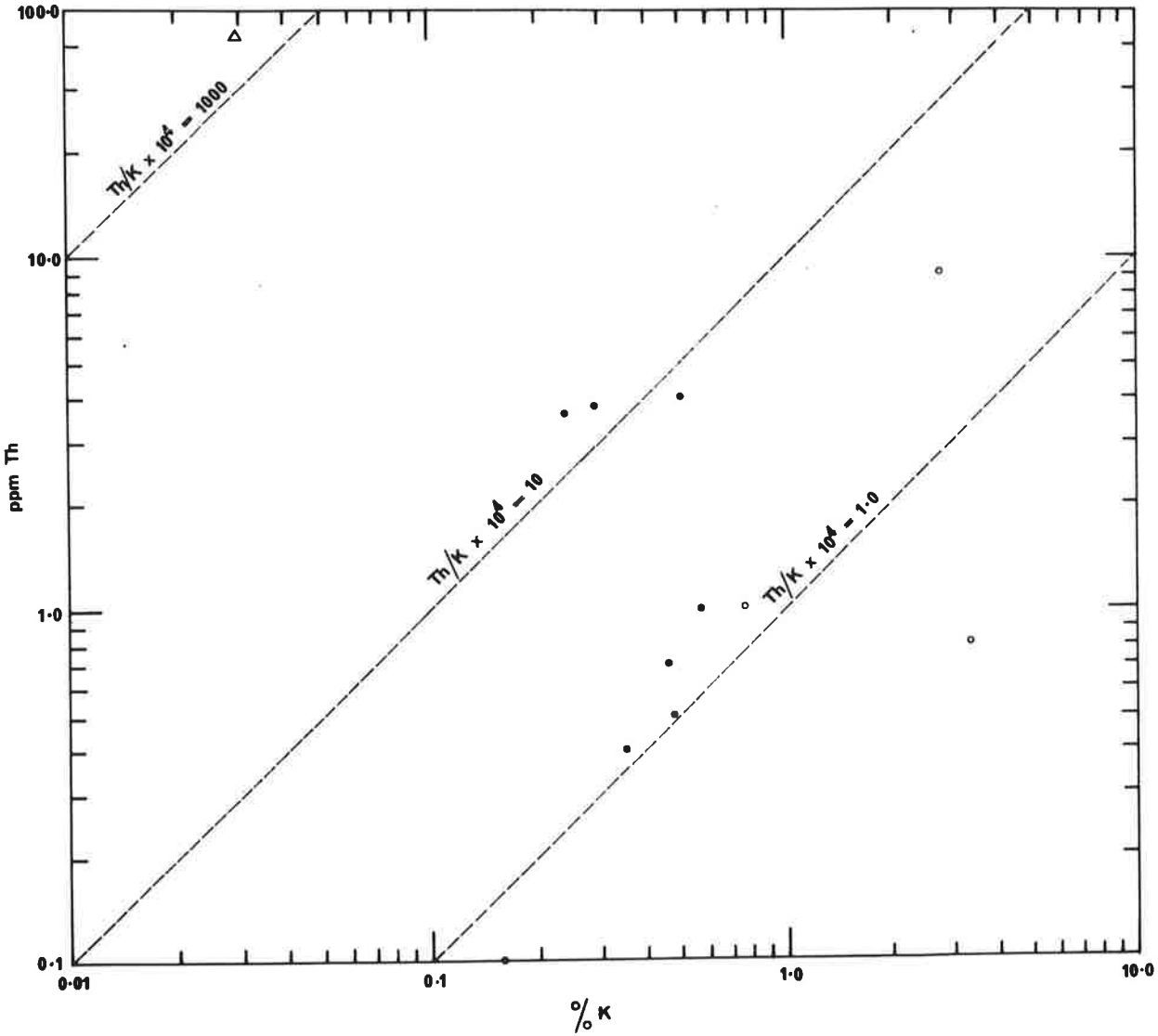
100·0
10·0
1·0
0·1
ppm Th
0·01
0·1
1·0
10·0
% K
Th/K x 10⁴ = 1000
Th/K x 10⁴ = 10
Th/K x 10⁴ = 1·0

FIGURE 4.15

(b) Th-K relationship for the transitional terrain lithologies.

Ornamentation:

small open circles - quartzo-feldspathic rocks
small closed circles - mica free mafic rocks
large closed circles - micaceous mafic rocks
square - ultramafic rock
triangle - calc silicate rock

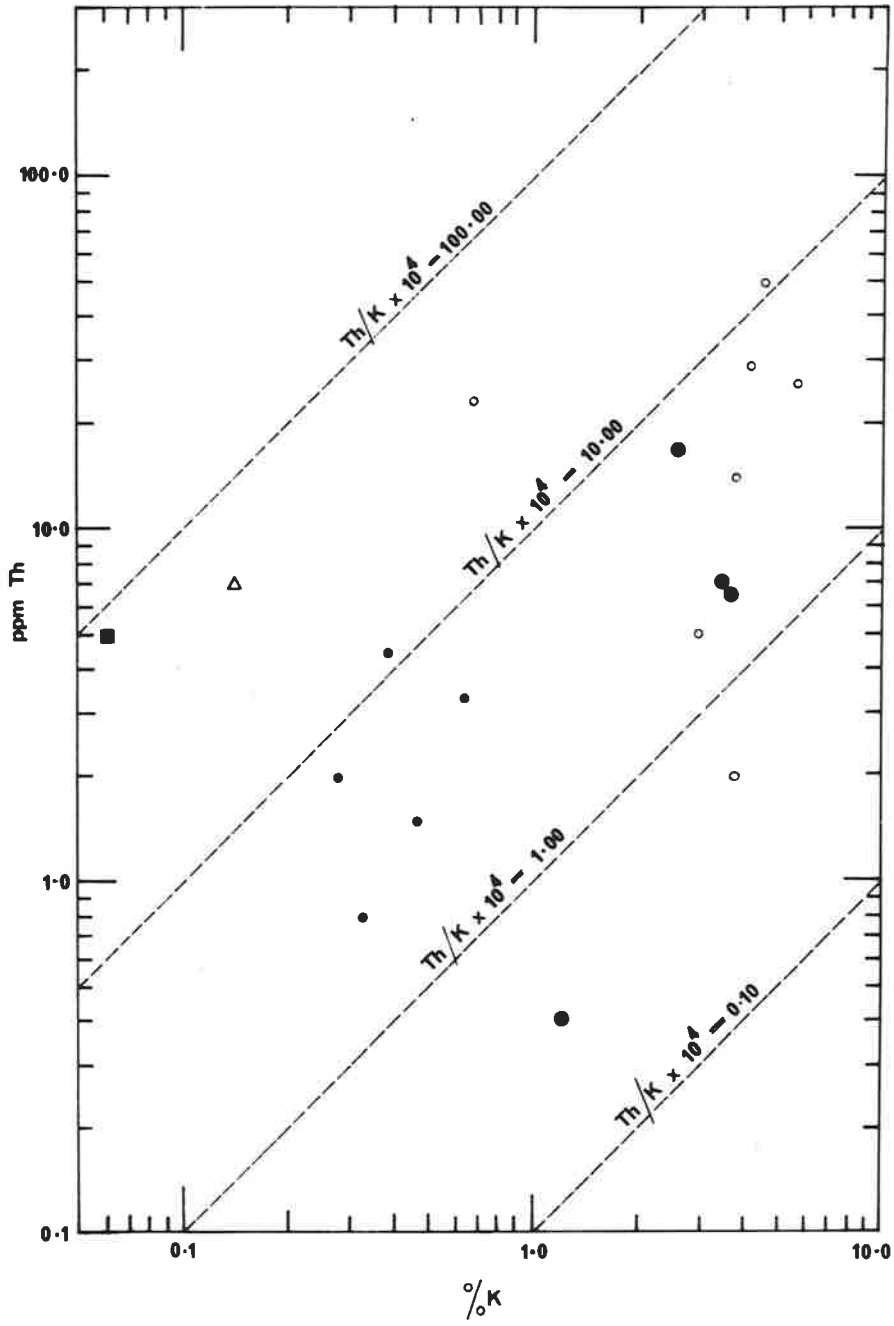
100·0
10·0
1·0
0·1
ppm Th
0·1
1·0
10·0
%K
Th/K x 10⁴ = 100·00
Th/K x 10⁴ = 10·00
Th/K x 10⁴ = 1·00
Th/K x 10⁴ = 0·10

FIGURE 4.15

(c) Th-K relationship for the amphibolite facies terrain lithologies.

Ornamentation:

open circles - quartzo-feldspathic lithologies

closed circles - mafic lithologies

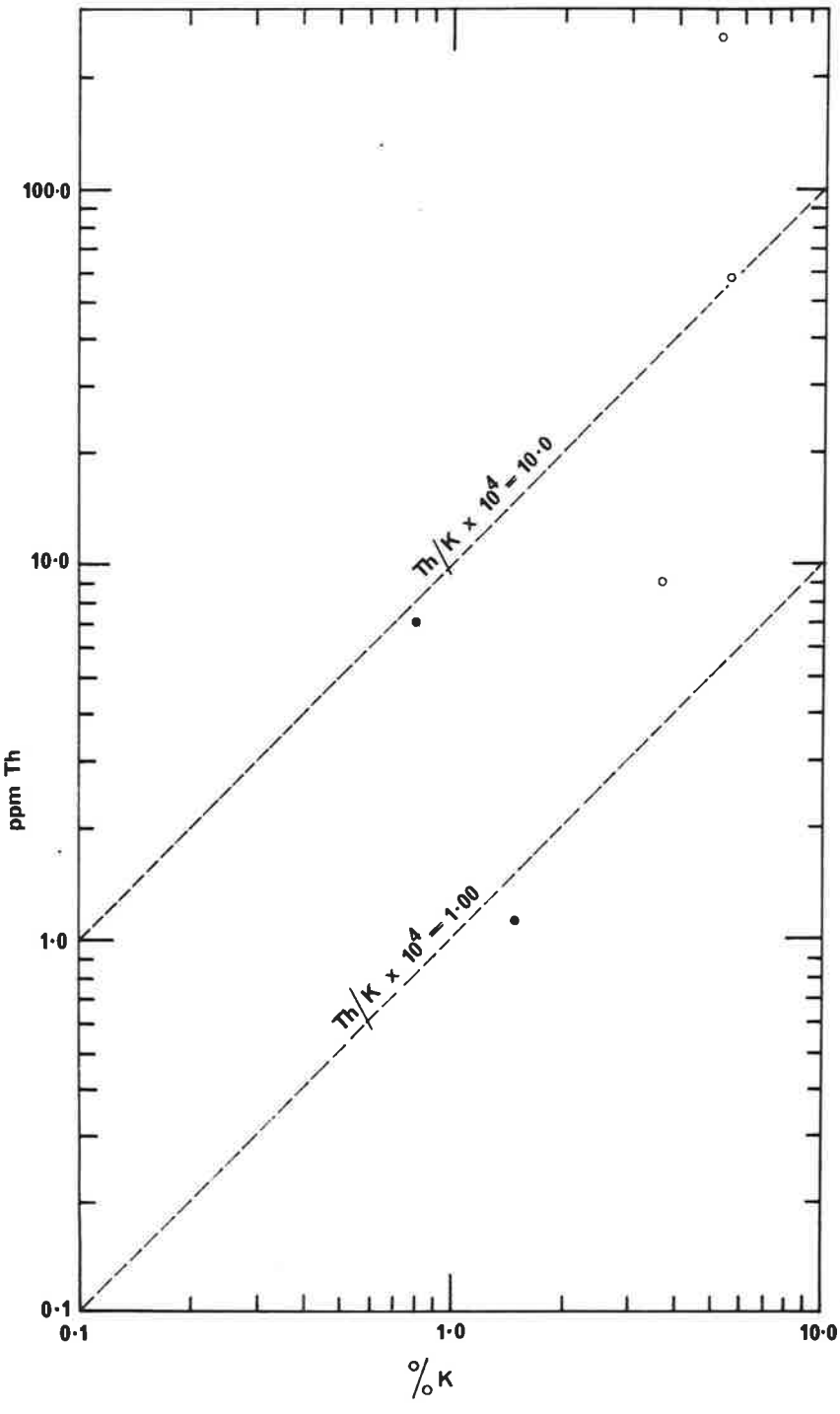
100·0
10·0
1·0
0·1
ppm Th
Th/K x 10⁴ = 10·0
Th/K x 10⁴ = 1·00
0·1
1·0
10·0
%K

FIGURE 4.16.1

Plot of relative modal percentage of hornblende (b) and orthopyroxene (a), from granulite facies terrain, against rock oxidation ratio.

Ornamentation:

open circles - quartzo-feldspathic lithologies
closed circles - mafic lithologies
square - ultramafic lithology

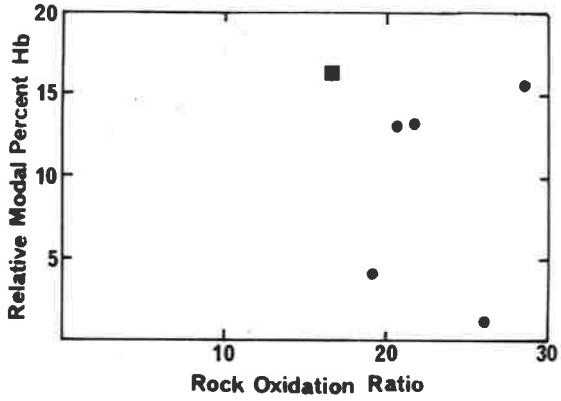
Relative Modal Percent Hb
20
15
10
5
10
20
30
Rock Oxidation Ratio

b

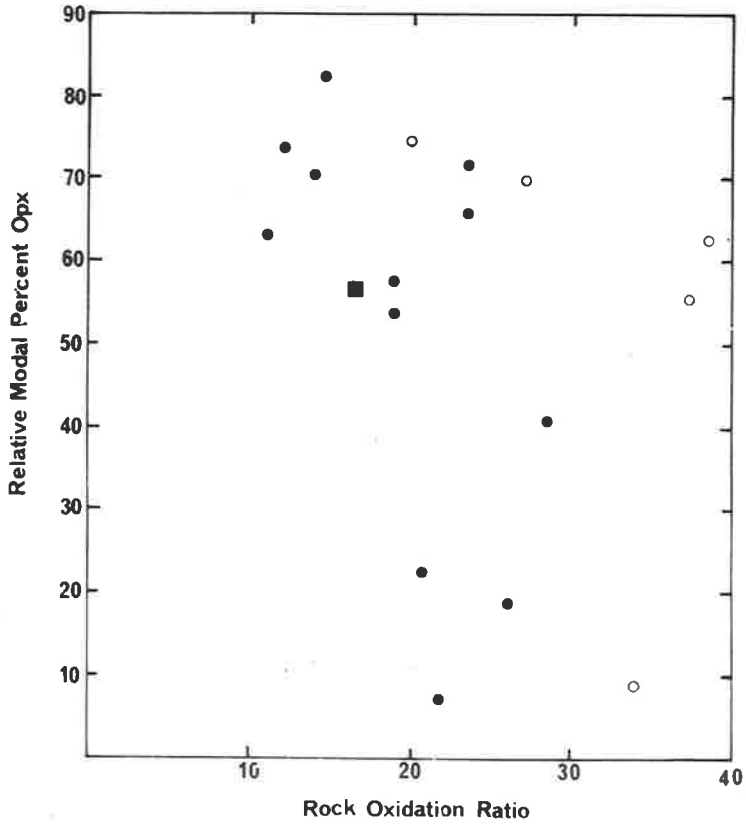
Relative Modal Percent Opx
90
80
70
60
50
40
30
20
10
10
20
30
40
Rock Oxidation Ratio

a

FIGURE 4.16.2

Plot of relative modal percentage of clinopyroxene, from granulite facies terrain, against rock oxidation ratio.

Ornamentation:

open circle - quartzo-feldspathic lithology
closed circle - mafic lithologies
closed square - ultramafic lithology
open square - manganiferous lithology

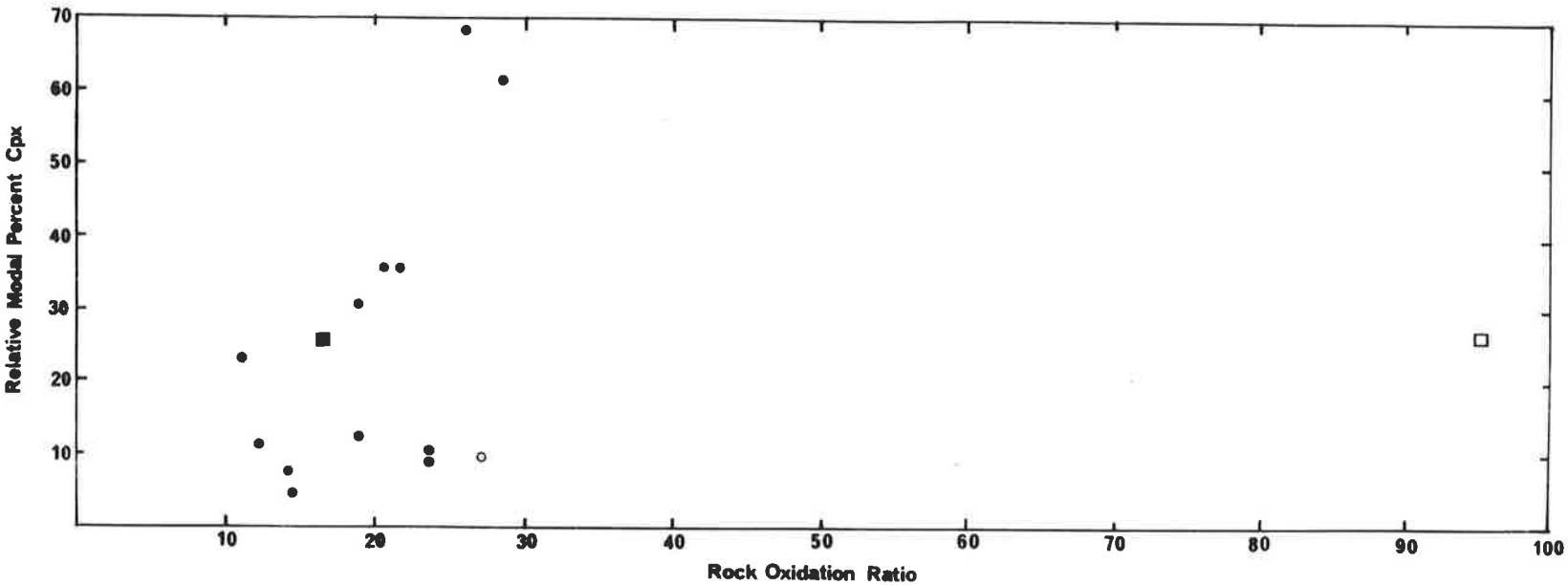
Relative Modal Percent Cpx
70
60
50
40
30
20
10
10
20
30
40
50
60
70
80
90
100
Rock Oxidation Ratio

FIGURE 4.16.3

Plot of relative modal percentage of opaque oxides, from granulite facies terrain, against rock oxidation ratio.

Ornamentation:

open circles - quartzo-feldspathic lithologies
closed circles - mafic lithologies
triangle - calc silicate lithology
open square - manganiferous lithology

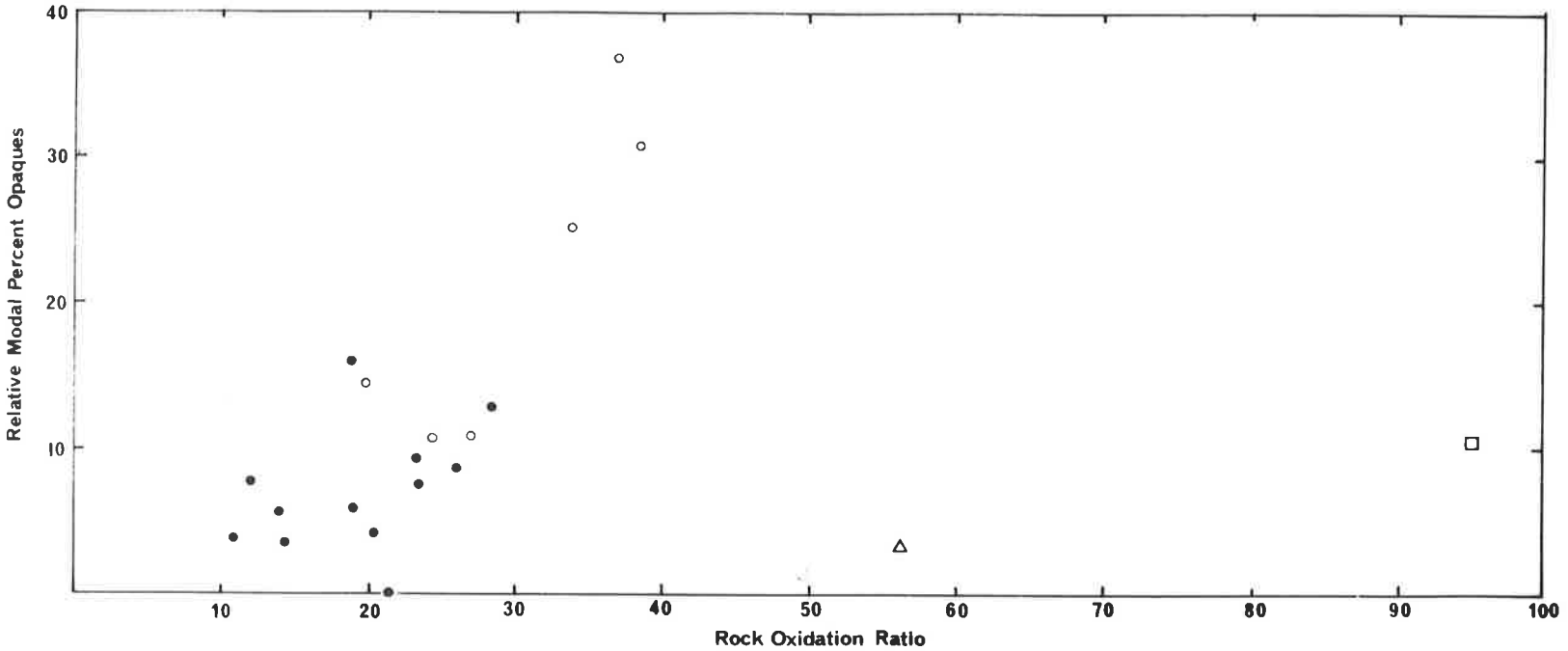
Relative Modal Percent Opaques
40
30
20
10
10
20
30
40
50
60
70
80
90
100
Rock Oxidation Ratio

FIGURE 4.16.4

(a) Plot of relative modal percentage of mica, from the transitional terrain, against rock oxidation ratio.

Ornamentation:

open circles - quartzo-feldspathic lithologies
large closed circles - micaceous mafic lithologies

(b) Plot of relative modal percentage of garnet, from the granulite facies terrain, against rock oxidation ratio.

Ornamentation:

open circles - quartzo-feldspathic lithologies
small closed circles - mafic lithologies
square - manganiferous lithology
triangle - calc silicate lithology

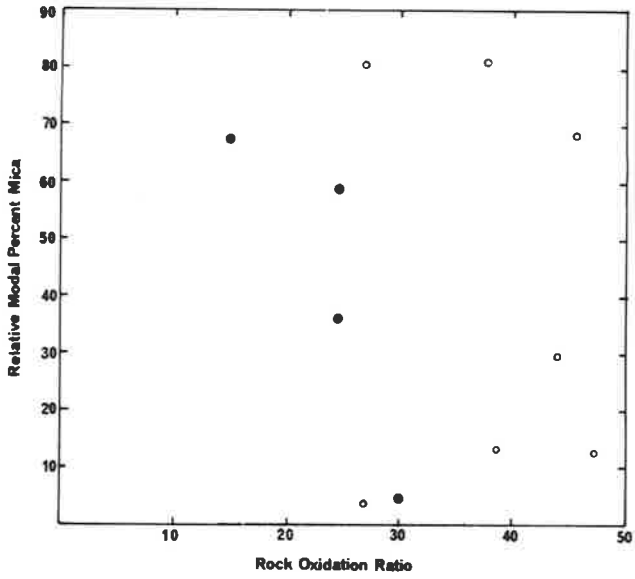
Relative Modal Percent Mica
Rock Oxidation Ratio
90
80
70
60
50
40
30
20
10
10
20
30
40
50

a

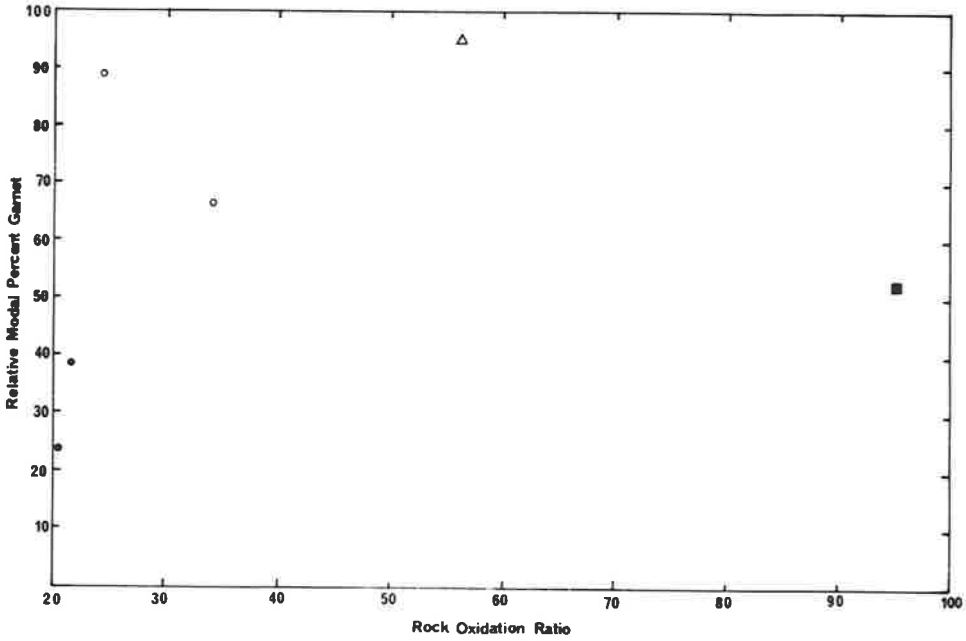
Relative Modal Percent Garnet
Rock Oxidation Ratio
100
90
80
70
60
50
40
30
20
10
20
30
40
50
60
70
80
90
100

b

FIGURE 4.16.5

Plot of relative modal percentage of (a) hornblende and clinopyroxene (b), from the transitional terrain, against rock oxidation ratio.

Ornamentation:

small open circles - quartzo-feldspathic lithologies with $K_2O \leq Na_2O$

inverted triangle - quartzo-feldspathic lithologies with $Na_2O \leq K_2O$

small closed circles - mica free mafic lithologies

large closed circles - micaceous mafic lithologies

square - ultramafic lithology

triangle - calc silicate lithology

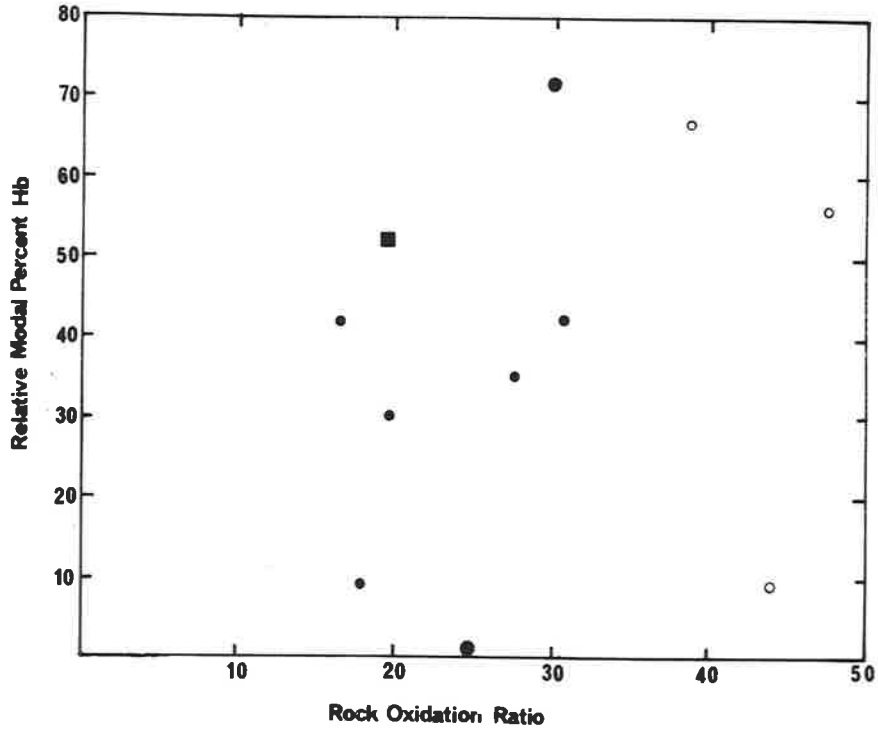
Relative Modal Percent Hb
80
70
60
50
40
30
20
10
10
20
30
40
50
Rock Oxidation Ratio

a

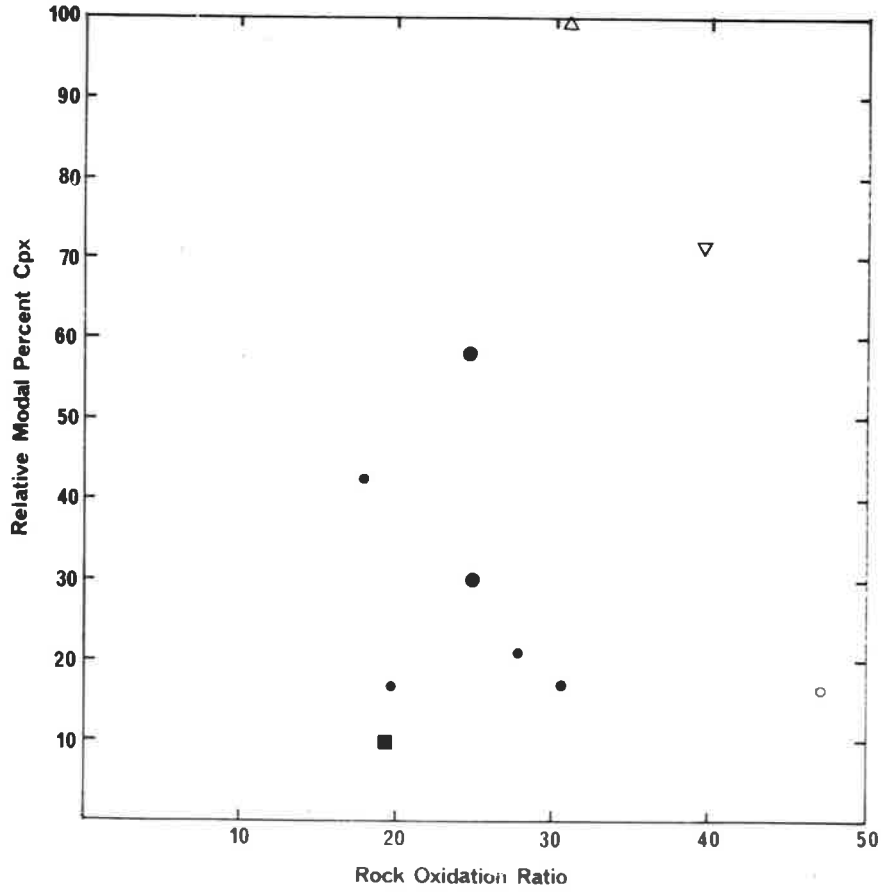
Relative Modal Percent Cpx
100
90
80
70
60
50
40
30
20
10
10
20
30
40
50
Rock Oxidation Ratio

b

FIGURE 4.16.6

Plot of relative modal percentage of opaque oxides (a) and orthopyroxene (b), from the transitional terrain, against rock oxidation ratio.

Ornamentation:
(the same as for Figure 4.16.5)

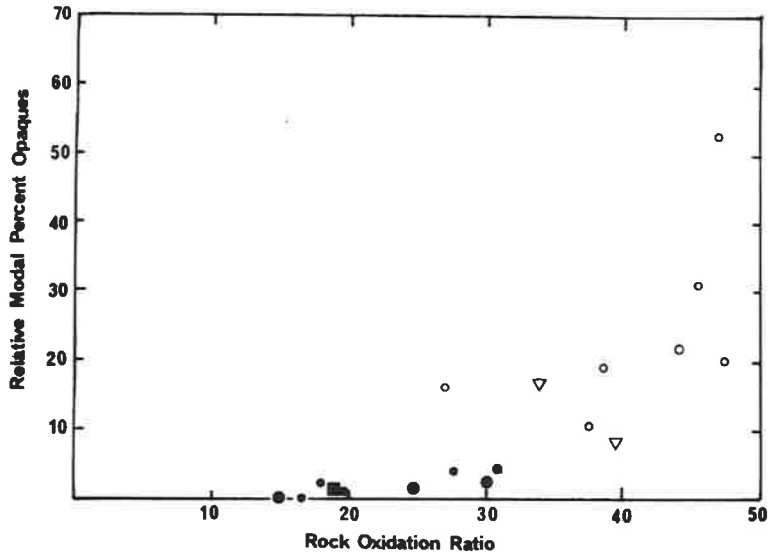
Relative Modal Percent Opaques
70
60
50
40
30
20
10
10
20
30
40
50
Rock Oxidation Ratio

a

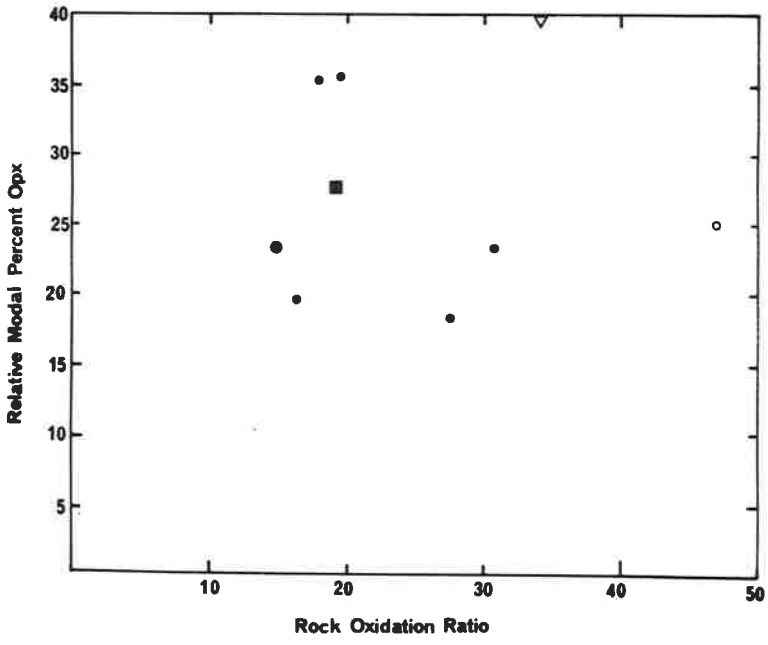
Relative Modal Percent Opx
40
35
30
25
20
15
10
5
10
20
30
40
50
Rock Oxidation Ratio

b

FIGURE 4.16.7

Plot of relative modal percentage of (a) opaque oxides, (b) hornblende and (c) biotite, from the amphibolite facies terrain, against rock oxidation ratio.

Ornamentation:
(the same as for Figure 4.15c)

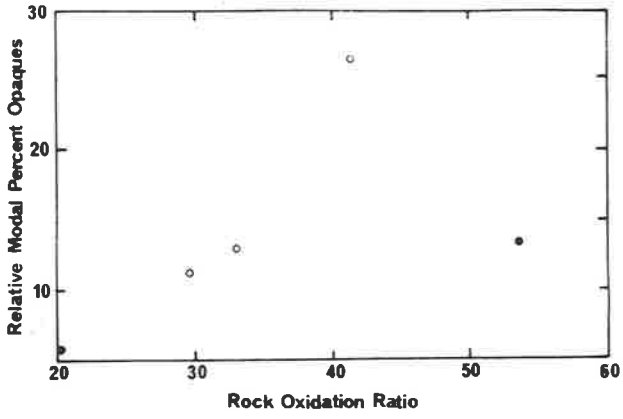
Relative Modal Percent Opaques
30
20
10
20
30
40
50
60
Rock Oxidation Ratio

a

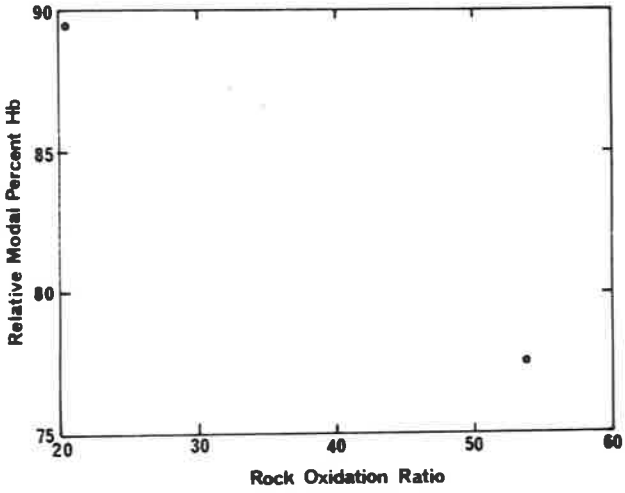
Relative Modal Percent Hb
90
85
80
75
20
30
40
50
60
Rock Oxidation Ratio

b

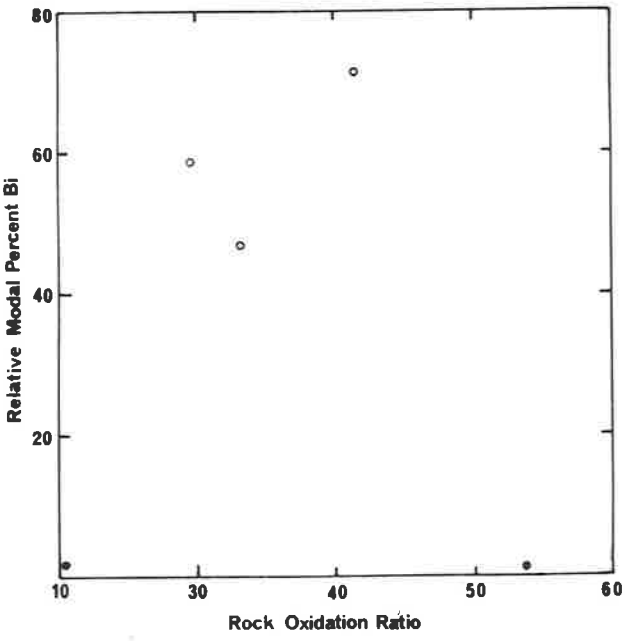
Relative Modal Percent Bi
80
60
40
20
10
30
40
50
60
Rock Oxidation Ratio

c

FIGURE 4.17.1

Plot of $Fe^{2+}/(Fe^{2+} + Mg)$ orthopyroxene (a) and hornblende (b) against rock oxidation ratio.

Ornamentation:

open circles - minerals from ilmenite-haematite assemblages
closed circles - minerals from magnetite-ilmenite-haematite assemblages
open triangles - minerals from magnetite-haematite assemblages
closed triangle - minerals from magnetite assemblages

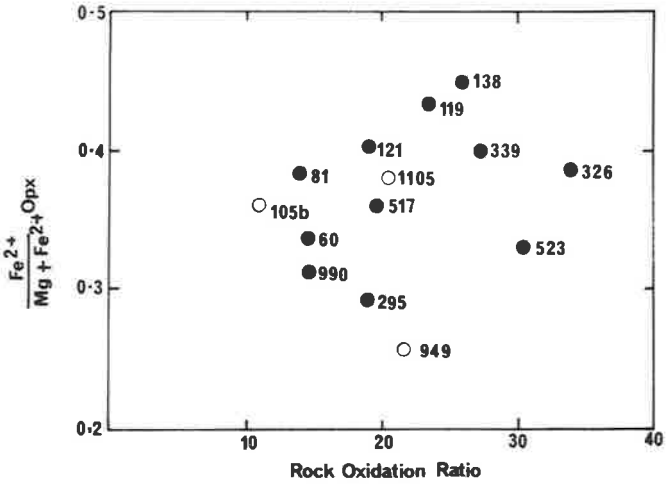
0·5
0·4
0·3
0·2
10
20
30
40
Rock Oxidation Ratio
$\frac{Fe^{2+}}{Mg+Fe^{2+}}$ Opx
138
119
121
339
326
81
1105
105b
517
60
523
990
295
949

a

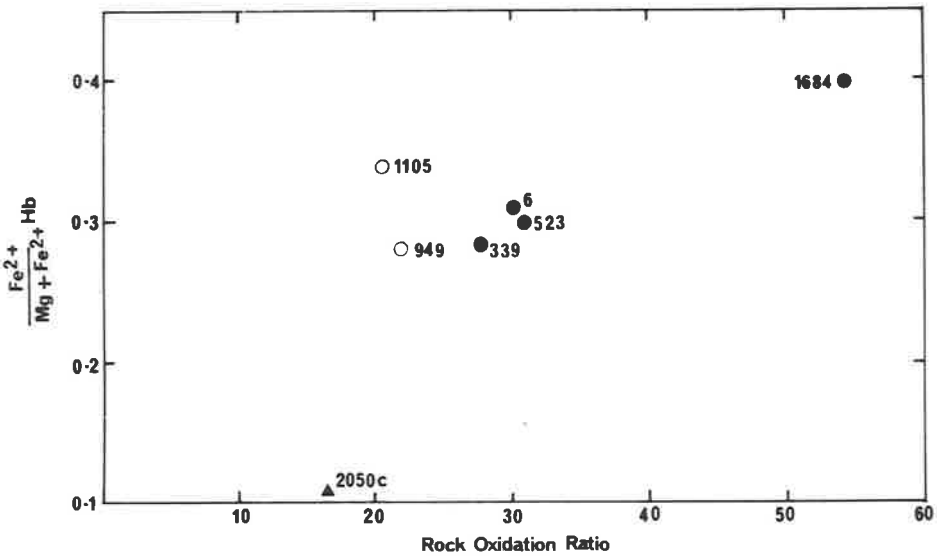
0·4
0·3
0·2
0·1
10
20
30
40
50
60
Rock Oxidation Ratio
$\frac{Fe^{2+}}{Mg+Fe^{2+}}$ Hb
1684
1105
6
523
949
339
2050c

b

FIGURE 4.17.2

Plot of $Fe^{2+}/(Fe^{2+} + Mg)$ clinopyroxene against rock oxidation ratio.

Ornamentation:
(the same as for Figure 4.17.1)

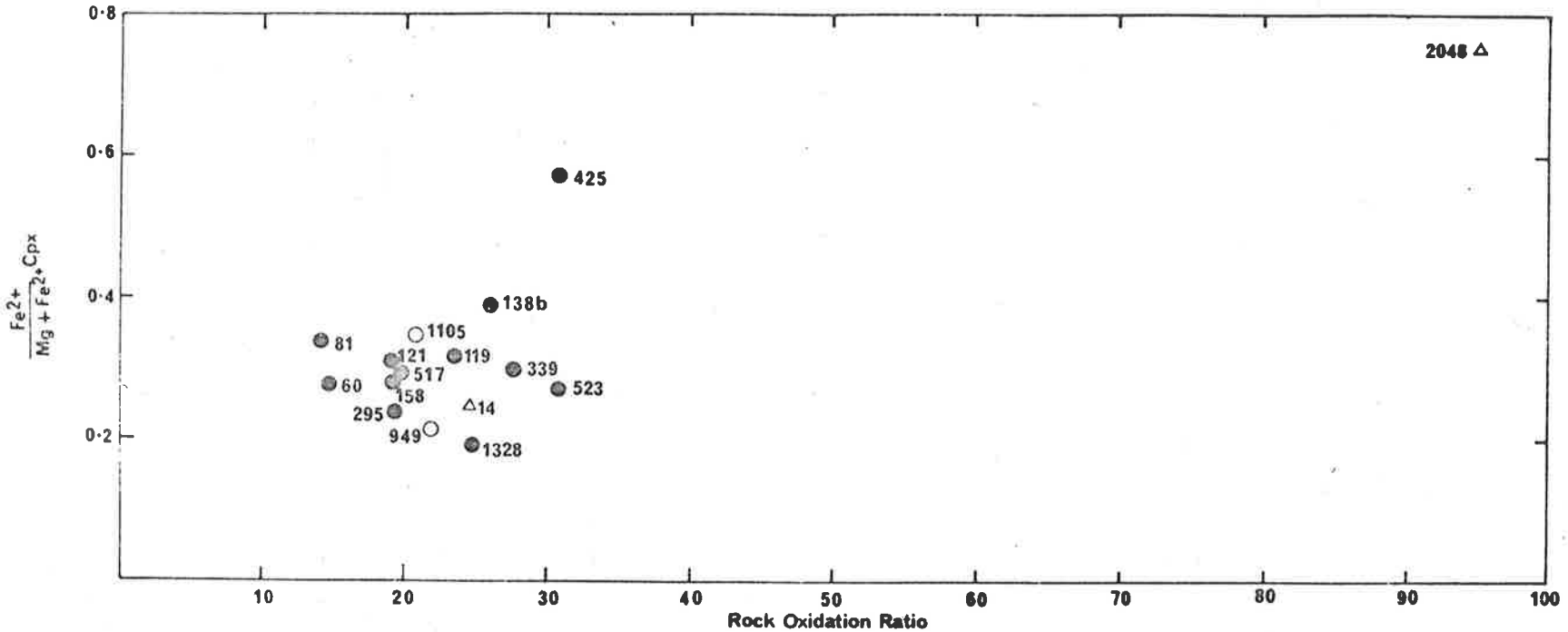
0·8
0·6
0·4
0·2
$\frac{Fe^{2+}}{Mg+Fe^{2+}}$ Cpx
2048 △
425
138b
1105
81
121
119
339
517
60
523
158
△14
295
949
1328
10
20
30
40
50
60
70
80
90
100
Rock Oxidation Ratio

FIGURE 4.17.3

Plot of $Fe^{2+}/(Fe^{2+} + Mg)$ mica (a) and garnet (b) against rock oxidation ratio.

Ornamentation:
(the same as for Figure 4.17)

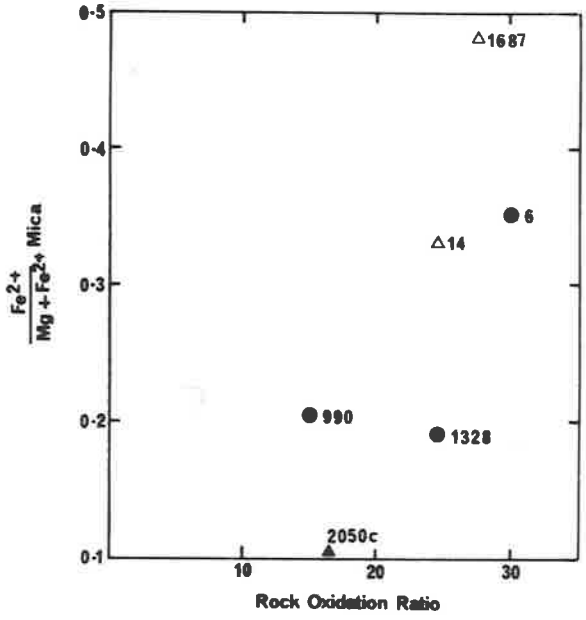
0·5
0·4
0·3
0·2
0·1
10
20
30
Rock Oxidation Ratio
$\frac{Fe^{2+}}{Mg+Fe^{2+}}$ Mica
△1687
● 6
△14
● 990
● 1328
2050c

a

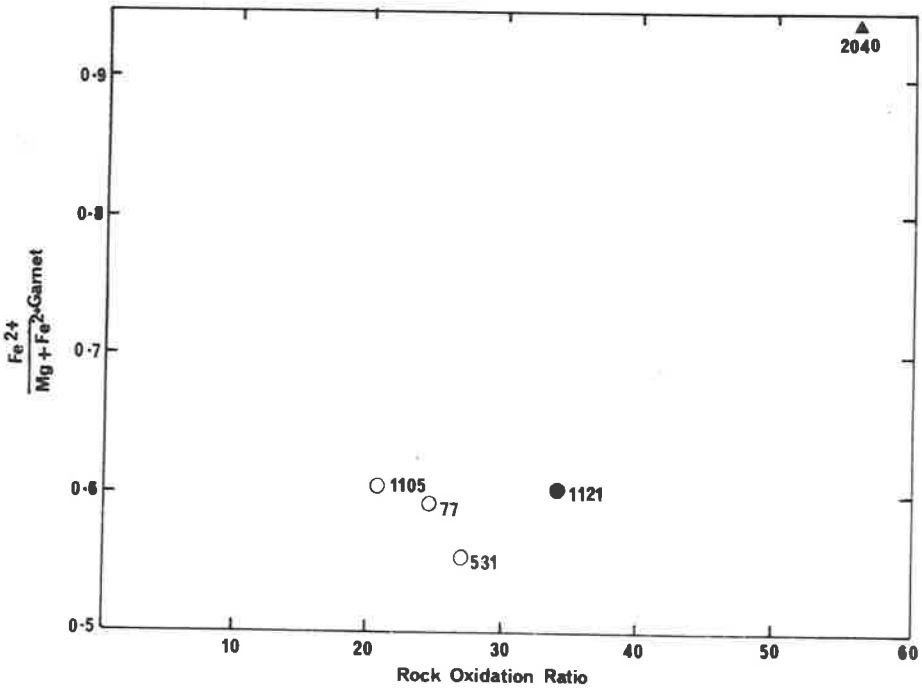
0·9
0·8
0·7
0·6
0·5
10
20
30
40
50
60
Rock Oxidation Ratio
$\frac{Fe^{2+}}{Mg+Fe^{2+}}$ Garnet
▲ 2040
○ 1105
○ 77
● 1121
○ 531

b

FIGURE 4.18.1

Plot of $Mg/(Mg + Fe^{2+})$ orthopyroxene (a) and hornblende (b) against rock oxidation ratio.

Ornamentation:
(the same as for Figure 4.17.1)

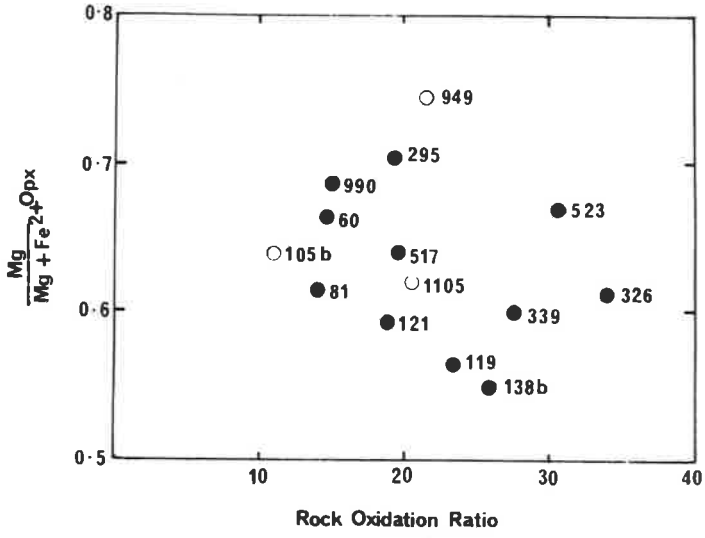
0·8
0·7
0·6
0·5
$\frac{Mg}{Mg+Fe^{2+}}$ Opx
949
295
990
523
60
105 b
517
1105
81
326
339
121
119
138b
10
20
30
40
Rock Oxidation Ratio

a

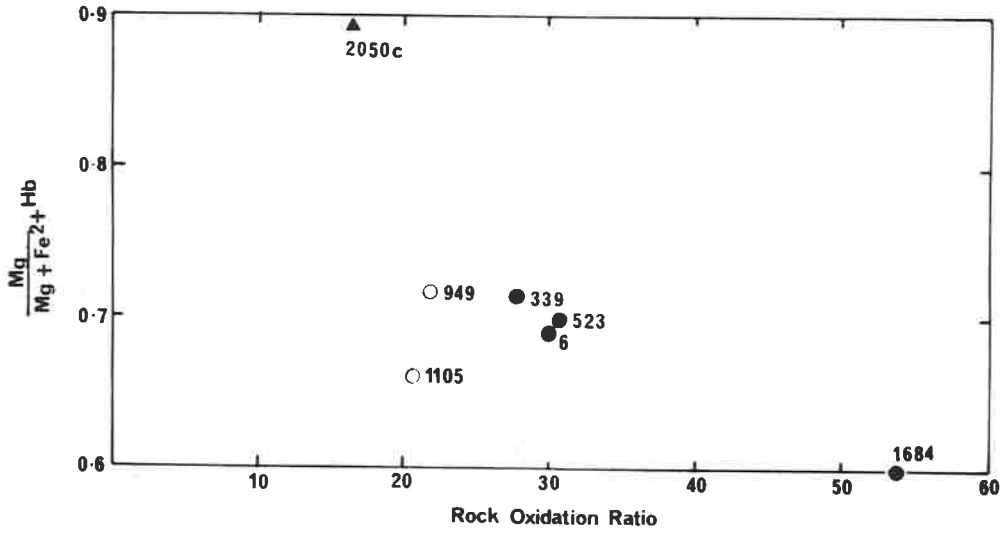
0·9
0·8
0·7
0·6
$\frac{Mg}{Mg+Fe^{2+}}$ Hb
2050c
949
339
523
6
1105
1684
10
20
30
40
50
60
Rock Oxidation Ratio

b

FIGURE 4.18.2

Plot of $Mg/(Mg + Fe^{2+})$ clinopyroxene against rock oxidation ratio.

Ornamentation:
(the same as for Figure 4.17.1)

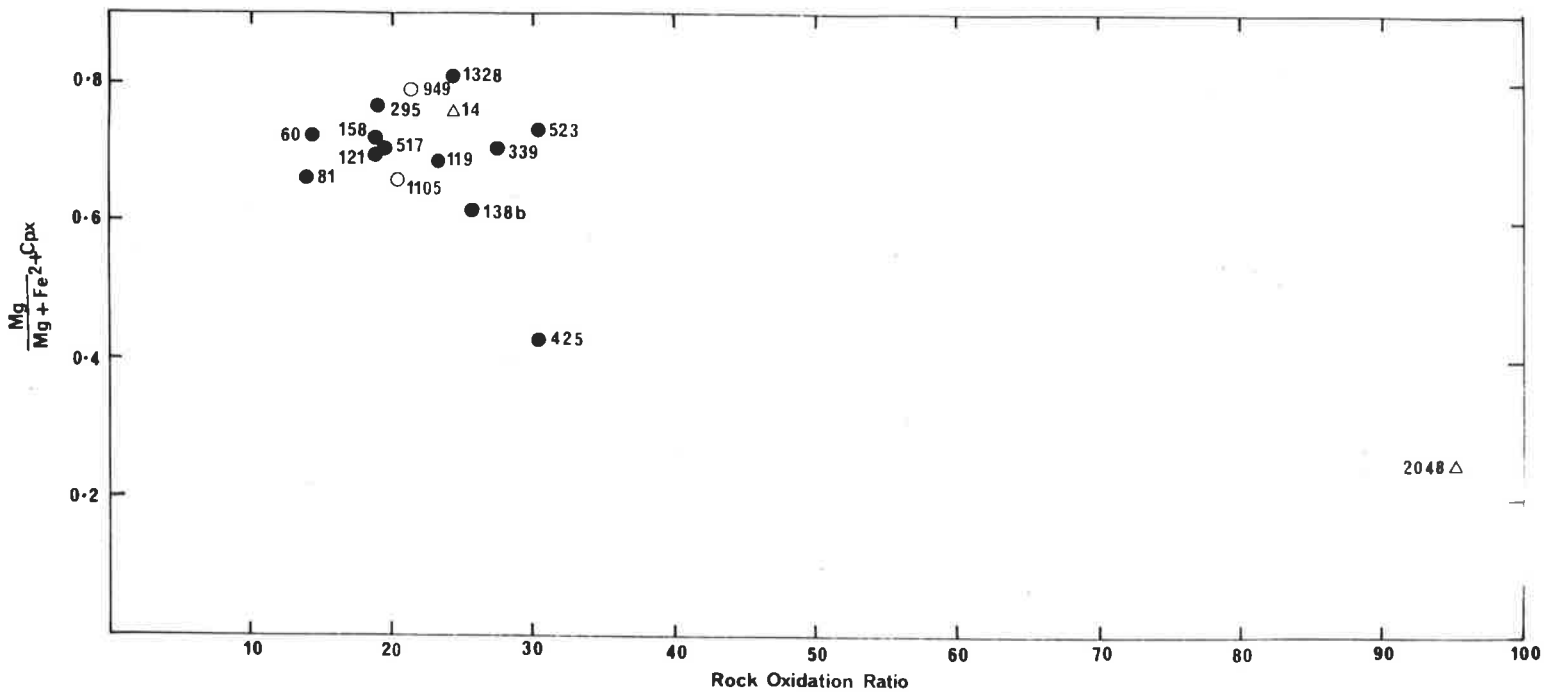
0·8
0·6
0·4
0·2
$\frac{Mg}{Mg+Fe^{2+}}$ Cpx
1328
949
295
14
60
158
523
517
121
119
339
81
1105
138b
425
2048
10
20
30
40
50
60
70
80
90
100
Rock Oxidation Ratio

FIGURE 4.18.3

Plot of $Mg/(Mg + Fe^{2+})$ mica (a) and garnet (b) against rock oxidation ratio.

Ornamentation:
(the same as for Figure 4.17.1)

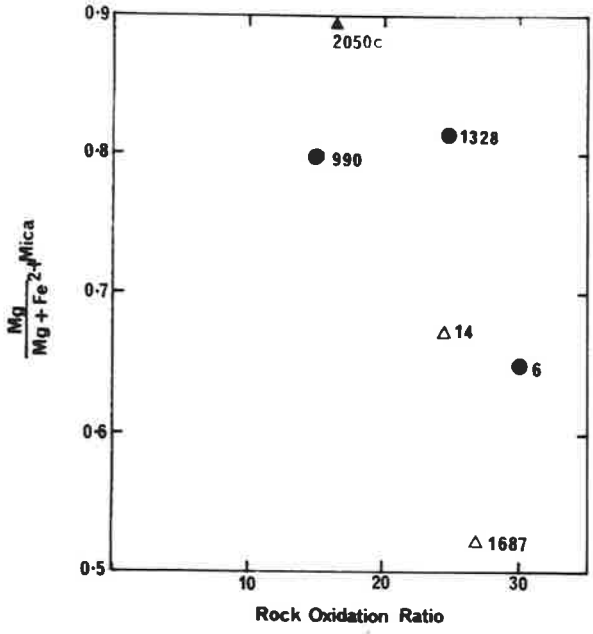
0·9
0·8
0·7
0·6
0·5
2050c
1328
990
14
6
1687
10
20
30
Rock Oxidation Ratio
Mg / Mg + Fe2+ Mica

a

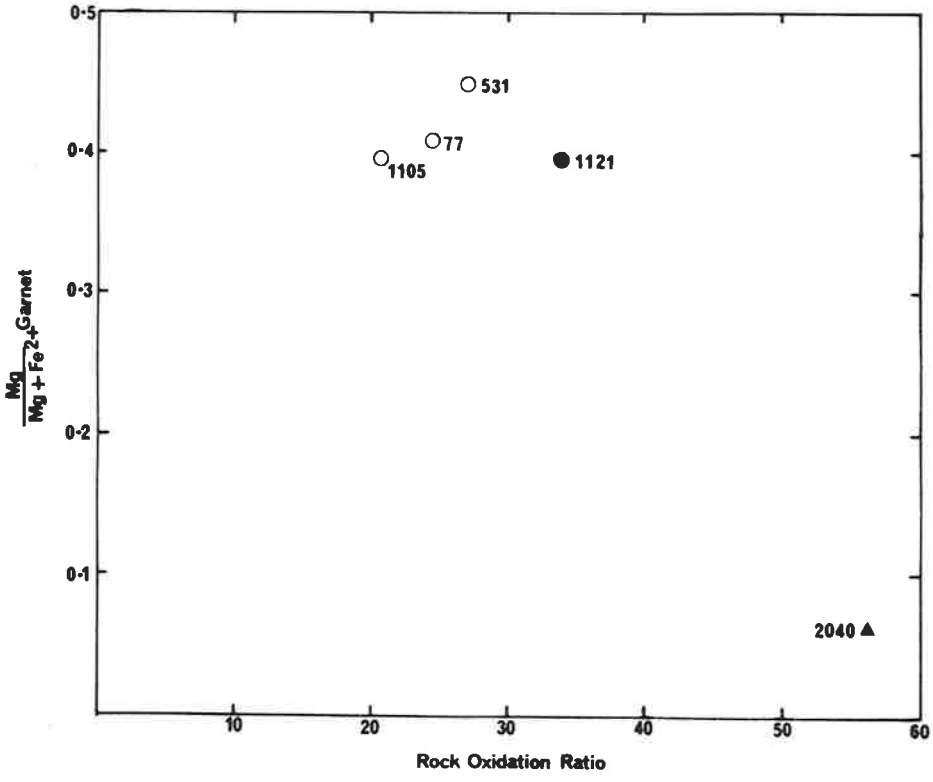
0·5
0·4
0·3
0·2
0·1
531
77
1105
1121
2040
10
20
30
40
50
60
Rock Oxidation Ratio
Mg / Mg + Fe2+ Garnet

b

FIGURE 4.19.1

Plot of rock oxidation ratio against rock 100.Mg/(Mg + Fe^{2+}) ratio for the granulite facies.

Ornamentation:

small open circles - quartzo-feldspathic lithologies
small closed circles - mafic lithologies
closed square - ultramafic lithology
triangle - calc silicate lithology
open square - manganiferous lithology

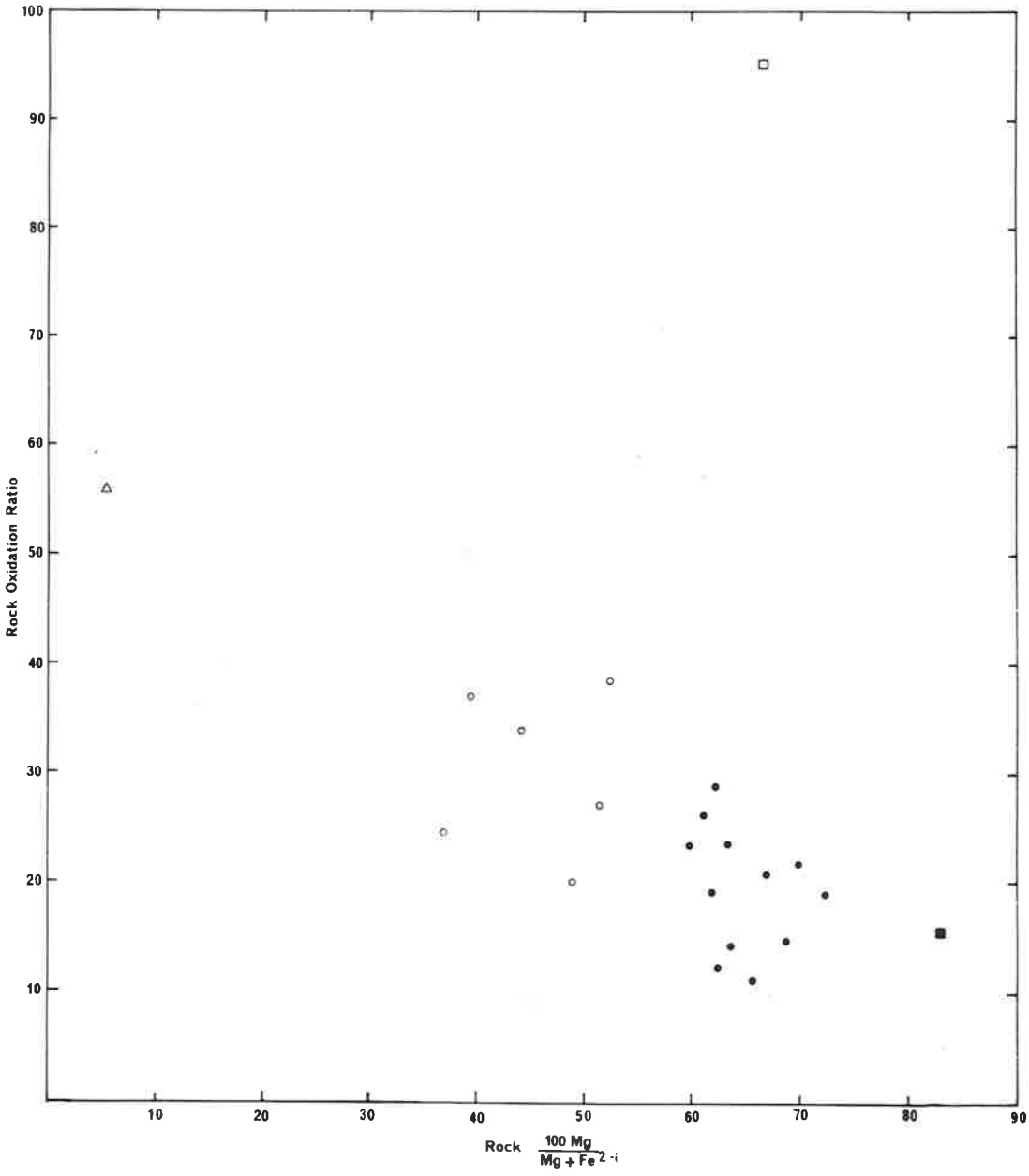
Rock Oxidation Ratio
100
90
80
70
60
50
40
30
20
10
10
20
30
40
50
60
70
80
90
Rock $\frac{100\ Mg}{Mg + Fe^{2+}}$

FIGURE 4.19.2

Plot of rock oxidation ratio against rock 100.Mg/(Mg + Fe^{2+}) ratio for the transitional terrain.

Ornamentation:

small open circle	- quartzo-feldspathic lithologies with K_2O > Na_2O
inverted open triangles	- quartzo-feldspathic lithologies with Na_2O > K_2O
small closed circles	- mica free mafic lithologies
large closed circles	- micaceous mafic lithologies
closed square	- ultramafic lithology
open triangle	- calc silicate lithology

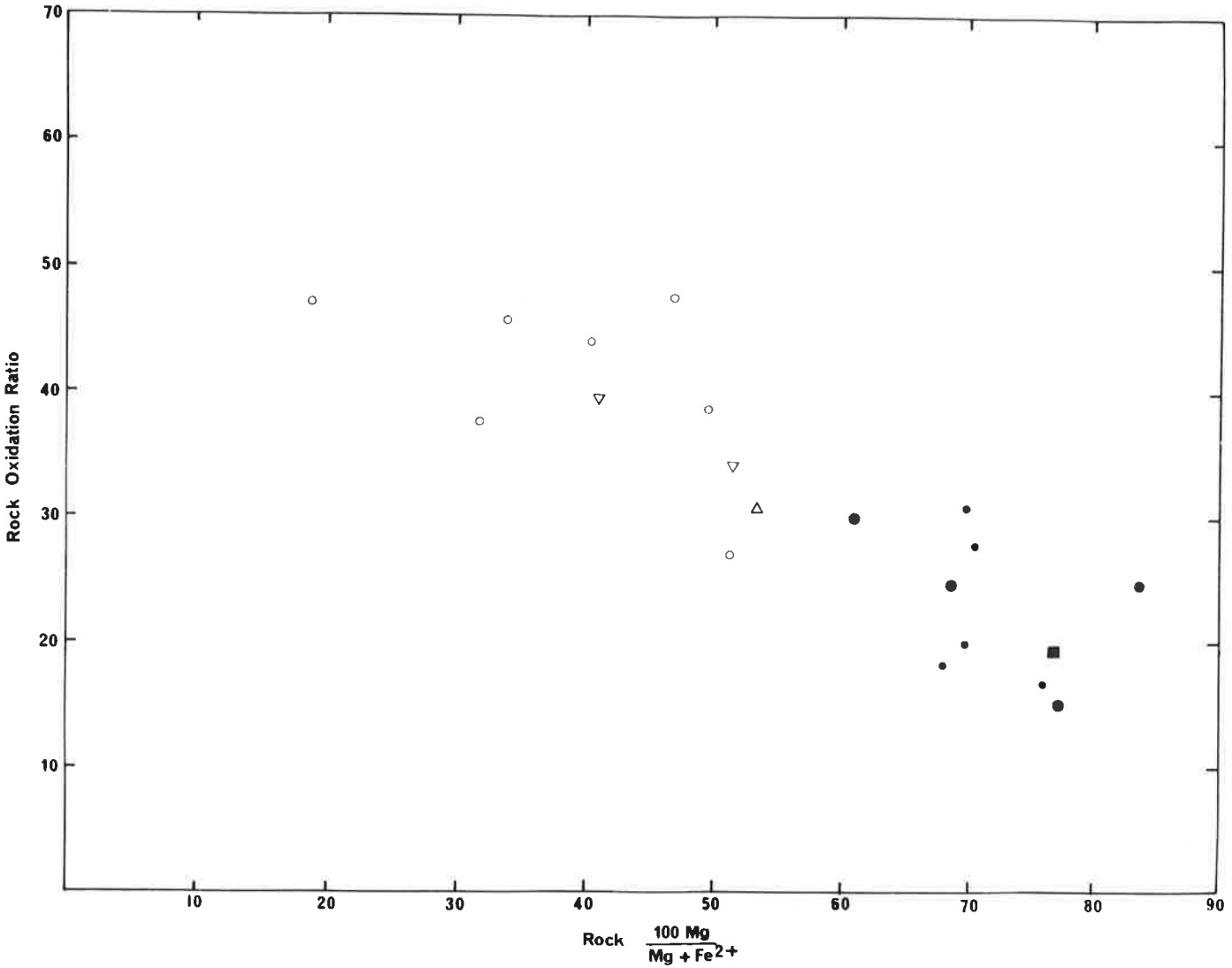
Rock Oxidation Ratio
70
60
50
40
30
20
10
10
20
30
40
50
60
70
80
90
Rock 100 Mg / Mg + Fe2+

FIGURE 4.19.3

Plot of rock oxidation ratio against rock 100.Mg/(Mg + Fe^{2+}) ratio for the amphibolite facies.

Ornamentation:

small open circle - quartzo-feldspathic lithologies
small closed circles - mafic lithologies
half open circle - pelitic lithology

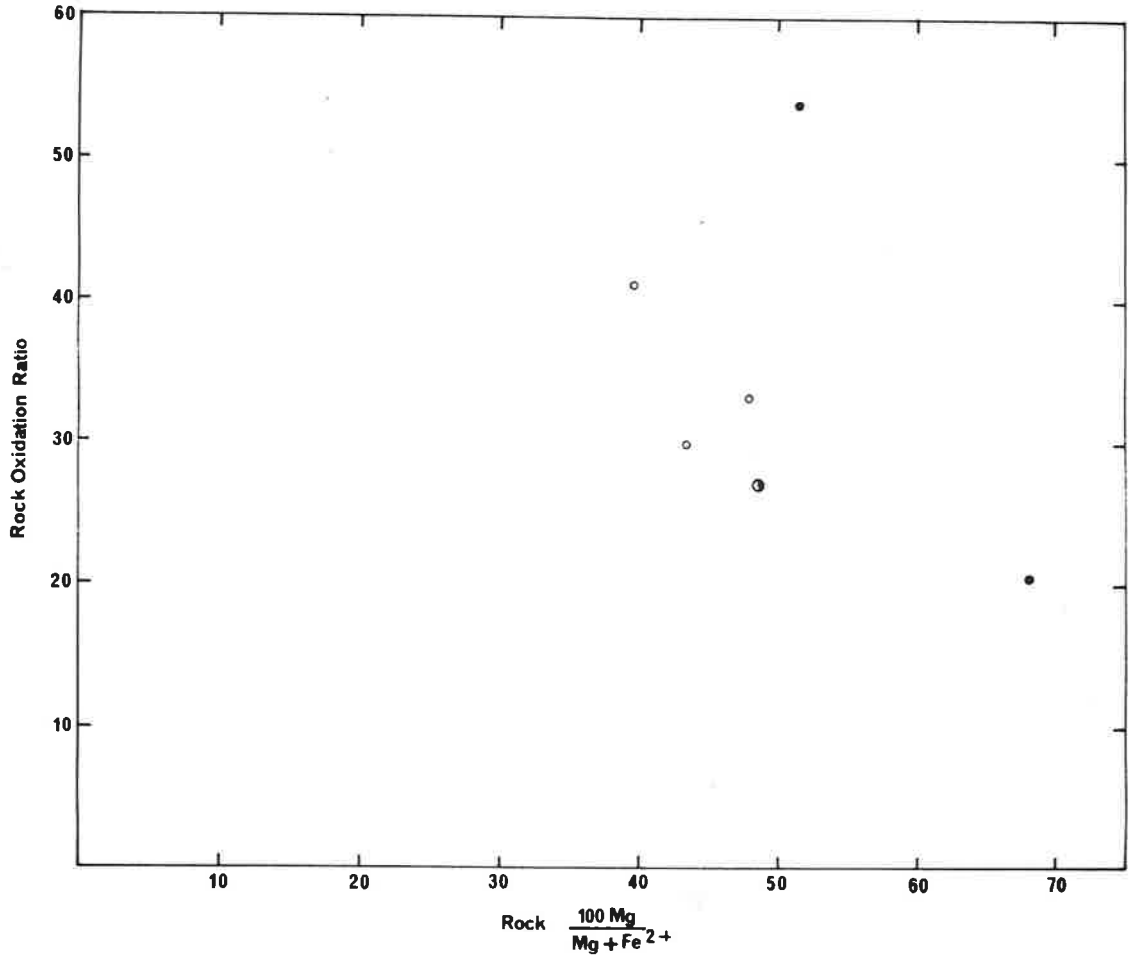
60
50
40
30
20
10
Rock Oxidation Ratio
10
20
30
40
50
60
70
Rock 100 Mg / Mg + Fe2+

FIGURE 4.20

Plot of $Fe^{3+}/(Fe^{3+} + Fe^{2+})$ ratio of orthopyroxene (a), hornblende (b), garnet (c) and mica (d) against rock oxidation ratio.

Ornamentation:
(the same as in Figure 4.17.1)

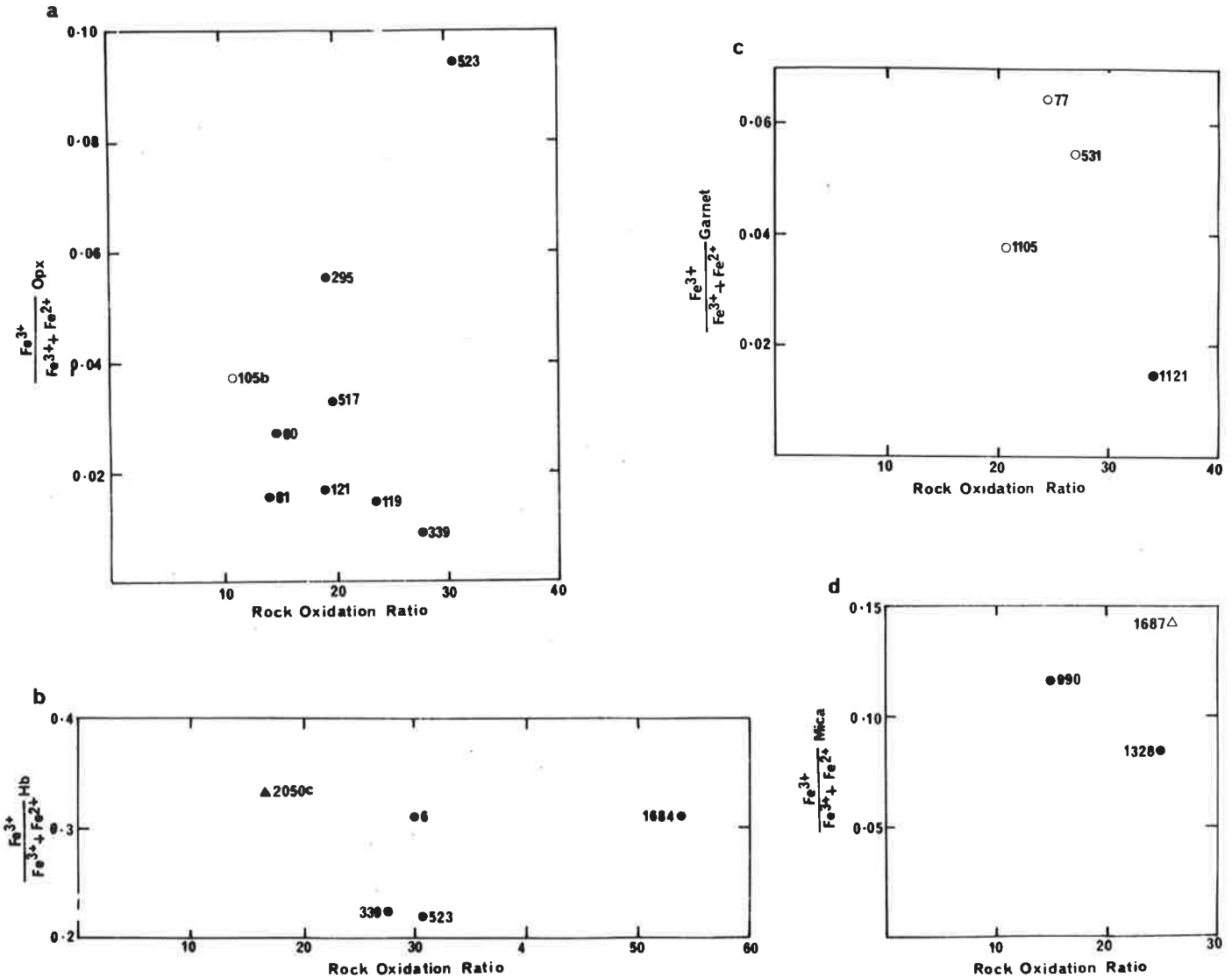
a
0·10
0·08
0·06
0·04
0·02
$\frac{Fe^{3+}}{Fe^{3+}+Fe^{2+}}$ Opx
●523
●295
○105b
●517
●80
●81
●121
●119
●339
10
20
30
40
Rock Oxidation Ratio
b
0·4
0·3
0·2
$\frac{Fe^{3+}}{Fe^{3+}+Fe^{2+}}$ Hb
▲2050c
●6
1684●
330●
●523
10
20
30
4
50
60
Rock Oxidation Ratio
c
0·06
0·04
0·02
$\frac{Fe^{3+}}{Fe^{3+}+Fe^{2+}}$ Garnet
○77
○531
○1105
●1121
10
20
30
40
Rock Oxidation Ratio
d
0·15
0·10
0·05
$\frac{Fe^{3+}}{Fe^{3+}+Fe^{2+}}$ Mica
1687△
●990
1328●
10
20
30
Rock Oxidation Ratio

FIGURE 4.21.1

Plot of [Mn/(Mn + Mg + Fe^{2+})] x 10^3 ratio of garnet (a) and hornblende (b) against rock oxidation ratio.

Ornamentation:
(the same as for Figure 4.17.1)

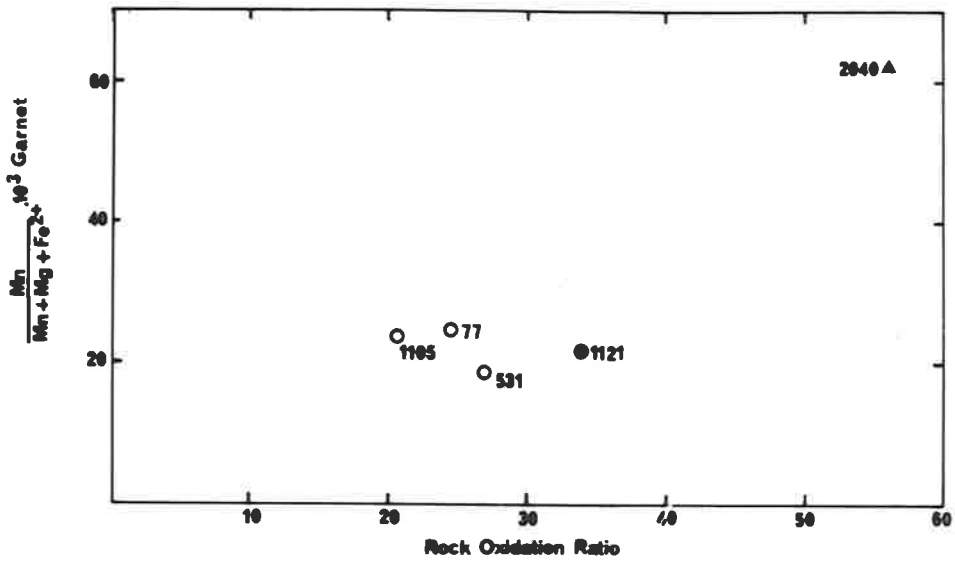
Mn / (Mn + Mg + Fe2+) .10^3 Garnet
60
40
20
2040
77
1105
1121
531
10
20
30
40
50
60
Rock Oxidation Ratio

a

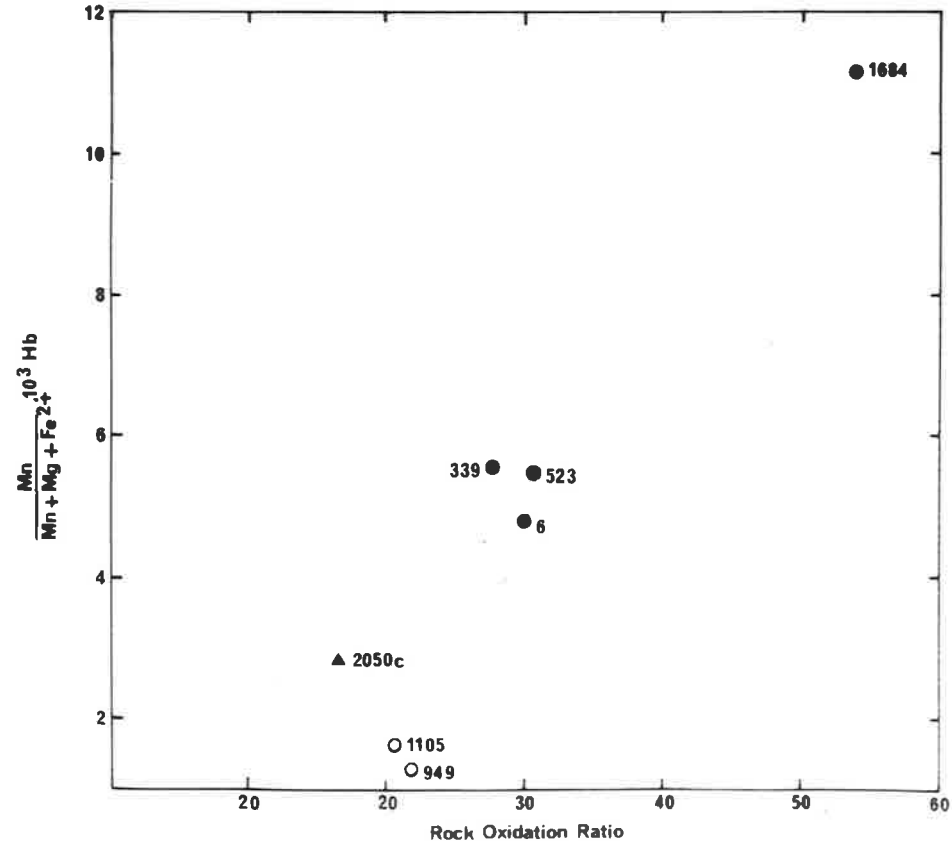
Mn / (Mn + Mg + Fe2+) .10^3 Hb
12
10
8
6
4
2
1684
339
523
6
2050c
1105
949
20
20
30
40
50
60
Rock Oxidation Ratio

b

FIGURE 4.21.2

Plot of [Mn/(Mn + Mg + Fe^{2+})] x 10^3 ratio of orthopyroxene against rock oxidation ratio.

Ornamentation:
(the same as for Figure 4.17.1)

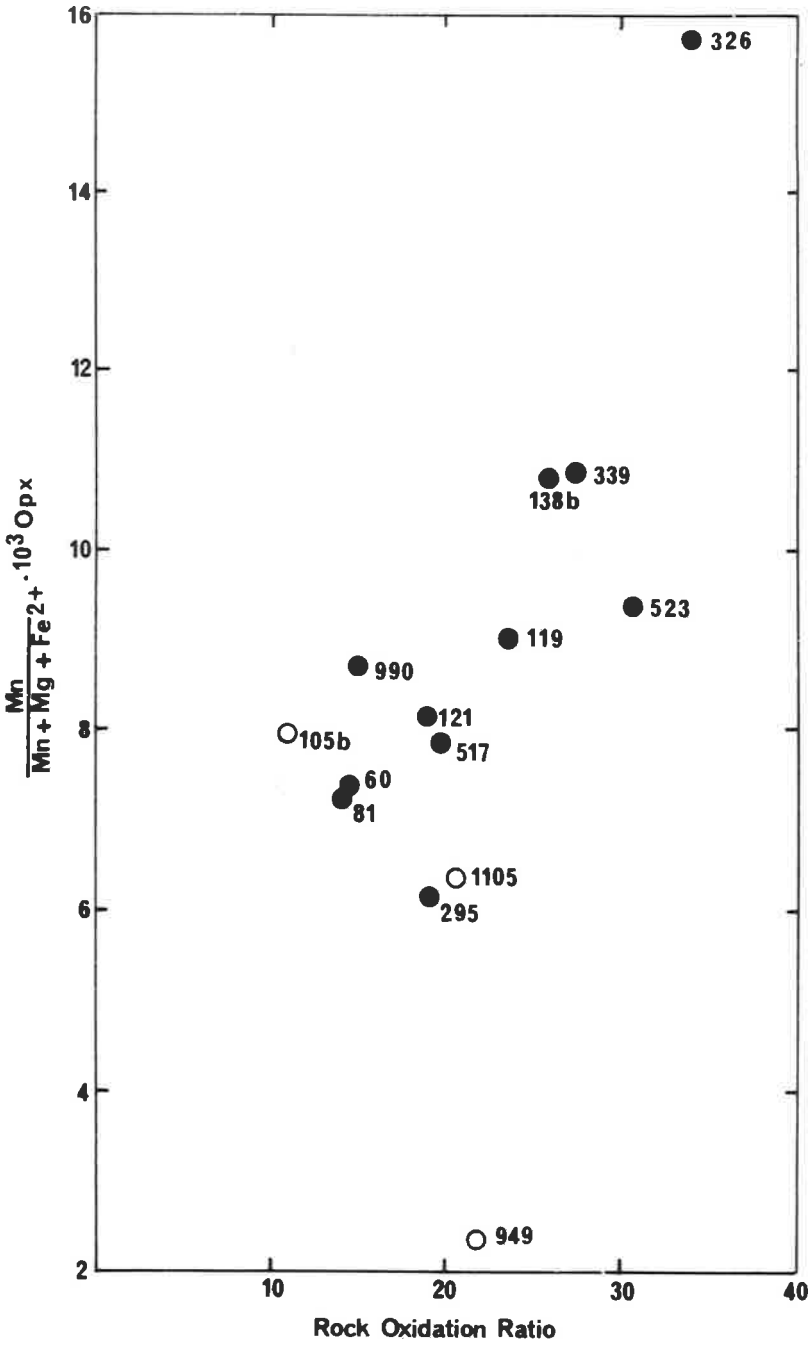
16
14
12
10
8
6
4
2
10
20
30
40
Rock Oxidation Ratio
$\frac{Mn}{Mn+Mg+Fe^{2+}} \cdot 10^3 Opx$
326
339
138b
523
119
990
121
105b
517
60
81
1105
295
949

FIGURE 4.21.3

Plot of [Mn/(Mn + Mg + Fe^{2+})] x 10^3 ratio of mica (a) and clinopyroxene (b) against rock oxidation ratio.

Ornamentation:
(the same as for Figure 4.17.1)

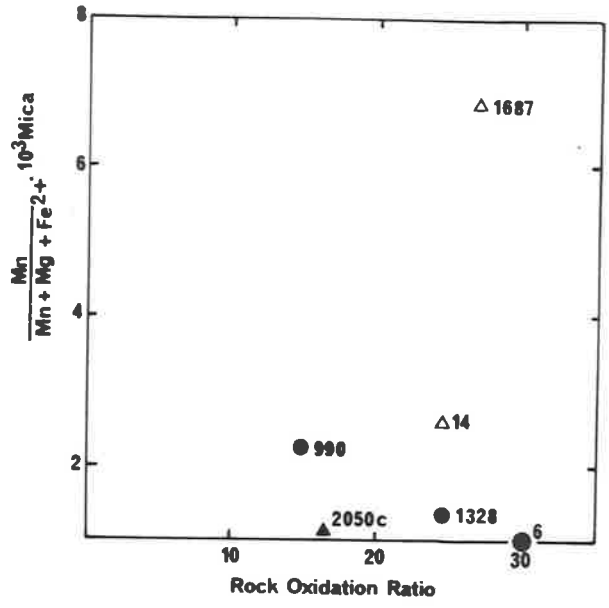
8
6
4
2
10
20
30
Rock Oxidation Ratio
$\frac{Mn}{Mn + Mg + Fe^{2+}} \cdot 10^3$ Mica
1687
14
990
2050c
1328
6

a

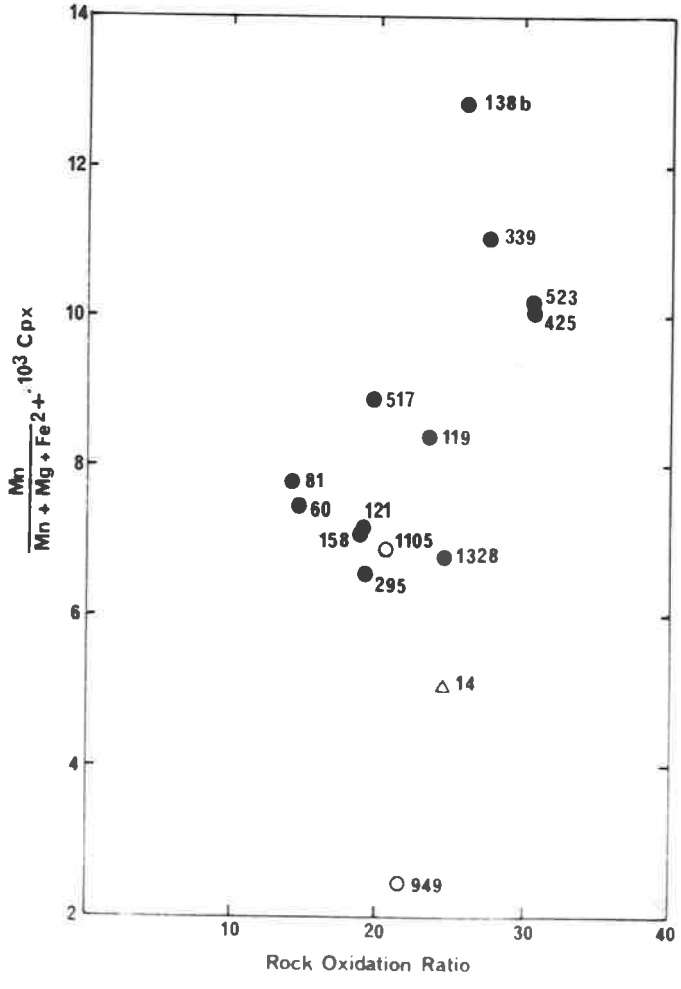
14
12
10
8
6
4
2
10
20
30
40
Rock Oxidation Ratio
$\frac{Mn}{Mn + Mg + Fe^{2+}} \cdot 10^3$ Cpx
138b
339
523
425
517
119
81
60
121
158
1105
1328
295
14
949

b

FIGURE 4.22.1

Plot of the $Mg/(Mg + Fe^{2+})$ ratios of (a) micas and (b) garnets, and the same ratios in parent rocks.

Ornamentation:

closed circles - minerals from granulite facies terrain

open circles - minerals from the transitional terrain.

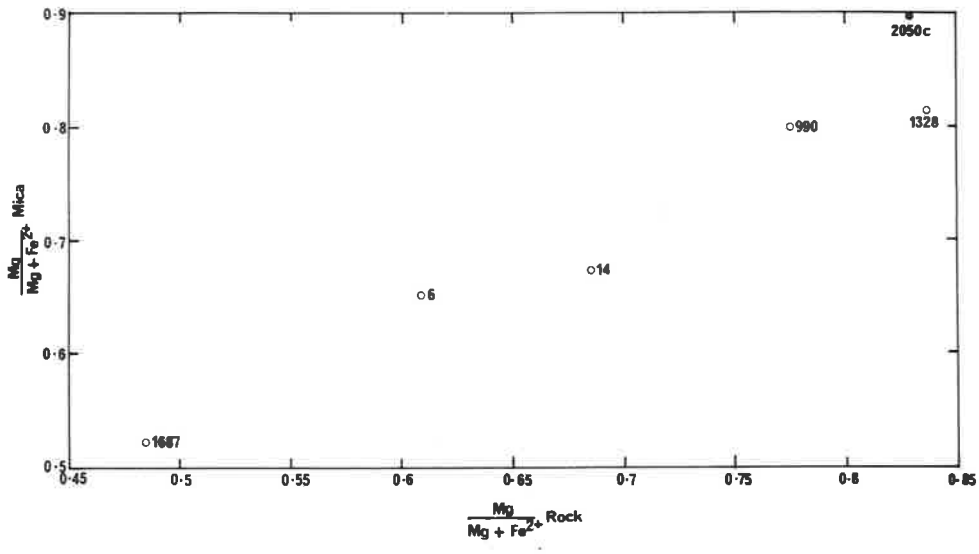
0·9
0·8
0·7
0·6
0·5
0·45
0·5
0·55
0·6
0·65
0·7
0·75
0·8
0·85
2050c
990
1328
14
6
1687
Mg / Mg + Fe2+ Mica
Mg / Mg + Fe2+ Rock

a

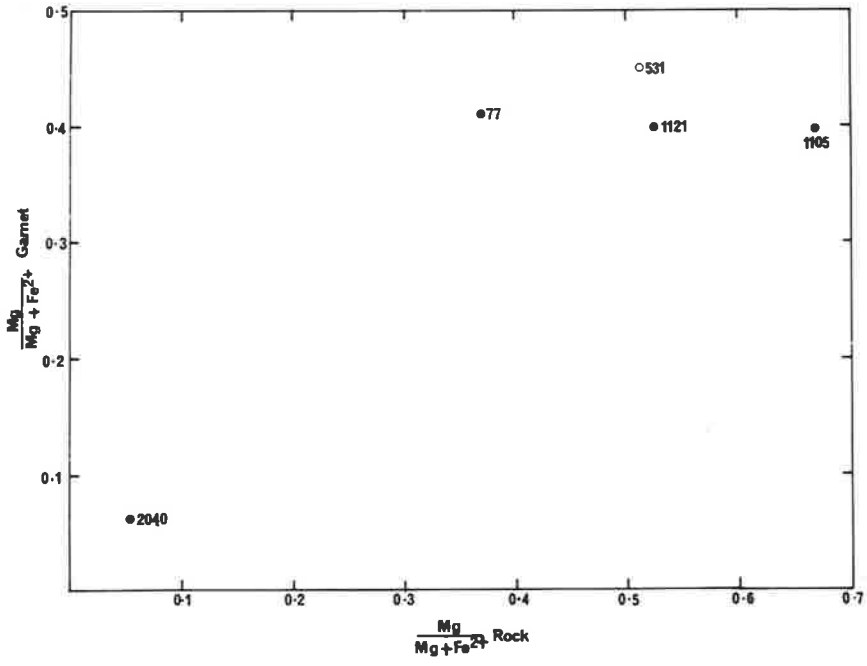
0·5
0·4
0·3
0·2
0·1
0·1
0·2
0·3
0·4
0·5
0·6
0·7
531
77
1121
1105
2040
Mg / Mg + Fe2+ Garnet
Mg / Mg + Fe2+ Rock

b

FIGURE 4.22.2

Plot of the $Mg/(Mg + Fe^{2+})$ ratios of (a) clinopyroxenes and (b) orthopyroxenes, and the same ratios in parent rocks.

Ornamentation:
(the same as for Figure 4.22.1)

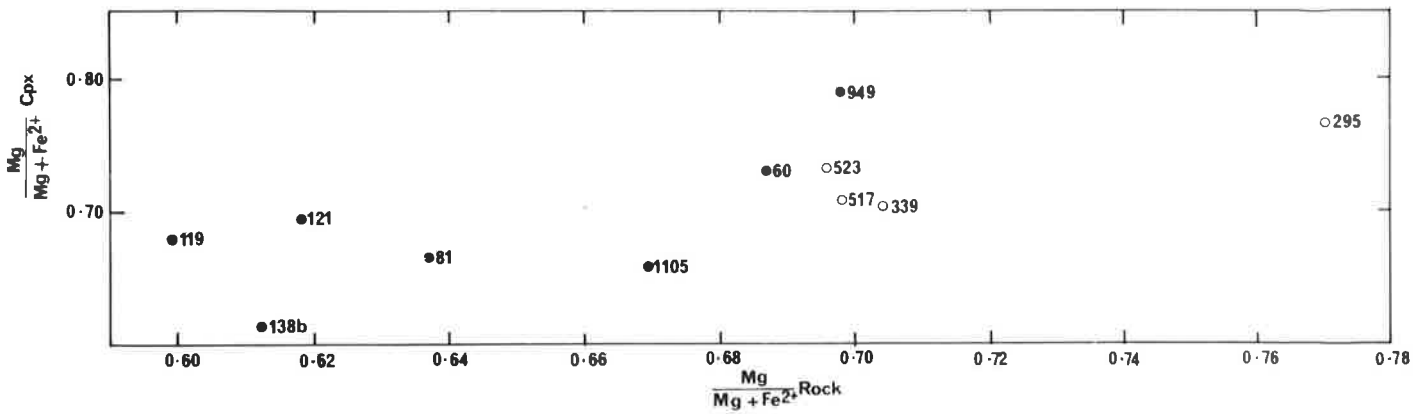
0·80
0·70
$\frac{Mg}{Mg+Fe^{2+}}$ Cpx
949
295
60
523
517
339
121
119
81
1105
138b
0·60
0·62
0·64
0·66
0·68
0·70
0·72
0·74
0·76
0·78
$\frac{Mg}{Mg+Fe^{2+}}$ Rock

a

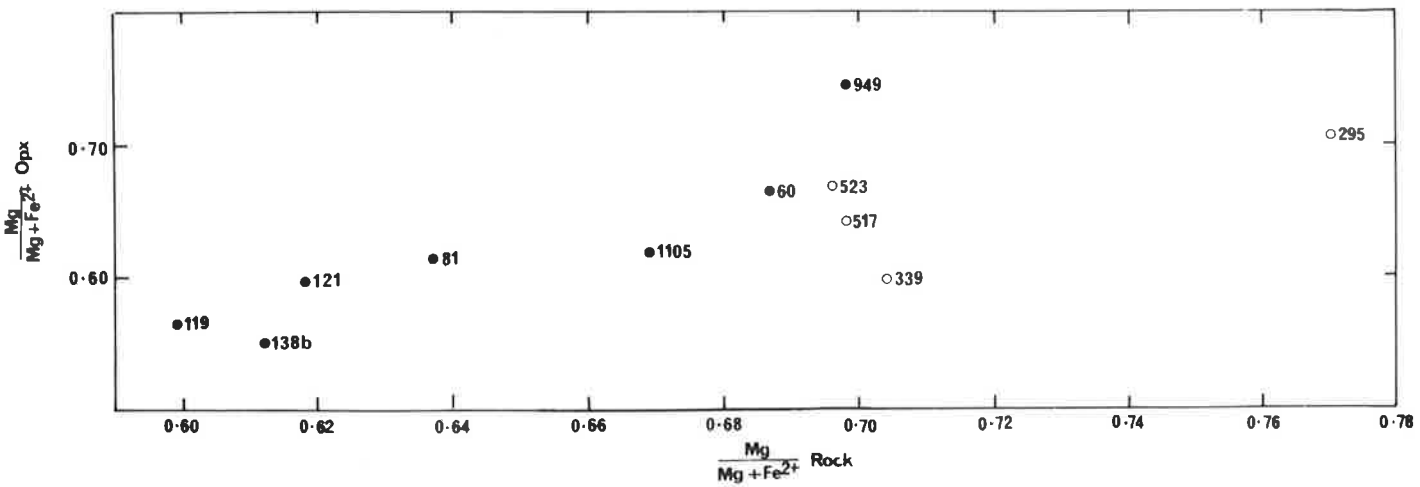
0·70
0·60
$\frac{Mg}{Mg+Fe^{2+}}$ Opx
949
295
60
523
517
81
1105
121
339
119
138b
0·60
0·62
0·64
0·66
0·68
0·70
0·72
0·74
0·76
0·78
$\frac{Mg}{Mg+Fe^{2+}}$ Rock

b

FIGURE 4.22.3

Plot of the $Mg/(Mg + Fe^{2+})$ ratios of hornblendes and parent rocks from Amata (ornamentation the same as in Figure 4.22.1).

Data compiled by Sen (1970) for hornblendes from Madras (open circles), Salem (open triangle), Adirondacks (closed circles), Broken Hill (closed square) and Pennsylvania and Delaware (closed triangle), are shown for comparison.

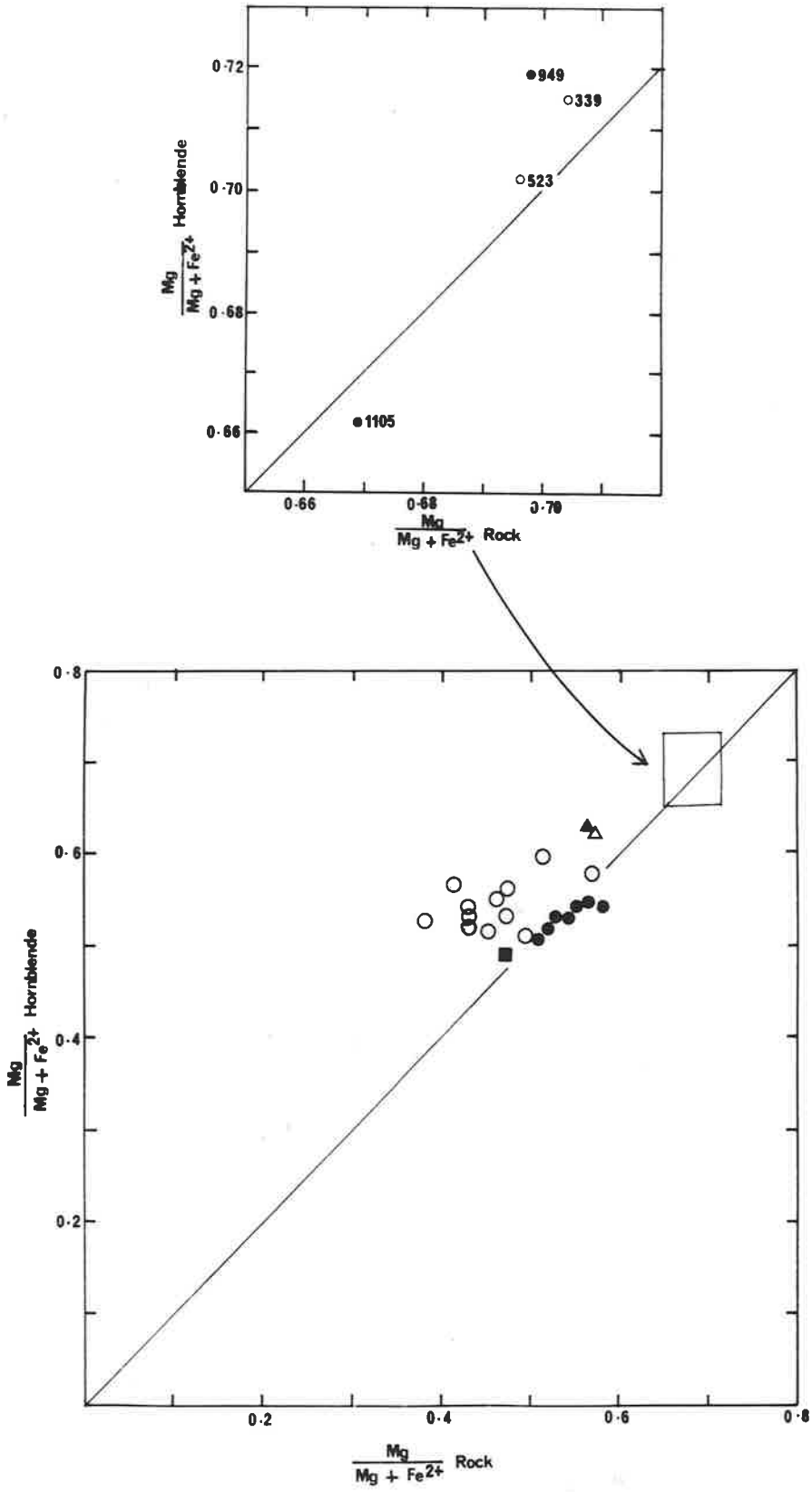
0·72
0·70
0·68
0·66
●949
○339
○523
●1105
0·66
0·68
0·70
Mg / Mg + Fe2+ Hornblende
Mg / Mg + Fe2+ Rock
0·8
0·6
0·4
0·2
0·2
0·4
0·6
0·8
Mg / Mg + Fe2+ Hornblende
Mg / Mg + Fe2+ Rock

FIGURE 4.23.1

Plot of the Mn/(Mg + Mg + Fe^{2+}) ratios of (a) clinopyroxenes and (b) orthopyroxenes, and the same ratio in parent rocks.

Ornamentation:
(the same as for Figure 4.22.1)

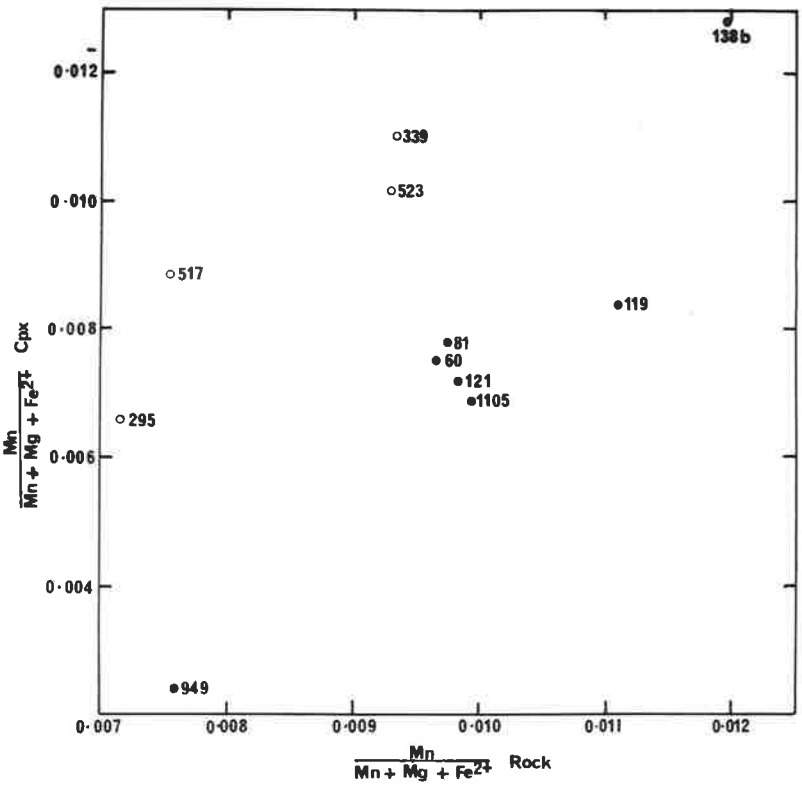
138b
339
523
517
119
81
60
121
1105
295
949
0·012
0·010
0·008
0·006
0·004
0·007
0·008
0·009
0·010
0·011
0·012
Mn / Mn + Mg + Fe2+ Cpx
Mn / Mn + Mg + Fe2+ Rock

a

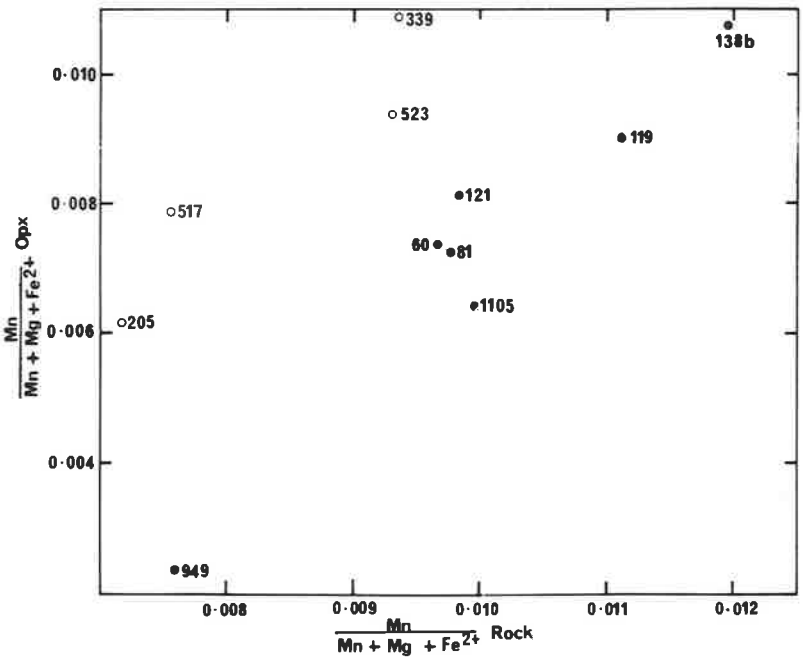
339
138b
523
119
121
517
60
81
1105
205
949
0·010
0·008
0·006
0·004
0·008
0·009
0·010
0·011
0·012
Mn / Mn + Mg + Fe2+ Opx
Mn / Mn + Mg + Fe2+ Rock

b

FIGURE 4.23.2

Plot of the [Mn/(Mn + Mg + Fe^{2+})] x 10^3 ratios of (a) hornblendes, (b) micas and (c) garnets, and the same ratio in parent rocks.

Ornamentation:
(the same as for Figure 4.22.1)

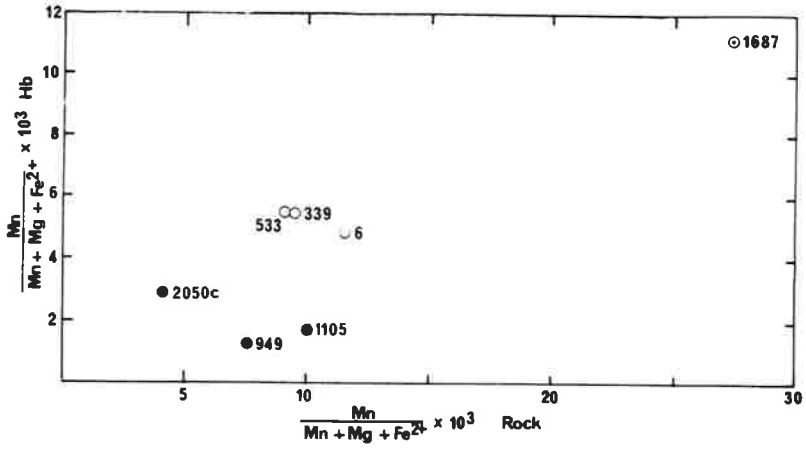
⊙1687
○339
533
○6
●2050c
●1105
●949
Mn / (Mn + Mg + Fe2+) x 10³ Hb
Mn / (Mn + Mg + Fe2+) x 10³ Rock

a

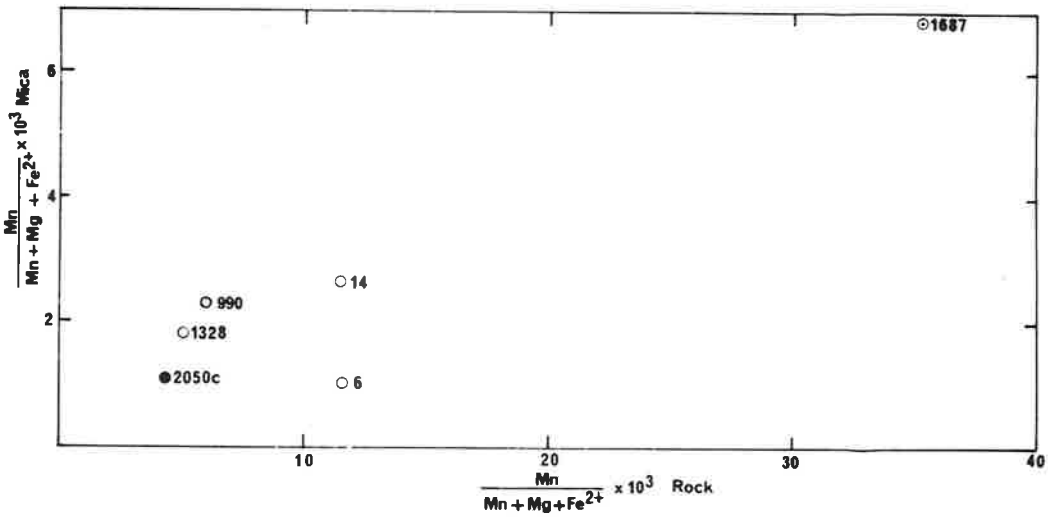
⊙1687
○14
○990
○1328
●2050c
○6
Mn / (Mn + Mg + Fe2+) x 10³ Mica
Mn / (Mn + Mg + Fe2+) x 10³ Rock

b

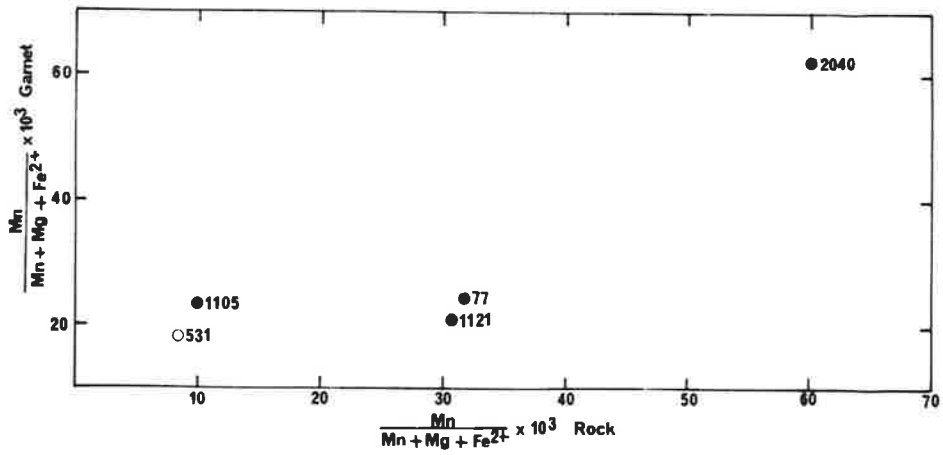
●2040
●1105
●77
●1121
○531
Mn / (Mn + Mg + Fe2+) x 10³ Garnet
Mn / (Mn + Mg + Fe2+) x 10³ Rock

c

FIGURE 4.24

Pyroxene quadrilateral En-Fs-Di-He showing compositions of pyroxenes from Amata.

Ornamentation:

open circles - clinopyroxenes
closed circles - orthopyroxenes

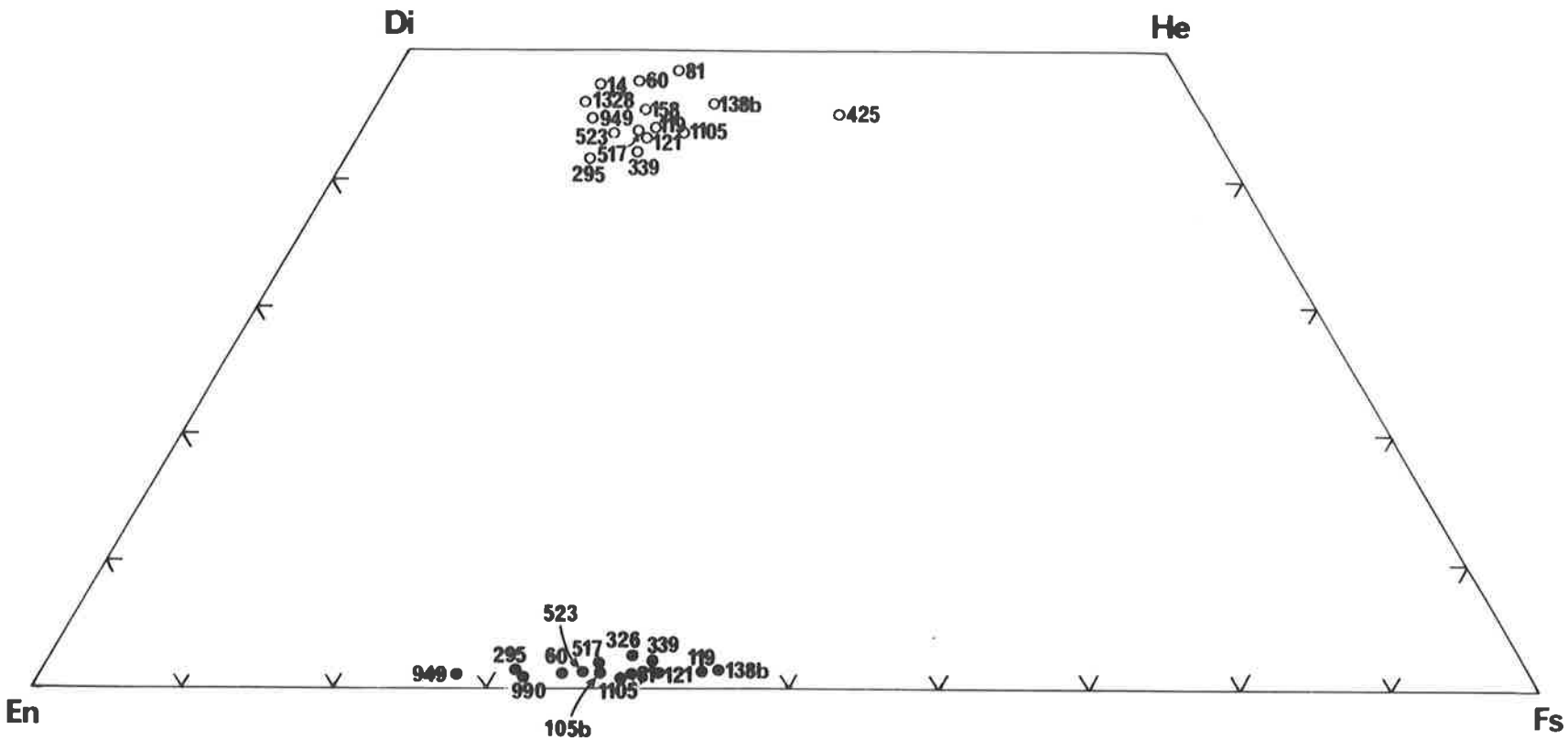
Di
He
En
Fs
14
60
81
1328
138b
425
949
523
1105
121
517
295
339
523
326
339
295
60
517
119
949
121
138b
990
1105
105b

FIGURE 4.25

Plot of the $Fe^{3+}/(Fe^{3+} + Fe^{2+})$ ratios of orthopyroxenes against

(a) Ti content in Y group; and
(b) $Al^{IV}/(Al^{IV} + Si)$.

Ornamentation:
(the same as in Figure 4.17.1)

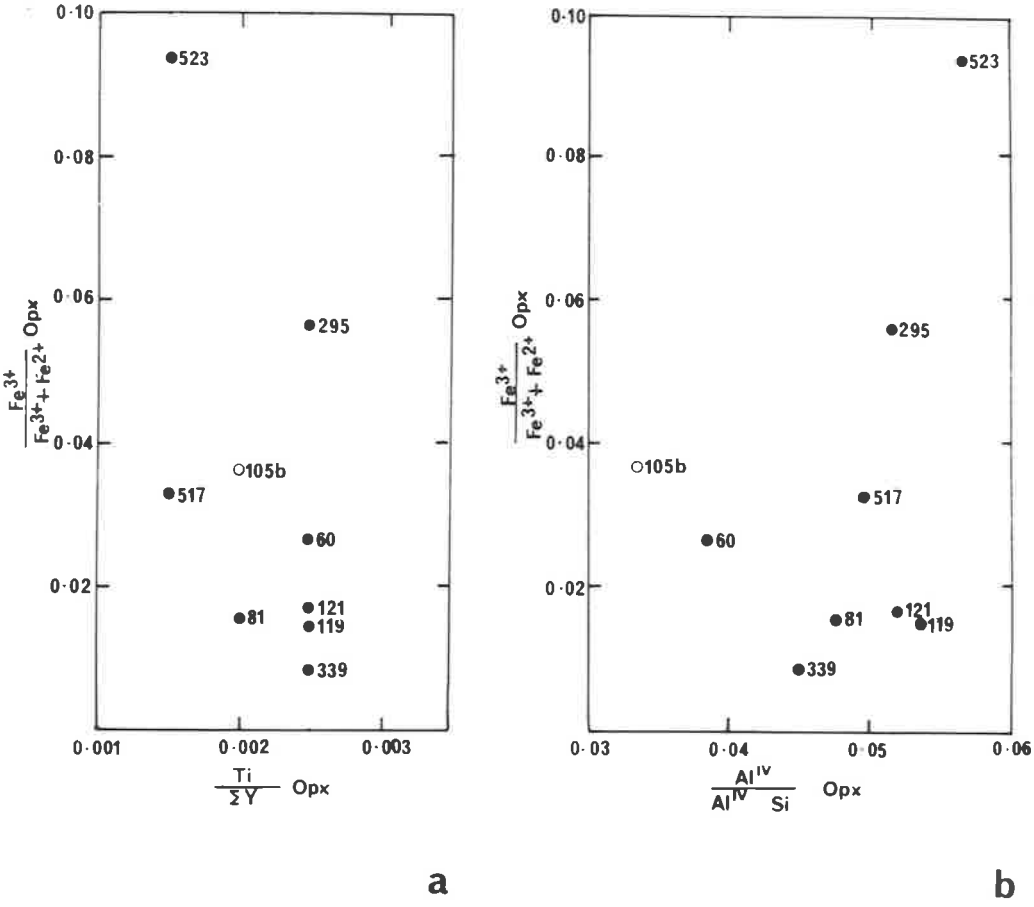
0·10
0·08
0·06
0·04
0·02
0·001
0·002
0·003
$\frac{Fe^{3+}}{Fe^{3+}+Fe^{2+}}$ Opx
$\frac{Ti}{\Sigma Y}$ Opx
●523
●295
○105b
●517
●60
●81
●121
●119
●339
0·03
0·04
0·05
0·06
$\frac{Al^{IV}}{Al^{IV}\ Si}$ Opx

a b

FIGURE 4.26

Plot of Al^{VI} against Al^{IV} for clinopyroxenes (after Aoki and Kushiro, 1968)

Ornamentation:
(the same as in Figure 4.22.1)

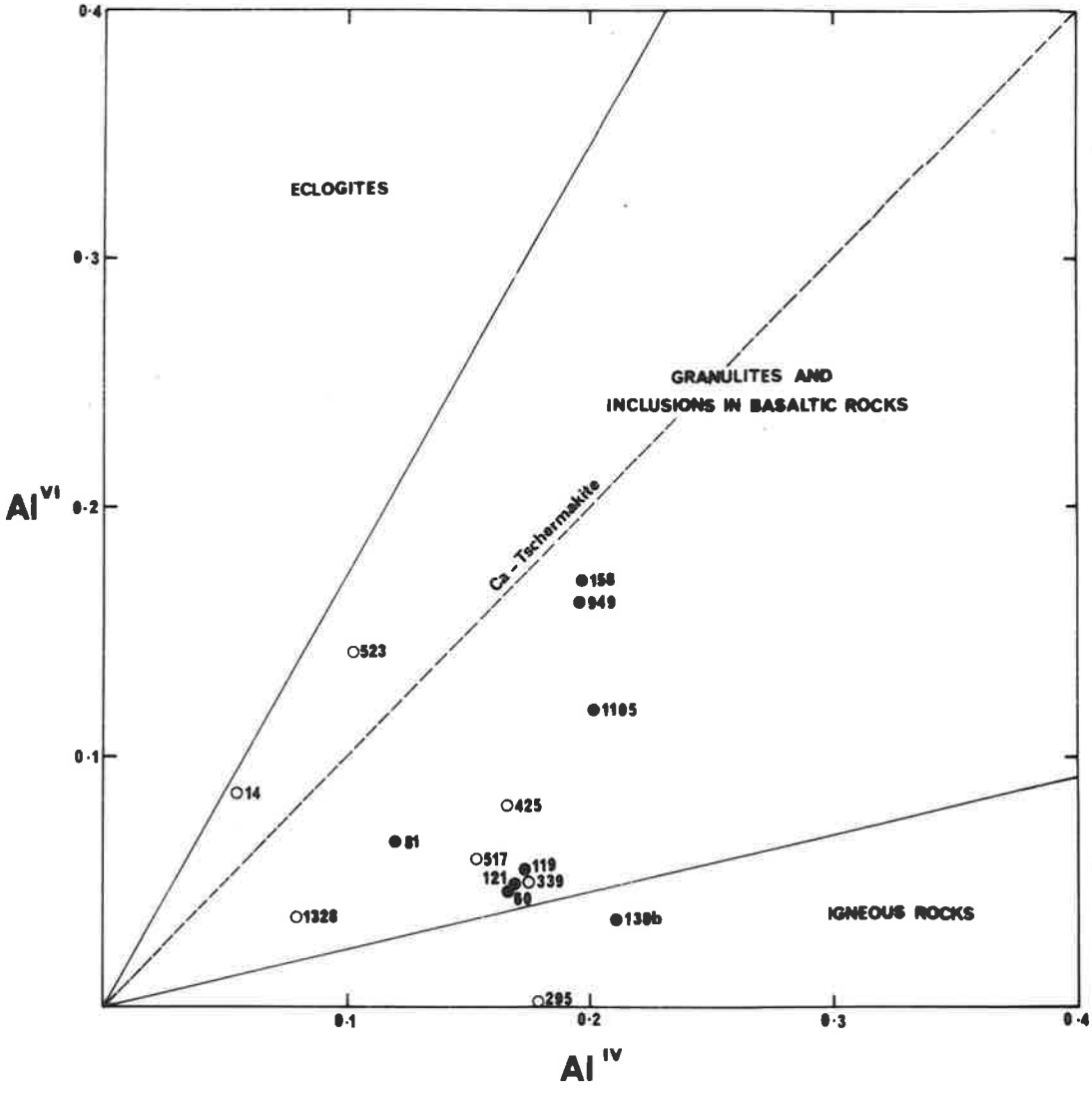
ECLOGITES
GRANULITES AND
INCLUSIONS IN BASALTIC ROCKS
Ca - Tschermakite
IGNEOUS ROCKS
0·4
0·3
0·2
0·1
0·1
0·2
0·3
0·4
Al VI
Al IV
158
949
523
1105
14
425
81
517
119
121
339
60
1328
138b
295

FIGURE 4.27

Chemical affinities of the Amata hornblendes.

Ornamentation:

closed circle - hornblende from the granulite facies terrain
open circle - hornblendes from the transitional terrain
open circle with dot - hornblende from the amphibolite facies terrain.

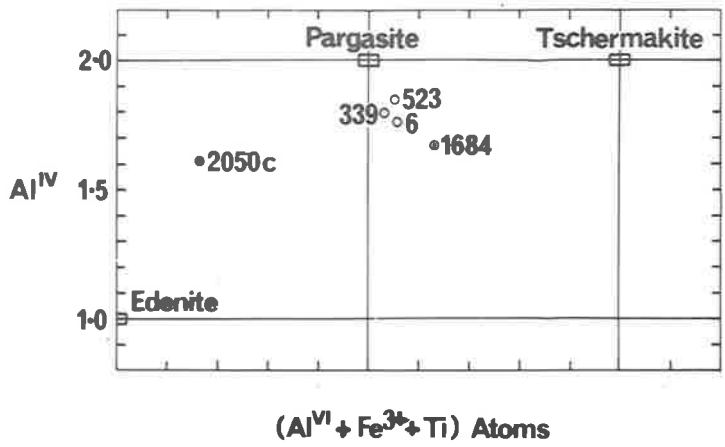
Pargasite
Tschermakite
2·0
1·5
1·0
Al^{IV}
523
339
6
1684
2050c
Edenite
$(Al^{VI} + Fe^{3+} + Ti)$ Atoms

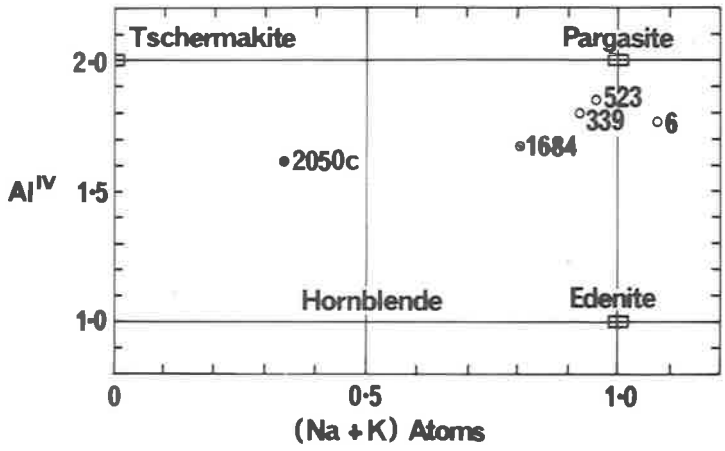
Tschermakite
Pargasite
2·0
1·5
1·0
Al^{IV}
523
339
6
1684
2050c
Hornblende
Edenite
0
0·5
1·0
(Na + K) Atoms

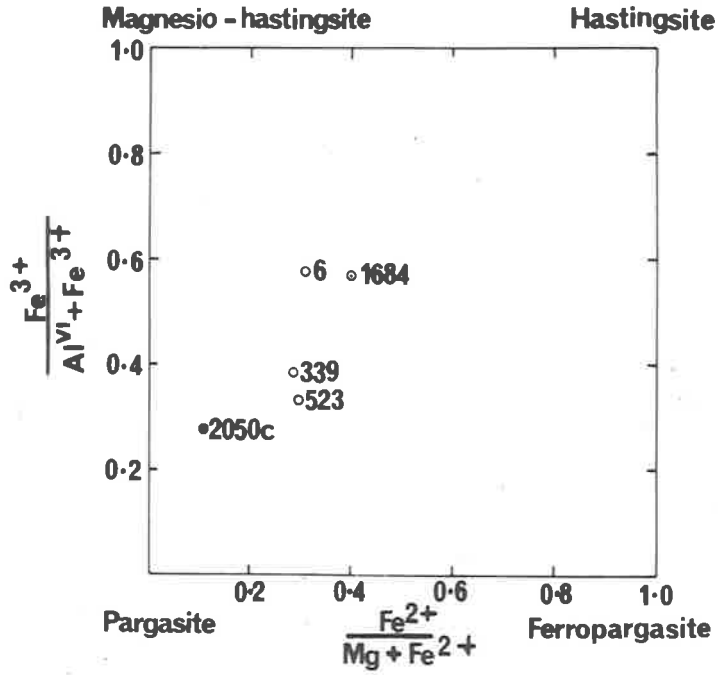
Magnesio - hastingsite
Hastingsite
1·0
0·8
0·6
0·4
0·2
$\frac{Fe^{3+}}{Al^{VI}+Fe^{3+}}$
6
1684
339
523
2050c
0·2
0·4
0·6
0·8
1·0
Pargasite
$\frac{Fe^{2+}}{Mg+Fe^{2+}}$
Ferropargasite

FIGURE 4.28

(a) Plot of Al^{VI} against Al^{IV} for the Amata hornblendes (after Binns, 1965a).

(b) Plot of Al^{VI} against Al^{IV} for hornblendes from other high grade rocks:

1) hornblendes from the Delegate pipe (Lovering and White, 1969)
2) R803 and A117 respectively

M1) hornblendes from eclogites (Mottana and Edgar, 1970)
M2) 3b and P2a respectively

K1) hornblende from garnet amphibolite (Kanisawa, 1969)

B1)
B2) hornblendes from amphibolite facies rocks in the Aracena
B3) Metamorphic belt (Bard, 1970)

Binns' (1965a) Broken Hill metamorphic zones are shown for comparison.

(c) Plot of titanium in the Y group against $Al^{IV}/(Al^{IV} + Si)$ for the Amata hornblendes.

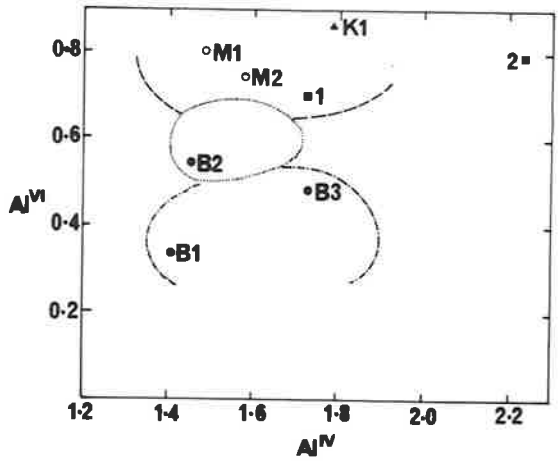
K1
M1
M2
1
2
B2
B3
B1
0·8
0·6
0·4
0·2
Al^VI
1·2
1·4
1·6
1·8
2·0
2·2
Al^IV

b

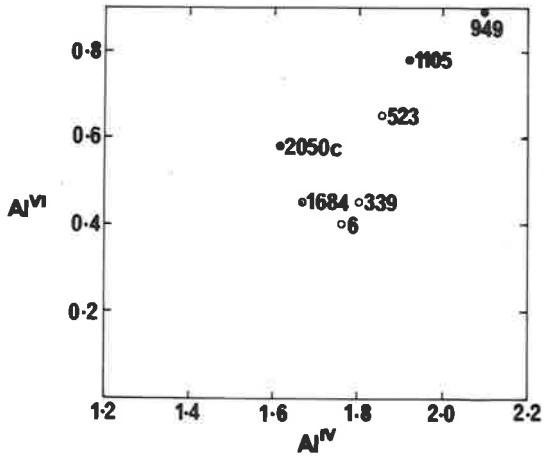
949
1105
523
2050c
1684
339
6
0·8
0·6
0·4
0·2
Al^VI
1·2
1·4
1·6
1·8
2·0
2·2
Al^IV

a

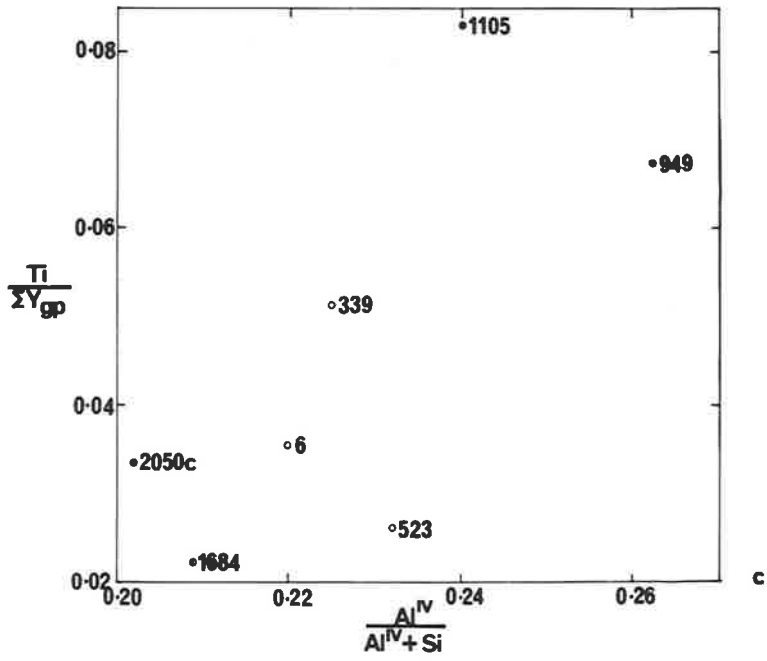
1105
949
339
6
2050c
523
1684
0·08
0·06
0·04
0·02
Ti / ΣY_gp
0·20
0·22
0·24
0·26
Al^IV / Al^IV + Si

c

FIGURE 4.29

Plot of the $Fe^{3+}/(Fe^{3+} + Fe^{2+})$ ratios of hornblendes against (a) titanium in the Y group, (b) $\frac{Al^{IV}}{Al^{IV} + Si}$

Ornamentation:
(the same as for Figure 4.17.1)

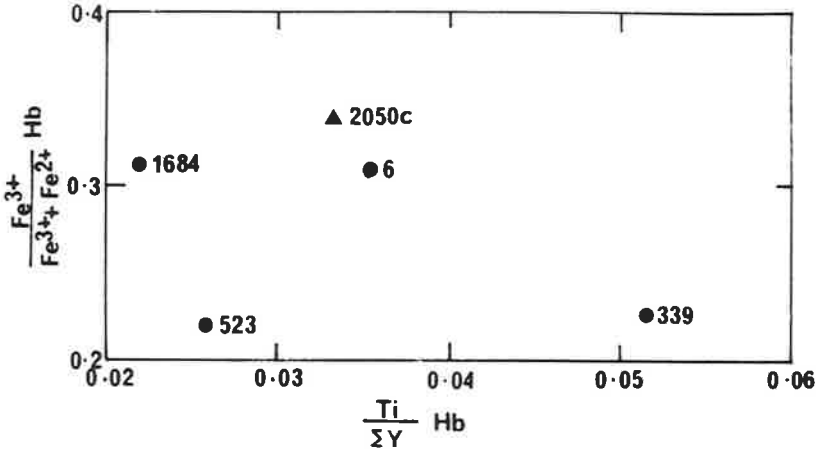
0·4
0·3
0·2
0·02
0·03
0·04
0·05
0·06
▲2050c
●1684
●6
●523
●339
$\frac{Fe^{3+}}{Fe^{3+}+Fe^{2+}}$ Hb
$\frac{Ti}{\Sigma Y}$ Hb

a

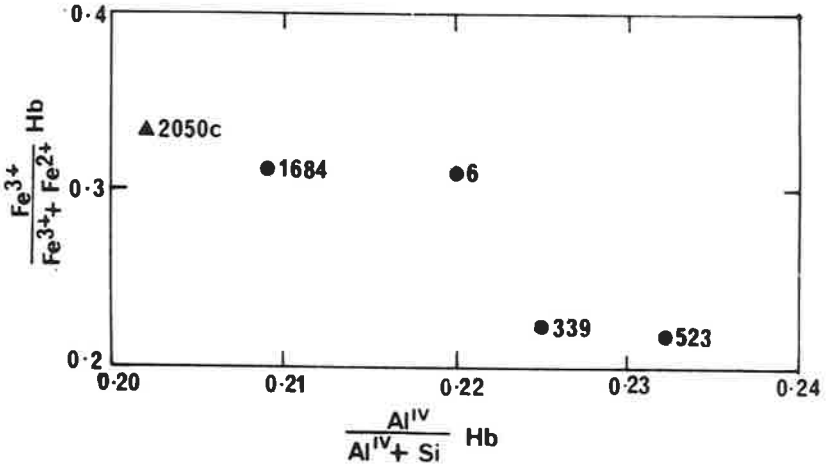
0·4
0·3
0·2
0·20
0·21
0·22
0·23
0·24
▲2050c
●1684
●6
●339
●523
$\frac{Fe^{3+}}{Fe^{3+}+Fe^{2+}}$ Hb
$\frac{Al^{IV}}{Al^{IV}+Si}$ Hb

b

FIGURE 4.30

Ternary plot of Fe^{2+} + Mn - Ca - Mg showing the compositions of the Amata pyralspite garnets. The compositional field of garnets from other granulite complexes (after White, 1969) is shown for comparison.

Ornamentation:
(the same as for Figure 4.22.1)

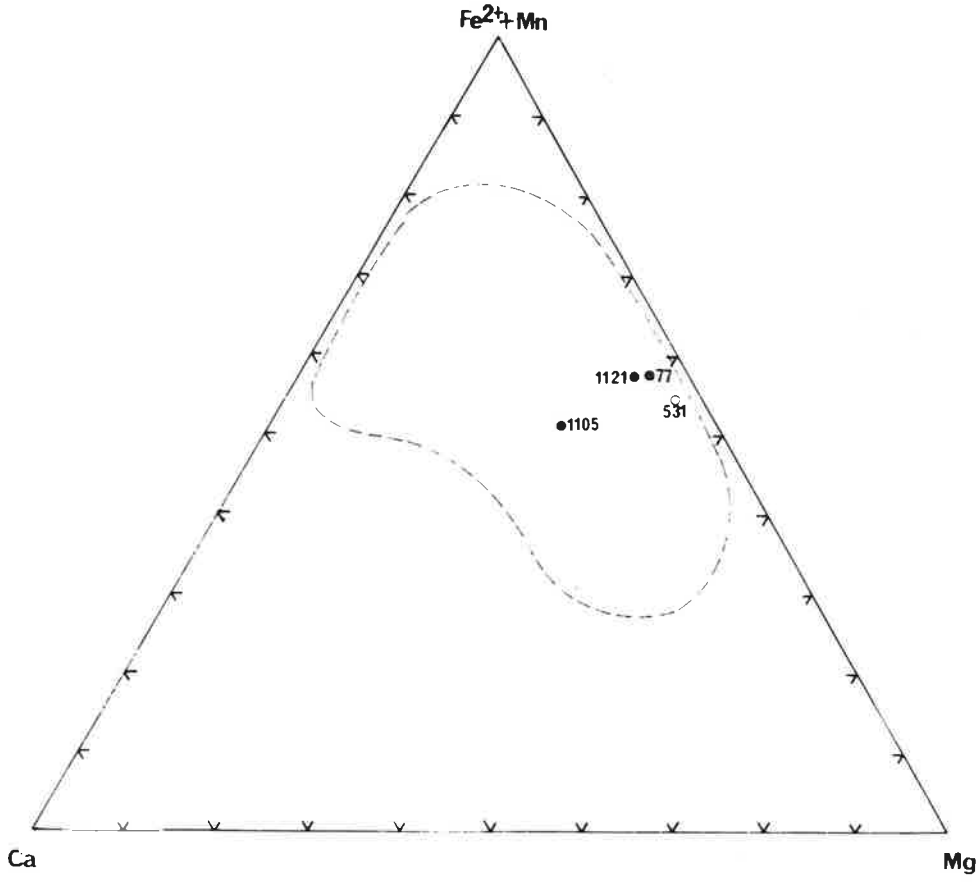
Fe2+Mn
1121
77
531
1105
Ca
Mg

FIGURE 4.31

Ternary plot of octahedrally co-ordinated atoms
($Mg:Fe^{2+} + Mn^{2+} : Al^{VI} + Fe^{3+} + Ti^{4+}$) for micas from the Amata area
(after Foster, 1960).

Ornamentation:
(the same as for Figure 4.22.1)

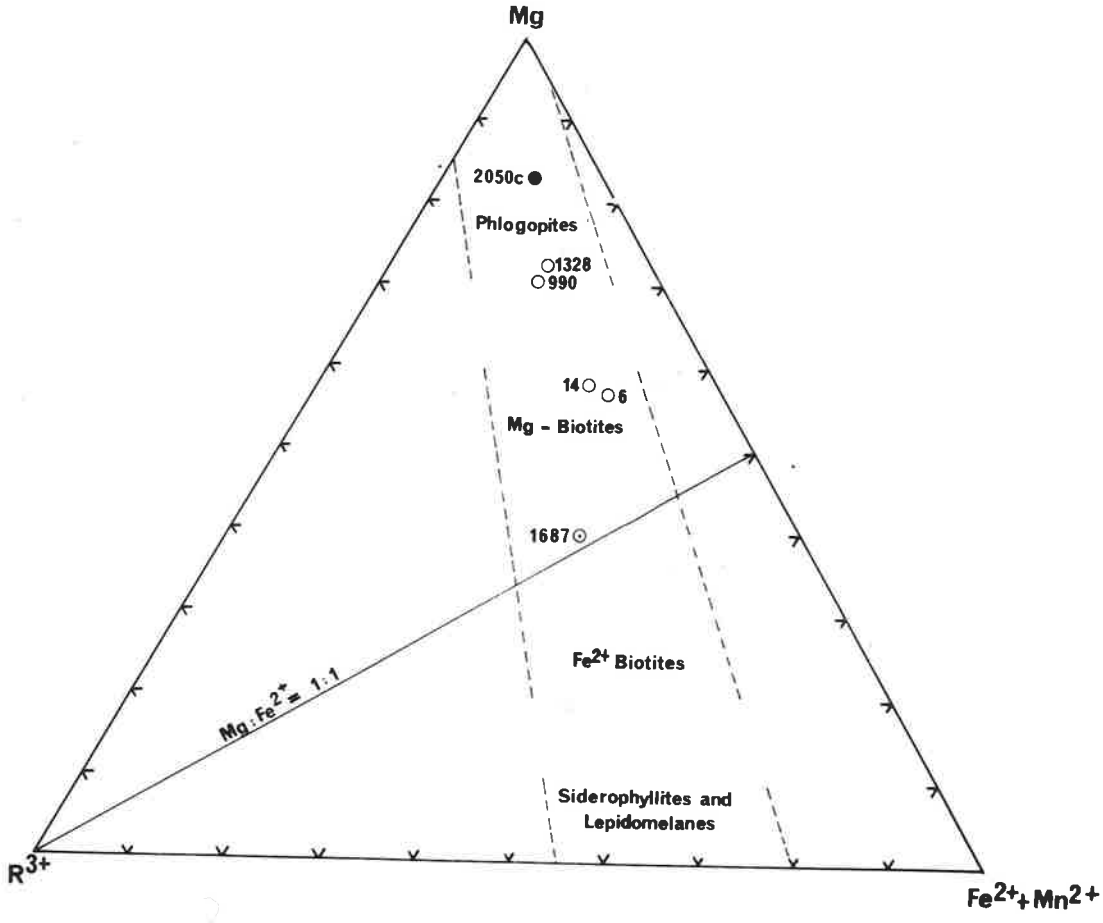
Mg
2050c
Phlogopites
1328
990
14
6
Mg - Biotites
1687
Fe2+ Biotites
Mg : Fe2+ = 1 : 1
Siderophyllites and
Lepidomelanes
R3+
Fe2+ + Mn2+

FIGURE 4.32

(a) Rounded grain of ilmenite (ilmeno-haematite) with bead-like exsolution blebs of haematite. Note the concentration of exsolution blebs along grain boundaries.
A325-6
Plane polarized light
Width of field: 0.21 mm.

(b) Equigranular to inequigranular granoblastic aggregates of magnetite in contact with ilmeno-haematite. The haematite exsolution blebs in the ilmenite are coarse to fine grained and appear to be absent close to the magnetite.
A325-81
Plane polarized light
Width of field: 0.21 mm.

(c) Flame-like exsolution lamellae of haematite in ilmenite showing secondary exsolution lamellae of ilmenite. Blade-like lamellae of corundum are present in the ilmenite.
A325-564
Plane polarized light
Width of field: 0.21 mm.

(d) Rounded grain of ilmenite almost totally enclosed in magnetite (showing martite alteration). The haematite exsolution in the ilmenite decreases in abundance towards the magnetite grains.
A325-564
Plane polarized light
Width of field: 0.21 mm.

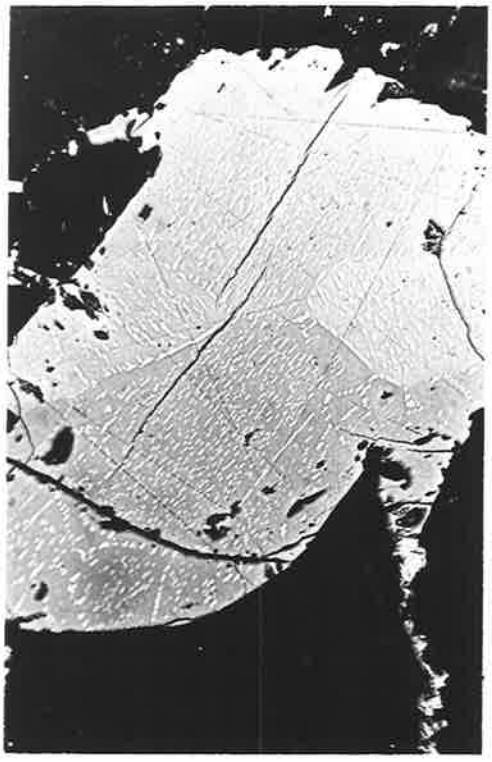

a

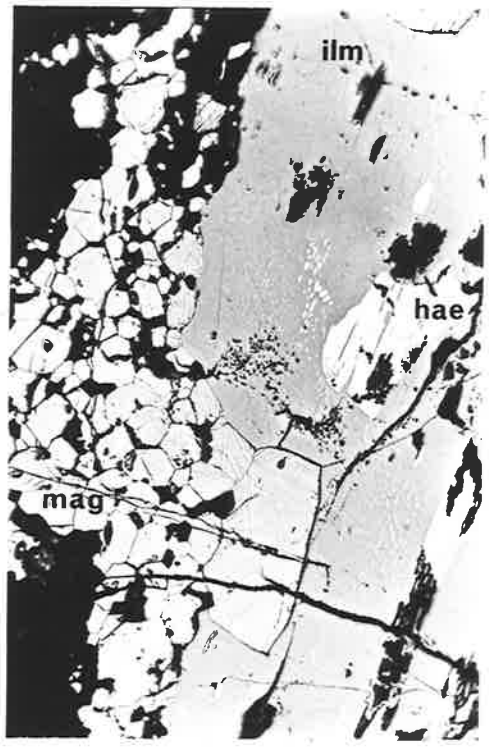

b

c

d

FIGURE 4.33

(a) Absorbed electron image of a grain of haemo-ilmenite with tabular intergrowths of magnetite (black).
A325-6
Width of field: 75μ

(b) FeKα radiation

(c) TiKα radiation

(d) Absorbed electron image of a grain of magnetite enclosed in haemo-ilmenite.
A325-538
Width of field: 75μ

(e) FeKα radiation

(f) TiKα radiation

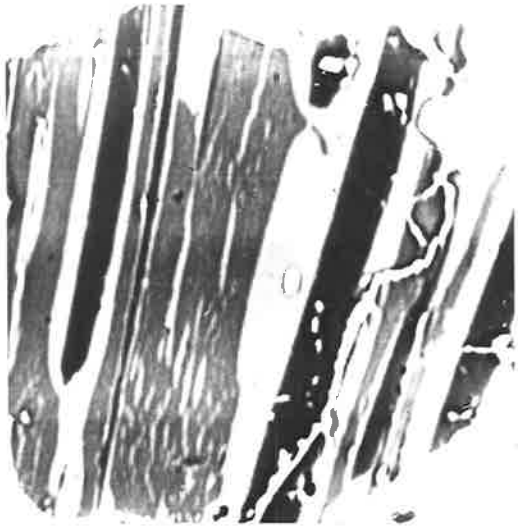

a

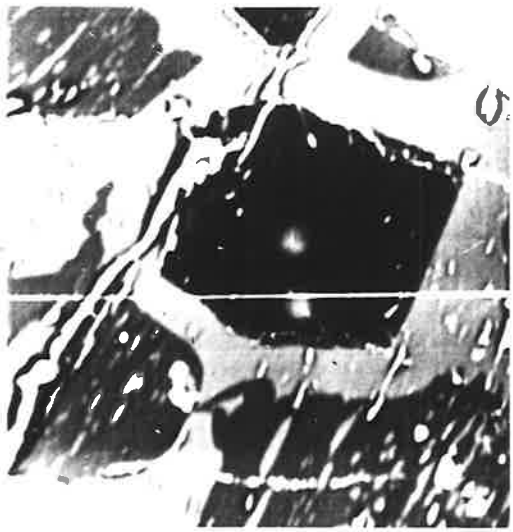

d

b

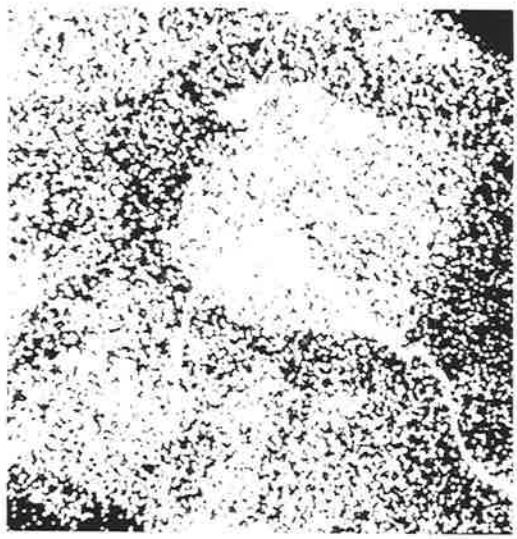

e

c

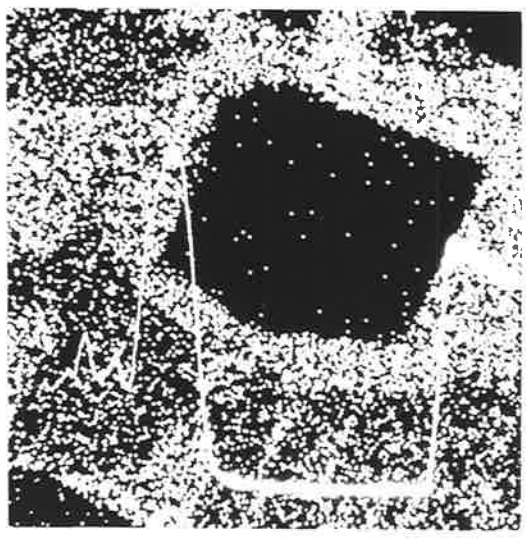

f

FIGURE 4.34

Ternary plot of Or-Ab-An showing the compositions of the Amata alkali feldspars.

Ornamentation:
(the same as for Figure 4.22.1)

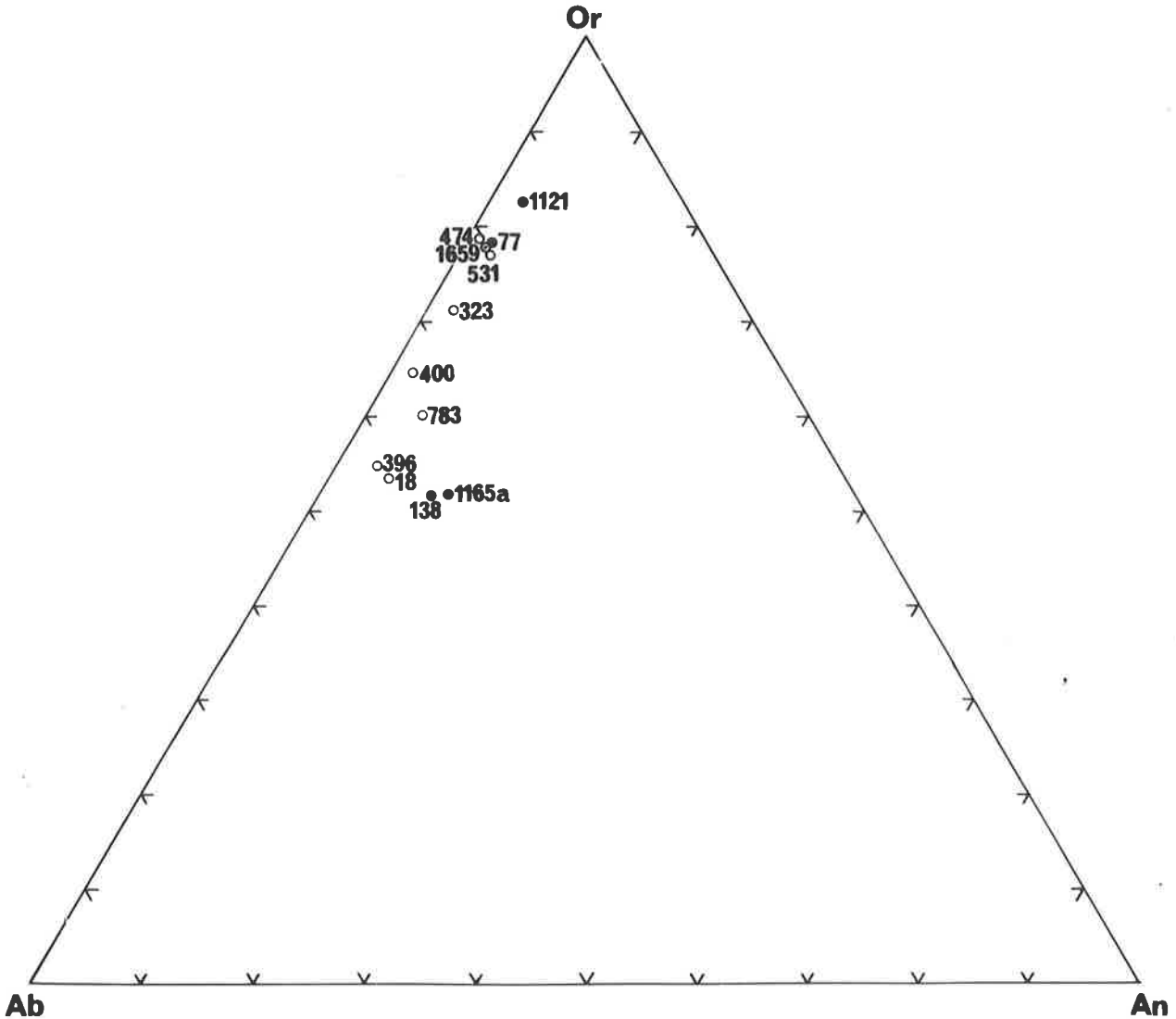
Or
1121
474
77
1659
531
323
400
783
396
18
1165a
138
Ab
An

FIGURE 4.35

Degree of order of the alkali feldspars shown by plotting on the degree of order v c*/b* graph of Jones (1966).

Ornamentation:

closed circles - granulite facies
open squares - transitional
closed squares - amphibolite facies

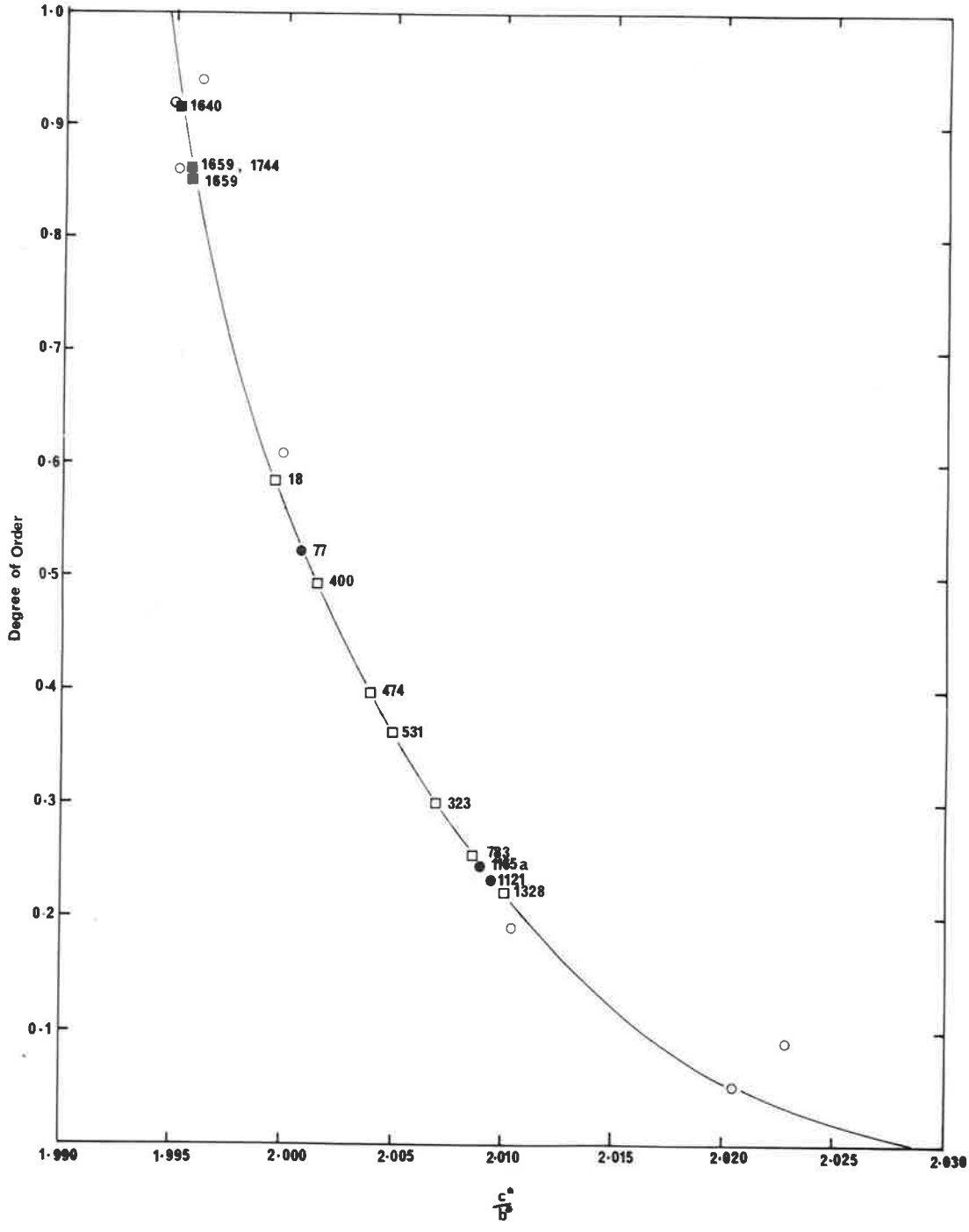
1·0
0·9
0·8
0·7
0·6
0·5
0·4
0·3
0·2
0·1
Degree of Order
1640
1659, 1744
1659
18
77
400
474
531
323
783
1121
1328
1·990
1·995
2·000
2·005
2·010
2·015
2·020
2·025
2·030
c*/b*

FIGURE 4.36

Potassium feldspars from Table 4.39 on b-c plot with cell edges of end members and equal Δbc lines from Stewart and Ribbe (1969) (after Crosby, 1971). The lengths of the bars show the b and c standard errors for each sample.

1. A325-1121
2. A325-77
3. A325-1165a
4. A325-1328
5. A325-323
6. A325-531
7. A325-783
8. A325-400
9. A325-18
10. A325-474 (homogenized)
11. A325-1640
12. A325-1659
13. A325-1744
14. A325-1659 (homogenized)

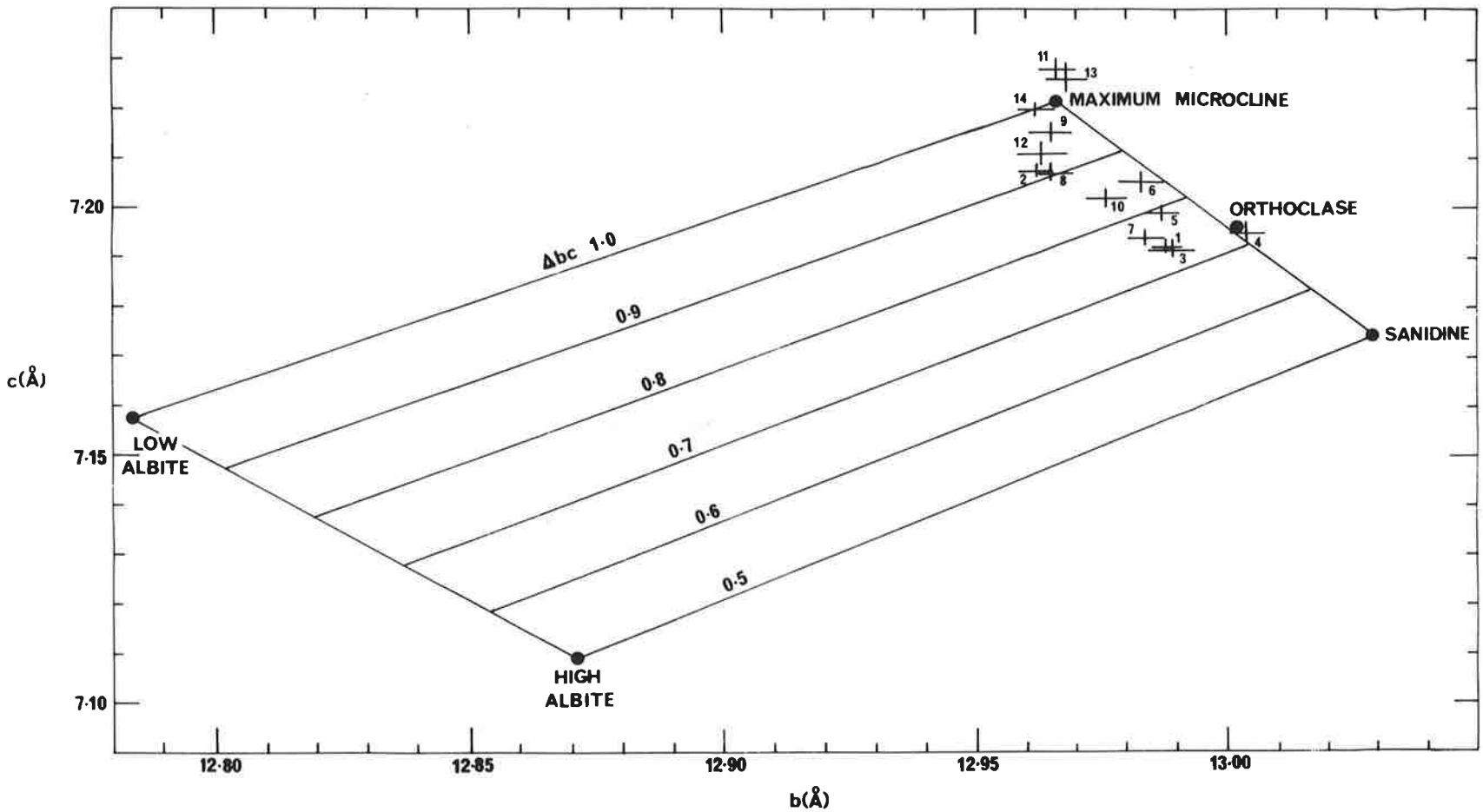
MAXIMUM MICROCLINE
ORTHOCLASE
SANIDINE
LOW ALBITE
HIGH ALBITE
Δbc 1·0
0·9
0·8
0·7
0·6
0·5
7·20
7·15
7·10
c(Å)
12·80
12·85
12·90
12·95
13·00
b(Å)
11
13
14
9
12
2
8
6
10
5
7
1
3
4

FIGURE 4.37

Distribution diagram for co-existing pyroxenes from the Amata area (atomic ratio $Fe^{2+}/(Fe^{2+} + Mg)$) for orthopyroxene is plotted against that of clinopyroxene.

Ornamentation:
(the same as for Figure 4.22.1)

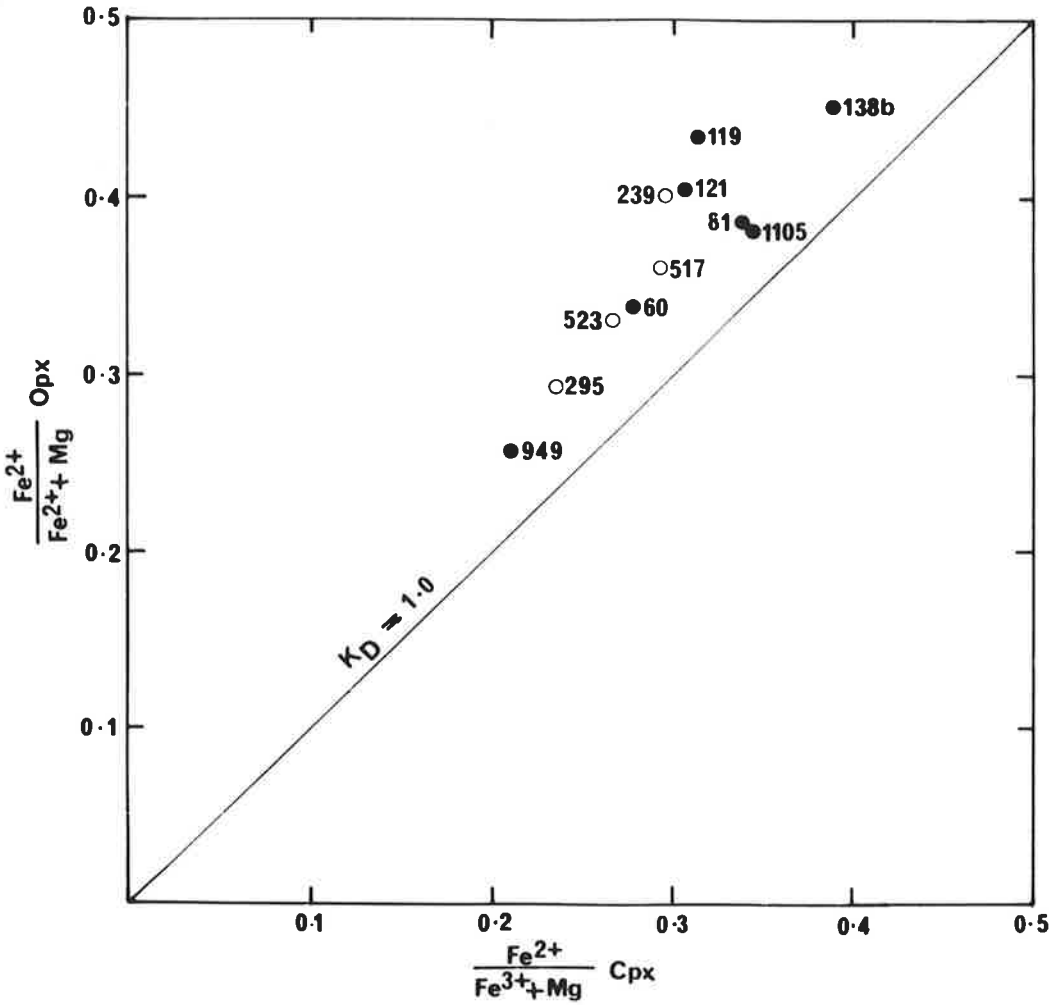
0·5
0·4
0·3
0·2
0·1
0·1
0·2
0·3
0·4
0·5
$\frac{Fe^{2+}}{Fe^{2+}+Mg}$ Opx
$\frac{Fe^{2+}}{Fe^{3+}+Mg}$ Cpx
$K_D = 1.0$
138b
119
239
121
81
1105
517
523
60
295
949

FIGURE 4.38

Plot of $Fe^{2+}/(Fe^{2+} + Mg)$ for orthopyroxene against the same ratio for clinopyroxene, for pyroxene pairs from other high grade terrains (after Binns, 1962). The field occupied by the Amata samples is outlined. The average distribution curves $K_D^{opx-cpx}{}_{Fe^{2+} - Mg}$ = 1.78 (dotted line) and = 1.00 (solid line) are drawn.

Ornamentation:

solid square - Broken Hill (Binns, 1962)
solid circle - Quairading (Davidson, 1968, 1969)
inverted open triangles - Scotland (Muir and Tilley, 1958; O'Hara, 1960, 1961a,b)
inverted solid triangle - Madras (Howie, 1955)
solid triangle - Lapland (Eskola, 1952)
open square - Varberg (Saxena, 1968a)

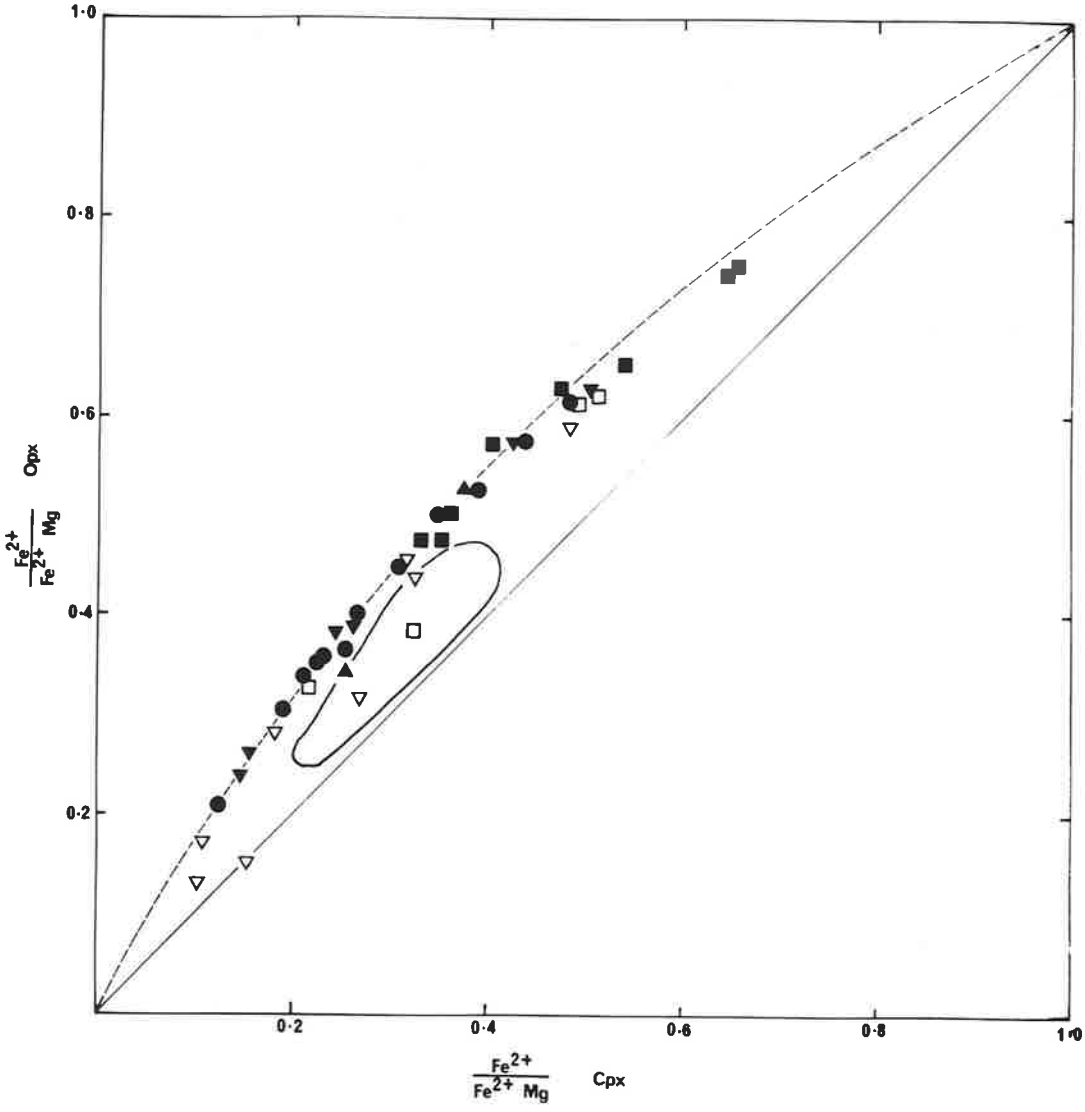
1·0
0·8
0·6
0·4
0·2
0·2
0·4
0·6
0·8
1·0
Opx
$\frac{Fe^{2+}}{Fe^{2+}\ Mg}$
$\frac{Fe^{2+}}{Fe^{2+}\ Mg}$ Cpx

FIGURE 4.39

Plot of $K_{D(Fe^{2+} - Mg)}^{opx-cpx}$ against:

(a) rock oxidation ratio

(b) rock $Fe^{2+}/(Fe^{2+} + Mg)$ ratio

(c) plot of $K_{D(Mg - Fe^{2+})}^{opx-cpx}$ against rock $Mg/(Mg + Fe^{2+})$ ratio.

Ornamentation:

(the same as for Figure 4.22.1)

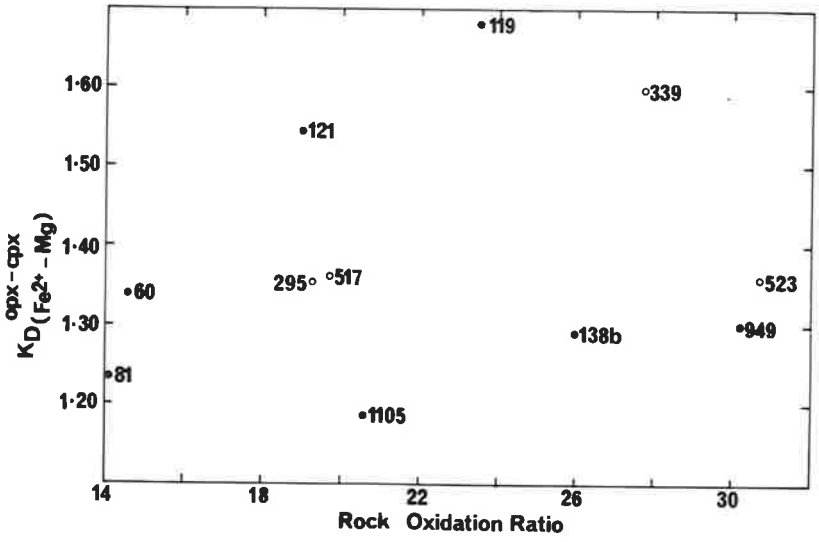
119
339
121
295
517
523
60
138b
949
81
1105
1·60
1·50
1·40
1·30
1·20
14
18
22
26
30
$K_{D(Fe^{2+}-Mg)}^{opx-cpx}$
Rock Oxidation Ratio

a

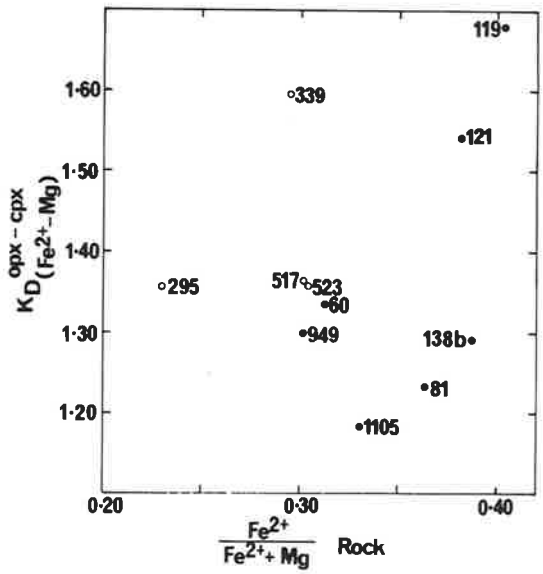
119
339
121
295
517
523
60
949
138b
81
1105
1·60
1·50
1·40
1·30
1·20
0·20
0·30
0·40
$K_{D(Fe^{2+}-Mg)}^{opx-cpx}$
$\frac{Fe^{2+}}{Fe^{2+}+Mg}$ Rock

b

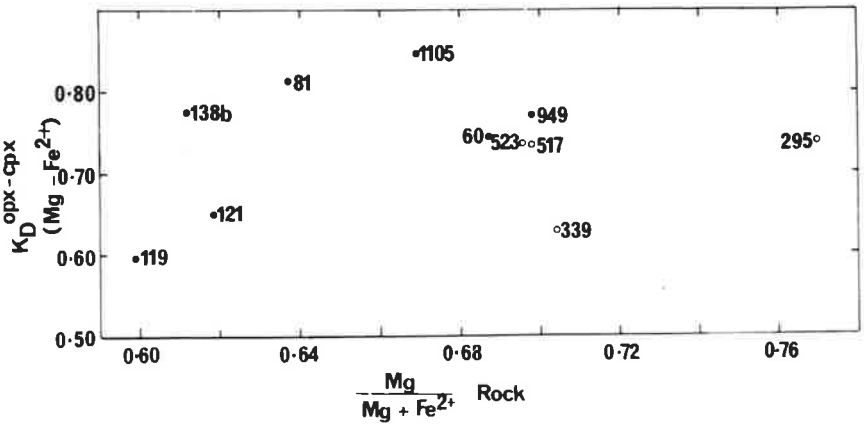
1105
81
138b
949
60
523
517
295
121
339
119
0·80
0·70
0·60
0·50
0·60
0·64
0·68
0·72
0·76
$K_{D\ (Mg-Fe^{2+})}^{opx-cpx}$
$\frac{Mg}{Mg+Fe^{2+}}$ Rock

c

FIGURE 4.40

Plot of the $Fe^{2+}/(Fe^{2+} + Mg)$ ratio of clinopyroxene (open circles) and orthopyroxene (closed circle) against the same ratio for co-existing hornblende.

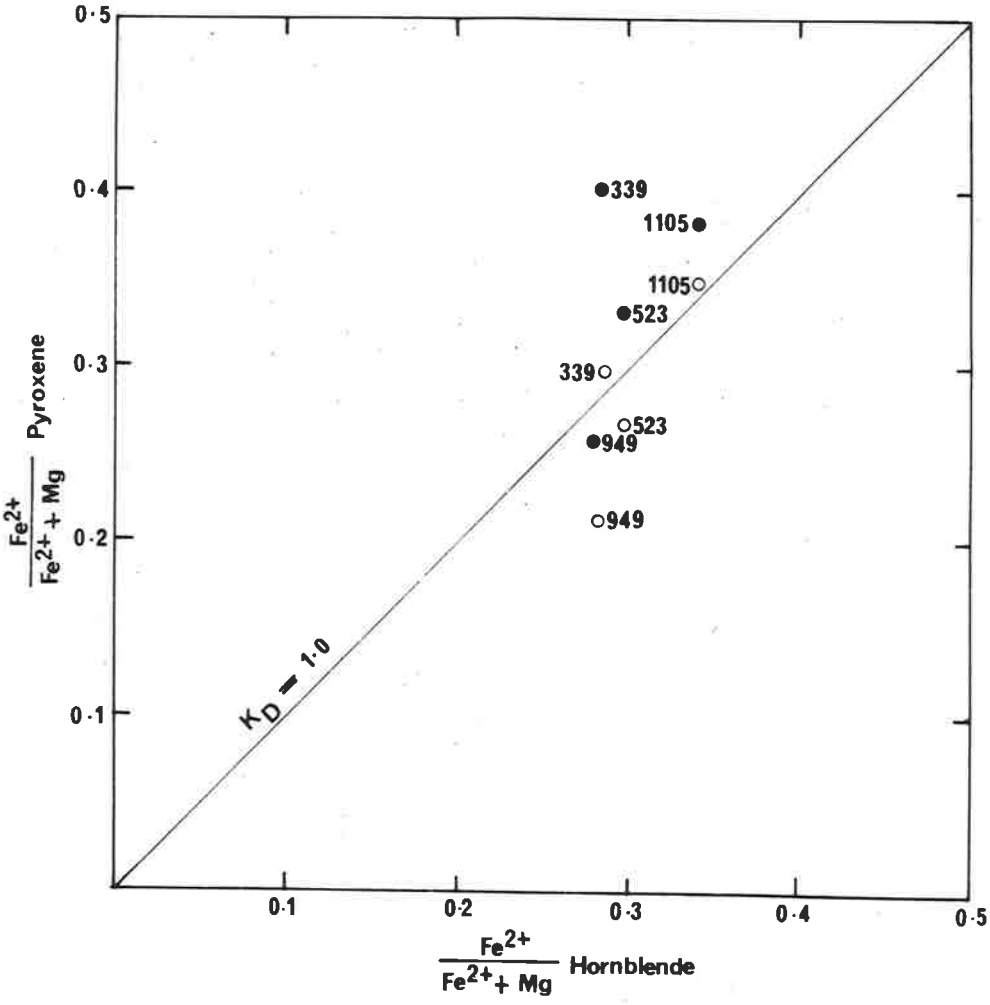
0·5
0·4
0·3
0·2
0·1
0·1
0·2
0·3
0·4
0·5
●339
1105●
1105○
●523
339○
○523
●949
○949
$K_D = 1·0$
$\frac{Fe^{2+}}{Fe^{2+}+Mg}$ Pyroxene
$\frac{Fe^{2+}}{Fe^{2+}+Mg}$ Hornblende

7. The critical line of the alkali feldspar solvus (after Morse, 1970).

The stippled areas indicate the ranges of pressure-temperature conditions estimated for the granulite facies (dotted) and amphibolite facies (dashed) terrains.

FIGURE 5.1

Petrogenetic grid

1. 1a Al_2SiO_5 triple point (after Althaus, 1969)
   1b Al_2SiO_5 triple point (after Richardson, Gilbert and Bell, 1969)

2. 2a Solidus for wet granite (after Luth et al., 1964)
   2b Solidus for wet granite (after Boettcher and Wyllie, 1968)
   2c Liquidus for granite with 2% water (after Tuttle and Bowen, 1958)
   2d Liquidus for anhydrous granite (after W.C. Burnham, pers.comm.)

3. 3 Upper stability limit of hornblende in the presence of excess water (after Nishikawa et al., 1971)

4. Subsolidus boundaries marking the first appearance of garnet in a variety of compositions:
   4a adamellite (after Green and Lambert, 1965)
   4b quartz tholeiite (after Green and Ringwood, 1967)
   4c high alumina basalt (after Green, 1967)
   4d olivine tholeiite (Ito and Kennedy, 1971)

5. 5a Upper stability limit of Mg-cordierite (after Schreyer and Yoder, 1964)
   5b) Upper stability limit of cordierite in rocks with $Mg/(Mg + Fe^{2+})$
   5c) ratios of 0.7 and 0.3 respectively (after Hensen and Green, 1971)
   5d Upper stability limit of Fe-cordierite (after Richardson, 1968)
   5e Extrapolated curve for $Mg/(Mg + Fe^{2+})$ ratio of 0.4

6. 6a) Experimentally determined curves for the reaction:
   6b) muscovite + quartz $\leq$ K feldspar + sillimanite + water
   (after Althaus et al., 1970 and Storre and Karotke, 1971 respectively)

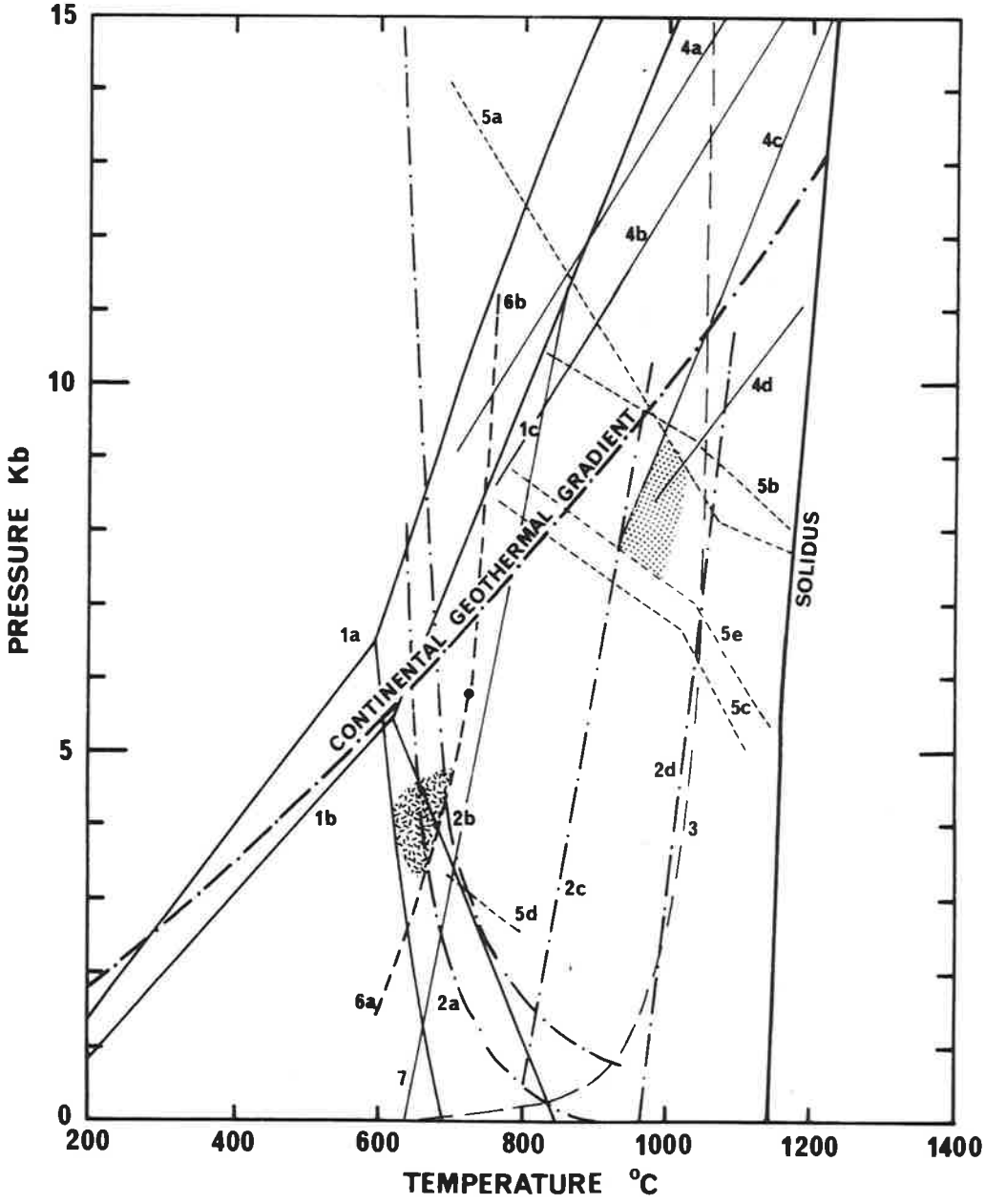
15
10
5
0
PRESSURE Kb
200
400
600
800
1000
1200
1400
TEMPERATURE °C
4a
5a
4c
4b
6b
4d
1c
5b
CONTINENTAL GEOTHERMAL GRADIENT
SOLIDUS
1a
5e
5c
2d
1b
2b
3
2c
5d
6a
2a
7

FIGURE 5.2

Frlationship between Niggli c and mg for the mafic rocks from the:

(a) granulite facies terrain;

(b) transitional and amphibolite facies terrains.

Dashed line outlines the pelitic area, solid curve indicates the trend of variation of igneous rocks (after Leake, 1964 and Van de Kamp, 1968).

Ornamentation:

(a) dots - mafic rocks
solid square - ultramafic rock

(b) small dots - mica free mafic rocks from the transitional terrain
large dots - micaceous mafic rocks from the transitional terrain
solid square - ultramafic rock
triangle - amphibolite

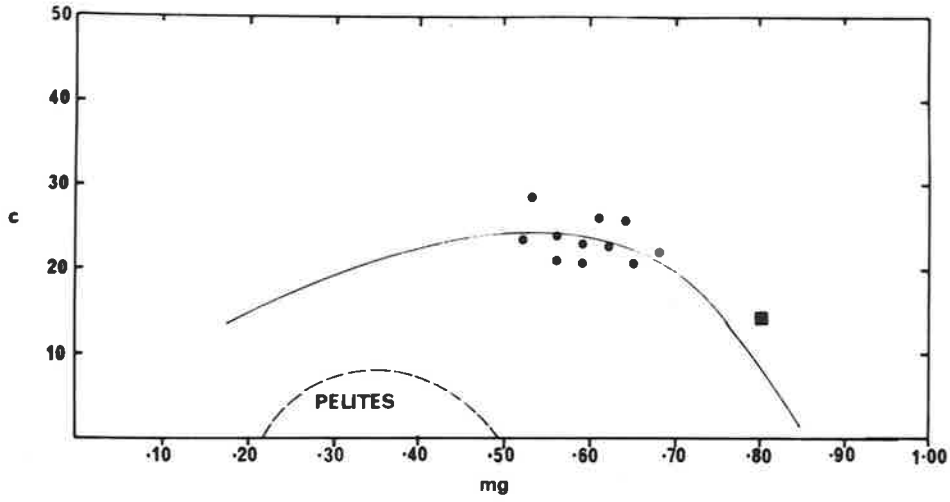
50
40
30
20
10
c
PELITES
·10
·20
·30
·40
·50
·60
·70
·80
·90
1·00
mg

a

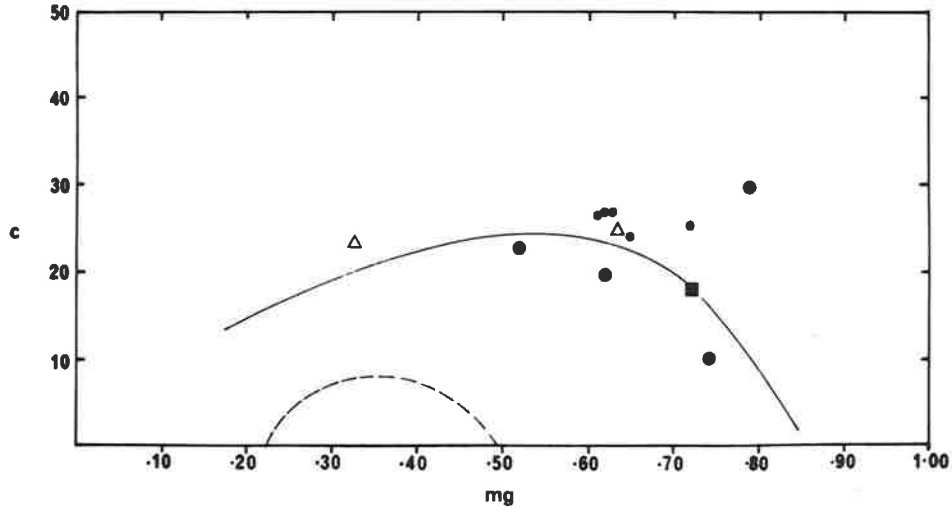
50
40
30
20
10
c
·10
·20
·30
·40
·50
·60
·70
·80
·90
1·00
mg

b

FIGURE 5.3

Relationship between Niggli al-alk and c for the:

(a) granulite facies terrain;

(b) transitional and amphibolite facies terrain

(after Van de Kamp, 1968).

Ornamentation:
(the same as in Figure 5.2)

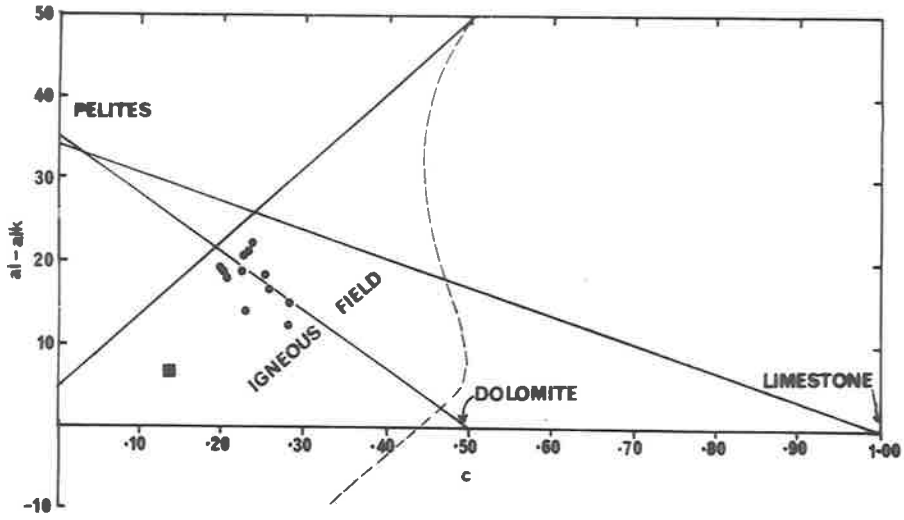
PELITES
FIELD
IGNEOUS
DOLOMITE
LIMESTONE
al - alk
c
50
40
30
20
10
-10
·10
·20
·30
·40
·50
·60
·70
·80
·90
1·00

a

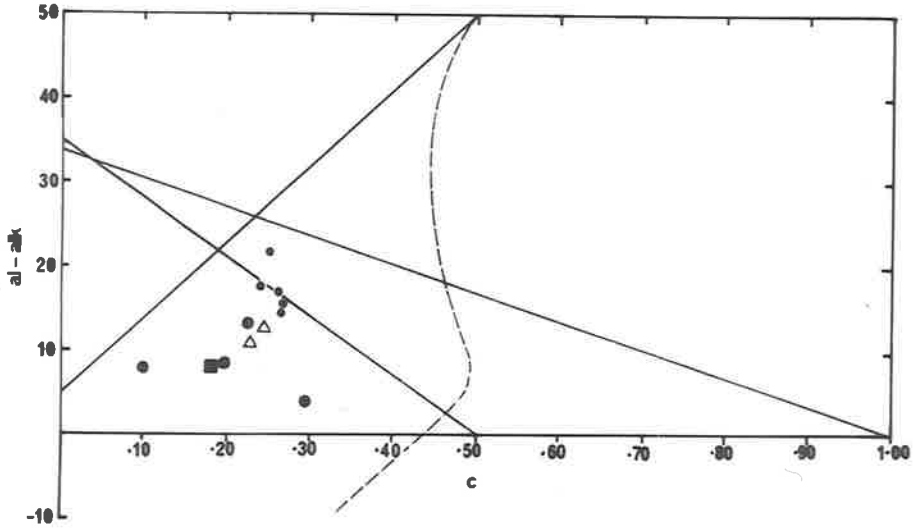
al - alk
c
50
40
30
20
10
-10
·10
·20
·30
·40
·50
·60
·70
·80
·90
1·00

b

FIGURE 5.4

Ternary plot of c, al-alk and 100.mg for the mafic rocks from the:

(a) granulite facies terrain

(b) transitional and amphibolite facies terrains.

Fine dashed curve illustrates the trend of variation of the Karroo Dolerites. (after Leake, 1964 and Van de Kamp, 1968).

Ornamentation:
(the same as in Figure 5.2)

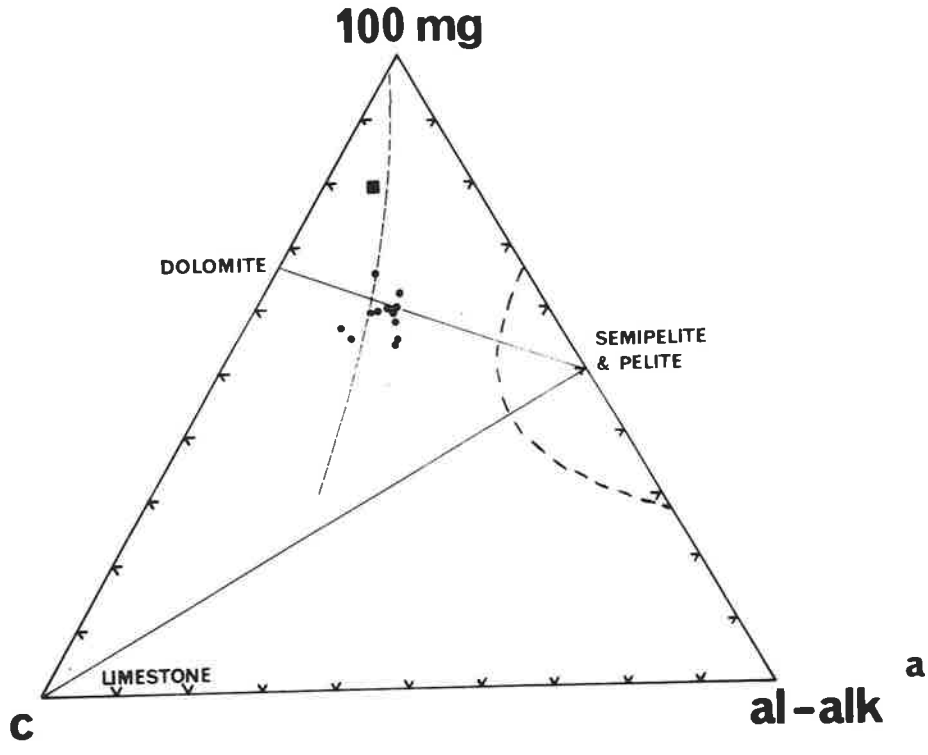
100 mg
DOLOMITE
SEMIPELITE
& PELITE
LIMESTONE
c
al-alk

a

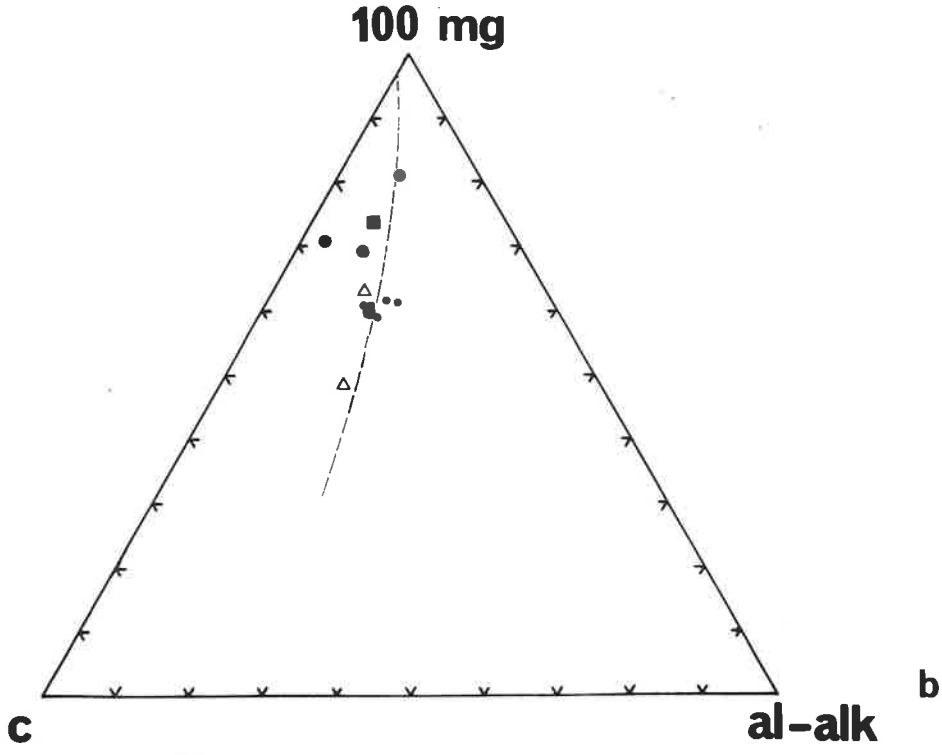
100 mg
c
al-alk

b

FIGURE 5.5

Plot of $Na_2O + K_2O$ against SiO_2 for the mafic rocks from the:

(a) granulite facies terrain;

(b) transitional and amphibolite facies terrains.

(after MacDonald and Katsura, 1964).

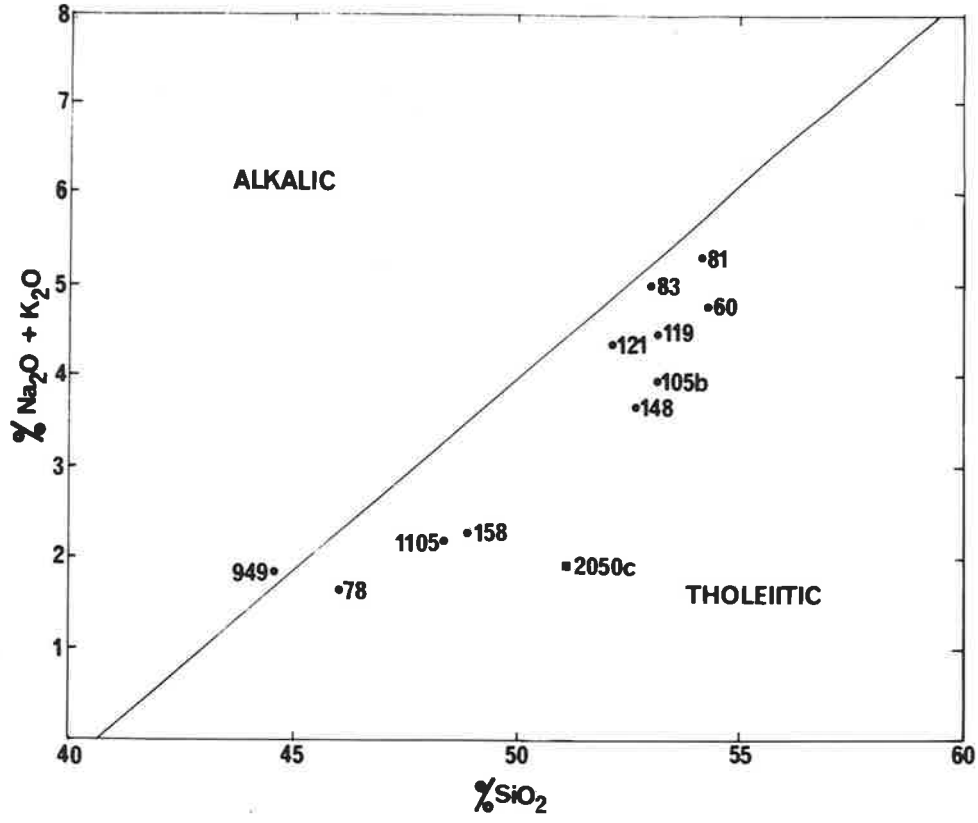
ALKALIC
THOLEIITIC
81
83
60
121
119
105b
148
158
1105
949
78
2050c
% Na2O + K2O
%SiO2
8
7
6
5
4
3
2
1
40
45
50
55
60

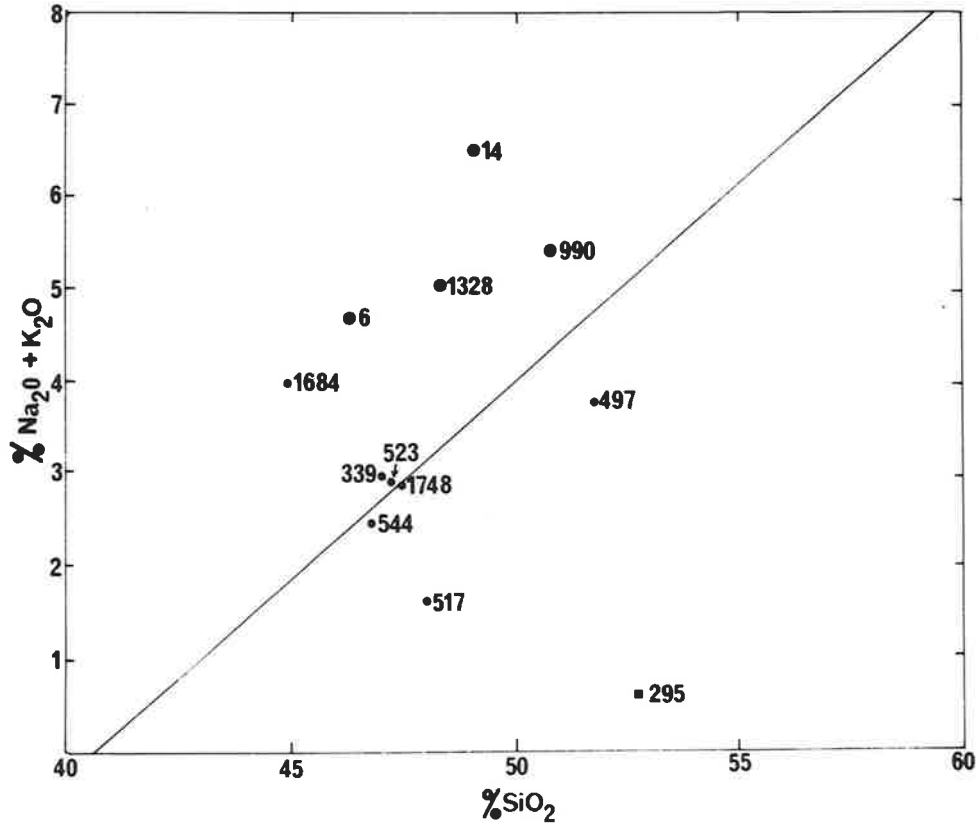
14
990
1328
6
1684
497
523
339
1748
544
517
295
% Na2O + K2O
%SiO2
8
7
6
5
4
3
2
1
40
45
50
55
60